An analysis of the nuclear interactions of high energy cosmic rays

Osborne, J.L.

An Analysis of the Nuclear Interactions of High Energy Cosmic Rays

A Thesis submitted to the
University of Durham for the
Degree of Doctor of Philosophy

by

J.L. Osborne, B.Sc.

March 1966

CONTENTS

		Page
ABSTRACT		i
PREFACE		iii
CHAPTER 1.	INTRODUCTION	1
1.1	The characteristics of nuclear interactions at high energies	2
1.2	Machine data on kaon production	4
1.3	The kaon to pion ratio from investigations of the muon flux	6
1.4	Weak interactions at high energies	8
1.5	Machine results on neutrino interactions	10
1.6	Cosmic ray studies of neutrino interactions	11
CHAPTER 2	THE VERTICAL MUON SPECTRUM AT SEA LEVEL	15
2.1	Introduction	15
2.2	The measured vertical muon spectrum	18
2.3	Energy loss and decay of muons in the atmosphere	24
2.3.1	Properties of the atmosphere	25
2.3.2	Rate of energy loss of muons in air	25
2.3.3	Survival probability calculations	26
2.4	Derivation of the muon spectrum from an assumed pion spectrum	27
2.5	The muon spectrum from kaon and pion decay	31
2.5.1	Directly produced muons	32
2.5.2	Muons produced by two-stage decay	34
2.5.3	The derived pion and kaon production spectrum	35

		Page
CHAPTER 3	CALCULATIONS OF THE MUON SPECTRUM AT LARGE ZENITH ANGLES	37
3.1	Introduction	37
3.2	Muon spectrum from pion parents	39
3.3	Muon spectrum from kaon and pion parents	41
3.4	Correction for scattering at large zenith angles	42
CHAPTER 4	DERIVATION OF THE KAON TO PION RATIO	49
4.1	Introduction	49
4.2	The measured muon spectrum at large zenith angles	50
4.2.1	The Durham horizontal spectrograph	50
4.2.2	Analysis of the data	51
4.2.3	Comparison of measured and predicted spectra	52
4.3	Electromagnetic cascades in the atmosphere	53
4.3.1	Experimental data	54
4.3.2	The production spectrum of initial photons	56
4.3.3	The predicted muon production spectra	58
4.3.4	The K/π ratio from electromagnetic cascade measurements	61
4.4	Measurement of the polarization of muons	63
4.4.1	The calculated muon polarization	64
4.4.2	Summary of the experimental data	67
4.5	Conclusions concerning the K/π ratio	70
CHAPTER 5	HIGH ENERGY NEUTRINO INTERACTIONS	73
5.1	Elastic interactions	73
5.2	Inelastic interactions	74

		Page
5.3	Production of the Intermediate Boson	76
5.3.1	Cross-sections for $W^{\pm}$ production	77
5.3.2	The energy of the 'prompt' muon	79
5.3.3	The energy of the 'decay' muon	81
5.3.4	The muonic branching ratio	81
5.3.5	Experimental data on the mass of the Boson	82
5.4	The Glashow resonance interaction	84
CHAPTER 6	THE FLUX OF NEUTRINOS AT SEA LEVEL	86
6.1	Introduction	86
6.2	Neutrinos produced in the atmosphere	88
6.2.1	Neutrinos from kaon and pion decay	88
6.2.2	Neutrinos from muon decay	90
6.3	Comparison with other results	95
6.4	Extra-terrestial neutrinos	97
CHAPTER 7	THE KOLAR GOLD FIELD NEUTRINO EXPERIMENT	104
7.1	The neutrino telescopes	104
7.2	The predicted numbers of events	106
7.2.1	The aperture of the telescopes	106
7.2.2	The flux of neutrino-initiated muons underground	106
7.2.3	The flux of atmospheric muons	112
7.3	The preliminary results of the KGF neutrino experiment	113
7.4	Discussion of the preliminary results	116
7.5	Results of the Case-Wits experiment	117

		Page
CHAPTER 8	CONCLUSIONS	121
8.1	The production of kaons in high energy nuclear interactions	121
8.2	The preliminary results of the neutrino experiment	126
ACKNOWLEDGMENTS		130
REFERENCES		131
APPENDIX A	The rate of energy loss of high energy muons	138
APPENDIX B	Properties of the atmosphere	142
APPENDIX C	Kaon decay modes and energy spectra of decay particles	144
APPENDIX D	Differential aperture of horizontally orientated telescopes	149
APPENDIX E	Celestial Coordinates of muons in the KGF neutrino experiment	151

Abstract

A study of kaon production in high energy nucleon-air nucleus collisions in the atmosphere has been made based on the muon momentum spectrum at sea level. Starting from the measured vertical momentum spectrum the spectra at zenith angles between 75° and 90° have been predicted for various admixtures of kaons and pions, taking into account all decay modes of both charged and neutral kaons. The predicted values are compared with the intensities measured using the Durham horizontal muon spectrograph. Although the method of computation allows the spectra to be predicted to an accuracy of 1% the present statistical errors on both the vertical and horizontal intensities are such that only an upper limit to R, the ratio of intensities at production of kaons to pions of all charge states, can be given; this has a value of about 40% over a range of meson energies from about 70 GeV to 1000 GeV.

In order to extend the determination of the value of R to lower and higher energies repectively, reviews have been made of measurements of muon polarization at sea level and of the intensity of the electromagnetic cascades at various heights in the atmosphere. Combining the three methods an estimate is given of R over a range of meson energies from 3 GeV to 5000 GeV. If R is taken to be independent of energy a value of 20% would fit the data best over the whole energy range, but the error on this value approaches $\pm$ 20%.

Comparing R with R_i, the observed ratio of numbers of non-pions to pions produced in individual interactions, it is concluded that, provided that the majority of non-pions are kaons, there is no evidence

for the effective mean energies of pions and kaons from individual nuclear interactions being different in the range of primary energies from 10 GeV to 10^5 GeV.

Using the measured vertical spectrum of muons the energy spectra and angular distribution of neutrinos at sea level are calculated. The information is used in the interpretation of the preliminary results from the Tata Institute-Osaka-Durham joint neutrino experiment in progress at the Kolar Gold Field. Comparison of observed rates of events with rates predicted from extrapolation to higher energies of machine results on neutrino-nucleus collisions indicates that the cross-section for inelastic interactions continues to rise above 10 GeV. Support for this conclusion is provided by the first results of the Case Institute-Witwatersrand University neutrino experiment. The possibility is discussed of detecting the hypothetical Intermediate Boson of weak interactions.

Preface

The studies reported in this thesis were made during 1962-1965 while the author was a Research Student, under the supervision of Professor A.W. Wolfendale, in the Cosmic Ray Group in the Physics Department of the University of Durham.

An analysis of one aspect of nucleon-air nucleus collisions at high energies, the production of kaons, has been made based on the momentum spectra of cosmic ray muons in the vertical and near horizontal directions, obtained by the author's colleagues at Durham. The results of this have been included in a recent paper by Ashton et al. (1966). In order to widen the range of energies covered, reviews have been made of the measurements of the polarization of cosmic ray muons and of the intensity of electromagnetic cascades in the atmosphere. The present work brings up to date studies made by Osborne (1964) and Osborne and Wolfendale (1964) of the data on these respective phenomena. The interpretation of the data is based on the vertical sea level muon spectrum derived by Osborne et al. (1964). An account of some earlier work on this subject (Osborne and Wolfendale (1963)) was presented at the International Conference on Cosmic Rays at Jaipur. In each case the analysis has been the responsibility of the author.

Using the ratio of kaons to pions produced in the atmosphere the spectra and angular distributions of neutrinos at sea level have been derived. Details of the author's calculations of these quantities are given here: the results have been reported by Osborne et al. (1965).

These are utilized in the interpretation of the preliminary results of an experiment to detect the nuclear interactions of high energy cosmic ray neutrinos, which is being performed at the Kolar Gold Field, India in a collaboration between Durham University, the Tata Institute of Fundamental Research, Bombay and Osaka City University, Japan. Results from this experiment, obtained by a team of workers from the three institutions up to 3rd November, 1965, are included in the present work. Interim reports on the experiment have appeared in three papers by Achar et al. (1965a,b,d).

A paper on the neutrino energy spectrum was given by the author at the Informal Conference on Experimental Neutrino Physics at CERN in January 1965.

Chapter 1

Introduction

Discoveries in the field of High Energy Physics are today contributing most to the fundamental understanding of nature. Pais has made an analogy between the present state of knowledge of High Energy Physics and the stage reached by chemists in the second half of the 19th Century when Mendeleev's Periodic Table of the elements had been constructed but its explanation in terms of Atomic Physics had not been found. Any basic advance in the transition from elementary particle 'chemistry' to elementary particle 'physics' must depend upon the detailed investigation of the interactions of particles at higher energies than at present attained.

Cosmic Ray physicists have always been in the vanguard of the advance to higher energies because of the existence of cosmic ray particles up to practically infinite energies when compared to those attainable by accelerators. Present day machines produce beams of protons up to energies of 30 GeV with a mean rate of the order of 10^{11} protons sec^{-1}. In two years' time the Sherpukov machine will raise this limit to 70 GeV, and concrete proposals have been made for the construction of 300 GeV machines and 30 GeV colliding beams. The latter arrangement would be equivalent to the incidence of 1000 GeV protons on a stationary target at a rate of 10^{5} sec^{-1}. The maximum energies of the beams of secondary particles, both hadrons and leptons, are fractions of the proton energy: for example, muon-neutrinos from the CERN P.S. have energies up to an effective limit $\sim$ 10 GeV. In comparison, cosmic ray protons are known to exist up to energies $\sim 10^{20}$ eV. At the top of the atmosphere the flux of nucleons with energy greater than 30 GeV is approximately 2.5×10^{-2} cm^{-2} sec^{-1}. The flux decreases rapidly

with energy and at 1000 GeV is about 10^{-4} cm^{-2} sec^{-1}. Beyond 10^{15} eV the flux of nucleons is so low that their initial interactions cannot be studied and investigations can only be made via the Extensive Air Showers that they produce. From a comparison of the fluxes it can immediately be seen that cosmic ray experiments cannot compete with those utilising machines in the region of overlapping energies. Present day cosmic ray research in the field of high energy physics is concentrated on the investigation of the characteristics, at still higher energies, of the behaviour of interactions that have already been observed at machine energies and the search for new phenomena (e.g. the production of massive unstable particles) which have threshold energies above the capabilities of present machines.

Both the strong and electromagnetic interactions of elementary particles have been examined using cosmic rays, and recently investigations of weak interactions have also been initiated. The work on electromagnetic interactions has been concentrated mainly on muons. Experiments have been performed to test the validity of quantum electrodynamical predictions at high energies and to examine 'nuclear' interactions of muons i.e. interactions between the nucleus and the virtual photon cloud surrounding the muon. A review of earlier work in this field has been made by Fowler and Wolfendale (1958) and some later experiments have been summarized by Rogers (1965). In the present work we shall first concentrate on one aspect of the investigation of strong interactions and then proceed to the description of an experiment on weak interactions involving the detection of interactions of cosmic ray neutrinos.

1.1 The Characteristics of Nuclear Interactions at High Energies

The characteristics of the interactions of cosmic ray protons with air

nuclei over a range from machine energies to 10^5 GeV have been investigated using nuclear emulsion stacks exposed near the top of the atmosphere and by ionisation calorimeters and emulsion stacks at mountain altitudes. Indirect information is also obtained from measurements of the intensities of secondary particles throughout the atmosphere. The main conclusions may be summarized as follows. The total cross-section for proton-proton collisions remains constant at about 40 mb over the whole energy range and the parameters of the interactions depend only weakly on the primary energy E_o. On the average in each interaction the primary particle loses just under half of its energy in the generation of secondary particles. The secondary particles are mainly pions, about one third of the primary energy going into pions. The mean transverse momentum of the pions, a Lorentz invariant quantity, is independent of E_o and has a value of $\sim$400 MeV/c. In cases where the non-pion secondaries are identified the lack of dependence on E_o of the mean transverse momentum has been confirmed, its value appearing to be proportional to the mass of the secondary particles. The total multiplicity of secondaries increases slowly with E_o. A dependence on energy of the form $n_s = 2.7\ E_o^{0.25}$ (where E_o is in GeV) fits the data well although a logarithmic dependence or one of the form $a + b\ E_o^{0.5}$ is not ruled out. The angular distribution of the secondaries suggests that the majority are produced isotropically from two centres or 'fireballs' moving in opposite directions in the c.m.s., although interactions are observed where the angular distribution of the secondaries does not fit this model.

Important parameters of the interactions are the proportion of non-pion secondaries produced in each interaction and the composition of these particles. Any model of the interaction, to be acceptable, must predict

the correct values for these parameters. Neutral pions produced in high energy nuclear interactions may be identified by the photons produced in their decay. Assuming charge symmetry in the production of pions it is concluded that, over the energy range in question, about 25% of all the charged and neutral particles produced in the interactions are not pions. The identification of the secondary particles and the measurement of their energy is very difficult. In nuclear emulsions measurements of the grain density versus scattering allow particles to be identified only up to 10 GeV, which restricts one to those travelling in the extreme backward direction in the c.m.s. The majority of the non-pions among these low energy particles are found to be kaons, in agreement with machine results. It has been suggested by Peters (1965) that a considerable fraction of the non-pions produced in the interactions could be nucleon-antinucleon pairs but there is no direct evidence for this yet.

It is possible, however, to obtain values of the ratio of kaon to pion production in these high energy interactions by more indirect methods involving the examination of the muons produced in their decay. It is to this problem that the first part of the present work is devoted. Before discussing this it is useful to summarize the data obtained from machine experiments.

1.2 Machine Data on Kaon Production

The production of kaons in proton-light nucleus collisions at angles from 5° to 20° has been studied by Baker et al. (1961) for proton energies from 10 to 30 GeV. It is found that the ratios of numbers of K^+ to π^+ varies between 15% and 30%. It increases with angle to the proton beam and also slowly with proton energy. The ratio of numbers of K^- to π^+ is smaller,

being typically 6%. The average value of the charge ratio K^+/K^- is about 4.0.

At 14 GeV, proton-nucleon interactions in emulsions have been examined by Csejthey-Barth (1964). Using this technique, the production of particles at all angles in an interaction can be studied. It is found that the ratio of the numbers of kaons to pions of both signs is a function of their energy, increasing from $11\pm2\%$ for particles of energy less than 0.9 GeV to $25\pm8\%$ for those with energies between 6 and 10 GeV. It appears that the mean c.m.s. momenta of kaons and pions are different, that of the former being 0.56 ± 0.03 GeV/c while the latter is 0.79 ± 0.14 GeV/c.

The most detailed study of kaon production has been made by Dekkers et al. (1965). Particle production by 18.8 and 23.1 GeV protons on protons was studied at 0° and 5.7°. At these small angles the angular distribution and energy spectra of K^+ and π^+ are similar, the ratio of their numbers being independent of secondary energy and equal to 10%. The observed production of π^+ in the extreme forward direction is explained by the authors in terms of isobar decay and the similarity between the K^+ and the π^+ spectra is interpreted as due to the production of kaons via the isobar decay $N^* \rightarrow K^+ + Y$. The spectra of K^- and π^- are different. As the secondary energy increases from 2 to 12 GeV the ratio of numbers of K^- to π^- decreases from 10% to 2% while the ratio of π^+ to π^- increases from unity to 3. Peters (1965) suggests that the spectrum of K^- is explained by the fact that at these energies one is still at the threshold for the production of $\bar{K}$, the K^- being produced via heavy isobars $N^* \rightarrow \bar{K} + K + N + n\pi$. The ratio of numbers of kaons to pions of all charges produced in the forward direction rises from 7% to 11% with increasing secondary energy.

1.3 The Kaon to Pion Ratio from Investigations of the Muon Flux

All muons produced in the atmosphere must come directly either from charged pion decay or from the decays of kaons in the $K^{\pm}_{\mu_2}$, $K^{\pm}_{\mu_3}$ or $K^{o}_{\mu_3}$ modes. Associated with the muons produced directly in kaon decay there will be a calculable number of muons coming from the pions produced by the other decay modes of the kaons. Throughout the present work it is assumed that the production of charged and neutral kaons in nuclear interactions is identical. This charge symmetry has been verified at machine energies by Shafer et al. (1963). From studies of the muon flux it is possible, in principle, to calculate the ratio of intensities at production of charged and neutral kaons to charged and neutral pions, R. The value of R may be a function of meson energy. The intensity at production is defined at the depth-rate of production of mesons, having a given energy at production, integrated over all heights in the atmosphere. It must be stressed that the value of R is not necessarily the same as the ratio of the numbers of kaons to pions produced in individual interactions. The two quantities are identical only if the mean energies of the kaons and pions produced in an interaction are the same.

For meson energies between ~70 GeV and a few thousand GeV the variation of muon intensity at sea level with zenith angle depends on the proportion of kaons among the parent mesons. This manifests itself as a maximum difference of ~30% at 1000 GeV between the predicted intensities of muons between zenith angles of 80° and 90° for the extreme cases of all muons coming from pions and all muons coming from kaons, the production spectra of the kaons or pions having been made to agree with the observed vertical intensities of muons. Measurements of the muon intensities by means of the

Durham horizontal and vertical muon spectrographs give values of the actual angular variation of intensity.

If the value of R is to be determined with reasonable accuracy from these results the calculation of the expected muon intensities at large zenith angles, as a function of R, must be performed to an accuracy of about 1%. This is done in Chapters 2 and 3. Detailed results are given, which are relevant to the derivation of the charge ratio of parent mesons from the observed muon charge ratio as well as to the present problem. First a review of previous calculations is made and the approximations involved in each are pointed out. There follows the derivation of the vertical muon spectrum at sea level upon which all subsequent calculations are based. From this, meson production spectra are derived, first for the case of pion parents only and then for admixtures of kaons in the meson flux. In Chapter 3, using these production spectra, the respective muon spectra at zenith angles above 75° are calculated. The evaluation of a correction to the intensities to take account of muon scattering in the atmosphere is described. In Chapter 4 the experimental results from the Mark I Durham horizontal spectrograph are given and an attempt is made to derive the value of R from a comparison between the predicted and measured spectra.

Two other methods of determining the K/π ratio are then considered, at low energies from measurements of the muon polarization and at higher energies from a comparison between the intensities of electromagnetic cascades in the atmosphere and muon intensities at sea level. The results from the three methods are then combined to give an estimate of the ratio of kaon and pion production spectra over a region of meson energies from 3 to 5000 GeV. In the final Chapter these results are compared with values of the proportion of non-pions produced in individual nuclear interactions that are

obtained from more direct measurements.

1.4 Weak Interactions at High Energies.

Following Pauli's postulation of the existence of the neutrino the theory of weak interactions was initiated by Fermi in explaining the beta decay of atomic nuclei. After the discovery of parity vidation the present V-A form of the weak interaction theory was developed by Feynman and Gell-Mann. The theory successfully describes, for example, beta decay and muon decay and absorption, but these cover only a limited energy region, the momentum transfers involved in beta decay and muon decay being only of the order of 1 MeV/c and 100 MeV/c respectively. The description given at low energies becomes not logically possible as the energy is increased. The cross-section for $e^- + \bar{\nu}_e \rightarrow \mu^- + \bar{\nu}_\mu$, for instance, increases proportionately with the square of the c.m.s. energy and above $\sim$ 300 GeV would exceed $\pi\lambda\!\!\!^{-2}$. Thus there must be deviations from the present theory before c.m.s. energies of this magnitude are reached. At c.m.s. energies $\sim$ 30 GeV Lee has remarked that weak and electromagnetic interactions would be of the same strength and this fact would suggest that the four-fermion interaction theory breaks down at energies lower than this. Thus, in order to learn more about weak interaction theory and perhaps, eventually, to derive a unified theory of strong, electromagnetic and weak interactions, it is vital that weak interactions should be studied to higher energies. Unfortunately because of the small mass of the electron, a neutrino laboratory energy of 10^5 GeV would be required in an interaction with an electron at rest in order to obtain a c.m.s. energy of only 5 GeV. This type of investigation is therefore not likely to be pursued in the foreseeable future. Possible experiments with colliding beams of electrons are also some years distant. Recent investigations have therefore been concentrated on neutrino-nucleon

interactions. Here the effects of strong interactions are expected to modify the interactions. A consequence of the Conserved Vector Current hypothesis is that the vector weak structure of the nucleon is identical to the electromagnetic structure. The latter is expressed by the Hofstadter form factor obtained from electron-nucleon scattering experiments. The result of this is that the momentum transfer in neutrino-nucleon elastic collisions, $\nu + N \rightarrow N + \ell$, is expected to be limited to about 1 GeV/c and any effects due to the breakdown of the weak interaction theory at higher energies will not be apparent. For inelastic collisions, where one or more additional hadrons are produced, the effect of the strong interactions on the form of the cross-section is in general different for each specific end product. The determination of the form of the variation with energy of the total inelastic cross-section and in particular the identification of a cut off energy at which the cross-section saturates might throw some light on the behaviour of the weak interactions at high energies.

An hypothesis that would explain the vector form of the four-fermion weak interaction and avoid some of the difficulties encountered at high energies is that the weak interactions are mediated by the exchange of an Intermediate Boson, W. Beta decay, for example, would then be a two step process, $n \rightarrow p^+ + W^- \rightarrow p^+ + e^- + \bar{\nu}_e$. The direct four-fermion interaction would still give an effective description of low energy processes such as weak decays. At high energies the increase in cross-section of the lepton-lepton interactions would be cut off at c.m.s. energies of the same order as the boson mass. The intermediate boson hypothesis of weak interactions was first suggested by Yukawa: in its present form it was presented by Lee and Yang (1960). Some of the basic properties of the hypothetical boson

are as follows. It must exist in both negative and positive charge forms in order to mediate the observed weak interactions. If the W^0 exists it must not mediate strangeness changing interactions since otherwise it would give rise to such unobserved kaon decays as $K \rightarrow \pi + \mu^+ + \mu^-$. The boson must be massive since the weak interactions are of short range, and its mass, m_W, must be greater than the mass of the kaon. Were this not so, the unobserved fast decay $K \rightarrow W + \gamma$ would be possible. The boson would also have spin 1 and magnetic moment $\frac{e}{2m_W}(1 + k)$, the anomalous magnetic moment, k, being unknown.

The simplest process by which a real Intermediate Boson might be produced and identified is in its semi-weak production by a neutrino in the Coulomb field of a nucleus, $\nu + Z \rightarrow Z + \ell + W$. The cross-section for $W^{\pm}$ production as a function of neutrino energy has been evaluated theoretically in terms of its mass (a summary of the results is given in Chapter 5). If a search for boson production in neutrino-nucleus interactions leads to a negative result a lower limit may be set to the mass, m_W.

1.5 Machine Results on Neutrino Interactions

The first investigation of neutrino-nucleus interactions using neutrinos from a proton synchrotron was made by Danby et al. (1962) at Brookhaven. This involved the study of interactions in a multi-plate aluminium spark chamber. Subsequently, rather more sophisticated experiments have been performed at CERN using aluminium and magnetised iron spark chambers (Bienlein et al. (1964)) and a heavy liquid bubble chamber (Block et al. (1964)). In each of these experiments, the calculated energy spectrum of neutrinos was peaked at a value below 1 GeV and extended effectively up to about 10 GeV. From these investigations the following conclusions were

drawn. Neutrinos from pion to muon decay (ν_μ) are different from beta decay neutrinos (ν_e): this has been tested to an accuracy of 1%. The conservation of lepton number has been confirmed with 94% certainty by searching for positive muons produced by ν_μ. The 'neutrino flip' hypothesis, whereby the neutrino associated with the electron in pion decay corresponds to the neutrino associated with the muon in $K_{\mu 2}$ decay, has been shown to be false with 90% certainty. The ratio of elastic events with no change in the charge of the lepton, viz. $\bar{\nu}_\mu + p \rightarrow \bar{\nu}_\mu + p$, to those with charge exchange, $\bar{\nu}_\mu + p \rightarrow \mu^+ + n$, is less than 3%: on the Intermediate Boson hypothesis this constitutes evidence against a W^o mediating interactions in which strangeness is conserved in addition to that already stated for strangeness changing interactions. The cross-sections of elastic and inelastic interactions were also studied and a search made for $W^\pm$ production. Further details of these cross-sections and a lower limit to m_W, obtained from the machine experiments, are given in Chapter 5.

1.6 Cosmic Ray Studies of Neutrino Interactions

Pursuing the general theme of the study of the interactions of elementary particles at energies above those available from machines we now turn to a description of preliminary experiments on the interactions of cosmic ray neutrinos. A clear distinction must be drawn between these experiments and those of the type recently initiated by Davis (1964) whereby low energy electron-neutrinos ($E \lesssim 15$ MeV) will be recorded by their inducing inverse beta decay in a large volume of detector. In these experiments the details of the neutrino interactions are assumed to be known and the quantity being measured is the flux of low energy electron-neutrinos at the Earth, the majority of which are assumed to come from the sun.

Neutrinos with energies greater than about 1 GeV at the Earth's surface are expected to come almost entirely from the decays of pions, kaons and muons in the atmosphere. Calculations of the flux of neutrinos are given in Chapter 6, using as a starting point the vertical muon sea level spectrum, and it is shown how the flux depends on the kaon to pion ratio, **R**. The result of the present analysis of the experimental data on R is used in order to set narrow limits to the values of neutrino intensities, energy spectra and angular distributions at sea level.

A simple calculation shows that for an interaction which has cross-section S cm^2 $nucleon^{-1}$ an Earth diameter represents approximately $4\ 10^{33}$S interaction lengths. All non-resonant neutrino-nucleon interactions that have so far been envisaged have cross-sections $\ll 10^{-33}$ cm^2 $nucleon^{-1}$ and thus the Earth is, for non-resonant interactions, effectively transparent to neutrinos. Thus values of neutrino intensities and angular distributions calculated at the Earth's surface are valid for underground locations, and in particular the flux of neutrinos travelling upwards from the lower hemisphere is identical to that travelling downwards. It is therefore apparent that as one goes deeper underground and the background intensity of atmospheric muons decreases, eventually it will become less than the intensity of particles produced by local neutrino interactions.

Since the cross-sections for neutrino interactions are so small, it might at first seem that a prohibitively large detector would be necessary to register them. Markov and Zheleznykh (1961) pointed out, however, that for neutrino interactions in which a muon is produced there will be an effective target thickness of rock surrounding the detector that is equal to the range of the muon in rock. In addition, the muon range, and thus the

dimensions of the target, is approximately proportional to the muon energy. This to some extent compensates, in interactions in which the energy retained by the muon is an approximately constant fraction of the initial neutrino energy, for the rapidly falling neutrino energy spectrum. It was concluded that with a detector of moderate size it should be possible to measure a significant rate of muons from neutrino interactions although the interactions themselves would not be seen.

The observation by Menon et al. (1963) of zero counts in 30 days using two vertical muon telescopes each of area 1.5 m^2 at a depth of 9200 ft at the Kolar Gold Field (KGF) demonstrated that depths sufficient to reduce the background flux of atmospheric muons to at least the same order as the flux of neutrino-induced muons are in fact attainable in practice. Following on this discovery, two experiments to observe cosmic ray neutrino interactions in deep gold mines were proposed, one, a collaboration between the Tata Institute, Bombay, the Osaka City University, Japan and Durham University, to be set up at KGF (Menon (1963)), the other, a collaboration between the Case Institute, Ohio and Witwatersrand University, at the East Rand Proprietary Mines, South Africa (Reines et al. (1963)). Both experiments are similar in basic conception, using detectors orientated to register muons incident predominantly in the horizontal direction where a slight peaking in the neutrino flux is expected and the atmospheric muon intensity, by virtue of its sharp peaking in the vertical direction, is negligible. The preliminary results of the former, the 'KGF Neutrino Experiment', are reported in Chapter 7 and are compared with results from the latter, the 'Case-Wits Experiment'. Tentative conclusions are drawn and the possibility of observing interactions that can be attributed to Intermediate Boson production is discussed.

It should, perhaps, be stressed at this stage that as well as the Lee and Yang intermediate boson that we discuss in the present work there have been a number of other theories of weak interactions proposed involving other intermediate bosons, each with different properties. For example, the theory of Tanikawa and Watanabe (1959) postulates the existence of an intermediate boson B possessing both baryon and lepton number. The neutrino-nucleon interaction would then proceed via $\nu_\ell + n \rightarrow B^0_\ell \rightarrow \ell^- + p^+$. It is apparent that at an energy $E_o = (m_B^2 - m_p^2)/2m_p$ there would be a resonance due to the production of a real boson and that this would result in a considerable flux of muons from neutrino interactions. From the zero count result of Menon (1963) a lower limit to the mass of this boson has already been set by Bahcall and Frautschi (1964) as 60 GeV.

Chapter 2

The Vertical Muon Spectrum at Sea Level

2.1 Introduction

In studying the spectra and properties of cosmic ray muons at sea level, in order to gain insight into the nuclear interactions of cosmic rays in the atmosphere, the vertical muon energy spectrum will be taken as the starting point; (N.B. for muons of energy above 1 GeV the energy and momentum are numerically identical and units of energy or momentum may be used interchangeably). From it the spectrum at large zenith angles is derived for comparison with the measured values and the polarisation of muons at sea level is predicted. The calculated spectrum of muons, obtained from measurements of γ-e cascades in the atmosphere, is compared with the vertical muon spectrum and, finally, it can be used to predict the energy spectrum of those neutrinos at sea level that are produced in the atmosphere. In section 2.2 methods that can be used to investigate the vertical muon energy spectrum at sea level are discussed and the spectrum that is used in all subsequent calculations is given.

From the vertical muon spectrum one may calculate the production spectrum of parent particles; the spectrum that is arrived at depends on the assumptions made concerning the relative contributions of kaon and pion decay to the muon flux. A number of calculations of this have been made previously under various simplifying assumptions. It is shown in Chapter 3 that the predicted muon spectrum at large zenith angles for energies up to 1000 GeV is not very sensitive to the assumed ratio of kaon to pion parents, when averaged over zenith angles from 80° to 90° the differences amounting only to 10%. It is therefore necessary to aim for an accuracy $\sim$ 1% in the calculation of the

predicted spectra.

Barrett et al. (1952) were the first to give the diffusion equation of pions in the atmosphere and the effects on the muon spectra of the change with energy of relative probability of decay and absorption of the pions. Their paper is concerned with the measurement of muon intensities far underground and they were interested only, therefore, in muons of sufficiently high energies that to a first approximation their energy loss in the atmosphere could be neglected and a simple expression for the probability of muon decay could be used. The effects of muons produced by kaon decay were discussed qualitatively but their quantitative results were uncertain because the mass, lifetime and branching ratios of the kaons were not accurately known at that time.

Smith and Duller (1959) investigated the expected zenith angular distribution of muons, following a similar procedure to that of Barrett et al. In the same way as the latter authors they used a unique relation between the muon and parent pion energies (whereas, in fact, there is a spread in the values of the fractional energy in the laboratory system taken by the muon in pion decay), and took a "flat earth" approximation. The latter approximation, which takes the thickness of the earth's atmosphere at a zenith angle θ at sea level to be proportional to sec θ, is valid only for $\theta \lesssim 65^{\circ}$. They took into account, however, energy loss of the muons in the atmosphere and gave muon spectra at various angles for muon energies from 40 to 160 GeV. No consideration was given to the production of muons by kaons.

Zatsepin and Kuz'min (1961), took the earth's curvature and the energy spread of muons from their parent mesons into account and produced muon spectra

for all zenith angles and for energies from 100 to 10^5 GeV. In treating the energy loss and decay of the muons it was assumed, as an approximation, that the muons traverse a large portion of their geometric path in an atmosphere of low density where the energy loss may be neglected and the probability of decay calculated, and that the only important energy loss occurs in the last fraction of the path which is so short that decay is not important. This simplification introduces negligible error for muon sea level energies above 100 GeV but cannot be used for lower energies. Results were presented for both pions and kaons as the parent mesons. In the latter case the dominant $K_{\mu 2}$ mode was the only one considered. This has the advantage that the calculations are the same as for the pion decay with only a change in values of mass and lifetime necessary. The authors acknowledge that the effect of ignoring other kaon decay modes is the most important source of error in their treatment.

Allen and Apostolakis (1961) have calculated the expected muon spectra from pion and $K_{\mu 2}$ decay for energies from 1 to 1000 GeV and for all zenith angles. In the pion case, energy spread of muons from the decay is neglected, which introduces an error of about 1%. For the $K_{\mu 2}$ case, in which the muons have a larger energy spread, this approximation is not made but to keep the calculation simple it was assumed that the muons are initiated at a single level of production; this involves an error of about 4%. At large zenith angles, for energies below about 30 GeV, geomagnetic deflexion and multiple scattering have important effects on the muon spectrum. Calculations of these two phenomena were made by these authors.

Maeda (1960, 1964) has made the most comprehensive examination of the muon

propagation problem. Starting with an accurate integral expression for the pion intensity it is shown how it reduces under given approximations to solutions of the diffusion equations used by previous authors. In the first paper spectra are given for energies from 1 to 40 GeV for pion parents only, and a detailed discussion of the effect of geomagnetic deflexion is given; (the scattering correction was also calculated but this was later seen to be wrong). In the second paper spectra were given up to 10^4 GeV for both pion and kaon parents but, as in previous work, only the $K_{\mu 2}$ mode was considered in the latter case.

In the present work there are two main refinements. In calculating the kaon contribution to the muon intensity all decay modes of both charged and neutral kaons with branching ratios greater than 1% are taken into account. This makes a significant difference to the calculated contribution from kaon decay. Previous workers have assumed that the production spectrum of pion or kaon parents can be expressed exactly as a power law. Here, as a first approximation, a power law spectrum is assumed but this is then relaxed to fit the measured sea level muon spectrum exactly. The relaxing factor is typically 5% in the energy region up to 1000 GeV. In addition the effect of scattering on the intensities at low energy has been re-calculated by a Monte Carlo method.

2.2 The Measured Vertical Muon Spectrum

Four methods have been used in attempting to obtain values of the vertical muon energy spectrum up to values of 10 TeV; direct measurement of momentum of muons using vertically orientated muon spectrographs; measurements of the variation of total muon intensity with depth underground; measurements of the spectrum of bursts of ionisation produced by muons in shielded ionisation

chambers and scintillators; and, indirectly, by measuring the γ-cascade spectra at various heights in the atmosphere and relating these to the muon spectrum at sea level. The last two methods are not used in the present analysis for the following reasons. To obtain an estimate of the muon spectrum from γ-cascade measurements it is necessary to know the relative numbers of kaons and pions produced in high energy nuclear interactions in the atmosphere. Hayman et al. (1963), for example, took the proportion of kaons produced to be negligible and then, from the γ-cascade measurements of Duthie et al. (1962) gave the muon spectrum from 700 to 7000 GeV. In the present work, however, the procedure is reversed, i.e., we intend, having deduced the muon sea level spectrum from other types of measurements, to calculate possible values of the K/π ratio that give agreement between it and the γ-cascade results (Chapter 4).

Burst spectrum measurements have been made by Higashi et al. (1964) and Krasilnikov (1964). The bursts are electromagnetic cascades produced by the bremsstrahlung, knock-on, pair-production and nuclear interactions of muons; of these processes the first is the most important. Because of uncertainty in the effective aperture of the apparatus used in the first experiment, the absolute intensity of muons is not known and only the slope of the spectrum can be given. In the second experiment, although a spectrum is quoted in which absolute intensities are given, uncertainty in the contribution to the bursts from residual nuclear active particles at sea level and the effects of fluctuations that are not allowed for make the intensities somewhat suspect. An important argument against using the burst spectra in the present analysis is that the quantity that is measured is not, in fact, the vertical intensity but the omnidirectional flux over a solid angle of almost 2π steradians. To

convert the latter to the vertical intensity the angular distribution of the muons must be assumed. This depends, however, at large zenith angles, on the K/π ratio and the experimental results are weighted towards large zenith angles; in the Higashi et al. experiment 75% of the bursts are produced by muons with zenith angles greater than 70°. When the muon spectra obtained from these burst experiments are compared with those obtained from depth-intensity measurements, it seems that the slopes of the former are somewhat smaller but, bearing in mind the objections stated above and taking the statistical accuracy into account, one can only say that the muon spectra from bursts are not inconsistent with those from other methods.

The results of the two other types of experiments have been used by Osborne et al. (1964) in deriving a best estimate of the vertical muon energy spectrum up to 7000 GeV. This is the spectrum used in the present work (referred to as the OPW spectrum); a short discussion of the details of the derivation is given here and it is compared with two other recent estimates of the muon spectrum. For muons of momenta from 0.4 GeV/c up to about 1000 GeV/c the spectrum has been measured directly using magnetic spectrographs. The maximum detectable momentum (m.d.m.) of a spectrograph, which depends on the line integral of the magnetic field strength and the accuracy of location of the muon track, is defined as the momentum at which the probable error in a deflexion measurement is equal to the magnetic deflexion of a particle. The vertical spectrograph with the highest m.d.m. reported to date (600 GeV/c) is that described by Hayman and Wolfendale (1962). This employs an air gap magnet and four trays of neon flash tubes to define the muon trajectory. These authors give a momentum spectrum up to 1000 GeV/c. The aperture of a spectrograph of this type is necessarily

small, (8 cm^2 steradian) and the rate of muons above 500 GeV/c is less than 1 in 5 days; thus the statistical accuracy is not good above this momentum. The Hayman and Wolfendale (HW) spectrum has to be corrected for selection bias in that 10% of the muons incident on the spectrograph were rejected, either because of accompaniment by a second muon or soft component that penetrated the 5.5 g cm^{-2} of lead shielding above the instrument, or because of knock-on electrons produced in the aparatus. The measured spectrum was normalised at 1 GeV/c to the intensity given by Rossi (1948) but the probability of a muon being rejected for one of the three reasons given above increases slowly with energy. The result (Gijsbers, private communication) is that the HW spectrum has to be increased by amounts ranging from 5% at 10 GeV/c to 20% above 200 GeV/c.

If the total intensity of muons is measured at a series of depths underground and the relation between the range and energy of muons is known, then the integral energy spectrum at the earth's surface may be simply calculated. Many measurements of the cosmic ray intensity deep underground have been made (Menon and Ramana Murthy (1965) give a review), the deepest being those of Miyake et al. (1964) who report results down to a depth of 8400 hg cm^{-2} of rock at the Kolar Gold Field (KGF). There is some difficulty in the derivation of a unique depth-intensity relation because of the rather large spread of intensities, obtained at comparable depths by different workers, which point to the possibility of some systematic errors. Differences in the best estimate of the depth-intensity relationship will therefore arise from different weightings of individual experimental results. A source of discrepancy between the various final values arrived at for the sea level muon spectrum at high energies is the uncertainty in the rate of energy loss of muons in rock. This

rate may be expressed as

$$-\frac{dE}{dx} = a + c \ln E_m + b E \quad \text{GeV g}^{-1} \text{ cm}^2 \qquad (2.1)$$

The first two terms represent energy losses due to ionisation and excitation E_m being the maximum transferable energy from a muon to an electron. The third term gives the losses due to bremsstrahlung, pair-production, and nuclear interaction and the constant may be written as the sum of these three terms, $b = b_b + b_p + b_{nuc}$, respectively. The values deduced by Hayman et al. (1963) and given in equation (A16) are, $a = 2.05\ 10^{-3}$, $c = 7.66\ 10^{-5}$, and $b = 4.0\ 10^{-6}$. There is general agreement concerning the values of a and c, but b is rather uncertain. For example for the nuclear interaction term Hayman et al. take $b_{nuc} = 0.7\ 10^{-6}$ while Menon and Ramana Murthy (1965) use $b_{nuc} = 0.28\ 10^{-6}$. Erlykin (1965) suggests, from a theoretical analysis, that the value of b_p that has been used previously is approximately 30% too low. The above values refer to 'standard' rock with $\frac{Z^2}{A} = 5.5$; for KGF rock $\frac{Z^2}{A} = 6.3$ and the value corresponding to $b = 4.0\ 10^{-6}$ for 'standard' rock is $4.4\ 10^{-6}$. Expression (2.1) gives the mean rate of energy loss of muons. By integrating, one obtains the 'average' range-energy relation. This, for KGF rock, is plotted in Fig. 2.1 (the values are taken from Ramana Murthy (1962)) and is used in Chapter 7 in calculating rates of neutrino interactions.

In deriving the 'average' range-energy relation it is assumed that the energy losses are continuous. This is true, to a good approximation, for ionisation and pair-production losses, but for bremsstrahlung and nuclear interaction processes, where the probability of a muon losing a fraction v of its energy in an interaction is proportional to $1/v$, the muon may lose a large fraction of its energy in a single interaction. Therefore, for high energies, where the energy proportional term in the energy loss equation becomes

Fig. 2.1 The Range of Muons in KGF Rock ($b = 4.4\ 10^{-6}\ g^{-1}\ cm^2$)

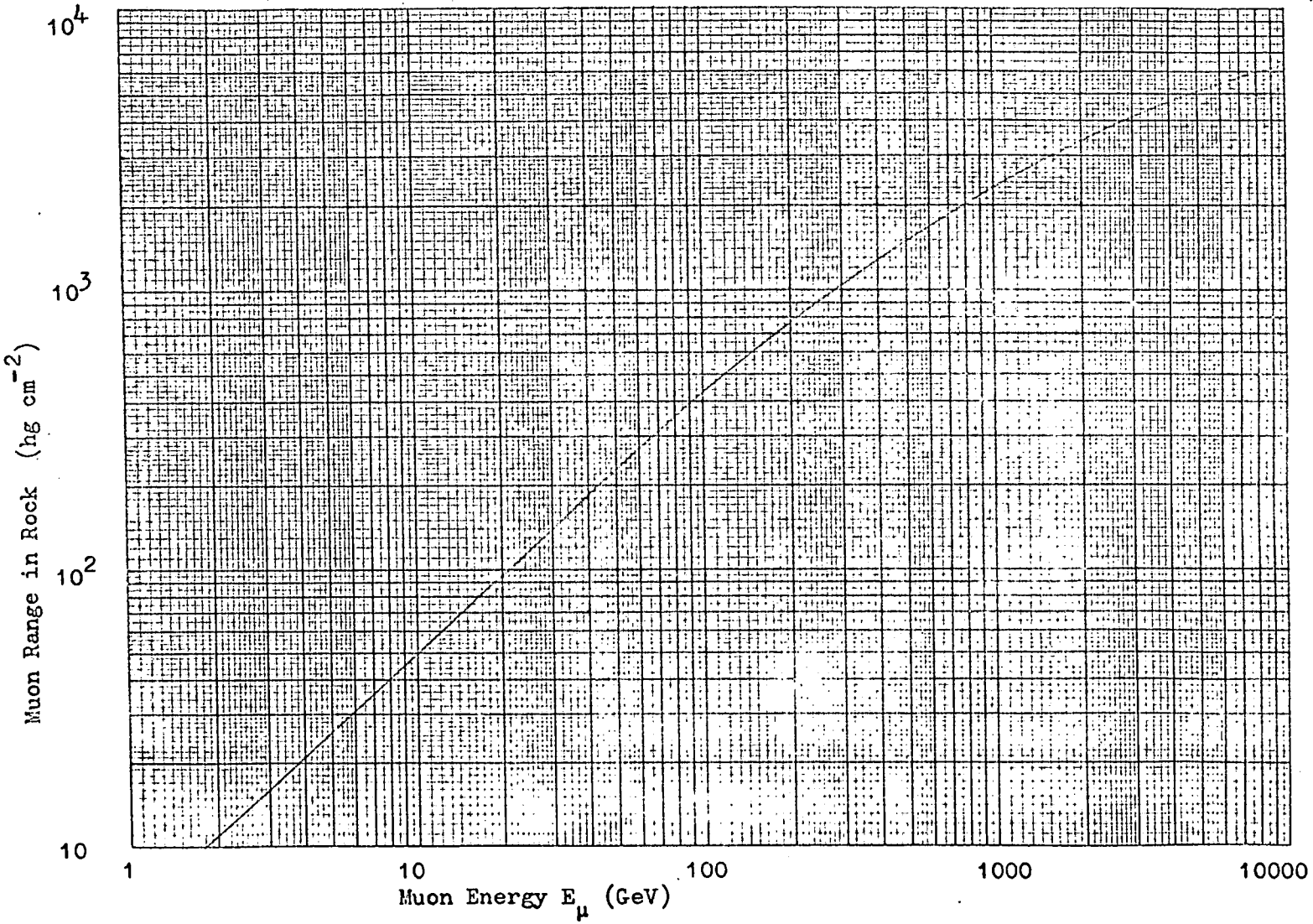

important, the effect of range straggling of muons of a given energy at the surface must be taken into account. This is done by calculating a correction factor $R(d) = I_m(d)/I_f(d)$ where $I_m(d)$ is the intensity at a depth d, calculated from an assumed muon sea level spectrum using the average range-energy relation and $I_f(d)$ is the intensity at the same depth when fluctuations are allowed for. R is found to be a function of γ, the exponent of the differential muon spectrum, b, and $\frac{b_f}{b_n} = \frac{b_b + b_{nuc}}{b_p}$, the ratio of the fluctuating to non-fluctuating parts of b. R has been calculated by various authors; the results of a Monte-Carlo calculation of Hayman et al. (1963) and the analytical calculations of Nishimura (1965) and Zatsepin and Mikhalchi (1961, 1965) are in good agreement for corresponding values of the parameters. From their own best estimate of the depth-intensity relation and using $b = 4.0\ 10^{-6}$ and $b_f/b_n = 1.5$, Osborne et al. (1964) have derived the muon sea level spectrum. The final OPW vertical muon sea level spectrum is then that which follows the latter spectrum above 200 GeV and the corrected HW spectrum at lower energies. This integral spectrum together with the estimated errors is given in table 2.1 and plotted in Fig. 2.2. Also shown for comparison is the HPW spectrum which followed the uncorrected HW spectrum below 100 GeV and at higher energies the spectrum of Duthie et al. (1962) from γ-cascade measurements at 220 g cm^{-2} when only pion production was considered. (It may be noted that the slope of this spectrum has been found to be somewhat steeper than would be expected from γ-cascade measurements at other depths). Hayakawa et al. (1965) have derived a composite spectrum (HNY) from the (uncorrected) HW spectrum below 100 GeV and depth-intensity experiments at high energies, taking, for rock, $b = 3.9\ 10^{-6}$ and $b_f/b_n = 1.25$. They find that the depth-intensity measurements under water of Higashi et al. (1965)

Table 2.1

The Integral Spectrum of Muons at Sea Level in the Vertical Direction ('OPW' Spectrum)

Energy (GeV)	Intensity ($cm^{-2} sec^{-1} sterad^{-1}$)	Estimated Error (%)
20	$2.62\ 10^{-4}$	4
30	$1.29\ 10^{-4}$	5
50	$4.81\ 10^{-5}$	6
70	$2.42\ 10^{-5}$	7
100	$1.19\ 10^{-5}$	9
150	$4.95\ 10^{-6}$	10
200	$2.64\ 10^{-6}$	11
300	$1.02\ 10^{-6}$	12
500	$2.86\ 10^{-7}$	14
700	$1.14\ 10^{-7}$	15
1000	$4.56\ 10^{-8}$	16
1500	$1.58\ 10^{-8}$	17
2000	$7.28\ 10^{-9}$	18
3000	$2.44\ 10^{-9}$	22
5000	$4.80\ 10^{-10}$	27
7000	$1.49\ 10^{-10}$	31

Fig. 2.2 Vertical integral muon sea level spectra

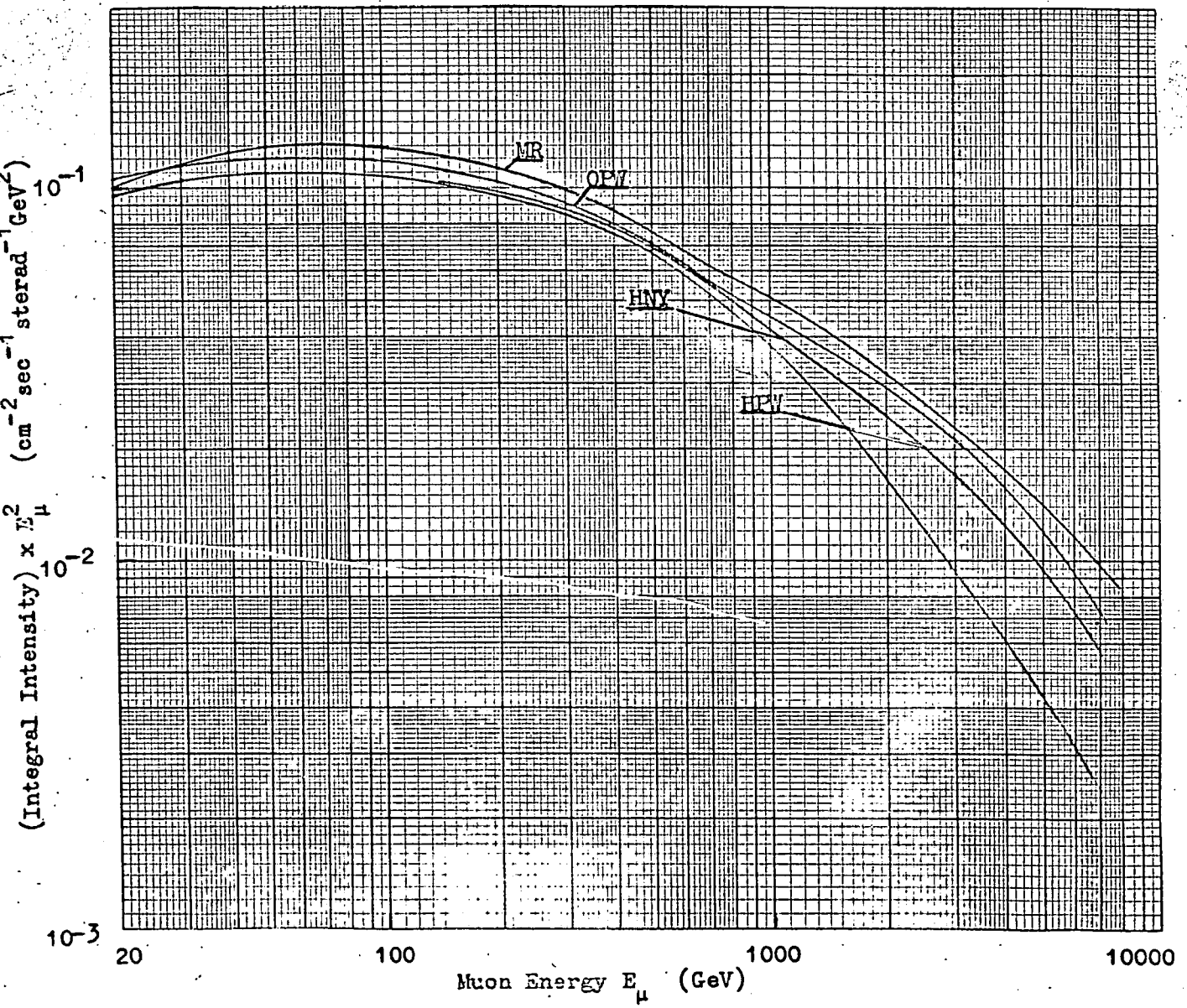

are in agreement with the HW spectrum, and, arguing that there is uncertainty in all depths measured under rock, normalise the under-rock results to those under-water by decreasing each depth by 10%. This has the effect, at the high energy end, of reducing the muon energy spectrum by $\sim$ 30%. Finally there is the composite spectrum of Menon and Ramana Murthy (1965) (MR). At high energies the conversion of the depth-intensity to sea level muon spectrum using $b = 3.6\ 10^{-6}$ and $b_f/b_n = 1.25$ and the inclusion of γ-cascade and burst measurements result in a somewhat higher muon spectrum. Below 100 GeV depth-intensity results under rock give a higher muon intensity than direct measurements. The overall result is that the derived spectrum is higher than the OPW spectrum over the whole energy range above 30 GeV.

It can be seen from Fig. 2.2 that the OPW spectrum lies between the MR and HNY spectra and that the latter two spectra are generally within the expected errors quoted in table 2.1. The differential momentum spectrum from the OPW spectrum is given in table 2.2.

2.3 Energy Loss and Decay of Muons in the Atmosphere

In all problems involving the propagation of muons in the atmosphere the values of energy loss and survival probability (i.e. $1 - P_d$, where P_d is the probability of $\mu \rightarrow e + \nu_e + \nu_\mu$ decay) are needed. To avoid the necessity of recalculating these quantities for each separate application it was decided to prepare tables of survival probability, $SP(x,E_o,\theta)$, and energy, $E(x,E_o,\theta)$, for standard values of x, the atmospheric depth measured vertically, (i.e. the pressure in g cm^{-2}), E_o and θ. SP is the survival probability from x to sea level and E is the energy of a muon at depth x which arrives at sea level at a zenith angle θ and with energy E_o. The tables may then be read into the store of a computer and intermediate values may be

Table 2.2

Differential Momentum Spectrum of Muons at Sea Level in the Vertical Direction ('OPW' Spectrum)

Momentum (GeV/c)	Intensity ($cm^{-2} sec^{-1} sterad^{-1} GeV/c^{-1}$)	Momentum (GeV/c)	Intensity ($cm^{-2} sec^{-1} sterad^{-1} GeV/c^{-1}$)
1	$2.45\ 10^{-3}$	100	$2.50\ 10^{-7}$
1.5	$1.95\ 10^{-3}$	150	$7.26\ 10^{-8}$
2	$1.50\ 10^{-3}$	200	$2.97\ 10^{-8}$
3	$9.01\ 10^{-4}$	300	$8.18\ 10^{-9}$
5	$3.96\ 10^{-4}$	500	$1.46\ 10^{-9}$
7	$2.15\ 10^{-4}$	700	$4.31\ 10^{-10}$
10	$1.07\ 10^{-4}$	1000	$1.15\ 10^{-10}$
15	$4.36\ 10^{-5}$	1500	$2.79\ 10^{-11}$
20	$2.20\ 10^{-5}$	2000	$9.88\ 10^{-12}$
30	$7.85\ 10^{-6}$	3000	$2.30\ 10^{-12}$
50	$1.94\ 10^{-6}$	5000	$3.28\ 10^{-13}$
70	$7.23\ 10^{-7}$	7000	$7.43\ 10^{-14}$

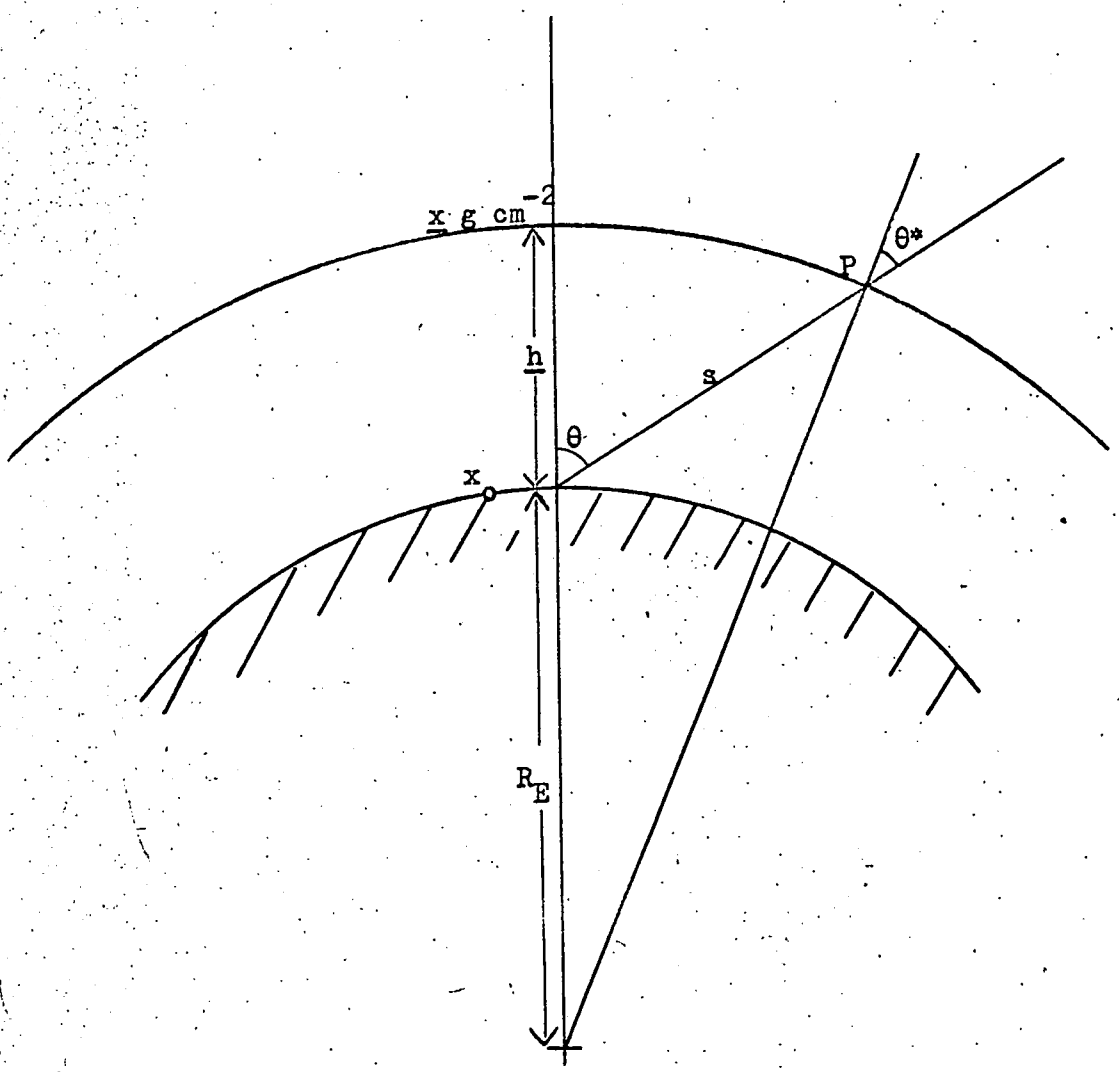

Fig. 2.3 Notation used in the calculation of muon propagation in the atmosphere

obtained by a simple 4-point interpolation procedure.

2.3.1 Properties of the Atmosphere

The following notation is used (see Fig. 2.3).

R_e is the radius of the Earth, 6370 km.

x_o is the air pressure at sea level, 1030 g cm^{-2}.

θ is the zenith angle of the muon trajectory at sea level.

x is the air pressure at P.

h is the altitude of P in km.

s is the linear distance from P to sea level along the trajectory.

θ^* is the zenith angle of the trajectory with the local vertical at P.

$\rho(x)$ is the air density at P in g cm^{-3}.

l is the depth measured in g cm^{-2} from the top of the atmosphere along the trajectory.

The relationships between ρ, x and h are given in Appendix B.

From Fig. 2.3 we have $$\sec\theta^* = \left[1 - \frac{\sin^2\theta}{(1 + h/R_e)^2}\right]^{\frac{1}{2}} \qquad (2.2)$$

and $$h = (R_e^2 + s^2 + 2R_e s\cos\theta)^{\frac{1}{2}} - R_e \simeq s\cos\theta + \frac{s^2\sin^2\theta}{2R_e} \qquad (2.3)$$

Then $$l(\theta,s) = \int_s^\infty \rho(x)\, ds \qquad (2.4)$$

Expressing $\rho(x)$ as a function of s using equations (2.3) and 6,7,10 and 11 of Appendix B the integral is evaluated numerically and leads to values of l versus pressure given in Table 2.3 and Fig. 2.4.

2.3.2 Rate of Energy Loss of Muons in Air

Expressions for the rate of energy loss of muons in air, $\frac{dE}{dl}$, are derived in Appendix A (equations A17 and 18). In the higher energy region the rate of energy loss is seen to depend on the air density (i.e. $\frac{dE}{dl}$ is a function of

Table 2.3

Atmospheric Depth measured along particle trajectory at Zenith Angle θ as a function of Vertical Depth

	Zenith Angle θ (degrees)						
x(g cm^{-2})	75	80	84	86	88	89	90
			$\ell(\theta,x)$ (g cm^{-2})				
3	10.13	14.18	18.86	21.83	21.16	24.91	25.02
5	17.30	24.01	32.23	37.46	41.86	43.27	43.62
10	35.36	48.96	66.62	78.10	88.44	91.79	92.85
25	90.11	125.4	174.1	207.3	239.5	250.4	254.0
50	182.3	255.3	360.7	436.2	513.9	541.1	550.9
75	275.0	387.0	552.9	675.8	807.3	854.7	872.3
100	368.2	519.9	749.1	923.2	1115	1187	1214
150	555.4	788.4	1150	1436	1768	1897	1946
200	743.4	1059	1560	1968	2462	2661	2740
400	1501	2161	3203	4240	5587	6209	6474
600	2264	3281	5039	6697	9253	10620	11259
800	3032	4415	6874	9315	13534	16256	17758
900	3417	4986	7810	10681	15954	19812	22315
950	3610	5273	8282	11379	17247	21888	25340
1030	3919	5733	9044	12514	19449	25882	36540

Fig. 2.4 Muon path length from the top of the atmosphere as a function of pressure, x, and zenith angle, θ

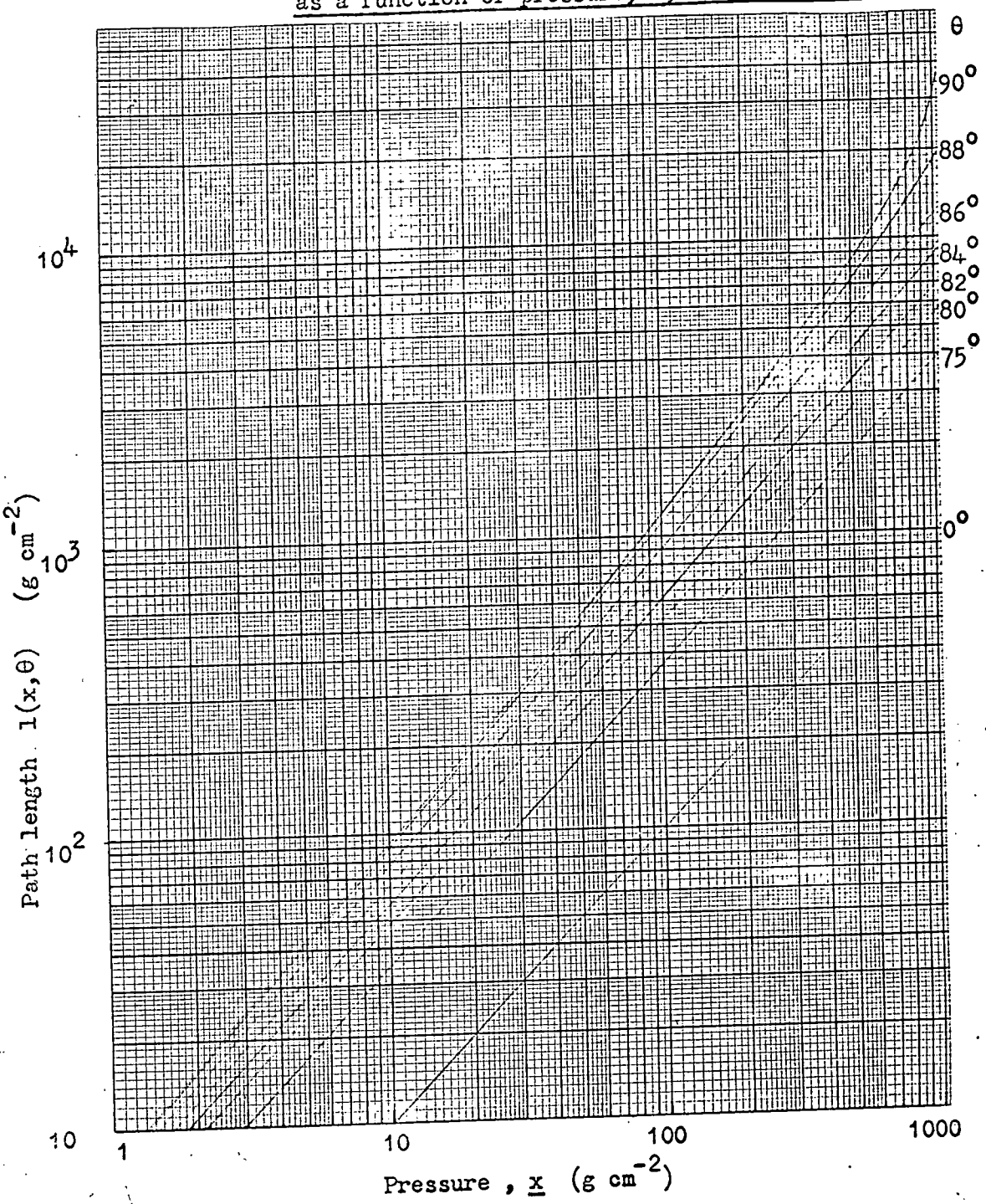

E and x). To show this dependence $\frac{dE}{dl}$ is plotted in Fig. 2.5 for two densities corresponding to sea level and x = 120 g cm^{-2} respectively. For comparison the expression used by Maeda (1964), $-\frac{dE}{dl} = 2.5\ 10^{-3}\ (1 + 10^{-3}E)$ GeV g^{-1} cm^{-2} is also shown.

2.3.3 Survival Probability Calculations

Graphs of muon survival probability from a depth x g cm^{-2} to sea level have been published by Maeda (1960). For the following reasons further calculations were necessary. The values given by Maeda are for E_o up to 43 GeV only; smaller intervals of E_o and θ are needed for accurate interpolation; the rate of energy loss had been taken to be independent of energy and equal to 2.5 10^{-3} GeV g^{-1} cm^2, which is not a very close approximation; tables of $E(x, E_o, \theta)$ are needed for the same values of x, E_o and θ as the survival probability.

The survival probability is given by the following expression;

$$SP(x,E_o,\theta) = \exp\left[-\frac{m_\mu c^2}{c\tau_\mu}\int_x^{x_o}\frac{\sec\theta^*}{E(x',E_o,\theta)}\frac{dx'}{\rho(x')}\right] \qquad (2.5)$$

where sec θ^* dx = dl, the increment in atmospheric depth along the trajectory. In the calculation the atmosphere was considered divided into 15 intervals, their bounds being given by the pressure $x_0, x_1, \ldots x_{15}$. The energy loss and survival probability from one bound to the next lower one were computed. Then the total energy loss is the sum of the losses, and the survival probability to sea level is the product of the survival probabilities in each interval below the given bound. Each interval was further subdivided so that, for example, for the lowest interval

$$SP(x,E_o,\theta) = \exp\left[-1.599\times10^{-6}\sum_{i=0}^{n-1}\int_{x_o-(i+1)\Delta}^{x_o-i\Delta}\frac{\sec\theta^* dx'}{E(x',E_o,\theta)\,\rho(x')}\right] \qquad (2.6)$$

where $\Delta = \frac{x_o - x_1}{n}$

Fig. 2.5 Rate of energy loss of muons in air

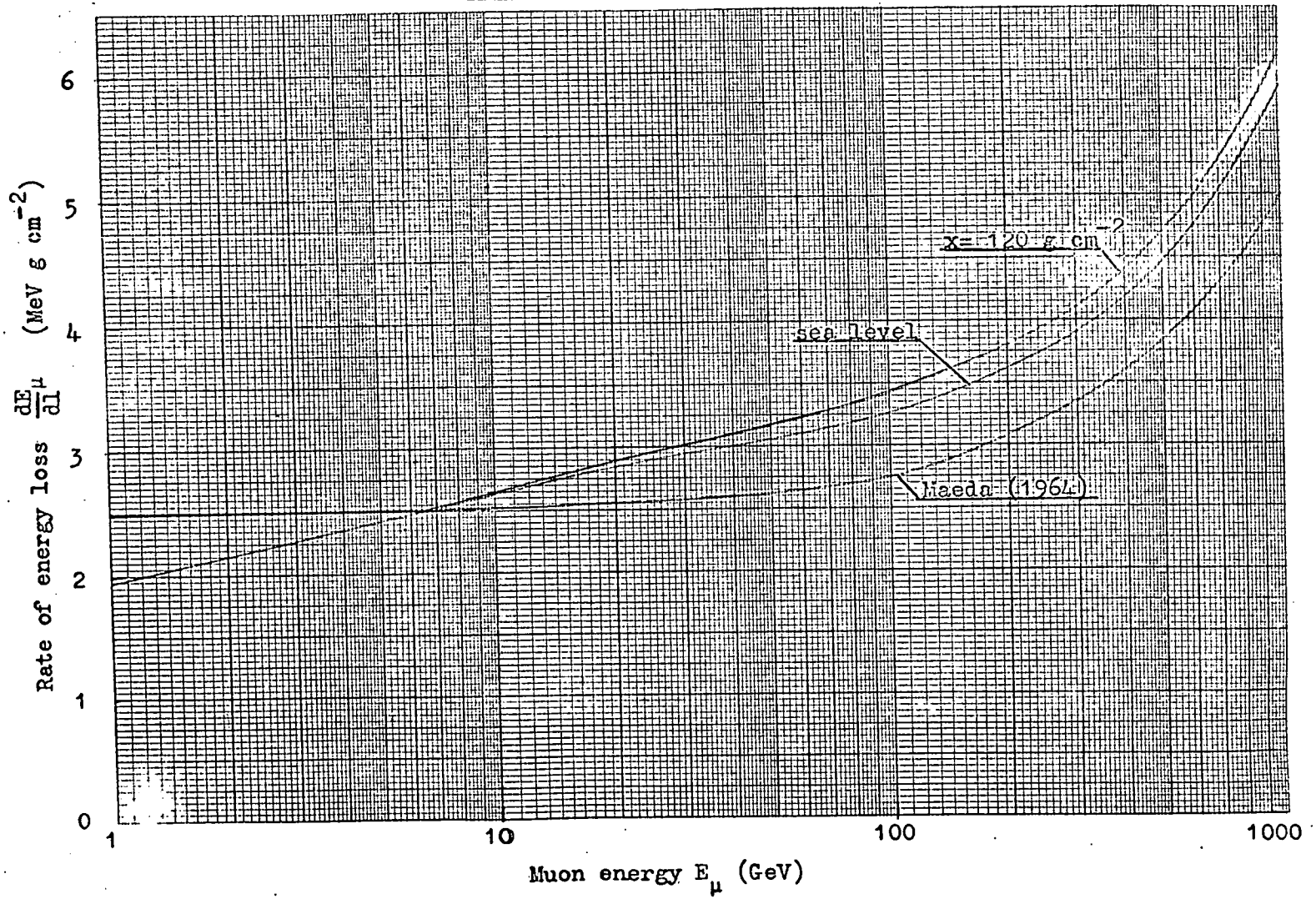

For n sufficiently large, the summation may be replaced by (omitting the E_o, θ parameters of E)

$$\sum_{i=0}^{n-1} \frac{2}{E(x_o - i\Delta) + E(x_o - (i+1)\Delta)} \int_{x_o-(i+1)\Delta}^{x_o - i\Delta} \frac{\sec\theta^* \, dx'}{\rho(x')} \qquad (2.7)$$

where $$E(x_o - (i+1)\Delta) \simeq E(x_o - i\Delta) + \frac{dE}{dl}(E(x_o - i\Delta), x_o - i\Delta).\Delta \qquad (2.8)$$

For each interval, the value of n was doubled until the difference between the values of $E(x,E_o,\theta)$ for successive values of n was less than 0.1%. The results of the calculations were tables of $SP(x,E_o,\theta)$ and $E(x,E_o,\theta)$ against x for θ = 0, 75, 80, 82, 84, 86, 88, 89 and 90 degrees and for E_o = 1, 1.5, 2, 3, 5, 7, 10..... 1000 GeV (19 values). In Figs. 2.6, 2.7, and 2.8 survival probabilities are plotted for θ = 0, 80 and 90 degrees. Some corresponding values from Maeda (1960) are shown for comparison as dashed lines.

2.4 Derivation of the Muon Spectrum from an Assumed Pion Spectrum

In order to calculate the pion production spectrum that gives rise to the measured vertical muon spectrum, if all muons originate in pion decay, it is assumed that the pion spectrum has the form $F_{\pi^+}(E)dE = A\,E^{-\gamma}\,dE$ and a general expression for the muon spectrum is derived. The theoretical spectra for various values of A and γ are calculated and the values that give the best fit to the measured spectrum are found. The pion spectrum is then relaxed to give an exact fit to the measured muon spectrum.

The general expression for the number of pions, travelling vertically with energy E at a depth x in the atmosphere is given by Maeda (1960) as

$$N_\pi(E_\pi, x) = \int_0^x \exp\left[-\int_{x'}^{x}\left(\frac{B_\pi}{E_\pi x''} + \frac{1}{L_\pi}\right)dx'' - \int_0^{x'}\frac{dx''}{L_n}\right]\frac{F_\pi(E_\pi)}{L_c}\,dx' \qquad (2.9)$$

where L is the absorption mean free path of pions,

L_n is the absorption mean free path of nucleons,

Fig. 2.6 Muon survival probability ($\theta = 0^{o}$)

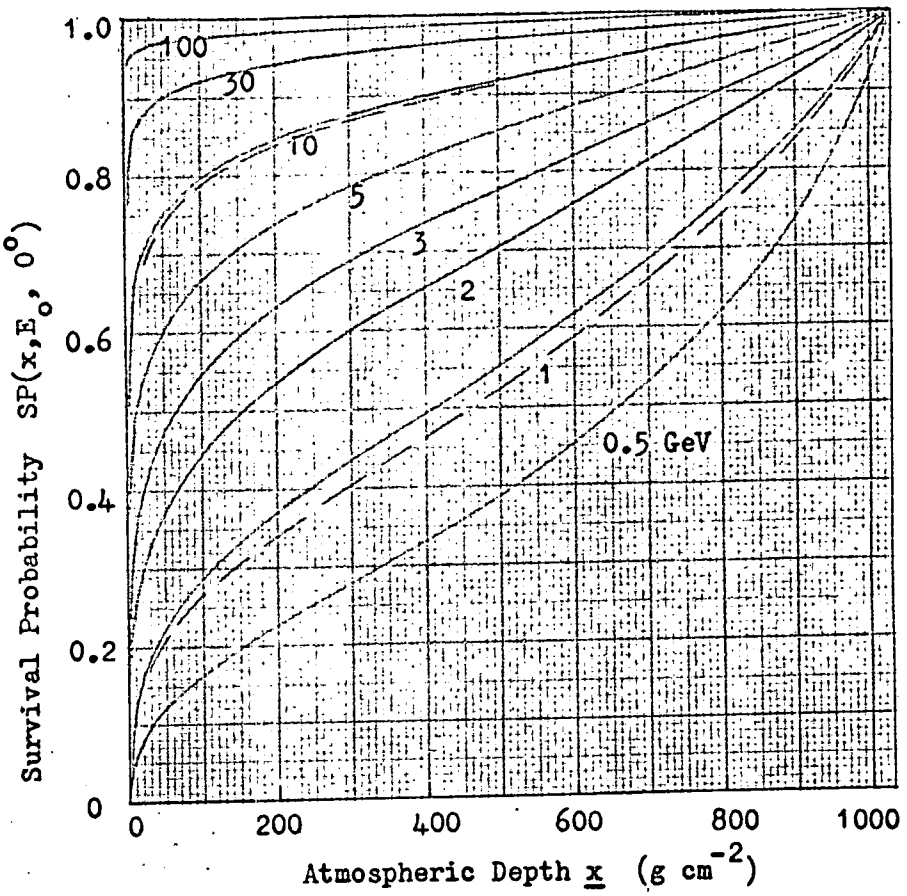

Fig. 2.7 Muon survival probability ($\theta = 80^{\circ}$)

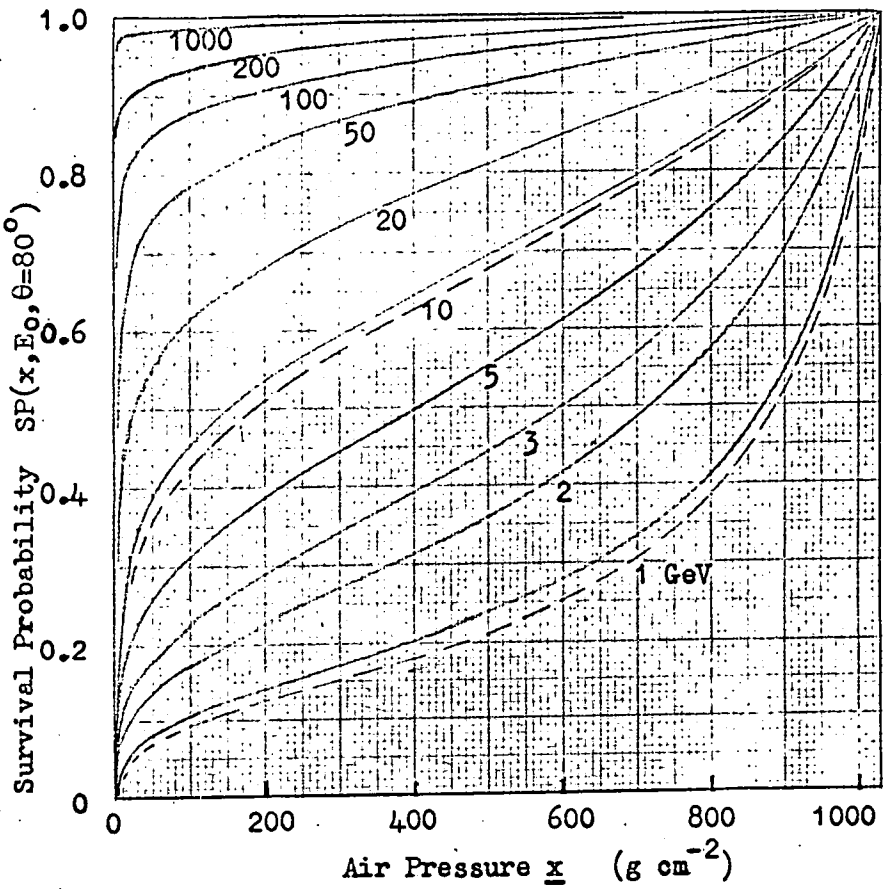

Fig. 2.8 Muon survival probability ($\theta = 90^{\circ}$)

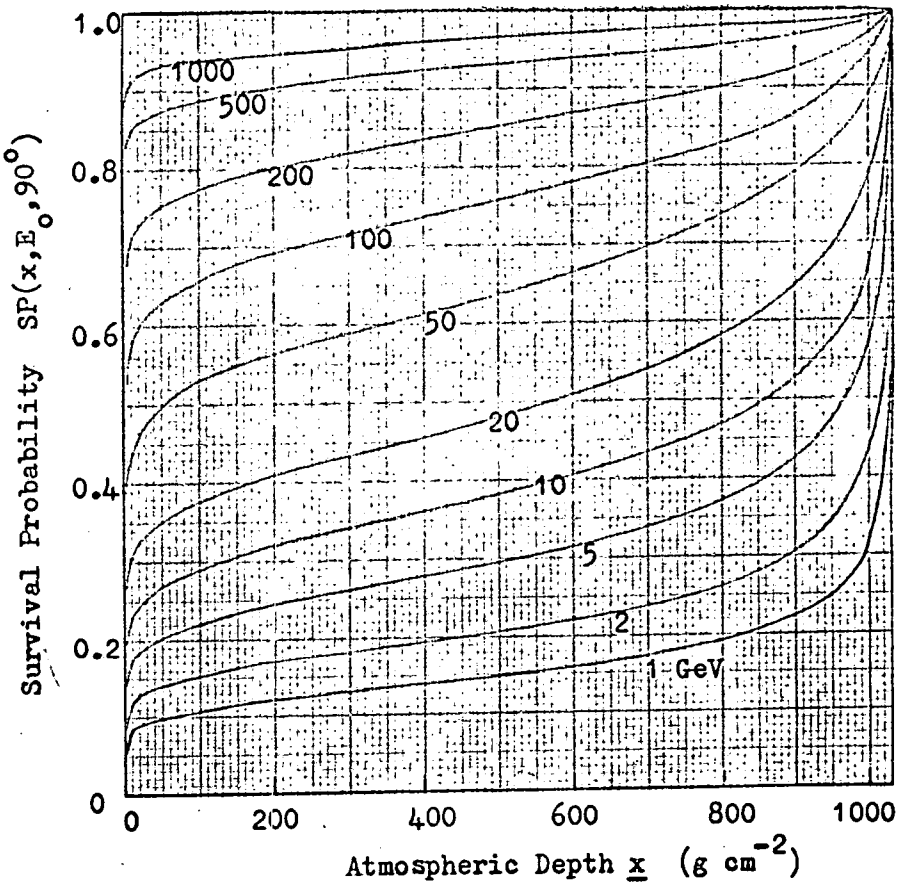

L_c is the collision mean free path of cosmic ray primaries,

and $$B_\pi = \frac{m_\pi c}{\tau_\pi} \frac{x''}{\rho(x'')} \qquad (2.10)$$

The first term in square brackets represents the decrease in intensity due to pion decay and absorption and the second represents the decrease of pion producing particles.

In order that this integral may be evaluated easily, certain approximations are now made. The effects of these approximations are small in themselves but their justification lies in the fact that, having obtained a pion production spectrum in this way, the muon spectrum at sea level at large zenith angles is calculated from the pion spectrum under the same approximations. In other words, we shall obtain by this method, from the OPW spectrum, an 'effective' pion production spectrum; this will be close to, but not exactly equal to, the true pion production spectrum. Provided that this 'effective' spectrum is used in calculating the muon spectrum at large zenith angles the effects of the approximations should be negligible. Firstly the energy loss of the pions between production and decay or absorption is neglected. At energies below about 50 GeV the range of the pions before decay is very short and the energy loss is very small. At high energies where the pion range is limited by absorption the fractional energy loss is small. Then, putting $E_{\pi''} = E_\pi$ and neglecting the weak dependence of B_π on $\underline{x}$ in (2.9), we have

$$N_\pi(E_\pi, x) = \frac{F_\pi(E_\pi)}{L_c} \exp\left(-\frac{x}{L_\pi}\right) \int_0^x \left(\frac{x'}{x}\right)^{\frac{\beta_\pi}{E_\pi}} \exp\left[x'\left(\frac{1}{L_\pi} - \frac{1}{L_n}\right)\right] dx' \qquad (2.11)$$

We shall further assume that the absorption lengths of pions and nucleons are the same, i.e. $L_\pi/L_n = 1$. Previous workers have generally taken smaller values for the absorption length of pions: for the ratio L_π/L_n Zatsepin and

Kuz'min (1961) and Duthie et al. (1962) use 0.63, while Maeda (1964) has made calculations using 0.5 and 1.0. The absorption length of nucleons, L_n, will be taken to be 120 g cm^{-2} but, provided that $L_\pi = L_n$, neither some change with energy nor the precise value of this quantity greatly affects the muon sea level spectrum. Shorter absorption lengths of the pion have been arrived at assuming that the pion interaction is catastrophic, there being no lower energy pions produced in the collision, and that the absorption length is therefore equal to the interaction length. It has been further assumed that the pion and nucleon interaction lengths are the same. Direct measurement of the pion intensity at sea level by Brooke et al. (1964), however, leads to pion absorption lengths of $\sim$ 150 g cm^{-2} at 2 GeV falling to $\sim$120 g cm^{-2} at 100 GeV. Maeda (1964), having calculated muon sea level spectra from pion decay at various zenith angles under the assumptions that L_π/L_n is equal to 0.5 and 1.0 concludes that the values obtained are sufficiently different that the measurement of the spectra of obliquely incident muons affords a method of determining the ratio of the absorption lengths rather than the K/π ratio. A pion production spectrum of the same slope, however, has been used by Maeda in both calculations, the vertical muon intensities being normalised at 40 GeV to the measured one. If the predicted vertical spectra are to fit the measured spectrum over the whole range then two different pion production spectra must be used and the differences between the predicted muon spectra at large zenith angles largely disappear.

For $L_\pi = L_n = \lambda$ (2.11) becomes

$$N_\pi(\epsilon_\pi, x) = \frac{F_\pi(\epsilon_\pi)}{L_c} \exp\left(-\frac{x}{\lambda}\right)\left(\frac{B_\pi}{\epsilon_\pi}+1\right)^{-(\gamma+1)} \qquad (2.12)$$

In two-body $\pi \rightarrow \mu + \nu_\mu$ decay the muon has a unique energy in the c.m.s. and the

angular distribution is isotropic. Because of this, in the laboratory system a pion of energy E_π produces a muon which has energy distributed with equal probability between $E_\pi (r_\pi)^2$ and E_π where $(r_\pi)^2 = (m_\mu/m_\pi)^2 = 0.5729$. Therefore the depth rate of production of muons at depth $\underline{x}$ is

$$n_\mu(E_\mu, x) = \int_{E_\mu}^{E_\mu/r_\pi^2} \frac{\beta_\pi}{E_\pi x}\left(\frac{1}{1-r_\pi^2}\right)\frac{dE_\pi}{E_\pi} N_\pi(E_\pi, x) \quad (2.13)$$

Substituting for (2.12) and writing $E_\mu = S\,E_\pi$ we have

$$n_\mu(E_\mu, x) = \frac{1}{1-r_\pi^2}\int_1^{1/r_\pi^2} \frac{dS}{S}\,\frac{F_\pi(E_\mu S)}{L_c}\exp\left(-\frac{x}{\lambda}\right)\left(1+\frac{S\epsilon_\mu}{\beta_\pi}\right)^{-1} \quad (2.14)$$

Which becomes, for $F_\pi(E_\pi) = A\,E_\pi^{-\gamma}$,

$$n_\mu(E_\mu, x) = \frac{2.341}{120} A\,E_\mu^{-\gamma}\exp\left(\frac{-x}{120}\right)\int_1^{1.746} S^{-(\gamma+1)}\left(1+\frac{S\epsilon_\mu}{\beta_\pi}\right)^{-1} dS \quad (2.15)$$

Here we have taken $L_c = 120$ g cm^{-2} although the exact value is not important. From (2.10) and appendix B, $B_\pi = 118.1$ GeV for $x \leq 253.3$ g cm^{-2} and $44.08\ x^{0.18}$ for ≥ 253.3 g cm^{-2}. Thus the contribution to the intensity of muons with energy E_o at sea level from a height of production $\underline{x}$ is

$$M(E_o, x) = n_\mu(E_\mu(x, E_o), x)\ .\ SP(x, E_o)\left[\frac{dE}{dl}(E_\mu, x)\Big/\frac{dE}{dl}(E_o, x_o)\right] \quad (2.16)$$

The third term, the ratio of rates of energy loss at $\underline{x}$ and at sea level, is a cell width correction. The energy E_μ and the survival probability $\underline{SP}$ are obtained by interpolation, as described in the previous section. Values of $N(E_o, x)$ are plotted in Fig. 2.9, for $E_o = 1$, 10 and 100 GeV, where each curve is normalised to the value at sea level. At high energies where the effects of muon decay and energy loss are small the shape of the curve is determined by the $\exp(-x/120)$ factor. At low energies the effect of the survival probability factor is to decrease the mean height of muon production. The total muon intensity at sea level obtained by integrating $M(E_o, x)$ over $\underline{x}$

Fig. 2.9 Relative contributions to the muon sea level intensity as a function of atmospheric depth

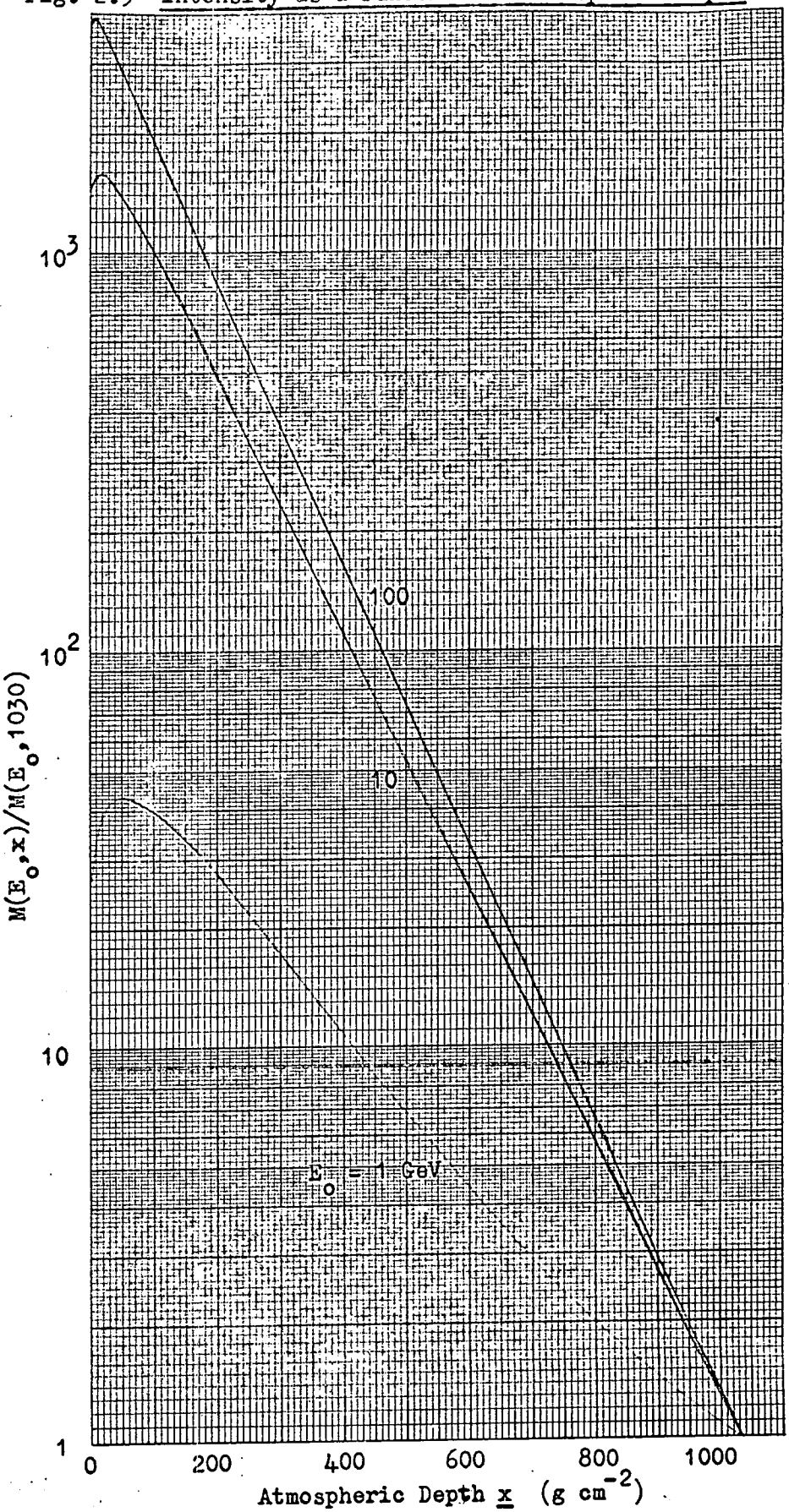

numerically, the atmosphere being divided into six sub-intervals limited by the bounds $\underline{x}$ = 0, 50, 100, 200, 300, 400, 1030 g cm^{-2}, an accuracy of 0.1% in the total intensity being required.

In the computations the value of γ was varied until the value of $\underline{A}$ in (2.15) derived by comparison between the calculated and OPW vertical spectra showed no systematic variation over the whole range of muon energies. It was found that a constant value of γ would not give a good fit over the entire range and that the exponent decreases at low energies. The pion spectrum giving the best fit is

$$F_{\pi^{\pm}}(E_\pi) = 7.16\ 10^{-2}\ E_\pi^{-1.93}\ \text{cm}^{-2}\ \text{sec}^{-1}\ \text{sterad}^{-1}\ \text{GeV}^{-1} \quad \text{for } E_\pi \leq 3.5 \text{ GeV}$$
$$F_{\pi^{\pm}}(E_\pi) = 1.76\ 10^{-1}\ E_\pi^{-2.65}\ \text{cm}^{-2}\ \text{sec}^{-1}\ \text{sterad}^{-1}\ \text{GeV}^{-1} : 3.5 \leq E_\pi < 2000 \text{ GeV} \qquad (2.17)$$

Using this pion spectrum the muon sea level spectrum was calculated and compared with the OPW spectrum in order to obtain a relaxation factor. The mean pion energy at production, to which each muon sea level energy corresponds, was found by re-running the program with γ replaced by γ-1. The values obtained by dividing the muon intensities so derived by the previous ones are the mean pion energies. A plot of these against muon sea level energy is given in Fig. 3.1. The relaxation factor to be applied to (2.17) for the case of all pion parents is given in Fig. 2.10.

2.5 The Muon Spectrum from Kaon and Pion Decay

An admixture of kaons in the flux of parent mesons that give rise to muons at sea level is now assumed. As a first approximation, the ratio of charged and neutral kaons to charged and neutral pions of a given energy at production is taken to be constant with energy. We denote the ratio $N(K^{\pm o})/N(\pi^{\pm o})$ by $\underline{R}$. If the production spectrum of all kaons and pions is of the form $F_{K\pi}(E) = C\ E^{-\gamma}$, then, assuming charge independence in the production

Fig. 2.10 Relaxation factor to be applied to the pion production spectrum of equation (2.17)

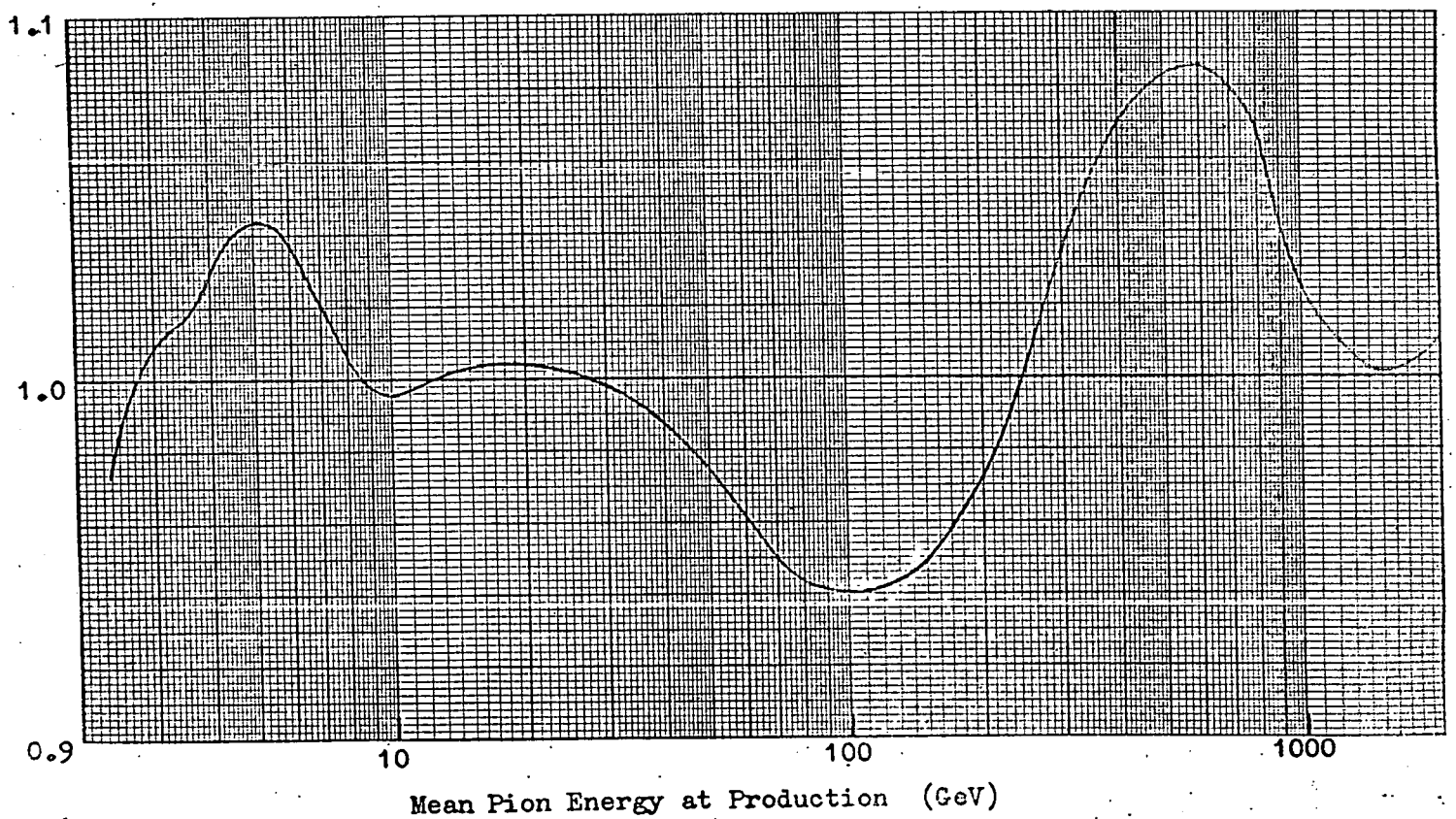

of pions, the production spectrum of charged pions is $C_\pi E^{-\gamma}$ where $C_\pi = \frac{2}{3}\frac{C}{R+1}$. We further assume that at production in high energy nuclear interactions the total numbers of charged and neutral kaons are the same, i.e. $N(K^\pm) = N(K^o + \bar{K}^o)$; this does not involve any assumption concerning the ratio of kaons to anti-kaons. Thus the production spectrum of charged kaons, $C_{K^\pm}E^{-\gamma}$, is equal to that of neutral kaons, $C_{K^o}E^{-\gamma}$, where $C_{K^\pm} = C_{K^o} = C_K = \frac{C}{2}\frac{R}{R+1}$. Using these production spectra, general expressions for the muon spectra at sea level from each decay mode may be obtained as in the previous section. (A list of kaon decay modes and branching ratios is given in Appendix C). The decay modes may be divided into two classes: those in which a muon is produced directly and those in which the muon comes from a pion produced in the decay of a kaon.

2.5.1 Directly Produced Muons

Muons are produced directly from the $K^\pm_{\mu 2}$, $K^\pm_{\mu 3}$, and $K^o_{\mu 3}$ decay modes of the kaons and from pions generated in the nuclear interactions. The expression for the rate of production of muons at depth x from these pions, $n^\pi_\mu(E_\mu, x)$, is identical to (2.15) except that the constant A is replaced by C_π. By analogy with (2.15) the depth-rate of muons from $K_{\mu 2}$ decay is

$$n^{K_{\mu 2}}_\mu(E_\mu, x) = \frac{0.58\,C_K}{120}\exp\left(\frac{-x}{120}\right)E_\mu^{-\gamma}\,1.048\int_1^{21.82} S^{-(\gamma+1)}\left(1+\frac{1.5E_\mu}{B_{K^\pm}}\right)^{-1} dS \qquad (2.18)$$

where $B_{K^\pm} = \frac{m_K c}{\tau_{K^\pm}}\frac{x}{\rho(x)} = 867$ GeV ($x \leqslant 253.3$ g cm^{-2}) and $322\,x^{0.179}$ GeV ($x \geqslant 253.3$ g cm^{-2}). In (2.15) the range of integration is from S = 1.0 to 1.746 and the integration was performed numerically. In (2.18) the range of integration is larger; however, the integral between S = 1.0 and 2.0, which represents 90% of the total, was evaluated numerically and in calculating the remainder of the integral use was made of the analytical approximation

$$\int_{S_1}^{S_2} S^{-(\gamma+1)}(1+\alpha S)^{-1} dS \simeq \frac{S_1^{-\gamma}}{\gamma+(\gamma+1)\alpha S_1}\left[1-\left(\frac{S_1}{S_2}\right)^{\gamma+\frac{\alpha S_1}{1+\alpha S_1}}\right] \qquad (2.19)$$

which is exact for $\alpha \to 0$ and $\alpha \to \infty$ and is valid for all α for $\gamma \geq 2$.

The calculations for the three-body decay modes of the kaon are complicated by the fact that the decay particles have a spectrum of energies in the c.m.s. instead of the unique energy associated with two-body decay. The derivation of the laboratory spectra from the c.m.s. spectra is given in Appendix C. All spectra are given in the general form

$$Q(\varepsilon) = a + b\varepsilon + c\varepsilon^2 + d\varepsilon^3 \quad \text{for } \varepsilon_{max} \gg \varepsilon \gg \varepsilon_{min} \qquad (2.20)$$

where $\varepsilon = E_i/E_K$, E_i being the laboratory energy of the decay particle i; a, b, c and d are constants. Now with $S = E_K/E_i = 1/\varepsilon$ the integral in equation (2.15) will be replaced, for three-body decay, by the general expression $\int_{1/\varepsilon_{max}}^{1/\varepsilon_{min}} Q\left(\frac{1}{S}\right)\left(1+\frac{E_\mu S}{B_i}\right)^{-1} S^{-(\gamma+1)} dS$

Thus we have for $K^{\pm}_{\mu 3}$ decay, from equation (C.5)

$$n_\mu^{K^\pm_{\mu 3}}(E_\mu, x) = \frac{0.04\, C_K}{120} \exp\left(\frac{-x}{120}\right) E_\mu^{-\gamma} \int_{1.091}^{20.16} \left(\frac{-0.3903}{S^{\gamma+1}} + \frac{19.70}{S^{\gamma+2}} - \frac{45.29}{S^{\gamma+3}} + \frac{26.69}{S^{\gamma+4}}\right)\left(1+\frac{E_\mu S}{B_{K^\pm}}\right)^{-1} dS \qquad (2.21)$$

The depth-rate of production of muons from $K^0_{\mu 3}$ is given by an expression identical to (2.21) except that the 4% branching ratio is replaced by 16% and the value of $B_{K_2^0}$ is 179 GeV (for $x \leq 253.3$ g cm^{-2}) and $66.4\, x^{0.179}$ GeV (for $x \geq 253.3$g cm^{-2}). Again the integration was performed numerically up to $S = 3$ and above $S = 3$ by use of the approximation (2.19). From each of the above expressions for the rate of muon production at depth x the vertical muon intensity at sea level was calculated as outlined in section 2.4.

2.5.2 Muons Produced by Two-stage Decay

The kaons that decay via modes in which charged pions are produced give a contribution to the muon sea level intensity through the decay of these pions. The production spectrum of these second stage pions is calculated and then used to derive the muon spectrum as shown above. The simplest case is the $K^{o}_{\pi 2} \rightarrow \pi^{+} + \pi^{-}$. The K^{o}_{1} has a very short lifetime, $9\ 10^{-11}$ sec, and therefore the probability of absorption of the kaon before decay is negligible for $E_{K^{o}} < 5000$ GeV ($B_{K^{o}_{1}} \simeq 1.2\ 10^{4}$ GeV). The rate of production of pions from this source is then,

$$\mathcal{N}_{\pi}^{K^{o}_{\pi 2}}(E_{\pi}, x) = \frac{0.345}{120} C_{K}\ E_{\pi}^{-\gamma} \exp\left(\frac{-x}{120}\right) \frac{2}{0.914 - 0.086} \int_{1.094}^{11.63} s^{-(\gamma+1)}\, ds \qquad (2.22)$$

In this case we have an analytical solution to the integral. We now compare this expression with the rate of production of directly produced pions, $\frac{C_{\pi} E_{\pi}^{-\gamma}}{120} \exp\left(\frac{-x}{120}\right)$, and find that the ratio of the former to the latter, substituting for C_{π} and C_{K}, is $0.625\ (0.914^{\gamma} - 0.086^{\gamma})\ (R/\gamma)$. Since this value, which represents the ratio of the production spectrum of pions from $K^{o}_{\pi 2}$ decay to that of directly produced pions, is independent of energy it also represents the ratio of muon intensities at sea level from the two sources.

The calculation is simple for the case of $K^{o}_{\pi 2}$ because, when the probability of decay can be taken as unity the shape of the spectrum of pions is the same as that of the parent kaons. For the other, longer lived, kaon decay modes the probability of kaon absorption instead of decay is appreciable and the shape of the pion spectrum is consequently modified. For instance the production spectrum of pions from $K^{\pm}_{\pi 2}$ decay is

$$\frac{0.26\ C_{K}\ E_{\pi}^{-\gamma}}{0.914 - 0.086} \int_{1.094}^{11.63} s^{-(\gamma+1)} \left(1 + \frac{E_{\pi} s}{B_{K^{\pm}}}\right)^{-1} ds \qquad (2.23)$$

This spectrum has a negative exponent of γ for $E_\pi \ll B_{K^\pm}$ but this increases with energy to $\gamma+1$ for $E_\pi \gg B_{K^\pm}$. The general expression for the other three-body modes, $K^0_{\mu 3}$, K^0_{e3}, $K^0_{\pi 3}$, $K^\pm_{\pi 3}$ and $K^\pm_{\pi 3}{}'$ is

$$br\ C_K E_\pi^{-\gamma} \int_{1/\varepsilon_{max}}^{1/\varepsilon_{min}} s^{-(\gamma+1)}\, Q(1/s)\left(1+\frac{\varepsilon_\pi s}{\beta}\right)^{-1} ds \qquad (2.24)$$

where br. is the appropriate branching-ratio and the spectrum Q and limits of integration are given in Appendix C. The total pion production spectrum from the sum of (2.23) and the five expressions represented by (2.24) was calculated. The resultant spectrum has a slope increasing steadily with energy, but, in order to be able to use the method of section 2.4 to calculate the muon sea level spectrum, a power law spectrum of constant negative exponent γ^* was fitted to it. It was found that $\gamma^* = \gamma + 0.2$ gave the best fit but that this spectrum had to be relaxed by up to $\pm$ 30%. This treatment leads to an error of 10% in the muon spectrum obtained, but since the muons from two-stage decay represent only a few per cent of the total intensity the effect of the approximation is not important.

2.5.3 The Derived Pion and Kaon Production spectrum

The K/π ratio R was first set equal to 0.4 and the value of γ was varied until the calculated vertical muon spectrum most nearly fitted the OPW spectrum. The production spectrum of pions and kaons was then

$$F_{\pi K}(E) = 0.335\ E^{-2.70}\ cm^{-2}\ sec^{-1}\ sterad^{-1}\ GeV^{-1} \qquad (2.25)$$

The relaxation factor that must be applied to (2.25) to give an exact fit to the measured muon spectrum is given in Fig. 2.11. The mean energy of the parent meson corresponding to a given muon energy at sea level was obtained as before by re-running the programs with γ replaced by $\gamma-1$. In Fig. 2.12 the intensities of muons at sea level coming from directly produced pions and

Fig. 2.11 Relaxation factors to be applied to the production spectrum of kaons and pions of equation (2.25) for R = 20% and 40%

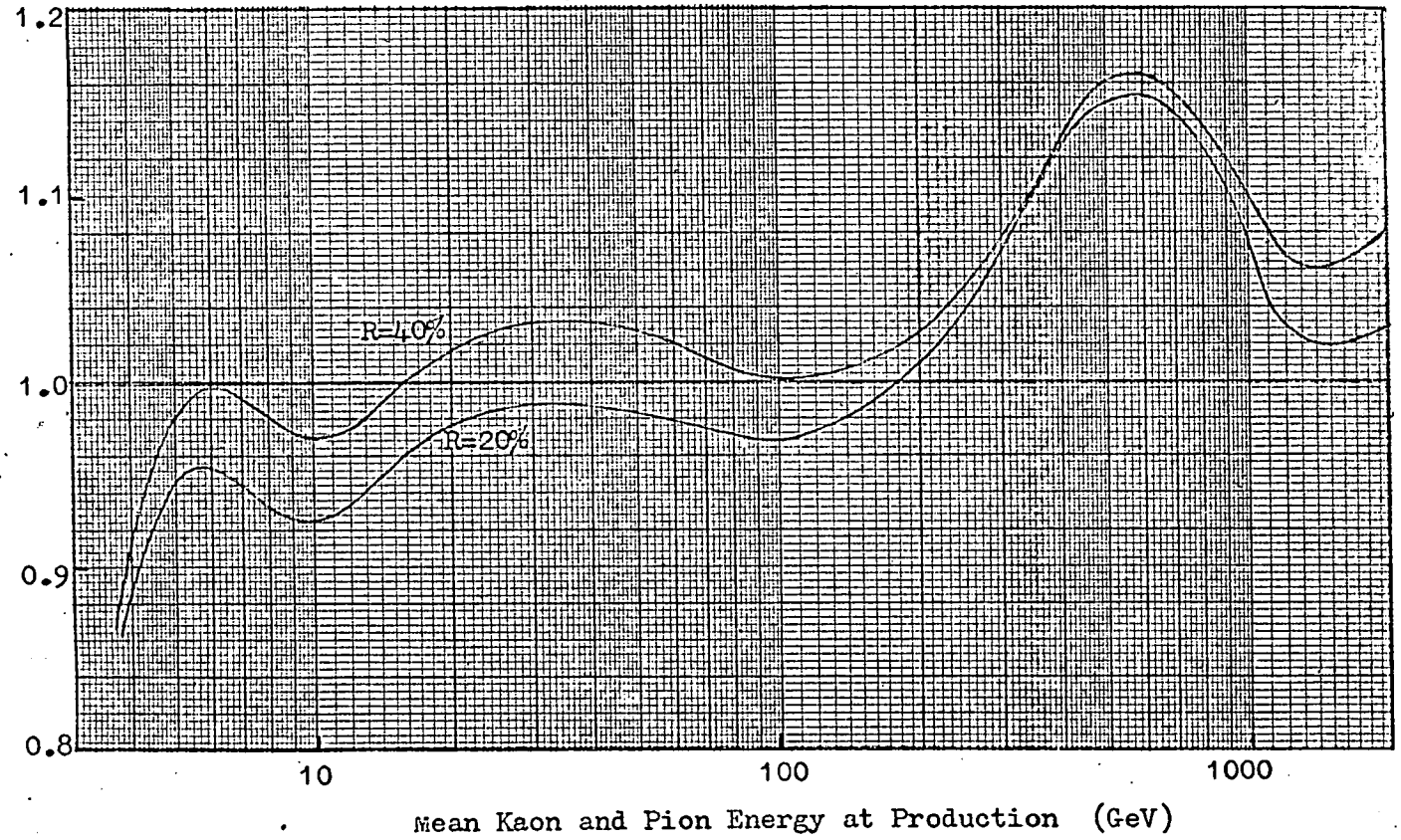

Fig. 2.12 Relative contributions of pions and the various decay modes of kaons to the sea level muon spectrum at $\theta = 0^{\circ}$ for R = 40%

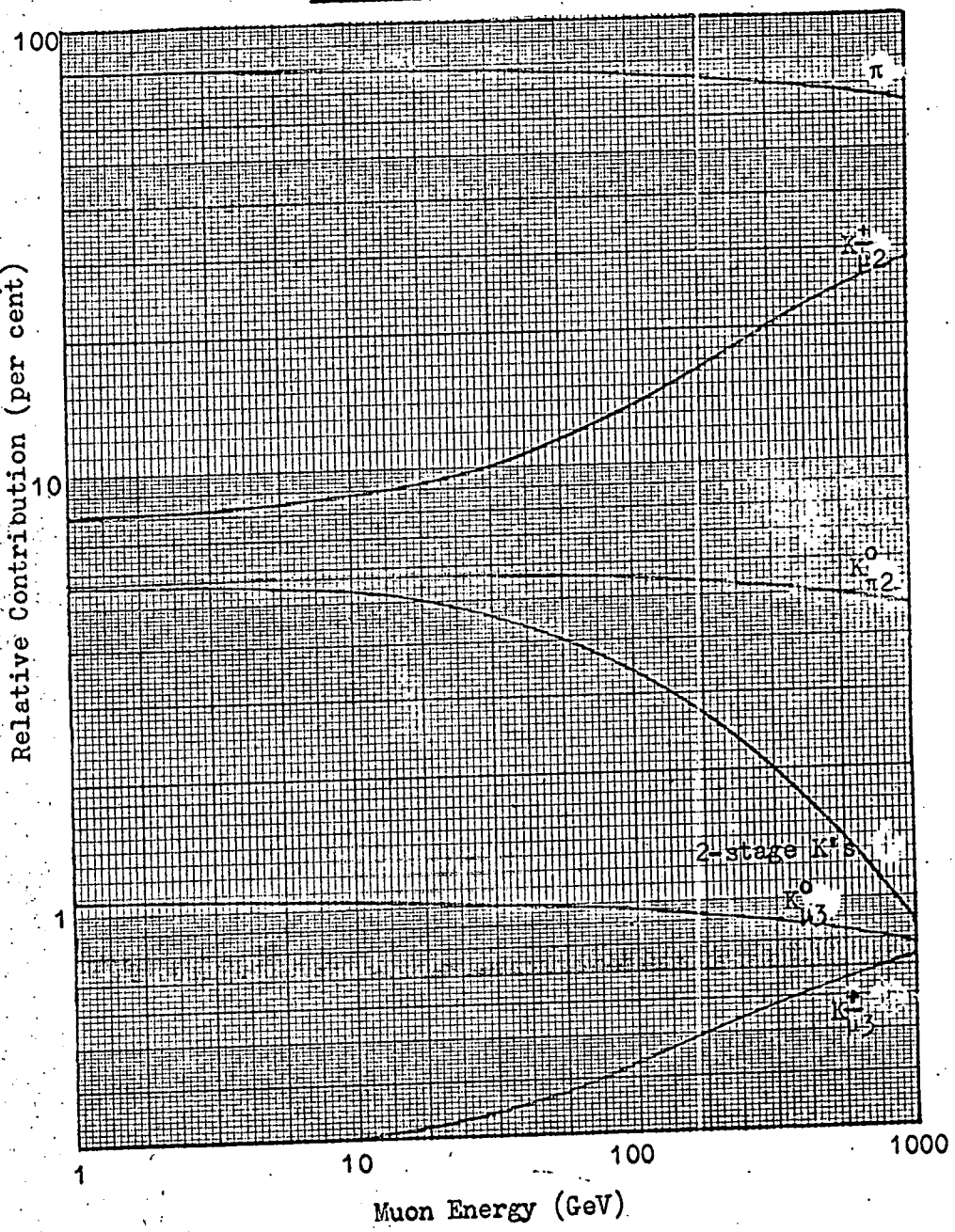

the various decay modes of the kaons are plotted as fractions of the total intensity for $K/\pi = 0.4$. It can be seen that the relative numbers of muons from $K^{\pm}_{\mu 2}$ and $K^{\pm}_{\mu 3}$ increase with energy and that the contribution from $K^{o}_{\mu 3}$ and $K^{o}_{\pi 2}$ remains constant relative to the direct pion contribution while the proportion of muons from the other two-stage decay modes decreases more rapidly with energy. The comparison of the calculated and observed muon spectra was repeated for R = 0.2. It was found that the production spectrum (2.25) would still give sufficiently close agreement between the calculated and OPW spectra. The relaxation factor is, of course, different for R = 0.2 and this is also plotted in Fig. 2.11. The slow systematic increase with energy indicates that a better value for the exponent of the pion and kaon production spectra for R = 0.2 would be $\gamma = 2.69$ instead of 2.70 but the difference is not important.

Chapter 3

Calculations of the Muon Spectrum at Large Zenith Angles

3.1 Introduction

In Chapter 2, starting with the measured muon sea level energy spectrum in the vertical direction, the production spectra of the muon parents were derived for three assumed admixtures of kaons and pions. It was pointed out that under the simplifying assumptions made, the 'effective' production spectra obtained would be close to but not identical to the true spectra. Here the effective spectra are used to derive spectra of muons at sea level at large zenith angles following the same approximations.

It will be seen that the treatment that has been used is one dimensional. In other words the direction of the muon trajectory at sea level is taken to be the same as that of the primary cosmic ray particle that initiated it. The effects of possible deviations from one dimensionality are most important at large zenith angles where, if the trajectory of a muon is not exactly a straight line, the actual thickness of the atmosphere traversed may be considerably different from that indicated by the direction of the particle at sea level. The angular spread of high energy mesons produced in nucleon-air nucleus collisions is very small and can certainly be ignored. Similarly the angle at decay between the muon and its parent meson is negligible. For example vertical muons of energy 1 GeV at sea level come from pions of mean energy ~ 3.5 GeV where the maximum possible angle between the directions of the two particles is ~ 0.01 radians; muons at large zenith angles

come from parent mesons of considerably higher energy. The two important phenomena that cause the muon trajectory to deviate from a straight line are bending of the track due to the Earth's magnetic field and Coulomb scattering of the particles on air nuclei. The geomagnetic effect on the muon survival probability has been studied by Maeda (1960).

It is a function of the direction, zenith angle and geomagnetic latitude of the observed particle as well as its momentum. Thus the correction for geomagnetic effects is, in general, dependent on the location and orientation of the detecting instrument. The experimental results used in the present work are obtained from the Durham horizontal spectrograph which is aligned with its axis 7.8° East of magnetic North. The muons accepted by the spectrograph travel in directions close to the magnetic meridian and thus have a minimal deflexion. The deflexion that does occur has its greatest component in the azimuthal plane where the effect on the survival probability is very small. In the zenithal plane the deflexions are small but tend to enhance the number of negative particles and decrease the number of positives. The result is that the effect on the total number of particles is negligible, although when measurements of the ratio of positive to negative particles are made a correction for geomagnetic deflexion must be applied. It should be emphasised that this argument applies only to spectrographs orientated in the North-South direction.

The correction due to Coulomb scattering at large zenith angles has been calculated by Allen and Apostolakis (1961) using an approximate analytical treatment: details of a new Monte Carlo calculation of the scattering are given at the end of this chapter.

3.2 Muon Spectra from Pion Parents

Starting again with the general expression for the number of pions with energy E_π at depth x, (2.9) becomes for pions at a local zenith angle $\theta^*(x)$

$$N_\pi(E_\pi, x, \theta^*) = \int_0^x \exp\left[-\int_{x'}^{x}\left(\frac{B_\pi(x'')}{E_\pi'' x''} + \frac{1}{L_\pi}\right)\frac{dx''}{\cos\theta^*(x'')} - \int_0^{x'}\frac{dx''}{L_\pi \cos\theta^*(x'')}\right]\frac{F(E_\pi'')dx'}{L_c\cos\theta^*(x')} \qquad (3.1)$$

Making the same approximations as before and changing the variable of integration from x to l (i.e. $dx/\cos\theta^*(x) = dl$) this becomes

$$N_\pi(E_\pi, l(x,\theta)) = \frac{F(E_\pi)}{L_c}\int_0^l \exp\left\{-\int_{l'}^{l}\left[\frac{B_\pi(x'')l''}{x''E_\pi l''}\right]dl'' - \frac{l}{\lambda}\right\}dl' \qquad (3.2)$$

Where l is a function of x and θ, the zenith angle at sea level. The term in square brackets may be written as $\frac{m_\pi c}{\tau_\pi}\frac{l''}{\rho(x'')}$. For the region of the atmosphere where pion production is important this expression is only weakly dependent on the pressure x and in (3.2) may be taken as a constant of value $\frac{m_\pi c}{\tau_\pi}\frac{l}{\rho(x)}$. This then gives the simplified expression for pion intensity as

$$N_\pi(E_\pi, l(x,\theta)) = \frac{F(E_\pi)}{L_c}\exp\left(-\frac{l}{\lambda}\right)\frac{l}{1+\frac{B_\pi(x)}{E_\pi}\frac{l}{x}} \qquad (3.3)$$

If we assume $F(E_\pi) = A\,E_\pi^{-\gamma}$, as before, then the rate of production of muons from pion decay at depth $l(x,\theta)$ is

$$n_\mu(E_\mu, l(x,\theta)) = \frac{2.341A}{120}E_\mu^{-\delta}\exp\left(-\frac{l}{120}\right)\int_1^{1.746} s^{-(\delta+1)}\left(1+\frac{sE_\mu}{B_\pi}\frac{\gamma c}{l}\right)^{-1}ds \qquad (3.4)$$

This expression should be compared with the corresponding one for vertical muons (2.15). The extra term, x/l, inside the integral gives the greater probability of pion decay at large zenith angles where the important first few interaction lengths are traversed at lower densities than in the vertical direction. The contribution of muons from a depth

$l(x,\theta)$ to the intensity of muons of energy E_0 and zenith angle θ at sea level is then

$$N(E_0, l(x,\theta)) = n_\mu(E_\mu(x, E_\nu, \theta), l(x,\theta))\, sp(x, E_\nu, \theta) \left[\frac{dE}{dl}(E_\mu, x) \Big/ \frac{dE}{dl}(E_\nu, x_0)\right] \qquad (3.5)$$

The values of $l(x,\theta)$ are obtained by interpolation from the data of Table 2.3. Using the pion production spectrum (2.17) the intensity of muons at sea level from 75° to 90° were obtained by integrating (3.5) over $\underline{l}$. For $\theta = 75^\circ$ the integration was performed over the whole range of $\underline{l}$ from 0 to 3919 g cm^{-2} but for larger zenith angles the integration was taken to $l = 3500$ g cm^{-2} only. The exponential term in (3.4) ensures that any contribution from heights corresponding to greater values of $\underline{l}$ are completely negligible. Mean pion energies corresponding to given sea level muon energies for each zenith angle were calculated and are plotted in Fig. 3.1. The calculated spectra were then relaxed using the relaxation factor of Fig. 2.10 and are plotted in Fig. 3.2. Here the full lines are the spectra corrected for Coulomb scattering as described in section 3.4 and the dashed lines are uncorrected spectra. The corrected sea level spectra are given in Table 3.1. At lower energies the muon intensity decreases with increasing zenith angle because the longer path lengths in the atmosphere lead to more muons being lost by decay and because muons of a given energy at sea level come from parents of higher mean energies. At sufficiently high energies that the muon survival probability is close to unity and the fractional energy loss is small the angular distribution is peaked close to 90° because of the greater chance of pion decay at the largest zenith angles.

Fig. 3.1 Mean pion energies&corresponding sea level muon energies for various zenith angles

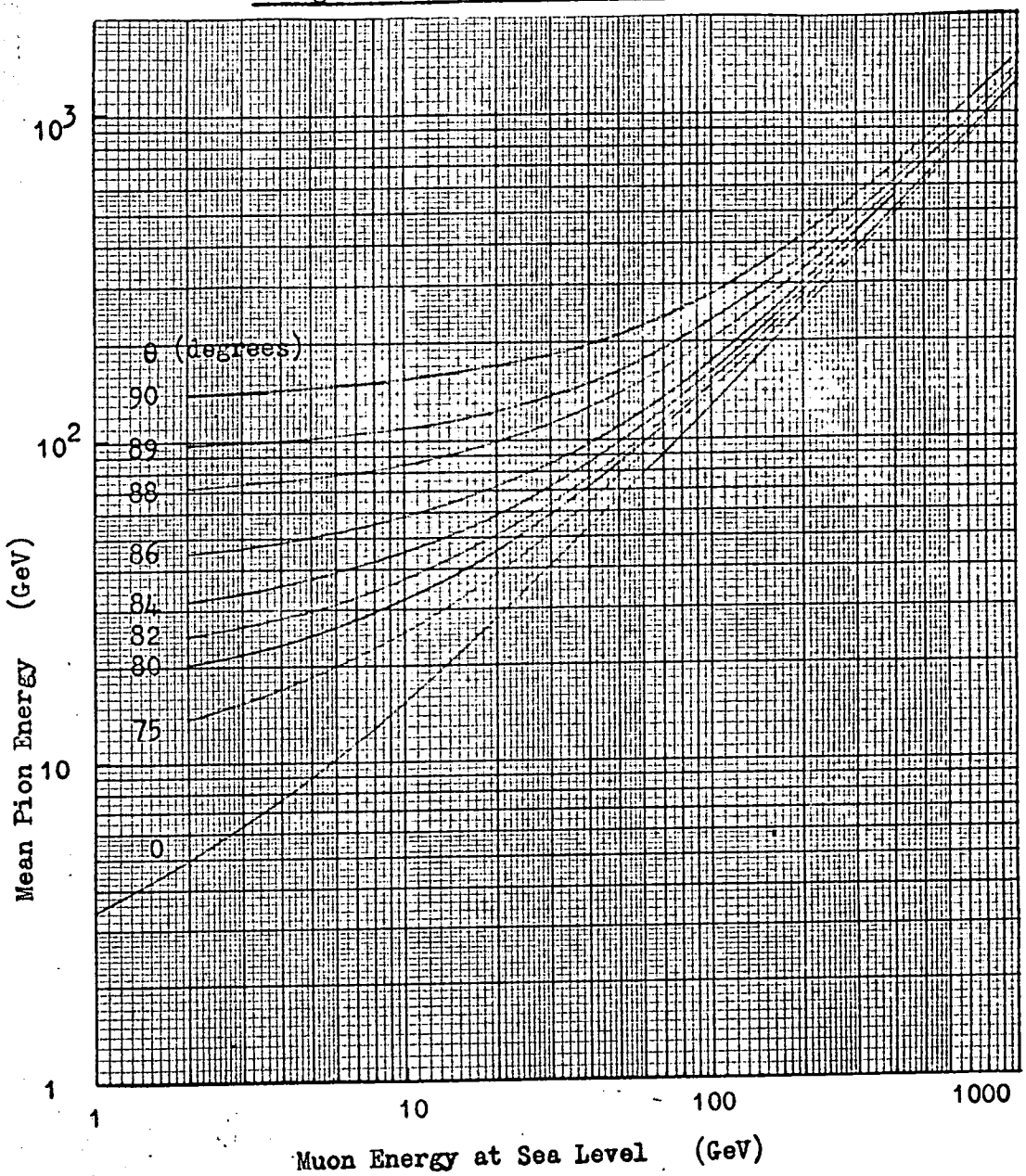

Table 3.1

Calculated Muon Sea Level Spectra at Large Zenith Angles from Pions Only

	Zenith Angle θ (degrees)							
	75	80	82	84	86	88	89	90
Energy (GeV)	Intensity ($cm^{-2} sec^{-1} sterad^{-1} GeV^{-1}$)							
5	2.70^{-5}	9.71^{-6}	5.56^{-6}	2.88^{-6}	1.30^{-6}	5.09^{-7}	3.21^{-7}	2.22^{-7}
7	2.22^{-5}	8.61^{-6}	5.07^{-6}	2.64^{-6}	1.17^{-6}	4.35^{-7}	2.56^{-7}	1.82^{-7}
10	1.66^{-5}	7.13^{-6}	4.38^{-6}	2.40^{-6}	1.06^{-6}	3.84^{-7}	2.15^{-7}	1.52^{-7}
15	1.06^{-5}	5.19^{-6}	3.39^{-6}	1.94^{-6}	9.29^{-7}	3.49^{-7}	1.95^{-7}	1.23^{-7}
20	7.11^{-6}	3.85^{-6}	2.65^{-6}	1.60^{-6}	8.11^{-7}	3.21^{-7}	1.82^{-7}	1.07^{-7}
30	3.67^{-6}	2.28^{-6}	1.68^{-6}	1.11^{-6}	6.14^{-7}	2.70^{-7}	1.58^{-7}	8.96^{-8}
50	1.36^{-6}	9.89^{-7}	7.98^{-7}	5.87^{-7}	3.71^{-7}	1.87^{-7}	1.18^{-7}	6.85^{-8}
70	6.52^{-7}	5.21^{-7}	4.42^{-7}	3.47^{-7}	2.40^{-7}	1.34^{-7}	8.81^{-8}	5.32^{-8}
100	2.82^{-7}	2.44^{-7}	2.18^{-7}	1.82^{-7}	1.37^{-7}	8.51^{-8}	5.92^{-8}	3.69^{-8}
200	4.82^{-8}	4.77^{-8}	4.60^{-8}	4.25^{-8}	3.64^{-8}	2.70^{-8}	2.10^{-8}	1.47^{-8}
300	1.57^{-8}	1.65^{-8}	1.64^{-8}	1.58^{-8}	1.43^{-8}	1.14^{-8}	9.37^{-9}	6.95^{-9}
500	3.30^{-9}	3.71^{-9}	3.82^{-9}	3.84^{-9}	3.68^{-9}	3.18^{-9}	2.74^{-9}	2.17^{-9}
700	1.08^{-9}	1.23^{-9}	1.32^{-9}	1.36^{-9}	1.34^{-9}	1.20^{-9}	1.06^{-9}	8.75^{-10}
1000	3.14^{-10}	3.79^{-10}	4.07^{-10}	4.29^{-10}	4.39^{-10}	4.13^{-10}	3.79^{-10}	3.25^{-10}

(N.B. the superscripts represent the power of ten)

Fig. 3.2 The predicted sea level intensities of muons at large zenith angles for R = 0

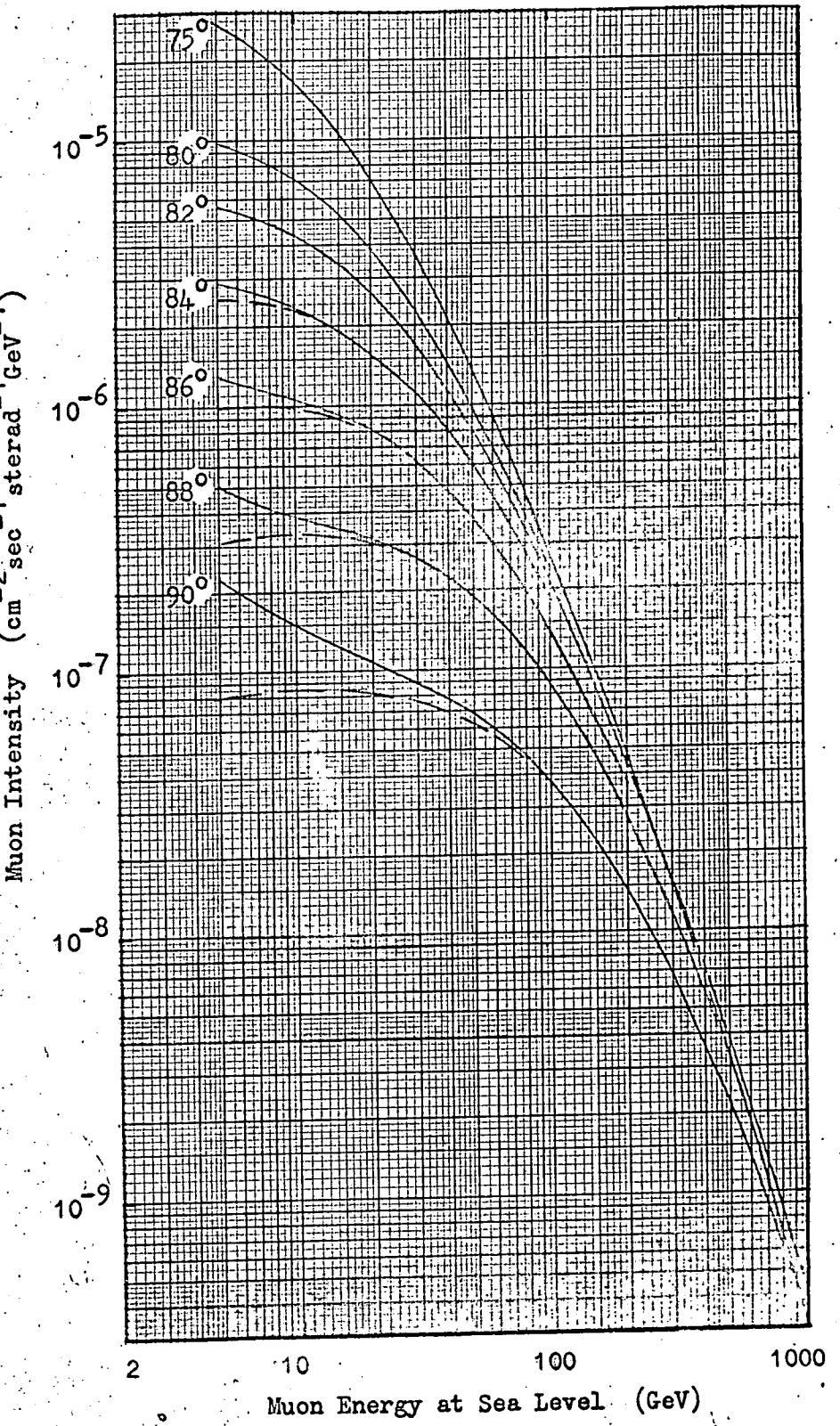

3.3 Muon Spectra from Kaon and Pion Parents

The expressions for the intensity of muons produced by a mixture of kaons and pions, which were derived in section 2.5 for the vertical direction, are modified in a similar way to those for pions as the only source when they are extended to large zenith angles. As before the contributions to the muon flux at sea level from each decay mode giving muons directly were computed separately and the contributions from two-stage decay were evaluated via the production spectrum of the secondary pions. Sea level muon intensities were calculated for values of the kaon to pion ratio, R, of 0.2 and 0.4 using the approximate power law expression (2.25) for the production spectrum of pions and kaons. The mean energy of the parent mesons for each sea level muon energy was found and the appropriate relaxation factors given in Fig. 2.11 were applied. The two sets of spectra, to which corrections for Coulomb scattering have been applied, are given in Tables 3.2 and 3.3. In Fig. 3.3 the relative contributions of the various decay modes to the muon sea level intensity at 90° are given for R = 0.4. This may be compared with the equivalent data for the vertical direction (Fig. 2.12). It can be seen that the variation with energy, over the range 1 to 1000 GeV, of the fractional contribution of each decay mode is smaller and that the two-stage decay modes are still significant at 1000 GeV. The predicted spectra for R = 0.2 and 0.4 are compared with those predicted for pions only in Figs. 3.4 and 3.5 respectively. Up to 1000 GeV the ratio for a given zenith angle decreases with energy. At energies not much greater than 1000 GeV the values will pass through a minimum, the energy

Fig. 3.3 Relative contributions of pions and the various decay modes of kaons to the sea level muon spectrum at $\theta = 90^{\circ}$ for R = 40%

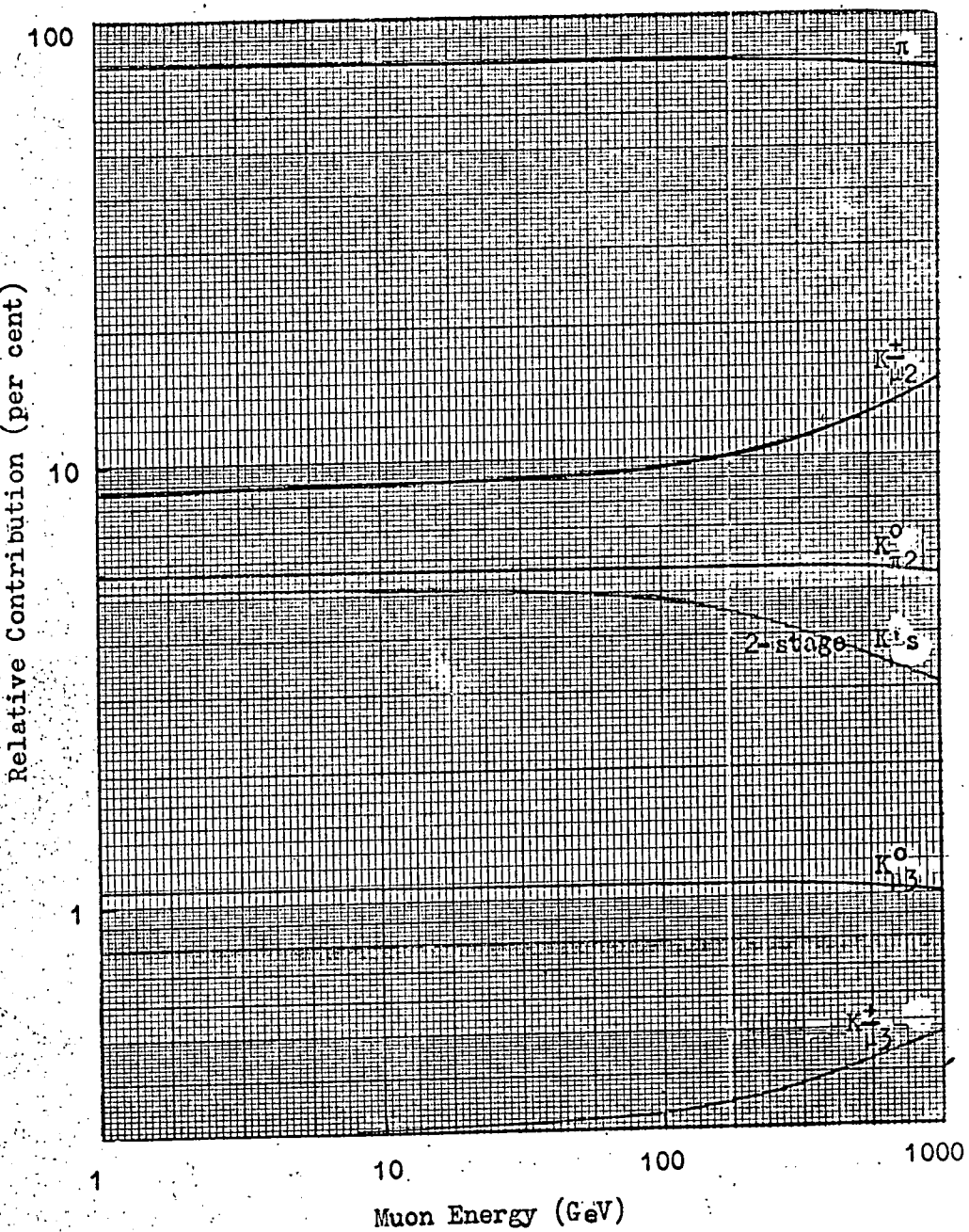

Table 3.2

Calculated Muon Sea Level Spectra at Large Zenith Angles (K/π = 20%)

	Zenith Angle θ (degrees)							
	75	80	82	84	86	88	89	90
Energy (GeV)	Intensity ($cm^{-2}sec^{-1}sterad^{-1}GeV^{-1}$)							
5	2.70^{-5}	9.71^{-6}	5.56^{-6}	2.87^{-6}	1.29^{-6}	5.03^{-7}	3.14^{-7}	2.16^{-7}
7	2.23^{-5}	8.60^{-6}	5.04^{-6}	2.62^{-6}	1.16^{-6}	4.29^{-7}	2.50^{-7}	1.77^{-7}
10	1.65^{-5}	7.11^{-6}	4.36^{-6}	2.33^{-6}	1.06^{-6}	3.78^{-7}	2.11^{-7}	1.48^{-7}
20	7.07^{-6}	3.82^{-6}	2.63^{-6}	1.59^{-6}	8.02^{-7}	3.14^{-7}	1.77^{-7}	1.03^{-7}
30	3.65^{-6}	2.26^{-6}	1.67^{-6}	1.10^{-6}	6.05^{-7}	2.64^{-7}	1.54^{-7}	8.65^{-8}
50	1.35^{-6}	9.75^{-7}	7.85^{-7}	5.75^{-7}	3.64^{-7}	1.82^{-7}	1.14^{-7}	6.59^{-8}
70	6.40^{-7}	5.10^{-7}	4.32^{-7}	3.38^{-7}	2.33^{-7}	1.28^{-7}	8.48^{-8}	5.08^{-8}
100	2.75^{-7}	2.37^{-7}	2.12^{-7}	1.77^{-7}	1.33^{-7}	8.16^{-8}	5.65^{-8}	3.50^{-8}
200	4.61^{-8}	4.55^{-8}	4.37^{-8}	4.03^{-8}	3.45^{-8}	2.94^{-8}	2.53^{-8}	1.99^{-8}
300	1.51^{-8}	1.58^{-8}	1.57^{-8}	1.51^{-8}	1.36^{-8}	1.08^{-8}	8.88^{-9}	6.55^{-9}
500	3.15^{-9}	3.50^{-9}	3.60^{-9}	3.59^{-9}	3.43^{-9}	2.94^{-9}	2.53^{-9}	1.99^{-9}
700	1.02^{-9}	1.14^{-9}	1.23^{-9}	1.24^{-9}	1.23^{-9}	1.10^{-9}	9.70^{-10}	7.98^{-10}
1000	2.96^{-10}	3.52^{-10}	3.76^{-10}	3.94^{-10}	4.00^{-10}	3.75^{-10}	3.43^{-10}	2.94^{-10}

(N.B. the superscripts represent the power of ten)

Fig. 3.4 Comparison of the predicted intensities of muons at large zenith angles for R = 20% with the intensities for pions only

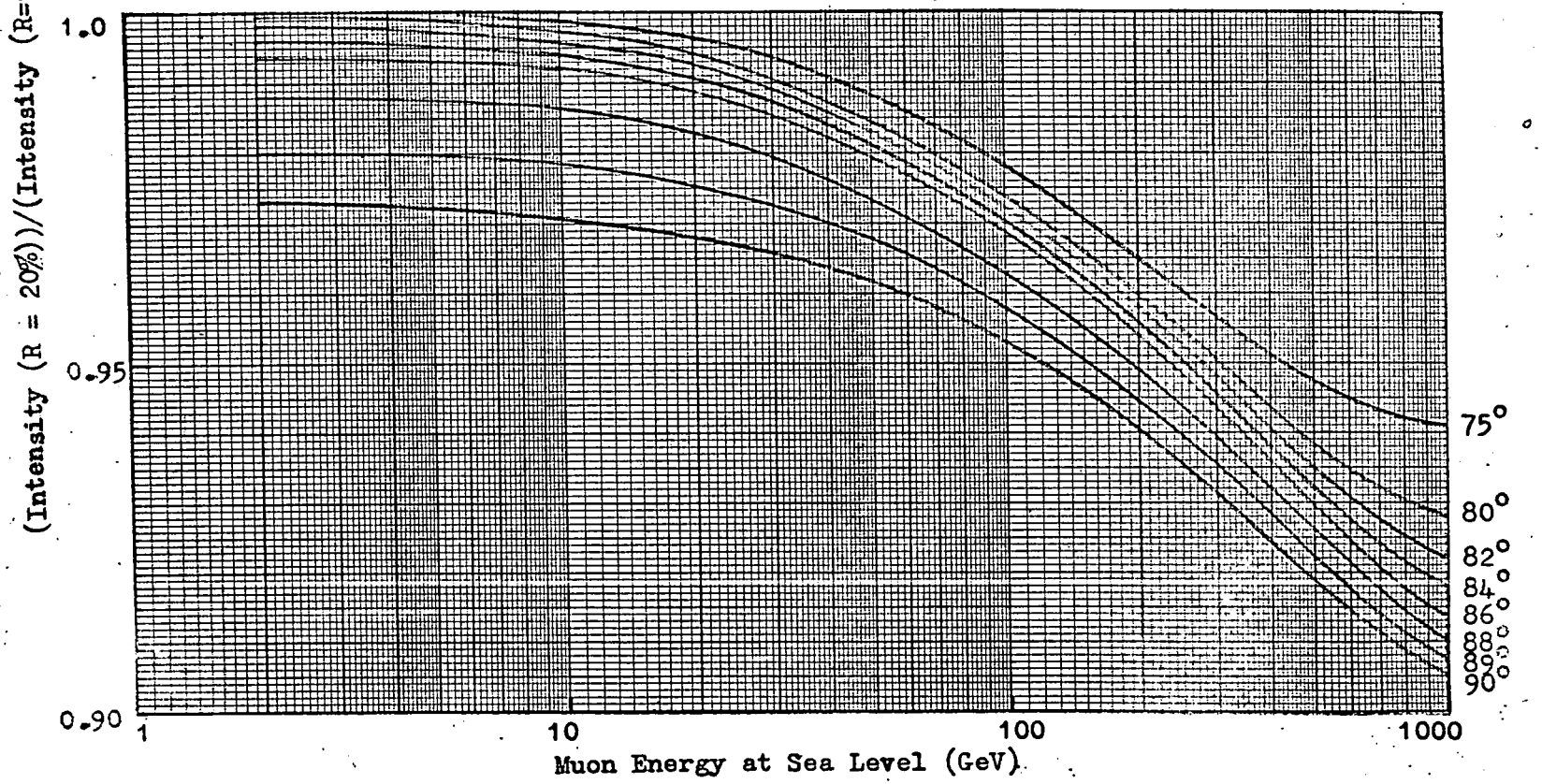

Table 3.3

Calculated Muon Sea Level Spectra at Large Zenith Angles (K/π = 40%)

	Zenith Angle θ (degree)							
	75	80	82	84	86	88	89	90
Energy (GeV)	Intensity ($cm^{-2}sec^{-1}sterad^{-1}GeV^{-1}$)							
5	2.70^{-5}	9.71^{-6}	5.56^{-6}	2.87^{-6}	1.29^{-6}	4.96^{-7}	3.11^{-7}	2.12^{-7}
7	2.22^{-5}	8.58^{-6}	5.05^{-6}	2.54^{-6}	1.16^{-6}	4.25^{-7}	2.48^{-7}	1.74^{-7}
10	1.65^{-5}	7.10^{-6}	4.37^{-6}	2.38^{-6}	1.05^{-6}	3.74^{-7}	2.08^{-7}	1.45^{-7}
20	7.05^{-6}	3.83^{-6}	2.62^{-6}	1.59^{-6}	7.98^{-7}	3.10^{-7}	1.75^{-7}	1.01^{-7}
30	3.65^{-6}	2.26^{-6}	1.66^{-6}	1.09^{-6}	6.04^{-7}	2.61^{-7}	1.51^{-7}	8.46^{-8}
50	1.34^{-6}	9.73^{-7}	7.83^{-7}	5.75^{-7}	3.59^{-7}	1.81^{-7}	1.12^{-7}	6.20^{-8}
100	2.71^{-7}	2.36^{-7}	2.09^{-7}	1.74^{-7}	1.30^{-7}	8.00^{-8}	5.52^{-8}	3.40^{-8}
200	4.51^{-8}	4.50^{-8}	4.31^{-8}	3.96^{-8}	3.36^{-8}	2.49^{-8}	1.92^{-8}	1.34^{-8}
300	1.47^{-8}	1.53^{-8}	1.51^{-8}	1.45^{-8}	1.30^{-8}	1.03^{-8}	8.40^{-9}	6.25^{-9}
500	3.04^{-9}	3.36^{-9}	3.45^{-9}	3.44^{-9}	3.27^{-9}	2.80^{-9}	2.39^{-9}	1.88^{-9}
700	9.73^{-10}	1.10^{-9}	1.17^{-9}	1.20^{-9}	1.16^{-9}	1.04^{-9}	9.13^{-10}	7.44^{-10}
1000	2.83^{-10}	3.36^{-10}	3.58^{-10}	3.75^{-10}	3.76^{-10}	3.55^{-10}	3.23^{-10}	2.75^{-10}

(N.B. the superscripts represent the power of ten)

Fig. 3.5 Comparison of the predicted intensities of muons at large zenith angles for R = 40% with the intensity for pions only

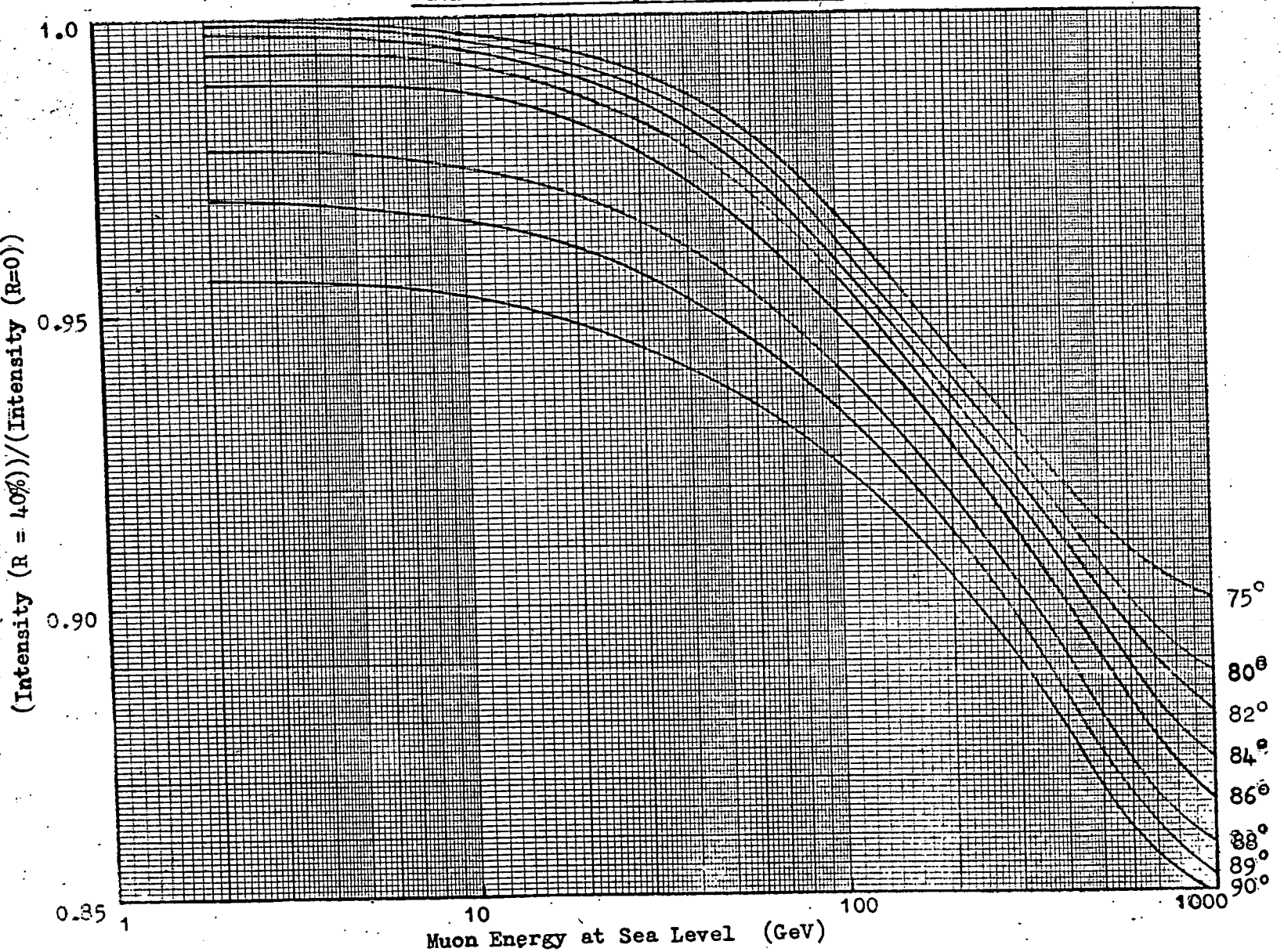

at which the minimum occurs being higher for larger zenith angles. At very high energies the ratio is 1.0 because the probability of decay of all types of parent particles becomes inversely proportional to their energy and the slopes of the muon sea level spectra at all zenith angles are equal and greater by unity than that of the parent meson production spectrum.

3.4 Correction for scattering at Large Zenith Angles

At very large zenith angles, Coulomb scattering of a muon as it traverses the atmosphere can lead to considerable variations in the length of the muon trajectory before it hits the earth. The calculations made so far have ignored scattering and assumed that the muon retains its original direction of travel until it reaches sea level. In this case the survival probability is uniquely determined. If scattering occurs then, for a muon of given energy and zenith angle at sea level, there will be a spread in its possible energy loss and survival probability about the value obtained with no scattering. Since particles which have higher survival probability and smaller energy loss have a higher intensity, the means of the two quantities weighted according to intensity will be shifted towards larger and smaller values respectively than given by the non-scattered calculation. Therefore intensities at large zenith angles, calculated taking account of scattering, will be higher than those ignoring scattering.

Allen and Apostolakis (1961) have used an approximate analytical approach to the scattering problem. If the zenith angular distribution of the muons, calculated ignoring scattering, can be approximated for a given energy at sea level by $I(\theta) = I \exp(-k\theta)$ then, following Lloyd

and Wolfendale (1955), the ratio of intensity with scattering to that without will be $I_s/I = \exp(k^2\sigma^2/2)$ provided that $\theta >> \sigma$. σ is the r.m.s. angle of scattering of the muon in the atmosphere, calculated taking account of the energy loss: it is a function of zenith angle and energy at sea level, increasing slowly with zenith angle and being approximately inversely proportional to the energy. Between 65° and 85°, being the region covered by the experimental results of these authors, the exponential is a good fit to the calculated unscattered distribution and the expression for the scattering correction given above should be close to the truth. Above 85°, however, the exponential form of the angular distribution no longer holds. In this region the scattering correction for low energies is very large and errors in its evaluation may have a profound effect on the predicted spectrum. It was therefore decided to recalculate the correction using a different method.

A Monte Carlo method was adopted whereby a number of 'particles' were followed in their path through the atmosphere and the effects of random scattering on survival probability and energy loss were examined. Since one is interested in standard values of energy and zenith angle at sea level, the trajectories of the particles were followed back from the earth's surface, the energy losses in each step being added to the previous energy. Scattering corrections were required for energies and zenith angles greater than 5 GeV and 75° respectively. The problem becomes much easier if one can separate the effects of scattering from the production process. This entails choosing a vertical height in

the atmosphere, $\underline{X}$ g cm^{-2}, above which muons are produced but the effects of scattering are negligible and below which little further muon production occurs but the values of energy loss and survival probability depend on scattering. Thus $\underline{X}$ must satisfy the following conditions. The contribution to the sea level muon intensity from heights above $\underline{X}$ must be $\gtrsim$ 85%. (The contribution becomes closer to 100% for increasing energy and zenith angle at sea level and is therefore limited by the value for 5 GeV at 75°). The intensity of muons at $\underline{X}$, $I_X(E_X,\theta_X)$, should not be strongly dependent on θ_X: it is found that the dependence on θ decreases as the energy increases. (The fulfilling of this condition ensures that any scattering correction to be applied to the intensity at $\underline{X}$ may be safely neglected). Finally, taking the first two conditions into consideration, $\underline{X}$ should be as large as possible in order to shorten the calculations. The value chosen for $\underline{X}$ was 100 g cm^{-2}. Then, of the 5 GeV muons at 75°, 88.6% are produced at heights above $\underline{X}$; this percentage increases to 99.97 for 90°. There are two reasons for being able to neglect the effects of scattering on the angular distribution at 100 g cm^{-2}. For the minimum zenith angle of 75° only muons of energy greater than about 20 GeV at 100 g cm^{-2} will contribute to the intensity of muons with energy greater than 5 GeV at sea level; Coulomb scattering of particles with energy above 20 GeV is small. Secondly, for an angular range at sea level from 75° to 90°, the corresponding range of local zenith angles (for no scattering) at 100 g cm^{-2} is only 74.5° to 85.9°. Even when scattering below $\underline{X}$ is allowed for, the chance of a muon, which has local zenith angle greater than 87°, reaching sea level

is very small. Thus the particles at extreme zenith angles at 100 g cm^{-2}, which may have experienced considerable scattering above this level, do not contribute at all to the sea level intensity.

Standard values of the intensity $I_{100}(E_{100},\theta_{100})$, that may be interpolated upon in the process of the calculation, are required. If these values are derived from the calculated unscattered intensities at sea level using the unique values of the survival probability and energy loss for the unscattered case, then they will automatically be greater than the true values by an amount which takes account of the small fraction of muons that are produced below 100 g cm^{-2}. A flow sheet of the computer program is given in Fig. 3.6. The notation follows that of section 2.3 with the following additions.

L is the path length in g cm^{-2}, measured along the trajectory from sea level.

R is the linear distance from the centre of the earth.

$\theta(h)$ is the angle of the particle trajectory with respect to the local vertical at altitude h.

Starting at sea level, the energy and zenith angles are set at E_o and θ. The first path length interval ΔL is fixed at 100 g cm^{-2}. x_1 is the pressure at the lower end of the interval and x_2 is that at the upper end. The mean air density over this interval, $\bar{\rho}$, is evaluated at a pressure $x_1 + \frac{L \cos\theta}{2}$ (approximation (i)). Then the linear path length increment is $\Delta s = \Delta L/\bar{\rho}$. The increment in altitude $\Delta h = (\Delta s^2(1 - \cos^2\theta))/2R + \Delta s \cos\theta$, and the pressure x_2 is evaluated for an altitude $h + \Delta h$. The energy loss is taken to be $\Delta E = \Delta L \frac{dE}{dl}(\bar{\rho},E)$ i.e. the rate of energy

Fig. 3.6 Flow sheet for Monte Carlo calculation

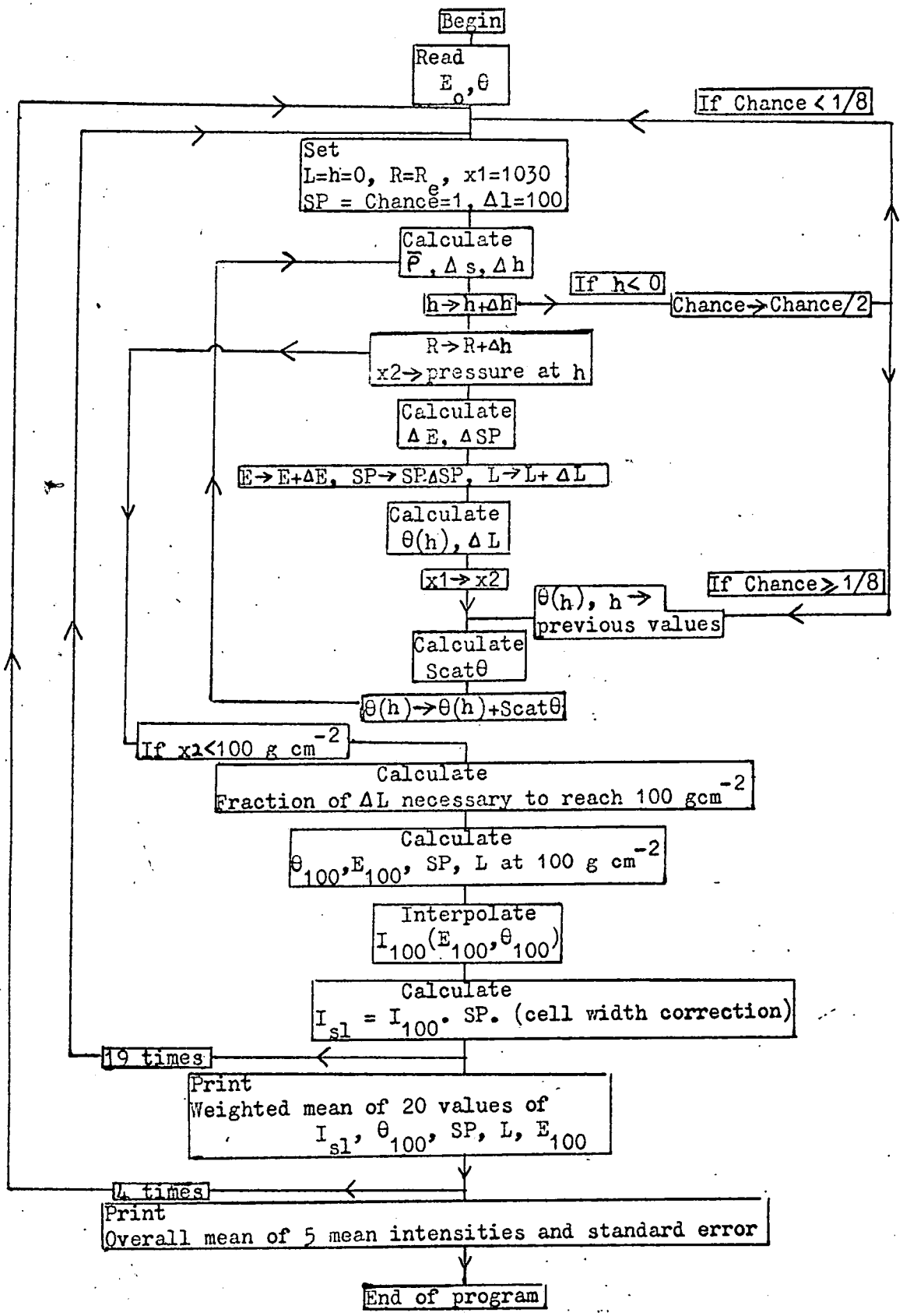

loss is evaluated at the energy corresponding to the lower end of the path interval (approximation (ii)). Then the survival probability over the interval is $\exp(-(m_\mu c^2 \Delta s)/(c\tau_\mu(E + \frac{\Delta E}{2})))$. The local zenith angle at the upper end of the interval is calculated for the case of no scattering using $\cos\theta\ (h_2) = (1 - (\frac{\sin^2\theta(h_1)}{1 + \frac{\Delta R}{R}})^2)^{\frac{1}{2}}$. The r.m.s. projected angle of scattering of a particle of energy E in a path length ΔL is $\frac{0.021}{E}\ (\Delta L/2\ X_o)^{\frac{1}{2}}$ radians where $X_o = 37.7$ g cm^{-2} for air. A random angle of scattering, scatθ, is chosen in accordance with a normal distribution with r.m.s. angle given above, and is added to the previous zenith angle. Now a second path length element ΔL must be chosen; it should be as large as possible with approximations (i) and (ii) still valid. Approximation (i), concerning the effective density over the path interval, demands that $\Delta x < 30$ g cm^{-2}; approximation (ii) holds well provided that the energy loss is less than 10% of the initial energy. Thus ΔL must be set equal to the smaller of 33E or $30/\cos\theta$ g cm^{-2}. With the new ΔL and zenith angle after scattering, a second value for Δh is calculated. If the scattering is in a downward direction it is possible, for 'particles' starting at extreme zenith angles, that Δh is negative and also, for the first few track intervals from sea level, that $\underline{h}$ will become less than zero. This corresponds to the 'particle' hitting the earth and this particular trajectory must be discounted. For 'particles' starting with $\theta = 90^\circ$ there is a high probability of this occuring within the first ten cycles. To reduce the number of false starts a facility is provided, if a random scattering results in $h < 0$, to return to the previous zenith angle and calculate a second random value for scatθ; the

weighting of this particular 'particle' is halved each time this occurs. The cycle for each path increment is repeated until x_2 becomes less than 100 g cm^{-2}. The final path increment is then reduced so that x_2 is equal to 100 g cm^{-2} and values of total path length, survival probability, energy and zenith angle are stored. By interpolation the intensity of muons at 100 g cm^{-2} at this energy and zenith angle, $I_{100}(E_{100},\theta_{100})$, is found, and, using the calculated survival probability, the corresponding intensity at sea level is derived. The procedure is repeated until 20 'particle' trajectories have been followed and the mean values of intensity at sea level, survival probability, total path length, and energy and zenith angle at 100 g cm^{-2}, all weighted according to intensity at sea level, are recorded. When the total number of 'particles' reaches 100 the overall mean intensity and the standard error on the mean is printed out.

To demonstrate the effects of scattering, a comparison is made in Table 3.4 between the mean path lengths and zenith angles at 100 g cm^{-2} for scattered muons of energy 5 GeV at sea level and the unique values for the case of no scattering.

At the smaller zenith angles and higher energies, 100 'particles' were sufficient to give the mean intensity to within a statistical accuracy of 1%, but at the largest zenith angles two or three times this number were needed to attain the required accuracy. The largest statistical error in the intensities was for 5 GeV at 90° where the following of 300 'particle' trajectories, involving over 15,000 separate scatterings, lead to a standard error of 5%.

Table 3.4

Comparison of Path Lengths and Local Zenith Angles for Scattered and Unscattered Muons

Zenith Angle (degrees)	Unique Values (No Scattering)		Mean Values (With Scattering)	
	L ($g\ cm^{-2}$)	θ_{100} (degrees)	L ($g\ cm^{-2}$)	θ_{100} (degrees)
75	3551	74.46	3537	74.35
80	5213	79.20	5165	79.01
82	6412	81.02	6347	80.78
84	8295	82.74	8155	82.46
86	11 590	84.28	11 000	83.85
88	18 330	85.44	16 540	84.99
90	35 330	85.91	24 560	85.65

Table 3.5

Correction Factor for Coulomb Scattering at Large Zenith Angles

Energy at Sea Level (GeV)	5	7	10	15	20	30
Zenith Angle			$C(E_o, \theta)$ (%)			
75^o	101.8	100.7	100.1	-	-	-
80^o	104.5	101.8	100.6	100.2	-	-
82^o	107.4	103.2	101.3	100.6	100.2	-
84^o	115.3	106.9	102.7	101.4	100.8	100.1
86^o	130.7	114.9	107.0	103.4	102.0	100.3
88^o	167.5	135.0	116.0	108.4	105.5	103.5
89^o	216.2	160.1	129.0	116.2	111.5	107.5
90^o	280.2	220.6	180.0	145.5	129.0	117.0

Fig. 3.7 The correction factor for muon scattering as a function of energy for various zenith angles

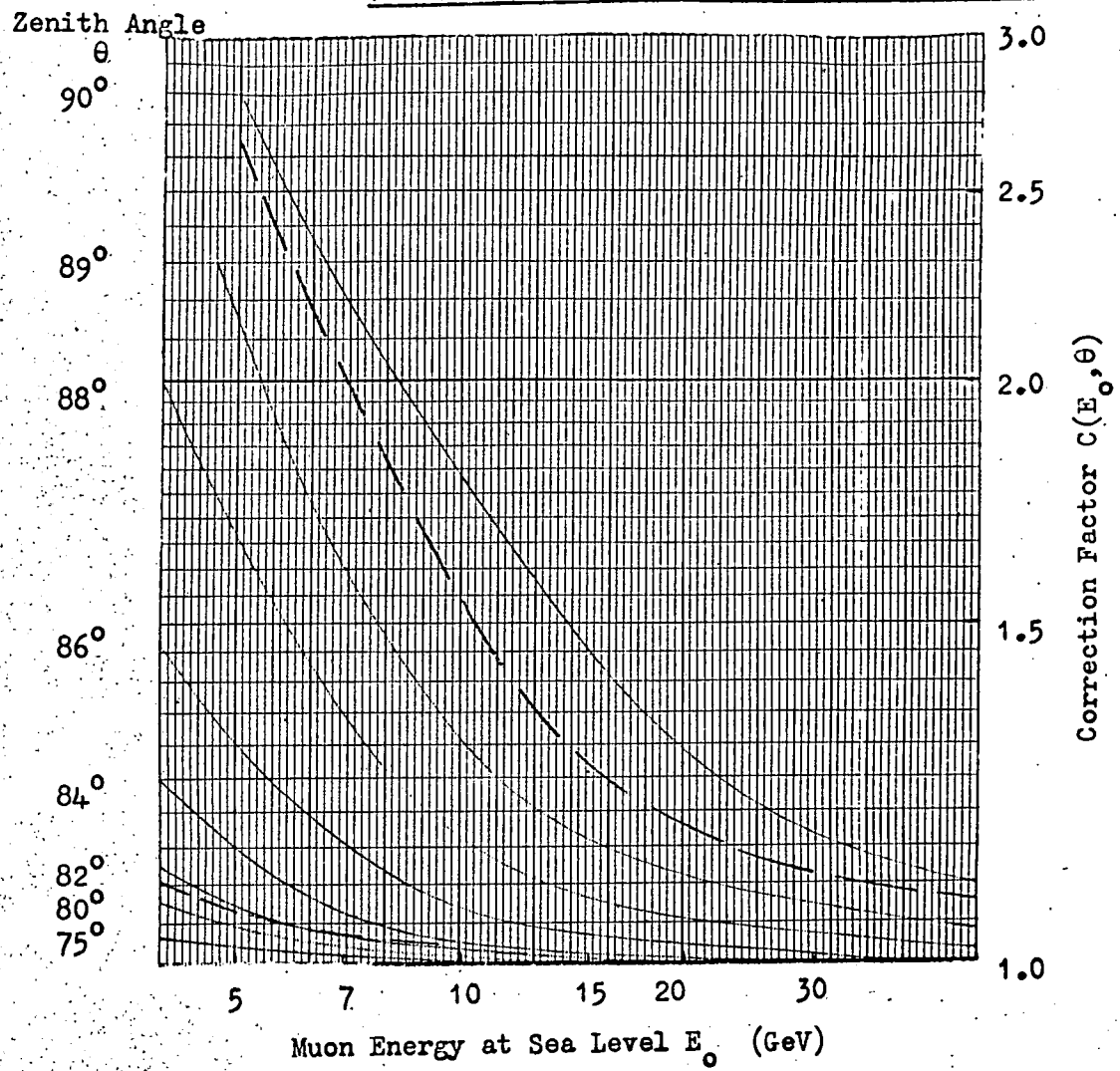

Fig. 3.8 The correction factor for muon scattering as a function of zenith angle for various sea level energies

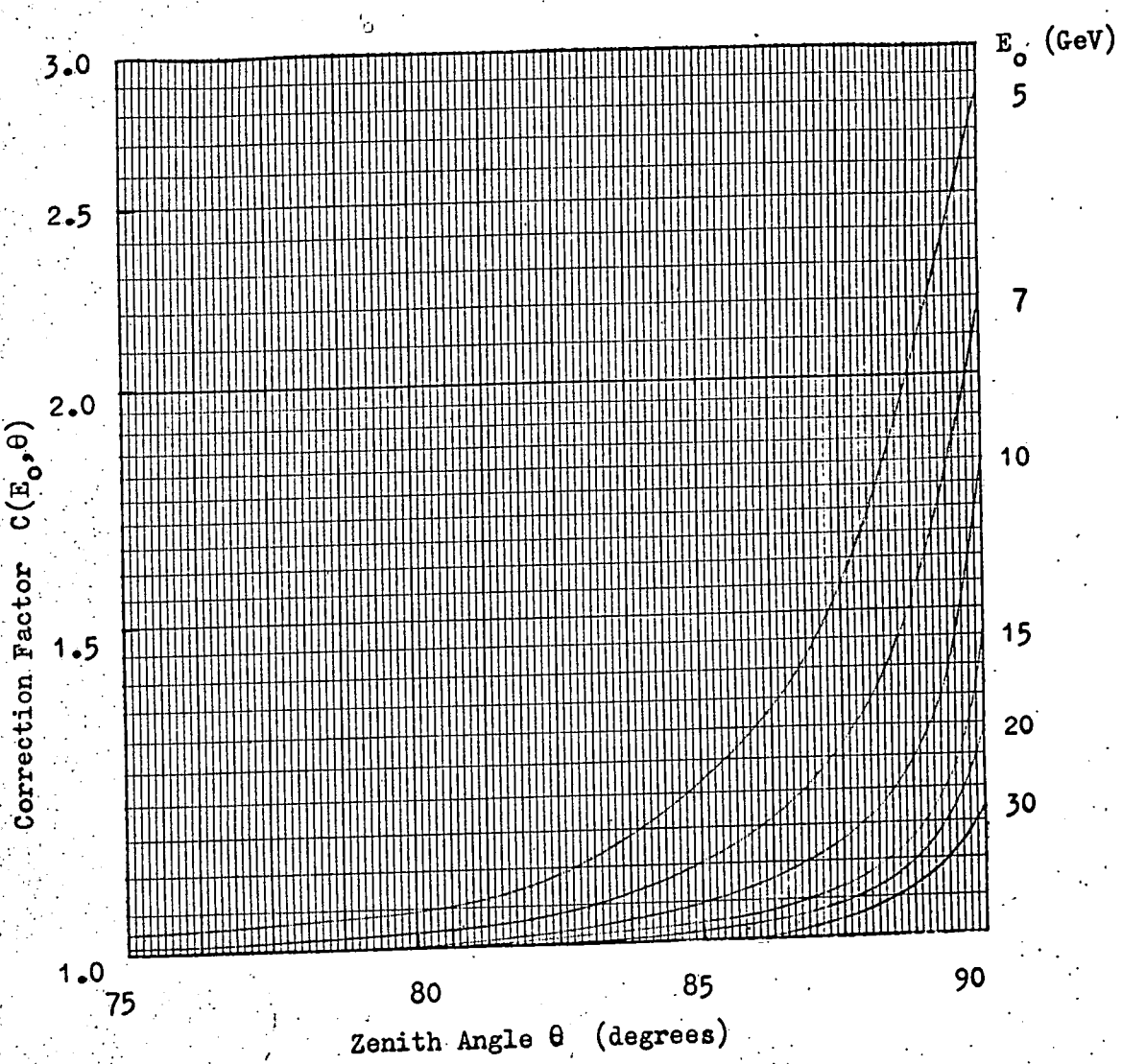

Having derived, in this way, the muon intensities corrected for scattering, values of the correction factor

$C(E_o,\theta)$ = (intensity with scattering)/(intensity ignoring scattering)

were obtained. The values are given in Table 3.5 and $C(E_o,\theta)$ is plotted versus E_o for constant θ in Fig. 3.7 and versus θ in Fig. 3.8. The correction factor was evaluated for the case of pion parents only, but at the relatively low energies for which scattering is important an admixture of kaons alters the muon spectrum very little and the correction factor may be equally well applied to these spectra.

For comparison, in Fig. 3.7 the correction factors of Allen and Apostolakis are shown as dashed lines for $\theta = 80^\circ$ and 90°. It seems that the analytical approximation slightly overestimates the correction by $\sim 2\%$ up to about 86°, but at zenith angles above this it does not increase sufficiently fast with increasing θ. At 90° it is too low by 10-20%.

Chapter 4

Derivation of the Kaon to Pion Ratio

4.1 Introduction

Having calculated the expected muon energy spectrum at large zenith angles as a function of R, the K/π ratio at a given mean energy at production, it should be possible, by comparing the calculated and measured values, to derive a value for R. In section 4.2 the results obtained from the Durham Horizontal Spectrograph are presented. The range of meson energies for which R can be obtained by this method with the present spectrograph is from about 70 to 1000 GeV.

At higher energies, as shown by Duthie et al. (1962) one may compare the measured intensities of electromagnetic cascades at various heights in the atmosphere with the vertical muon intensities at sea level, the relation between the two depending on R. Osborne and Wolfendale (1964) using electromagnetic cascade measurements reported up to June 1964 together with the OPW muon spectrum determined R by this method. The procedure used is outlined in section 4.2. The results have been brought up to date by including more recent cascade measurements and a new estimate of the K/π ratio is given.

At lower energies the polarization of stopping muons can be measured: this is also dependent upon R. Osborne (1964) gave a review of the experimental results up to November 1963. The interpretation of the results given in this paper differed from the previous ones in that all decay modes of the kaons were taken into account in calculating the mean polarization of muons from kaons. These calculations are summarised in

section 4.3 and the subsequent measurements of Asatiani et al. (1964) are included in the analysis. In the final section the results of these three indirect methods are combined to give experimental limits to the K/π ratio over a wide energy range.

4.2 The Measured Muon Spectrum at Large Zenith Angles

4.2.1 The Durham Horizontal Spectrograph

Up to the present time the measurements of the muon spectrum at extreme zenith angles that have the greatest statistical accuracy and cover the widest range of energy have been made using the Durham Horizontal Spectrograph (Ashton et al. 1966). Details of the spectrograph and the analysis of the data obtained from it have been given by MacKeown (1965). A brief summary is given here. The spectrograph (Fig. 4.1) is aligned 7.8° East of magnetic North. It has a solid iron magnet 68.4 cm thick in which the magnetic induction is 15.8 K gauss. Particles are selected by six trays of Geiger counters, A to F, the coincidence requirement being $ABCD\bar{E}\bar{F}$. The last two trays in anti-coincidence reduce the number of extensive air showers which trigger the apparatus. Four trays, each containing eight columns of flash tubes which have their centres 1.905 cm apart in the vertical direction, define the particle trajectories. The neon flash tubes are 1 m long and have an external diameter of 1.8 cm. When the necessary coincidence has been obtained a 9.5 KV pulse is applied to the flash tubes and all four trays are photographed by a single camera through a system of mirrors. The muon trajectories were reconstructed from the photographs and the deflection in the vertical plane measured. The deflexion was expressed

Fig. 4.1 The Durham horizontal muon spectrograph

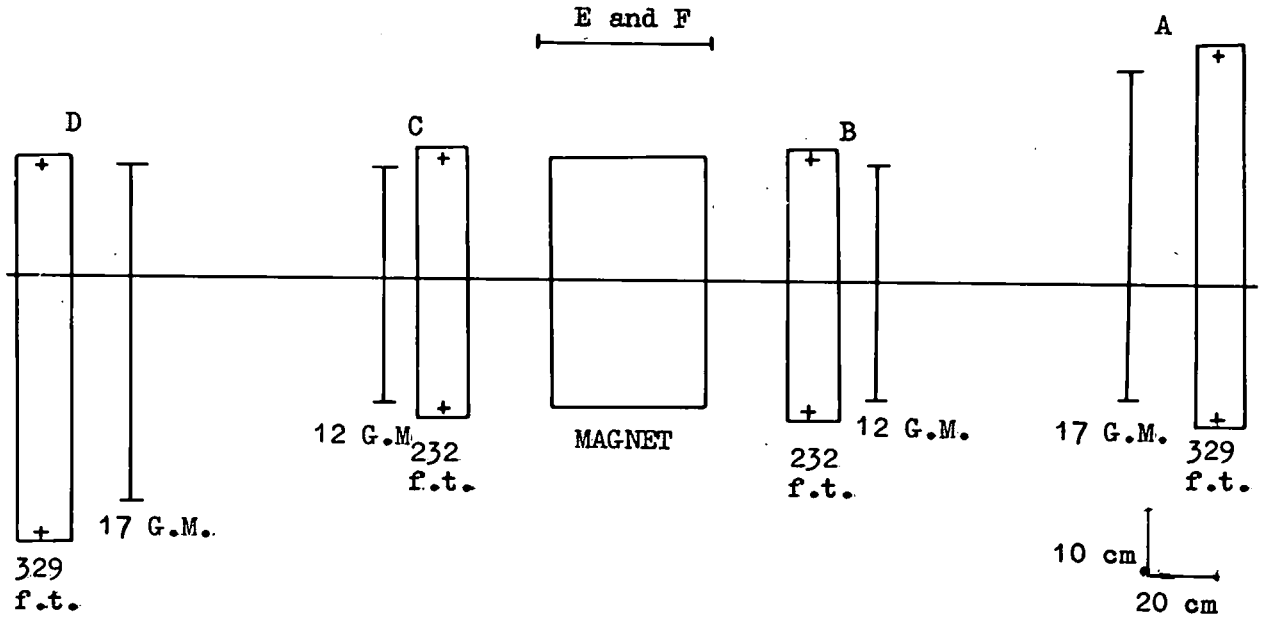

as the distance, Δ, measured at the fourth column of flash tube tray D, between the track through C and D and the extrapolation of the track through A and B. The momentum is then given by $p = \frac{43.87}{\Delta}$ GeV/c, where Δ is in cm. The accuracy with which Δ could be determined for very fast particles was such that the maximum detectable momentum of the spectrograph was 293 GeV/c.

4.2.2 Analysis of the Data

In a total running time of 1508.6 hours 10,080 particles with zenith angles > 77.5° and momenta > 3.7 GeV/c were accepted. The particles were assigned to five 2.5° zenith angle cells from 77.5° to 90° and further subdivided into seven momentum cells between 3.7 GeV/c and 215 GeV/c together with an eighth for particles with higher momenta. The calculated mean momentum of particles in this final cell was 447 GeV/c. In order to convert the measured number of muons to intensities, the spectrograph acceptance function was calculated. This depends on the differential aperture of the spectrograph, (a function of both zenith angle and displacement, Δ) and the efficiency of the Geiger trays. Rejection of events because of the production of a knock-on shower in the spectrograph, paralysis of the instrument by an immediately previous particle or excessive scattering of the muon in the magnet were also taken into account. The measured intensities are given in Fig. 4.2, where the errors are purely statistical. Corrections have been made for systematic errors in the intensities at high momenta caused by uncertainties in the determination of momentum due to scattering in the magnet and inaccuracies in track location. The full lines are the predicted

Fig. 4.2 The measured muon momentum spectra at large zenith angles

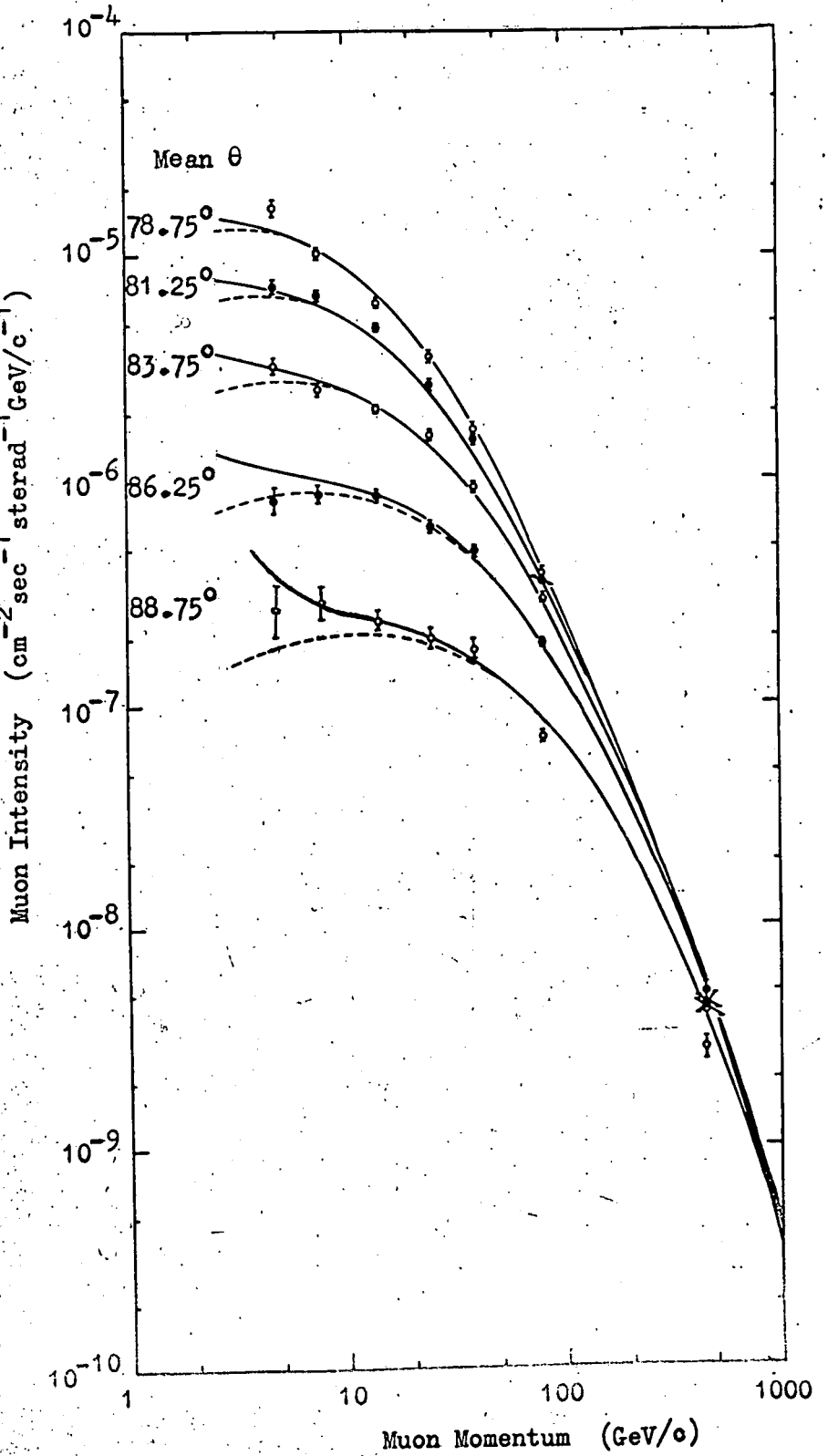

muon spectra, corrected for scattering, for pion parents only. They are derived by interpolation from the data given in Table 3.1. The dashed lines show the spectra with no scattering correction.

4.2.3 Comparison of Measured and Predicted Spectra

From Fig. 4.2 it can be seen that there is general agreement between the measured intensities and those predicted for pions as the only parents. The discrepancy between the lowest momentum point at 78.75° and the predicted intensity may be explained by the rapid variation of the aperture of the spectrograph with deflexion and zenith angle in this region. For greater statistical accuracy the 8,601 muons with zenith angles > 80° were combined and their number compared with the predicted mean intensities over the range 80° to 90°. In Fig. 4.3 the measured intensities are shown together with the predicted values for various admixtures of pions and kaons. All intensities are compared with those predicted for pions only. As well as the ratios for R = 0.2 and 0.4, of which details are given in Chapter 3, the value for the case of all kaon parents is given. For comparison, the relative intensities for the $K_{\mu 2}$ decay mode of kaons as the only source of muons is also shown. This simplification was used in previous analyses, e.g. Ashton and Wolfendale (1963) and Judge and Nash (1965).

The vertical error flags on the experimental points represent statistical errors. The uncertainties in the predicted intensities at large zenith angles due to statistical errors in the vertical intensities, from which they are derived, must also be taken into account. They are shown by the inclined error flags on the experimental points.

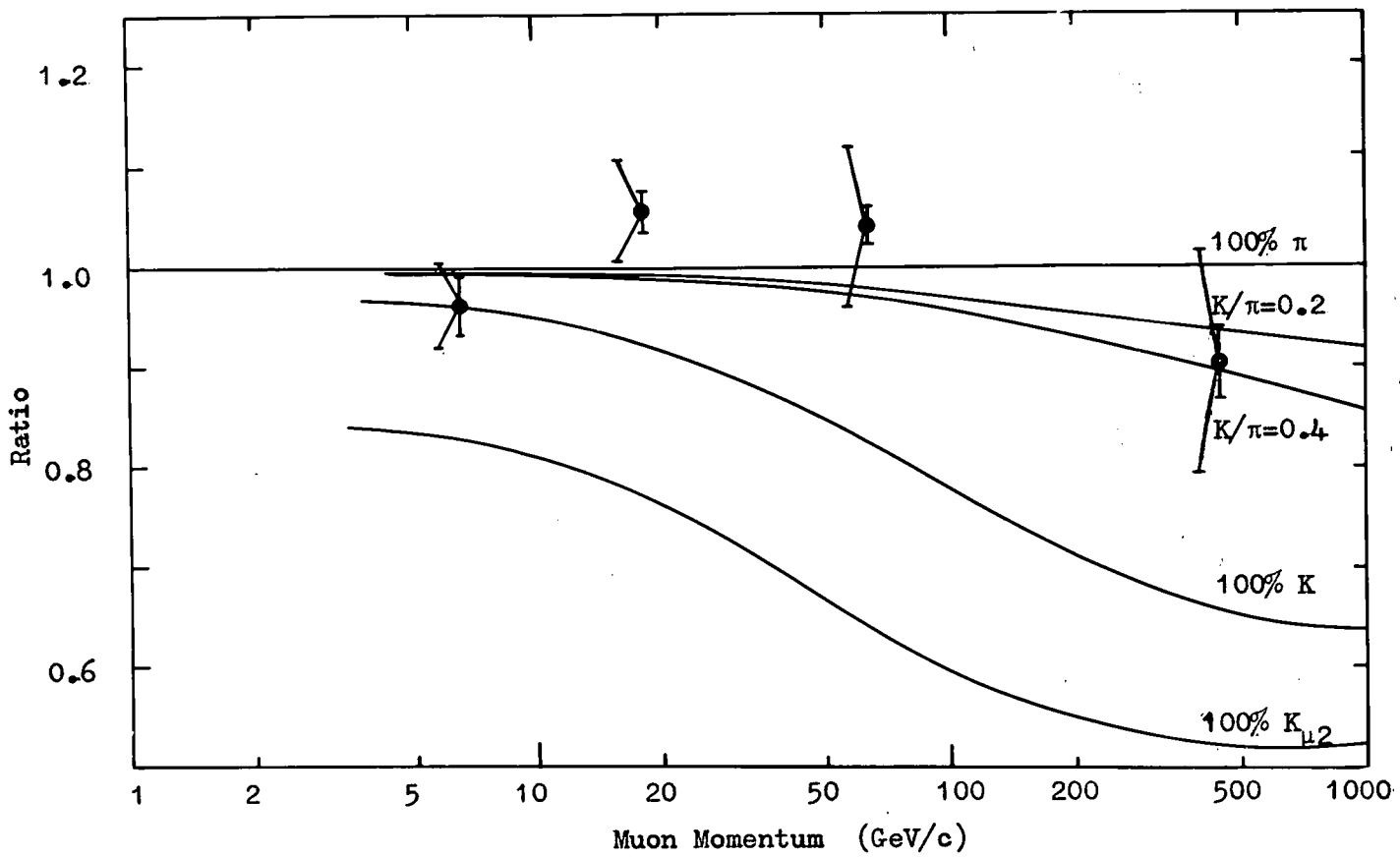

Fig. 4.3 Comparison of measured and predicted intensities with those for pions as the only parents

These errors are significant even at low momenta because the corresponding vertical momenta are comparatively high. (see Fig. 3.1).

It can be seen that, when the diluting effect of contributions from all kaon decay modes is taken into account, the small sensitivity of the inclined muon spectra to the value of R at low momenta means that measurements at momenta < 10 GeV/c cannot give information about the K/π ratio. The effect of an increase of pion absorption length with decreasing energy, for pion energies below 100 GeV, that was indicated by Brooke and Wolfendale (1964) would be to decrease the predicted intensities at low momenta. This might explain the point of lowest momentum in Fig. 4.3 but, as pointed out in section 2.4, the effect is small and furthermore it would be more noticeable at the smaller zenith angles. This does not agree with the data of Fig. 4.2.

It is clear that the derivation of the value of R from these measurements of muon spectra at large zenith angles is very difficult. At present only an upper limit can be set; this appears to be at a value of about 0.4. To obtain a more exact value of R more accurate measurements of both the vertical and horizontal muon intensities at momenta above 100 GeV/c are needed.

4.3 Electromagnetic Cascades in the Atmosphere

Under the hypothesis that all γ-e cascades in the atmosphere are initiated by the decay of neutral pions, the production spectrum of these pions can be obtained from the measurements of cascade intensities at various heights. If these pions are produced directly in nuclear interactions then, assuming charge independence in pion production, the

production spectrum of muons from charged pions can be calculated. On the other hand, if the neutral pions come from the decay of kaons produced in nuclear interactions, the same flux of photons implies a different spectrum of muons from kaon decay. By comparing the two calculated muon spectra with the measured one a value for the K/π ratio is obtained.

4.3.1 Experimental Data

A summary of the experimental data used in the analysis is given in Table 4.1. The results are given in the form of integral intensity spectra of individual photons and electrons. The atmospheric depth quoted is the mean depth at which measurements were made; this is not, in all cases, the same as the 'effective' depth, which depends on the variation of cascade intensity with zenith angle and the known differential aperture of the apparatus.

All of the measurements of the Bristol group have been made with nuclear emulsion-heavy element sandwich stacks. The 'Bristol-Balloon' results refer to a series of flights between 8 g cm^{-2} and 28 g cm^{-2}. From these a spectrum was obtained for an effective depth of 40 g cm^{-2}. The 'Bristol-Comet' data are from four exposures in Comet aeroplanes at 220 g cm^{-2}. In the two series of results the authors used measurements of the angular distribution for $E \geq 470$ GeV in order to obtain intensities over ranges of effective depths from 10 to 62.5 g cm^{-2} and from 230 to 430 g cm^{-2} respectively. The results from the 'Bristol-India' balloon flights are expressed as the rate of production of photons at the top of the atmosphere. The data from this exposure used in the previous

Table 4.1

Summary of Experimental Data on Electromagnetic Cascades

Experiment	Atmospheric Depth ($g\ cm^{-2}$)	Key for Figs. 4.6 4.7 and 4.8	References
Bristol-India	22	■	Malhotra et al. (1965)
Bristol-Balloon	8-28	X	Bowler et al. (1962); Duthie et al. (1962)
Chicago	~9	●	Abraham et al. (1963)
Japanese E.C.	58	▼	Fujimoto et al. (1959)
Bristol-Comet	220	×	Duthie et al. (1962)
Mt. Chacaltaya	550	△	Akashi et al. (1965); Hayakawa et al. (1965)
Mt. Norikura	730	○	Fujimoto et al. (1964)

analysis of Osborne and Wolfendale (1964) was preliminary in that it had been derived from a scan of only half the stack. The result of the full scan is that the previous intensities are reduced by about 10%. The 'Chicago' results are from four balloon exposures of stacks containing only nuclear emulsions. Vertical intensities are given but the effective depths have not been calculated. We have therefore normalised the results to a depth-intensity curve obtained from the other measurements for $E \geq 470$ GeV and arrive at an effective depth of 28 g cm^{-2}. The three remaining experiments were performed with emulsion chambers, consisting of nuclear emulsion sandwiched between horizontal layers of lead. In the two series of mountain exposures x-ray film was incorporated in the stacks to facilitate naked eye scanning for ultra-high energy cascades. No further results have been reported from Mt. Norikura where the total exposure is 24.8 m^2 yr. At Mt. Chacaltaya an exposure during 1964 has brought the total to 9.6 m^2yr. The construction of the latter chamber was such that only very high energy cascades were detected with high efficiency and intensities are quoted only for $E \geq 3000$ GeV. An important alteration to the mountain altitude data has been made due to the recalculation of the cascade development in the lead of the chambers resulting in a 15% increase in the energy scale of all events (Akashi et al. 1965). This is approximately equivalent to a 30% increase in measured intensities.

The combined data give values of the vertical integral intensity spectra of photons and electrons with energy from 300 to 3000 GeV in the atmosphere between 0 and 730 g cm^{-2}. Below 300 GeV only the pure

emulsion stacks give sufficiently high detection efficiencies and above 3000 GeV only the mountain exposures are long enough to give significant number of events.

4.3.2 The Production Spectrum of Initial Photons

Using the stationary solutions of cascade theory obtained by Rossi (1952) under approximation A, the measured intensities of photons and electrons may be used to derive the production spectrum of 'initial' photons, i.e. those produced directly in the decay of neutral pions. The expression for the intensity at depth x of photons and electrons of energy greater than E is of the form

$$F_{\gamma e}(x,>E) = N_{\gamma}(0,>E)\ f\ (x,\lambda_a,s) \qquad (4.1)$$

where $N_{\gamma}(0,E)$ is the rate of production of initial photons per g cm^{-2} at the top of the atmosphere. It is assumed in obtaining the solutions that the integral intensity spectrum at a given depth can be represented by a power law of constant exponent, $-s$, and that the absorption length of the nuclear-active component, λ_a, is independent of energy. Constant values of λ_a and s must be chosen so that the $f(x,\lambda_a,s)$ factor in (4.1) which determines the shape of the depth-intensity curve best fits the measured data. Examination of the spectrum at each depth of observation shows that the choice of the best unique value of s is not simple. In each case, although a power law fits the data well below 1000 GeV the spectrum shows a tendency to steepen at higher energies. The 'knee' in each of the spectra occurs at energies quite close to our upper limit of 3000 GeV, however, so that one may assume a single exponent over the energy range that we use. The value of this exponent is not constant but shows a tendency to increase with increasing depth of observation.

Fig. 4.4 The variation of $f(x, \lambda_a, s)$ with $\underline{x}$ and $\underline{s}$

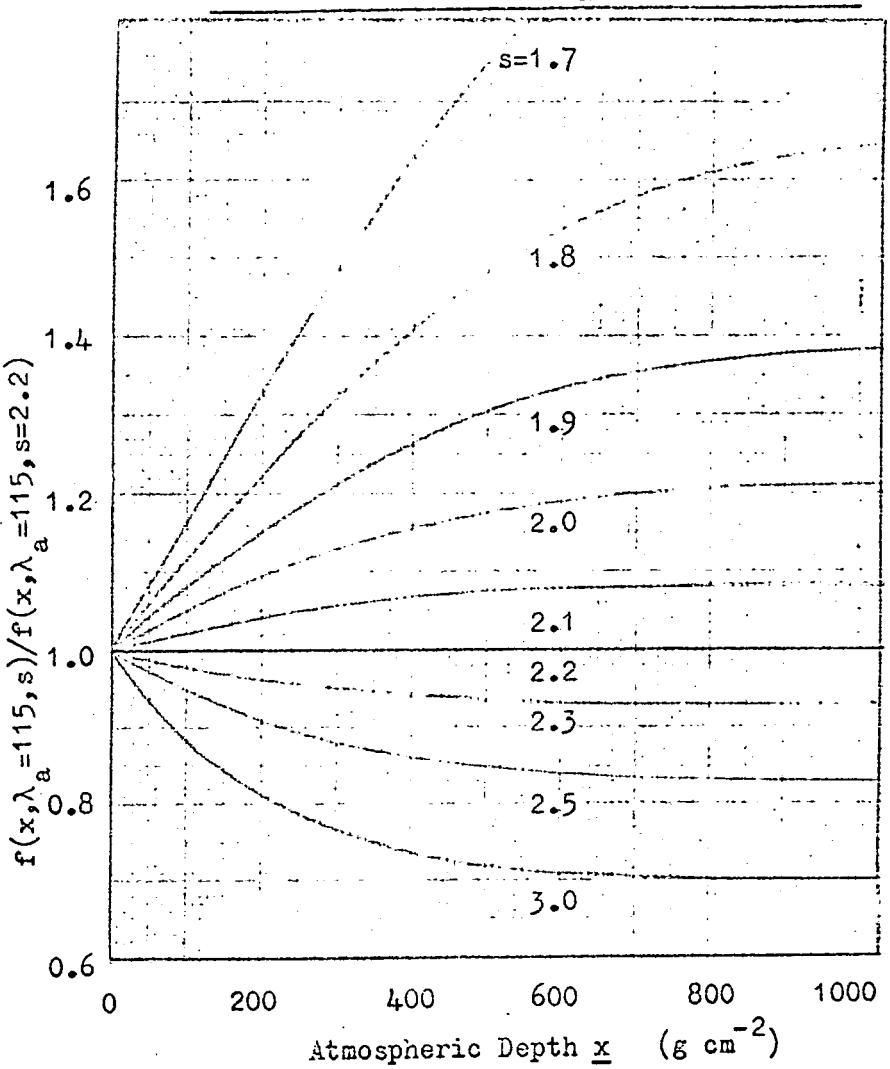

This effect, remarked upon by Malhotra et al. (1965a), is most apparent in the 'Bristol-India' and 'Bristol-Comet' spectra which have exponents of 1.67 ± 0.10 and 2.3 ± 0.20 respectively. The sensitivity of the calculated depth-intensity curves to $\underline{s}$ is shown in Fig. 4.4 where $f(x,\lambda_a = 115,s)$ is plotted against depth, $\underline{x}$, for various values of, $\underline{s}$, normalised to the expression for $s = 2.2$. It can be seen that at balloon altitudes ($x < 60$ g cm^{-2}) the calculated intensity is only weakly dependent on $\underline{s}$ but for aeroplane and mountain exposures ($x > 220$ g cm^{-2}) $\underline{s}$ must agree with the measured exponents of the spectra to within 0.1. Accordingly $\underline{s}$ is taken to be 2.2.

The effect of varying λ_a is shown in Fig. 4.5 where $f(x,\lambda_a,s=2.2)$ is plotted against $\underline{x}$ with λ_a as a parameter, normalised to the expression with $\lambda_a = 100$ g cm^{-2}. It is seen that the ratios are approximately linear functions of $\underline{x}$ for $x > 800$ g cm^{-2} and λ_a close to 100 g cm^{-2}. If the measured intensities, $F_{ye}(x,>E)_m$, at a given energy, $\underline{E}$, are divided by

$$f(x,\lambda_a=100,s=2.2) = -241.2\exp(-x/66.1) + 6.07\exp(-x/20.5) + 235.1\exp(-x/100) \text{ g cm}^{-2} \quad (4.2)$$

and plotted against $\underline{x}$ then they should lie on a straight line, whose slope gives the value of λ_a that would best fit the data and whose intercept with the $x=0$ axis gives the rate of production of initial photons at the top of the atmosphere corresponding to this value of λ_a. This was done for seven energies between 300 and 3000 GeV; graphs for $E>470, >700, >1500$ and >3000 GeV are given in Figs. 4.6 and 4.7. The apparent values of λ_a were obtained from the slopes of the lines given by weighted least squares fits to the experimental points and are listed

Fig. 4.5 The variation of $f(x,\lambda_a,s)$ with x and λ_a

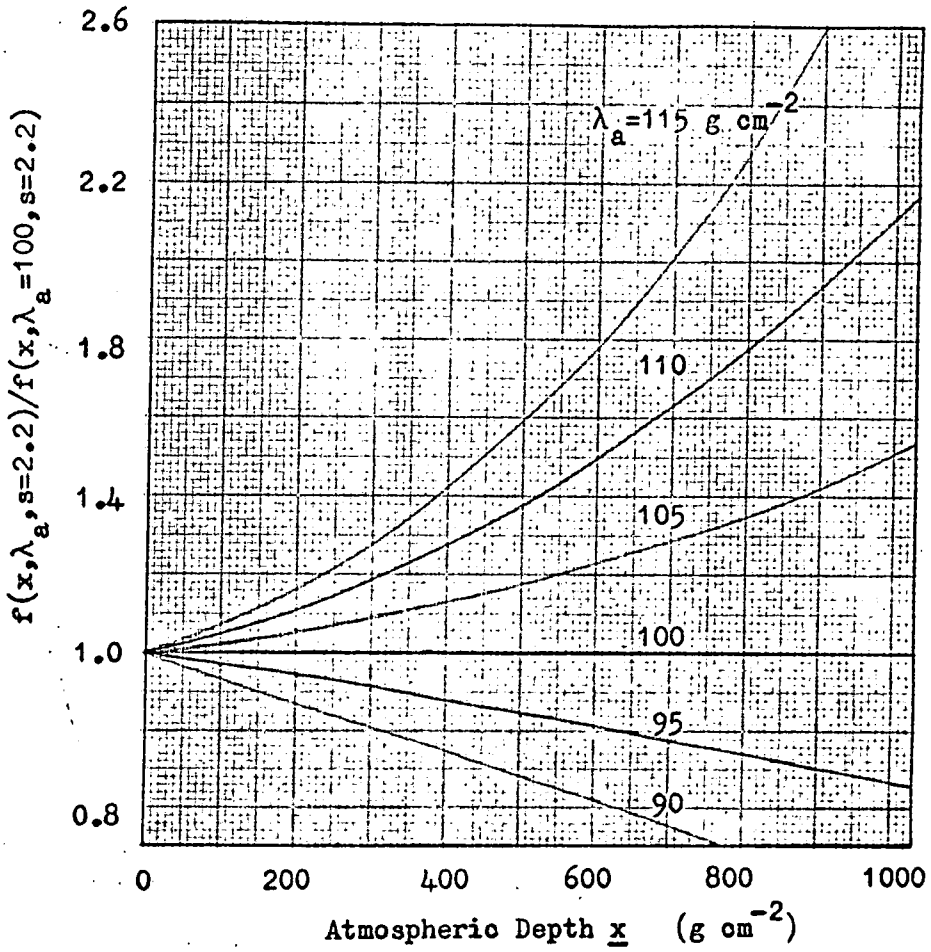

Measured intensities of electromagnetic cascades

Fig. 4.6a Energies greater than 470 GeV

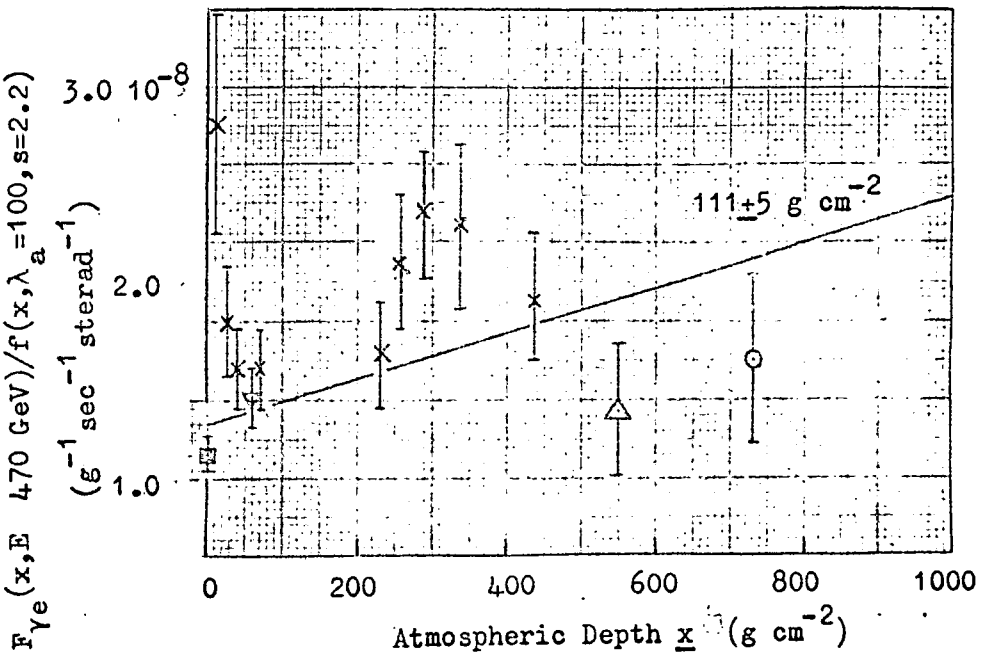

Fig. 4.6b Energies greater than 700 GeV

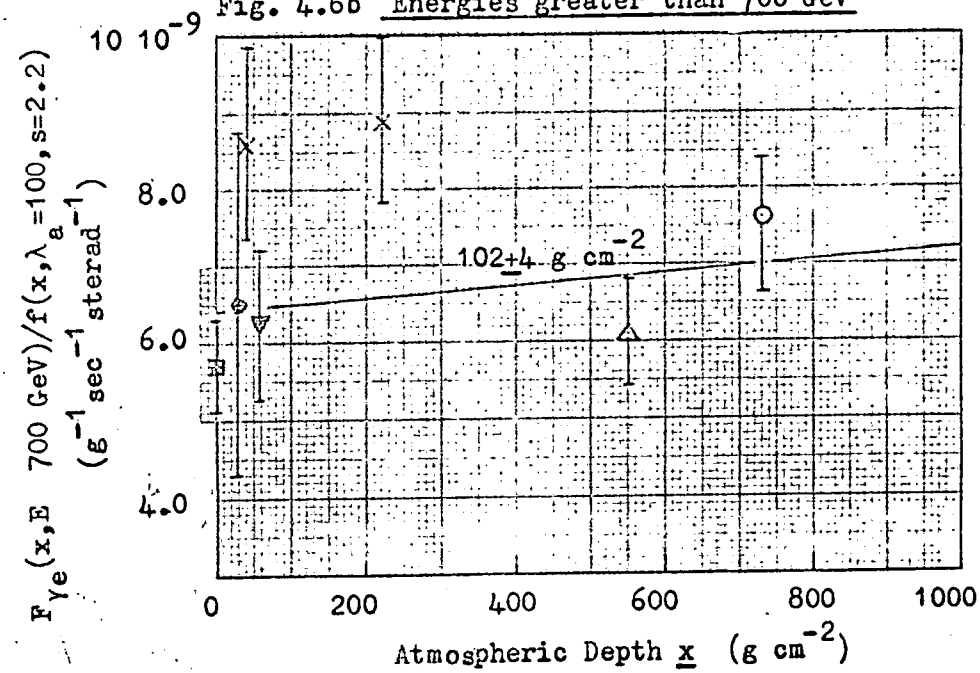

Measured intensities of electromagnetic cascades

Fig. 4.7a Energies greater than 1500 GeV

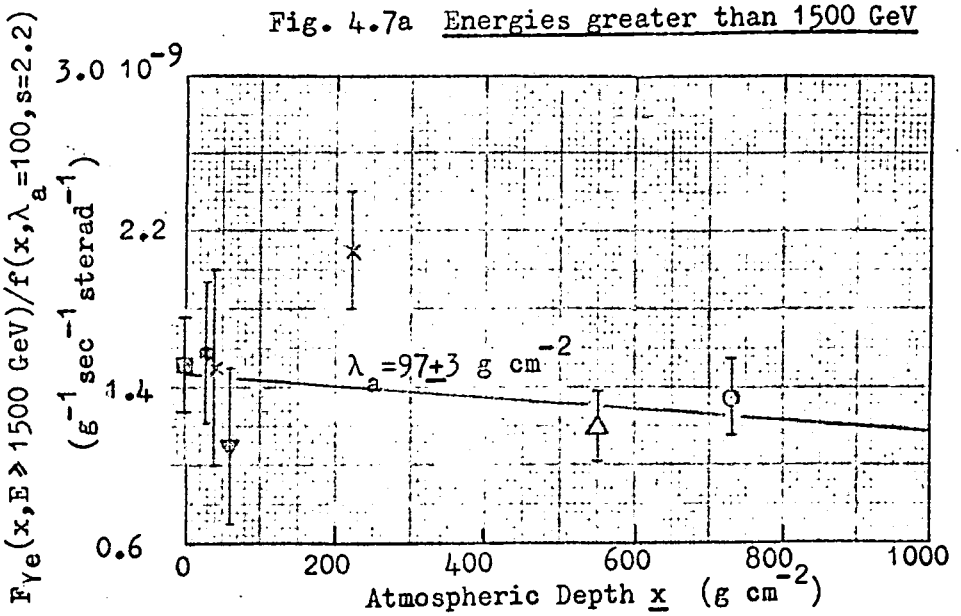

Fig. 4.7b Energies greater than 3000 GeV

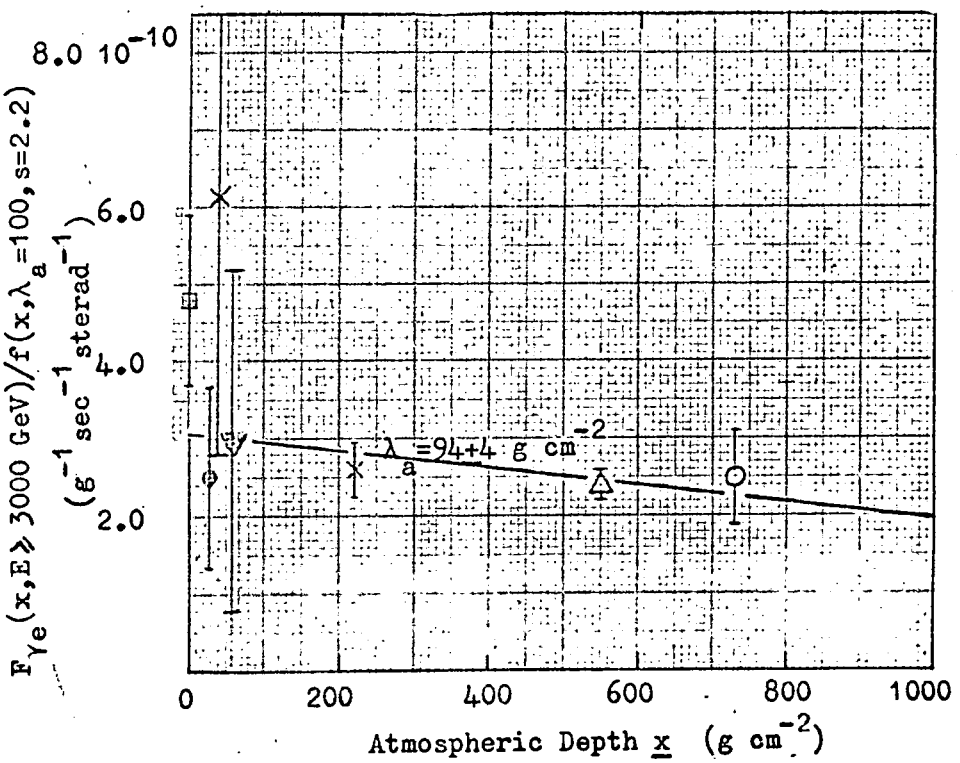

in Table 4.2. These values are from 5 to 10 g cm^{-2} greater than those obtained in the previous analysis because of the increased intensities from the mountain exposures, but they show the same apparent slow decrease of absorption length with increasing energy. It must be remembered, however, that the solution of the cascade propagation that has been used is not strictly valid if the exponents of the intensity spectra change with depth and therefore the apparent values of λ_a may not be identical with the actual absorption lengths of nuclear-active particles. In order to be consistent with our initial assumptions the weighted mean of the values of Table 4.2 is taken giving a constant value, $\lambda_a = 100 \pm 3$ g cm^{-2}. The intensity at production of initial photons of energy greater than E is given by

$$F_\gamma(>E) = \lambda_a \, N_\gamma(0,>E) \text{ cm}^{-2} \text{ sec}^{-1} \text{ sterad}^{-1} \qquad (4.3)$$

This is not sensitive to the precise value chosen for λ_a since a decrease in this parameter cause a corresponding increase in the derived mean value of $N_\gamma(0,>E)$. Using

$$F_\gamma(>E) = 100 \left\langle \frac{F_{\gamma e}(x,>E)_m}{f(x,\lambda_a=100,s=2.2)} \right\rangle \text{ cm}^{-2}\text{sec}^{-1}\text{sterad}^{-1} \qquad (4.4)$$

the production spectrum of initial photons, given in Table 4.3, is obtained. In Fig. 4.8 the depth-intensity expression $F_{\gamma e}(x,>1000)$, calculated using $\lambda_a = 100$ g cm^{-2}, $s = 2.2$ and $N_\gamma(0,>1000) = 3.53\ 10^{-9}$ $g^{-1}sec^{-1}sterad^{-1}$, is compared with the measured intensities.

4.3.3 The Predicted Muon Production Spectra

In order to derive muon spectra from the spectrum of photons using expressions similar to those given in Chapter 2 it is necessary to

Table 4.2

Energy E (GeV)	300	470	700	1000	1500	2000	3000
λ_a (g cm^{-2})	110±5	111±5	102±4	101.5±2.5	97±3	93.5±3	94±4

Table 4.3

The Production Spectrum of Initial γ-quanta

Energy, E (GeV)	$F_\gamma(E)$ (cm^{-2} sec^{-1} sterad^{-1})
300	$(2.49\pm0.25)\ 10^{-6}$
470	$(1.42\pm0.11)\ 10^{-6}$
700	$(6.63\pm0.45)\ 10^{-7}$
1000	$(3.53\pm0.16)\ 10^{-7}$
1500	$(1.42\pm0.11)\ 10^{-7}$
2000	$(6.95\pm0.51)\ 10^{-8}$
3000	$(2.51\pm0.16)\ 10^{-8}$

Fig. 4.8 Variation with depth in the atmosphere of the intensity of electomagnetic cascades ($E_{\gamma e} \geq 1000$ GeV)

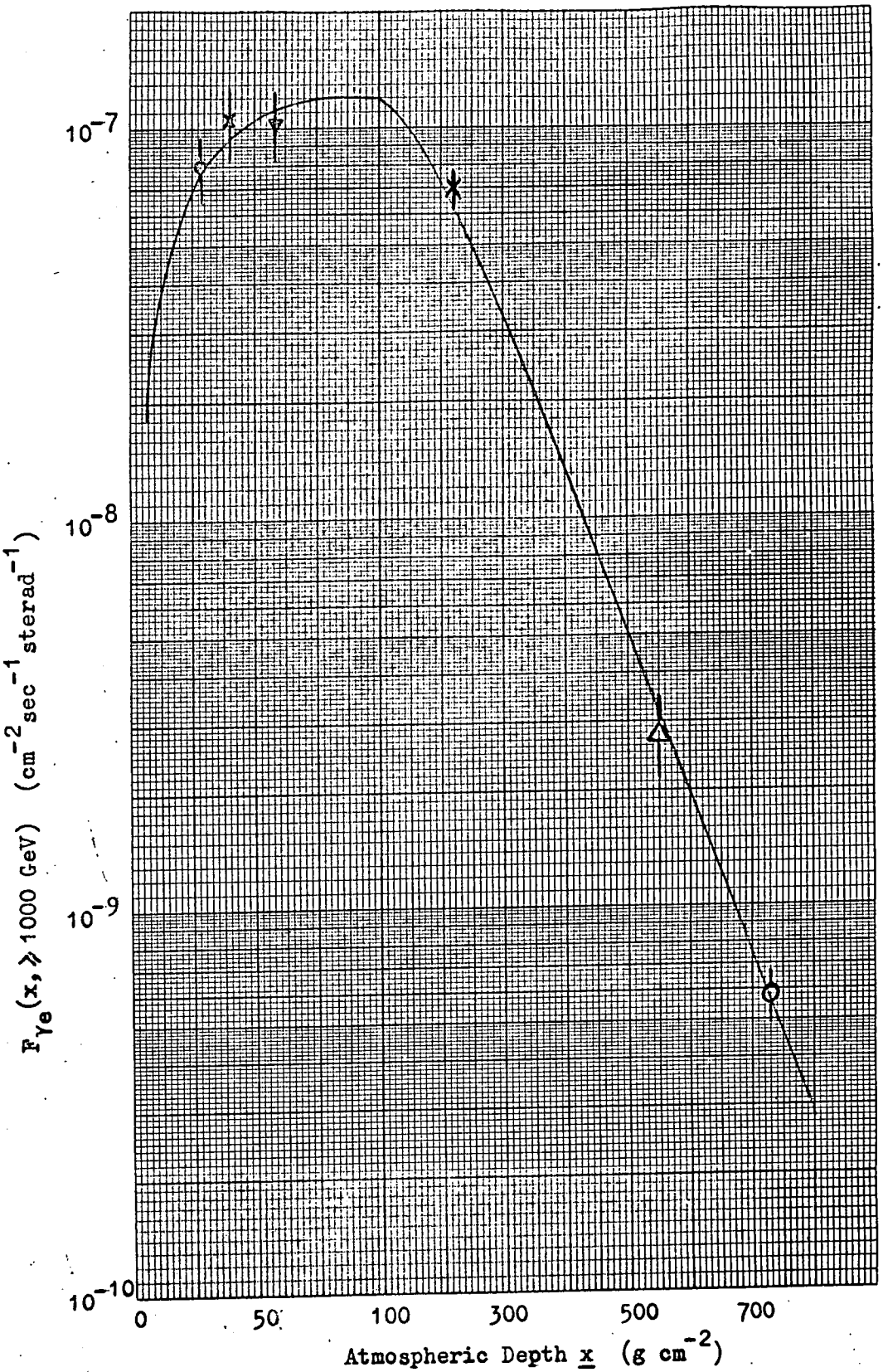

express the latter as a power law. The slope of the photon spectrum increases slowly with energy, however, and a close fit cannot be obtained. Over a limited energy range one may express a spectrum of this form as the difference of two power law spectra. The best fit to the integral photon production spectrum is then, for 300<E<3000 GeV,

$$F_\gamma(>E) = (3.20\ 10^{-2})E^{-1.6} - (1.84\ 10^{-4})E^{-1.0}\ \text{cm}^{-2}\text{sec}^{-1}\text{sterad}^{-1} \quad (4.5)$$

From the kinematics of neutral pion decay, if $F_\gamma(>E) = CE^{-(\gamma-1)}$, the differential production spectrum of neutral pions is

$$F_{\pi^o}(E) = \frac{\gamma(\gamma-1)}{2}\ CE^{-\gamma} \quad (4.6)$$

Then (4.5) gives

$$F_{\pi^o}(E) = (6.66\ 10^{-2})E^{-2.6} - (1.84\ 10^{-4})E^{-2.0}\ \text{cm}^{-2}\text{sec}^{-1}\text{sterad}^{-1}\text{GeV}^{-1} \quad (4.7)$$

For the case of all muons coming from pion decay the muon production spectrum is obtained in terms of the pion spectrum by integrating (2.15) over atmospheric depth (a constant value, $B_\pi = 118.1$ GeV, may be assumed since, at high energies, a large majority of the muons are produced at depths $x<253.3$ g cm^{-2}). Then, with charge independence in the production of pions, the muon production spectrum from pions is

$$N_\pi(E_\mu) = 4.68\ F_{\pi^o}(E_\mu)\ \left[\int_1^{1.74} s^{-(\gamma+1)}\left(1+\frac{sE_\mu}{\beta_\pi}\right)^{-1} ds\right] \quad (4.8)$$

In this case this is evaluated as the difference between two integrals for the two values of γ of (4.7). The spectrum is shown in Fig. 4.9 where the ordinate is the intensity multiplied by E_μ^2. The experimental points correspond to the measured photon intensities of Table 4.3.

If, on the other hand, only kaons are produced directly in nuclear interactions then the kaon production spectrum can be calculated from the neutral pion spectrum. Taking all kaon decay modes into account,

Fig. 4.9 Comparison of the 'OPW' spectrum with the muon spectra from electromagnetic cascade measurements

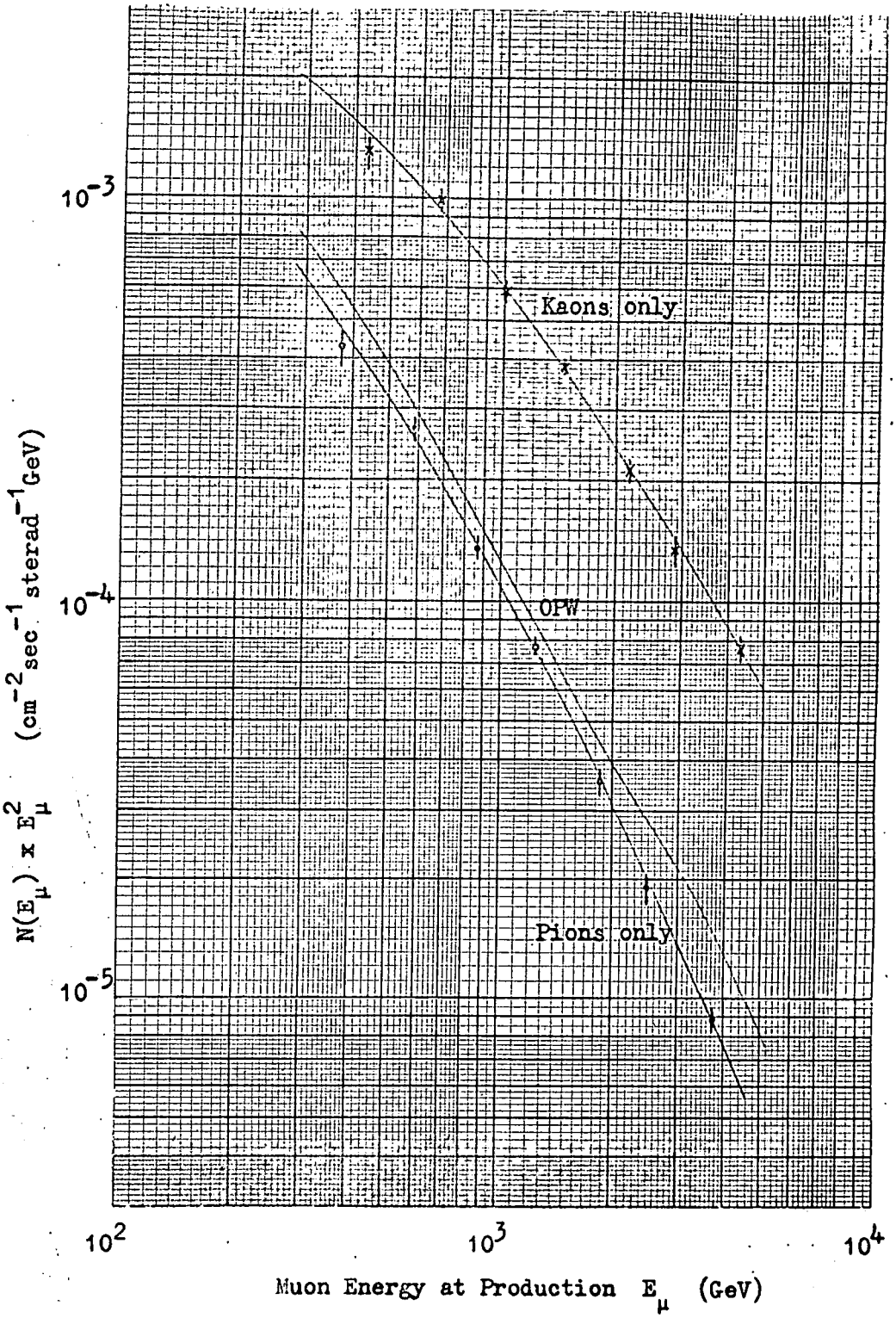

the relation between the two spectra is given by the following expression, when the kaon spectrum is of the form $F_{K^\pm}(E) = F_{K^0}(E) = KE^{-\gamma}$

$$F_{\pi^0}(E_\pi) = \left[0.155 \ \frac{2.42}{\gamma}\left(0.914^{\gamma} - 0.086^{\gamma}\right) F_{K^\pm}(E_\pi)\right](1 + R_{\pi^0}) \qquad (4.9)$$

The term in square brackets is the contribution from the dominant $K^0_{\pi 2}, \rightarrow \pi^0 + \pi^0$ decay mode and $R_\pi o$ is the fraction of this that is the contribution from the other decay modes (see Appendix C). $R_\pi o$ is a function of energy and also depends on γ. As the energy increases from 300 to 3000 GeV $R_\pi o$ decreases from about 0.8 to 0.2. From (4.9) and (4.7) the kaon production spectrum is obtained, again as the difference of two power law spectra,

$$F_{K^\pm}(E) = (6.67\ 10^{-2})E^{-2.12} - (1.72\ 10^{-3})E^{-1.96} \ \text{cm}^{-2}\text{sec}^{-1}\text{sterad}^{-1}\text{GeV}^{-1} \qquad (4.10)$$

The production spectrum of muons from kaons is of the form

$$N_K(E_\mu) = \left[0.58\ F_{K^\pm}(E_\mu)\ 1.05 \int_1^{22} s^{-(\gamma+1)}\left(1 + \frac{s E_\mu}{B_{K^\pm}}\right)^{-1} ds\right](1 + R_\mu) \qquad (4.11)$$

The term in square brackets is the contribution from the $K_{\mu 2}$ mode, derived from (2.18) with $B_{K^\pm} = 867$ GeV. R_μ is the relative contribution of the other decay modes and decreases from about 0.5 to 0.2 over the energy range considered. The spectrum obtained from (4.10) and (4.11) is shown in Fig. 4.9.

The two predicted spectra are then compared with the muon production spectrum derived from the OPW sea level spectrum; the energy loss and survival probability were allowed for, assuming all muons to be produced at the median height of 83 g cm^{-2}. The correction is small in the vertical direction at high energies, amounting to 4% at 300 GeV and becoming negligible above 2000 GeV.

4.3.4 The K/π Ratio from Electromagnetic Cascade Measurements

In Fig. 4.9 it can be seen that the observed muon intensities are greater than those predicted from electromagnetic cascade intensities if pions are the only source. Using the relations between the spectra given above the production spectra of pions and kaons were adjusted until the calculated intensities of muons and photons from both sources together were in agreement with the observed values. The ratio of kaons to pions thus obtained is given in Fig. 4.10 as a function of their energy at production. The dashed lines give the limits of error of one standard deviation resulting from the uncertainties in both the OPW spectrum and the photon intensities.

There appears to be a minimum in the K/π ratio at meson energies of about 1500 GeV but statistical errors are such that a constant value of 20% over the range of pion and kaon energies from 400 to 5000 GeV is not inconsistent with the measured data. The apparent relatively rapid increase in $\underline{R}$ below an energy at production of 600 GeV is rather suspect. From Fig. 4.9 it can be seen that this is due to the muon spectrum predicted from electromagnetic cascade measurements being less steep, at energies corresponding to photons of 300 to 500 GeV, than the OPW spectrum. This is the region just above the low energy cut off, which is imposed upon the heavy element-nuclear emulsion sandwich stack data by reduced detection efficiency. It seems possible that the detection efficiency may have been over-estimated in this region for some of the measurements resulting in an under-estimate of the photon intensity. In particular the 'Bristol-India' spectrum, which contributes

Fig. 4.10 Values of the K/π ratio from electromagnetic cascade measurements

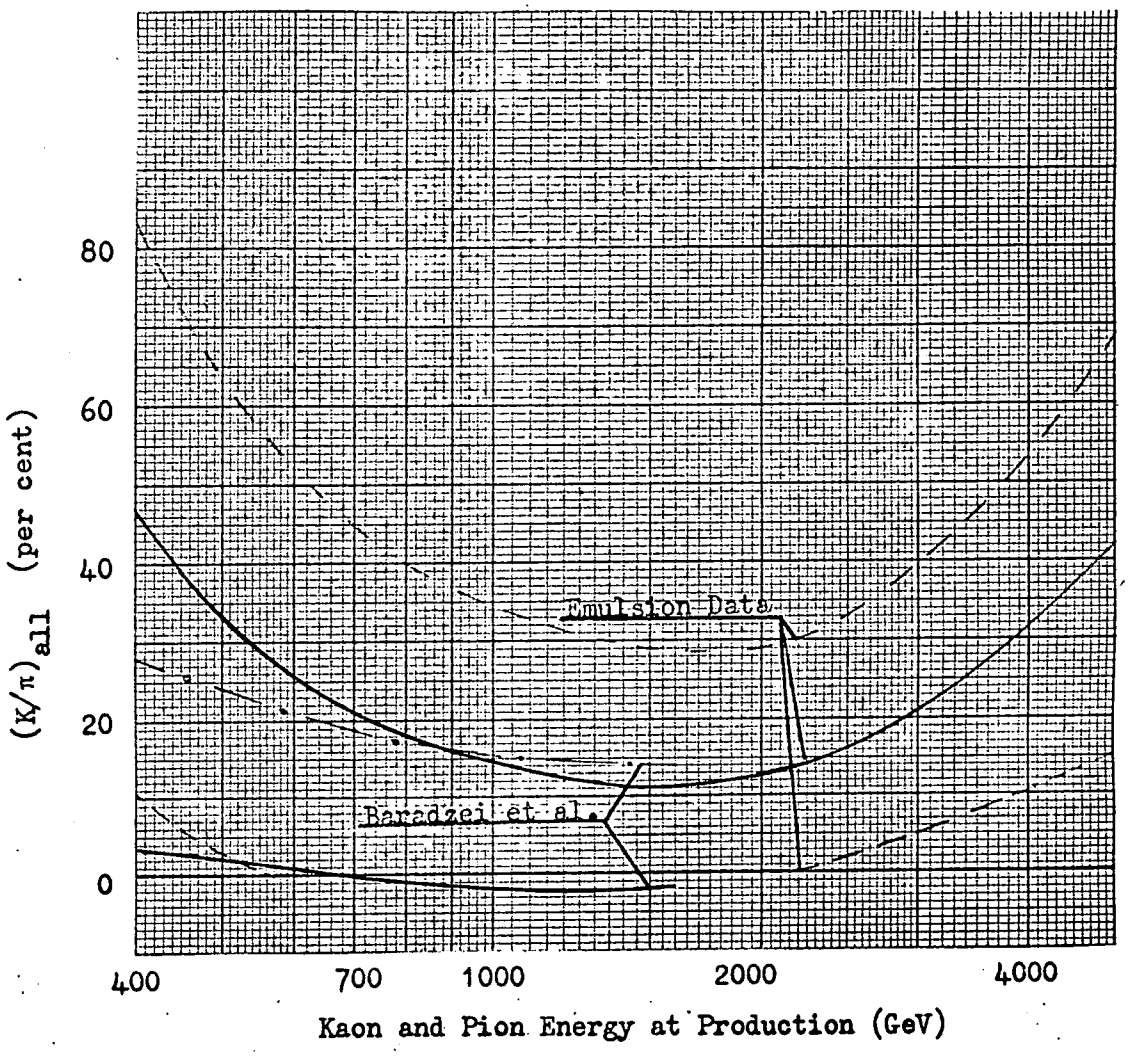

most of the weight at low energies (see Fig. 4.6a), has a significantly smaller slope than the 'Chicago' spectrum in this region (1.57 ± 0.08 compared with $1.9^{+0.3}_{-0.2}$). These measurements were made at similar atmospheric depths but the 'Chicago' results were from pure emulsion stacks in which the detection efficiency remains high to photon energies below 100 GeV.

Measurements of electromagnetic cascades have also been made by Baradzei et al. (1964) using arrays of ionisation chambers flown at atmospheric depths of 197 g cm^{-2} and 310 g cm^{-2}. From the intensities of individual photons and electrons incident on their arrays they derived the muon spectrum at sea level for pions as the only parents by a method similar to that given above. This spectrum follows the OPW spectrum very closely up to about 1500 GeV above which it becomes progressively larger. The authors point out, however, that, because of the finite resolution of their counters, it is possible for groups of relatively low energy photons to simulate single high energy photons. They calculate that, for this reason, their measured photon spectrum will be enhanced above 2000 GeV. In Fig. 4.10 the K/π ratio derived by us from these results is given up to 1500 GeV together with the upper limit of one standard deviation of their quoted statistical errors. The ionisation chamber data seems to indicate a smaller value of $\underline{R}$ than the combined emulsion data but, because of the large experimental errors, the two results are not contradictory. Unlike the emulsion measurements, where each cascade could be studied in detail, the ionisation chamber measurements did not allow those events caused by incident photons or

electrons to be distinguished from bursts produced by nuclear interactions in the array. The quoted intensities of photon-initiated bursts are the total intensities redued by approximately 25% to allow for these nuclear interactions. If this calculated reduction were too small by ~10% then the major part of the difference between the ionisation chamber and emulsion results would disappear but there would still be no rapid increase of R with decreasing energy below 600 GeV from the ionisation chamber results.

4.4 Measurement of the Polarization of Muons

The mean polarization of cosmic ray muons depends upon whether the parent mesons are kaons or pions. In the rest system of pion decay or two-body decay of kaons in the $K_{\mu 2}$ mode the muon is completely polarized along its momentum. (All the experiments that have been performed up to the present have measured the polarization of positive muons only. In two-body decays the positive muon is polarized anti-parallel to its momentum: for simplicity in the present discussion, we define this to be a positive polarization.) In the laboratory system the overall polarization will be reduced because those muons moving backwards in the rest system will be transformed to forward directions and will have polarizations of opposite sign to those moving forward in the rest system. If one considers muons of a given laboratory energy, then those that were produced by forward decays in the rest system will have come from parent mesons of lower energy than those from backward decays. The rapidly falling energy spectrum of pions and kaons favours muons from forward decays. It can be seen that the muon polarization will

depend on the parent meson spectrum and the energy available to the muon in the rest system.

4.4.1 The Calculated Muon Polarization

An expression for the polarization of muons from two-body decays has been given by Hayakawa (1957). If $\underline{E}$ and $\underline{p}$, and $\underline{E}^*$ and $\underline{p}^*$ are the energy and momentum of the muon in the laboratory system and the rest system respectively, then the polarization is

$$P = \frac{EE^*}{pp^*} - \frac{\epsilon m_\mu^2}{pp^*} \qquad (4.12)$$

where ϵ is the parent meson energy in terms of its rest mass, Mc^2. Now for all muon energies that we shall consider $v = p/E$ can be taken as unity and $v^* = p^*/E^* = (M^2 - m_\mu^2)/(M^2 + m_\mu^2)$ has values 0.272 and 0.921 for pions and $K_{\mu 2}$ respectively. If the differential production spectrum of parent mesons is a power law of exponent γ the mean polarization averaged over this spectrum is (c.f. equation (4.8))

$$\overline{P} = \frac{\int_1^r s^{-(\gamma+1)}\left(1+\frac{sE_\mu}{B}\right)^{-1}\left[\frac{1}{v^*} - \frac{m_\mu^2}{p^* M}s\right]ds}{\int_1^r s^{-(\gamma+1)}\left(1+\frac{sE_\mu}{B}\right)^{-1}ds} \qquad (4.13)$$

Where, as before, for pions and $K_{\mu 2}$ respectively, $r = (1+v^*)/(1-v^*)$ has values of 1.74 and 21.82 and B = 118.1 GeV and 867 GeV. For $E_\mu \lesssim 10$ GeV, which is the energy range covered by the experimental results, the probability of absorption rather than decay of the parent mesons is negligible and the factor $(1 + SE_\mu/B) \to 1$. In this case (4.13) becomes

$$\overline{P} = \frac{1}{v^*} - \left(\frac{1}{v^*} - 1\right)\frac{\gamma(r^\gamma - r)}{\gamma - 1(r^\gamma - 1)} \qquad (4.14)$$

(N.B. in the original paper, Hayakawa (1957), there is a mistake in the

derivation of this formula which has been pointed out by later authors). Therefore, if the meson spectrum has a constant exponent the muon polarization will be independent of energy and height of production in the atmosphere.

If all muons come from pion decay then, data from magnetic spectrograph measurements of the vertical muon spectrum indicate that the pion production spectrum has a constant exponent, $\gamma = 2.65$ from 5 GeV/c to beyond 20 GeV/c. Substituting this value in (4.14) the mean polarization of muons from pions is found to be 0.327. Thus the predicted polarization will be constant at this value down to a muon momentum at sea level of 2 GeV/c which corresponds to the 5 GeV/c pion production momentum (see Fig. 3.1). Below 5 GeV/c the slope of the pion spectrum becomes smaller. Since muons of a given momentum at sea level are produced by pions whose momentum is a function of the altitude at which the muon is produced, the calculation of the expected polarization in this momentum region requires detailed knowledge of the behaviour of the pion production spectrum and the altitude dependence of the rate of production of muons at low momenta. Although the muon polarization has been predicted by Berezinskii and Dolgoshein (1962) down to 100 MeV/c using the pion production spectrum of Olbert (1954) and the calculations of muon production versus altitude of Sands (1950), we do not consider that, at very low momenta, these quantities are well enough established for the polarization to be calculated with sufficient accuracy to allow a quantitative comparison with measured values below 1 GeV/c. The calculated polarization of muons from pion decay is shown in Fig. 4.11 down to 1 GeV/c.

Before the polarization of muons from kaons can be calculated it is necessary to know the form of the kaon production spectrum, which depends on the variation of the K/π ratio with energy. The procedure adopted here is to take the simplest case, in which the ratio is assumed to be constant and then to ascertain whether any change in the ratio with energy is indicated by a comparison between the predicted polarization and the measured values. Because the production spectrum of kaons then has the same shape as that of pions and since muons having sea level momentum of 1 GeV/c come from kaons of mean momentum 5.4 GeV/c or greater, depending on the mode of decay, the slope of the spectrum is constant at $\gamma = 2.65$ over the relevant momentum range. The production spectra of charged and neutral kaons are taken to be identical, $F_{K^{\pm}}(E) = F_{K^o,\bar{K}^o}(E) = AE^{-2.65}$, and all decay modes are considered. The muons may be divided into three groups. Those from $K_{\mu 2}$ decay, when the appropriate values of $\underline{v}^*$ and $\underline{r}$ are substituted in (4.14), have a mean polarization of 0.943. From (2.24) it can be seen that at low momenta the production spectrum of pions from kaon decay has the same slope as the kaon spectrum, so that muons produced in two-stage kaon decays have polarization 0.327. Muons from $K^{\pm}_{\mu 3}$ and $K^{o}_{\mu 3}$ have a range of energies in the kaon rest system and varying polarizations correlated to these energies. These have been calculated by Brene et al. (1961) for various values of a parameter ξ (see Appendix C.3). In the previous analysis the mean polarization, averaged over the production spectrum of kaons was calculated to be 0.273, assuming $\xi = 1$. A recent accelerator experiment on the polarization of muons from $K_{\mu 3}$ (Borreanni et al. (1965)) confirms that ξ lies between 0 and 1. For

$\xi = 0$ the mean polarization would be a few per cent greater than for $\xi = 1$. The polarization of positive muons from $K_{\mu 3}$ is of opposite sign to that of muons from the two-body decays.

The relative numbers of positive muons of a given energy are given in Table 4.4: the spectra are expressed as fractions of the kaon production spectrum. If we define $r_K = F_{K^+}(E)/F_{K^\pm}(E)$ then the overall polarization of positive muons from kaons is

$$\bar{P}_K = (0.039 + 0.238 r_K)/(0.148 + 0.311 r_K) \qquad (4.15)$$

The value of r_K is not known precisely. If all muons did come from kaon decay only then $r_K = 0.6$ would give agreement with the observed positive to negative ratio of muons of 1.23. The predicted polarization then is 0.542; this is shown in Fig. 4.11. On the other hand if only a small fraction of muons came from kaons r_K could be larger without contradicting the observed muon charge ratio. At lower, machine, energies the observed value of r_K is ~ 0.8 and one would expect the value to fall rather than rise with increasing energy. Therefore $r_K = 0.8$ is taken as an upper limit and the measured data is interpreted below for both values or r_K.

4.4.2 Summary of the Experimental Data

All measurements of the polarization of cosmic ray muons that have been made up to the present time have involved stopping the particles in a copper, brass or aluminium absorber and examining the angular distribution of the positrons produced in their decay. In some cases a multiplate cloud chamber was used while in the others the positrons

Table 4.4

The Production Spectra and Polarizations of Muons from Kaons

Decay Mode	Production Spectrum of Muons $\pm F_{K^\pm}(E)$	Production Spectrum of Positive Muons $\pm F_{K^\pm}(E)$	Polarization
$K^\pm_{\mu 2}$	0.229	$0.299 r_K$	0.943
$K^\pm_{\pi 2}$	0.064	$0.064 r_K$	0.327
$K^\pm_{\pi 3}$	0.021	$0.007(r_K+1)$	0.327
$K^\pm_{\pi 3'}$	0.002	$0.002 r_K$	0.327
$K^\pm_{\mu 3}$	0.008	$0.008 r_K$	-0.273
$K^o_{\pi 2}$	0.168	0.084	0.327
$K^o_{\pi 3}$	0.015	0.008	0.327
$K^o_{\mu 3}$(*)	0.033	0.017	-0.273
$(K^o_{e3}+K^o_{\mu 3})$(**)	0.066	0.033	0.327

(*) Directly produced muons only

(**) Includes muons from $K^o_{\mu 3}$ via two-stage decay only

were recorded electronically by a delayed coincidence technique. The positive muons are automatically separated from the negative muons by this method because the latter are absorbed by copper nuclei within $\sim 10^{-7}$ sec. The sea level momentum of the muons stopping in the absorber could be altered by placing a variable thickness of 'moderator' over the apparatus, by siting the instrument underground. The measurements thus cover a range of sea level momenta from 0.113 GeV/c to 8.7 GeV/c. Those above 1.0 GeV/c are listed in Table 4.5 and plotted in Fig. 4.11. The results of three experiments by Soviet workers reported by Asatiani et al. (1964) were not included in the previous analysis. The predicted polarizations obtained in the previous section refer to the value at production: depolarization in the air and moderator has to be taken into account. Hayakawa (1957) has calculated the fractional depolarization due to multiple Coulomb scattering to be $\delta = 4.4\ x/p_o X_o$, where x is the thickness of air and moderator in g cm^{-2} and p_o is the momentum of the muon at production in MeV/c. At the momenta under consideration the range, x, is very nearly proportional to p_o and δ is practically constant at 5%. Where it had not already been done by the authors the measured polarizations have been corrected by this amount. Corrections to the measured values due to depolarization of the muon after stopping and Coulomb scattering of the positron, in the absorber, and decay of negative muons have been discussed by the various authors and are generally considered to be negligible. Instrumental assymetries could have an important effect on the measured polarization; in the 'delayed coincidence' experiments this was combated by regularly exchanging upper and lower

Fig. 4.11 Measured and predicted values of muon polarization

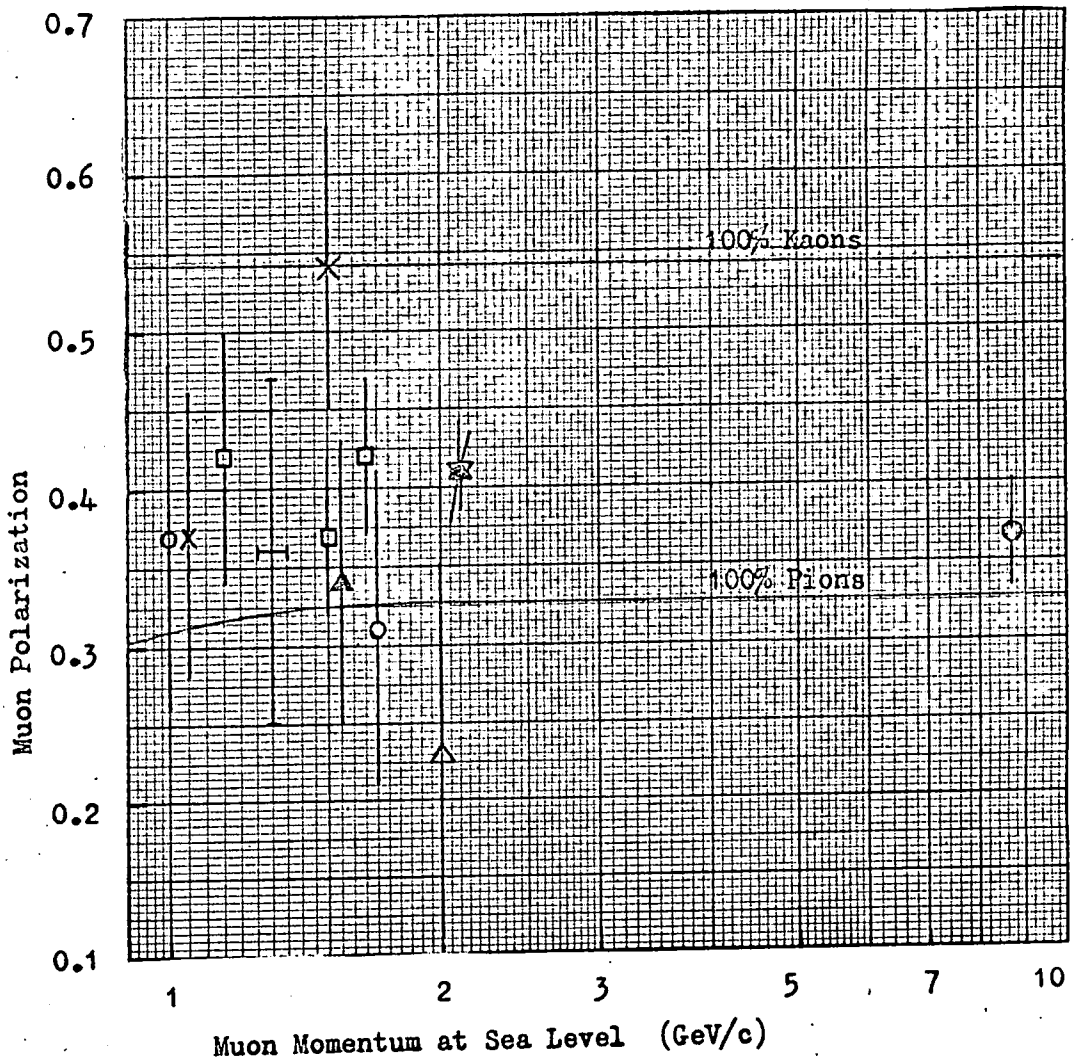

Table 4.5

Measurements of Muon Polarization

Muon Sea Level Momentum (GeV/c)	Muon Polarization at Production	Reference	Key to Fig. 4.11
1.00	0.37 ± 0.11	Barmin et al. (1960)	o
1.05	0.37 ± 0.09	Alikhanyan (1959)	x
1.15	0.42 ± 0.08	Dolgoshein et al. (1962)	□
1.3 - 1.4	0.36 ± 0.11	Sen Gupta and Sinha (1962)	┼
1.50	$(kP=0.23 \pm 0.03)^{*}$	Bradt and Clark (1963)	●
1.50	0.37 ± 0.05	Dolgoshein et al. (1962)	□
1.50	0.54 ± 0.09	Alikhanyan (1959)	x
1.55	0.34 ± 0.09	Asatiani et al. (1964)	▲
1.65	0.42 ± 0.05	Dolgoshein et al. (1962)	□
1.70	0.31 ± 0.10	Barmin et al. (1960)	o
2.0	0.23 ± 0.12	Kocharyan et al. (1960)	△
2.1	0.41 ± 0.033	Asatiani et al. (1964)	▲
2.1	0.41 ± 0.025	Asatiani et al. (1964)	▽
8.7	$(kP=0.21 \pm 0.02)^{*}$	Bradt and Clark (1963)	●

*See text

detectors or by measuring the up-down ratios with a depolarizing magnetic field applied to the absorber. Bradt and Clark (1963) do not attempt to estimate the absolute polarization, however, but investigate its change with sea level momentum. Their results are given as $\underline{k}P$, where $\underline{k}$ is a constant that contains the unevaluated systematic errors. If their result at 1.50 GeV/c is normalised to the mean of the other measurements then the absolute value at 8.7 GeV/c is 0.367 ± 0.035. It can be seen from Fig. 4.11 that there is a wide spread in the measured values of polarization at comparable momenta. Although, because of the large statistical errors, no two sets of results are definitely contradictory, it seems likely that there are systematic errors in some of the measurements that have not been accounted for. The fact that all except two of the points lie above the line for pions only suggests strongly, however, that there must be at least a small admixture of kaons among the muon parents. For each point the K/π ratio was determined for $r_K = 0.6$ and 0.8, using the expression

$$\frac{K^{\pm o}}{\pi^{\pm o}} = \frac{4}{3} \frac{0.68 r_\pi}{(0.148 + 0.311 r_K)} \left(\frac{P_m - P_\pi}{P_K - P_m}\right) \qquad (4.16)$$

P_m, P_K, and P_π are the measured and predicted polarizations respectively; the production spectrum of positive muons from pions is $0.68 r_\pi F_{\pi^\pm}(E)$. r_π, the fraction of charged pions that are positive, is assumed to have the value 0.552, to agree with the observed positive excess of muons. The twelve values between 1.0 and 2.1 GeV/c were then divided into three groups according to momentum and the mean values were calculated. (Because of possible systematic errors the individual values were not

Fig. 4.12 Values of the K/π ratio from polarization measurements

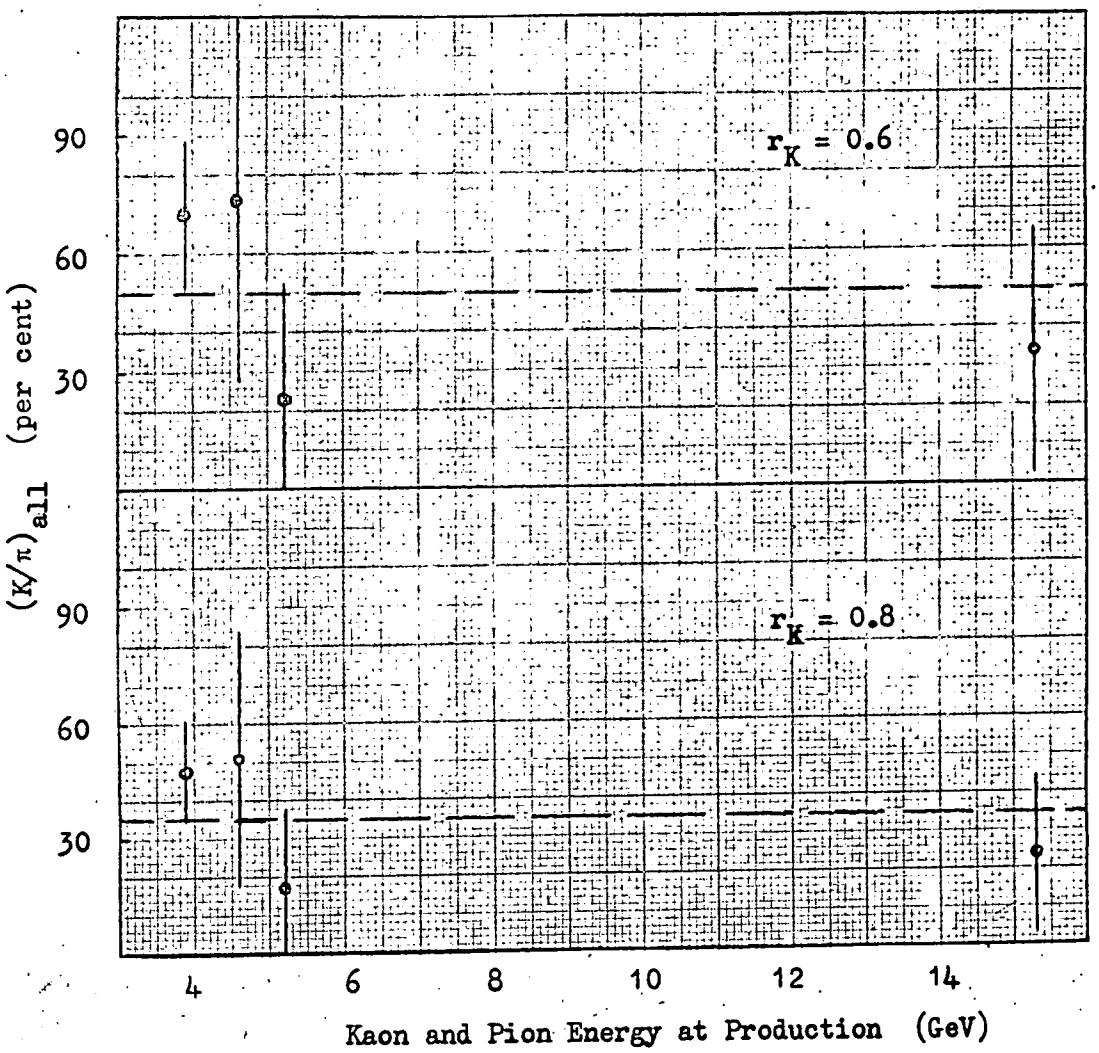

weighted according to the quoted statistical errors). These points, together with that from the measurement at 8.7 GeV/c are plotted in Fig. 4.12 as a function of the corresponding kaon and pion energies, for the two values of r_K. The large statistical errors make it impossible to draw detailed conclusions about the behaviour of the K/π ratio, R. An increase of R over the meson energy range 4 GeV to 16 GeV can be ruled out with reasonable confidence. If a constant ratio is assumed then the values are $(50 \pm 15)\%$ and $(35 \pm 10)\%$ for $r_K = 0.6$ and 0.8 respectively. A decrease of R by a factor of two between 4 GeV and 16 GeV would, however, be in accord with the data. As stated above, this would alter the predicted polarization of muons from kaons and thus the absolute values of the ratio obtained from (4.16). For example, if the slope of the kaon spectrum were assumed to be $\gamma = 3.15$ to account for this factor of two, the predicted kaon polarization would be increased such that R would be reduced to $\sim 91\%$ of the values given in Fig. 4.11.

4.5 Conclusions concerning the K/π Ratio

The three methods of examining the K/π ratio may be combined to give an overall estimate over a range of meson energies from 3 GeV to 5000 GeV. This is shown in Fig. 4.13, where limits are plotted corresponding to one standard deviation on the measured data. Because of the reservations stated above concerning the behaviour of the photon production spectrum at the low energy end, obtained from the nuclear emulsion measurements, the measured value is taken as the upper limit at 400 GeV It is seen that the results for all three methods can give with certainty only an upper limit to the ratio, although the polarization results at

Fig. 4.13 Combined values of the ratio of Kaon and Pion production spectra

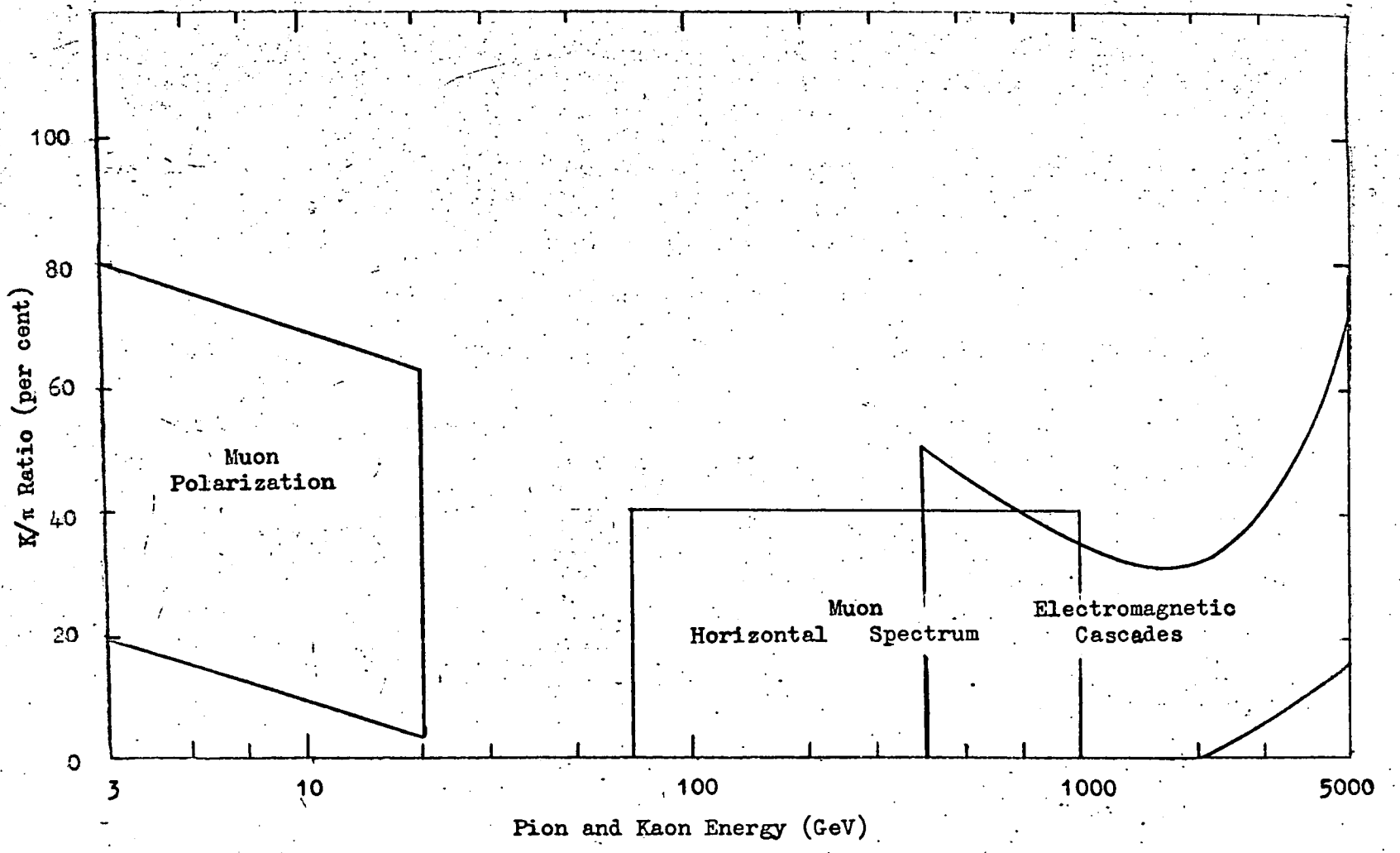

the very lowest energies strongly indicate a finite number of kaons. If the ratio is assumed to be independent of energy then a value of 20% would fit the measured data best, but the error on this value approaches $\pm$ 20%.

Any substantial improvement in the determination of the ratio is probably limited to the horizontal spectrum results. The Durham horizontal spectrograph has already been enlarged, increasing its m.d.m. to ~ 1950 GeV/c (MacKeown (1965)), thus allowing the determination of the muon intensity in the region close to 1000 GeV/c where it is most sensitive to the K/π ratio. Further measurements by the Bristol group should improve our knowledge of the photon production spectrum in the region of 400 GeV. Measurements incidental to the two neutrino experiments described in Chapter 7 will give greater accuracy to the data on the variation of muon intensity with depth and thus lead to a more accurate value of the muon sea level spectrum at high energies. This should indicate whether the apparent increase in the K/π ratio above 2000 GeV is real. It must be noted, however, that there are systematic errors in the determination of the energy of cascades in nuclear emulsions that may amount to 10%. This means that there is an inherent uncertainty in the absolute intensities of the photons, and hence in the K/π ratio, that cannot be much smaller than that represented by the present statistical limits. As pointed out be Asatiani et al. (1964) the measurements of the muon polarization could be improved by calibrating the apparatus in a beam of muons of known polarization from an accelerator. This method of removing systematic errors has not been used up to the present time. However, even if the

polarization were known exactly, there would still be uncertainties in the interpretation due to the largely unknown charge ratio of kaons and the lack of knowledge of the exact shape of the kaon spectrum.

The results given in Fig. 4.13 refer to the ratio of the production spectra of kaons and pions averaged over all interactions of the primary particles. This is the same as the ratio of kaons and pions produced in individual nuclear interactions only if the effective mean energies of the two types of mesons from the interactions are the same. The indirect results given above are compared with the direct results from the study of the individual interactions in the final Chapter.

High Energy Neutrino Interactions

From the study of muons arising from the products of the interactions of cosmic ray primaries we now turn to particles produced in conjunction with the muons or in their decay: high energy neutrinos. In this Chapter a summary is given of the present state of knowledge on high energy neutrino interactions from accelerator measurements and the possible modes of behaviour, at higher energies, predicted by various theories. The predicted rates of interactions deep underground may then be calculated and compared with the preliminary measurements. With the present type of detector of cosmic ray neutrinos only those interactions in which a muon of kinetic energy $\gtrsim 100$ MeV is produced will be registered. These may be conveniently divided into four groups: elastic and inelastic interactions, the production of the hypothetical Intermediate Boson in the Coulomb field of a nucleus, and resonance interactions.

5.1 Elastic Interactions

The interaction between a neutrino and a nucleon in which the charge of the lepton changes but no additional hadrons are produced is termed an 'elastic interaction'. For the case of incident muon-neutrinos we have

$$\nu_\mu + n \rightarrow \mu^- + p \qquad (5.1) \qquad \text{and} \qquad \bar{\nu}_\mu + p \rightarrow \mu^+ + n \qquad (5.2)$$

The cross-sections for these interactions have been calculated by Yamaguchi (1961). Below 1 GeV the total cross-sections increase approximately linearly with energy, that of (5.1) being about three times that of (5.2). Near to 1 GeV the effects of strong interactions in restricting the four-momentum transfer to the nucleon limit this increase. This effect manifests itself as four form-factors in the expression for the differential cross-

section. The Conserved Vector Current hypothesis predicts that, of these, the two vector form-factors are identical to the Hofstadter electromagnetic form-factor for electron-proton scattering, viz. $(1 + q^2/0.8\ m_p^2)^{-2}$, where q^2 is the four-momentum transfer. The form of the two axial-vector form-factors is not known but it is, arbitrarily, taken to be identical to the electromagnetic one. Under this assumption, the total cross-sections for both (5.1) and (5.2) tend at high energies to a constant value of $0.75\ 10^{-38}\ cm^2$, the former from above and the latter from below.

The variation with q^2 of the differential cross-section for elastic interactions has been measured in the CERN heavy liquid bubble chamber (Block et al. (1964)) confirming that, for this interaction, the vector and axial-vector form-factors are similar. The present neutrino telescopes do not differentiate between positive and negative muons, and since $Z/A = 0.5$ for the surrounding rock one may take the mean of the cross-sections for (5.1) and (5.2) giving a constant value of $0.75\ 10^{-38}\ cm^2\ (n\text{-}p\ pair)^{-1}$ down to 1 GeV. Because of the restriction on the momentum transfer the muon may be assumed to retain effectively the whole of the neutrino energy. This cross-section was derived under the assumption that the Intermediate Boson has infinite mass. To take account of a boson of mass m_W the form-factors would be multiplied by an additional factor $(1 + q^2/m_W^2)^{-1}$. With the present lower limit to m_W this would have only a marginal effect on the cross-section.

5.2 Inelastic Interactions

Under this heading are considered all interactions in which one or more hadrons are generated excluding those in which a real Intermediate Boson is produced. The processes may be very diverse; Paty (1965) gives a summary of

the many theoretical works on the subject. At energies available to machine experiments an important mechanism seems to be the production of a single pion via the 1236 MeV $(\frac{3}{2}, \frac{3}{2})$ isobar

$$\nu_\mu + N \rightarrow \mu^- + N^* \rightarrow \mu^- + N + \pi \qquad (5.3)$$

Berman and Veltman (1965) have calculated the total cross-section for this interaction and have found that it behaves similarly to the elastic cross-section if the same form-factors are assumed, but saturates at a higher value. This is in agreement with the bubble chamber results for single pion production. The number of channels through which the inelastic interaction can occur increases with neutrino energy. For each channel the asymptotic form of the cross-section depends on the generally unknown behaviour of the relevant form-factors at large momentum transfers. (Cabibbo and Chilton (1965) show that for $f(q^2)$ tending to K, K/q^2 and K/q^4 the asymptotic cross-section is proportional to E^2, lnE and constant respectively). Since with the present detector it is not possible to differentiate between the channels through which the inelastic interaction occurs, only the total inelastic cross-section for all channels is of interest. If we take arbitrary forms for the variation of cross-section with energy, with the restriction that they shall agree with the machine results at low energies then the predicted and observed rates of events underground may be compared. The inelastic cross-section has been obtained experimentally in the HLBC from 1 to 10 GeV but at the high energy end the statistics are very poor and there is some uncertainty in the neutrino flux. It seems that an approximately linear increase with energy is indicated, and, under this assumption, a least squares fit to the data gives $\sigma_{inel} = 0.45\ 10^{-38}\ E_\nu\ cm^2\ nucleon^{-1}$. If, however, a quadratic increase is fitted to the data then $\sigma_{inel} = 0.19\ 10^{-38}\ E_\nu^2\ cm^2 nucleon^{-1}$.

In Chapter 7 the predicted rates of events are given for these cross-sections with various cut off energies above which the cross-section is assumed to become constant. For the energy region where the cross-section is steadily increasing we assume that the muon retains half of the neutrino energy. In the region where the cross-section is constant due to the restriction on the momentum transfer the muon is assumed to retain effectively the whole of the neutrino energy. Lee (1961), using the fact that the total inelastic cross-section is expected to be proportional to $\langle q^2 \rangle$, the average of the square of the four-momentum transfer, has predicted its form by assuming that, at very high energies, the behaviour of the multiplicity and transverse momentum distribution of the secondaries from inelastic interactions is similar to that in nucleon-nucleon collisions. Then the dependence of the cross-section on neutrino energy is the same as the dependence of the multiplicity on nucleon energy, i.e. $\sigma_{inel} \propto E_\nu^\beta$ where $0.25 \lesssim \beta \lesssim 0.5$. This type of behaviour is, however, obviously not the case in the energy region in which machine results have been obtained.

5.3 Production of the Intermediate Boson

If the Intermediate Vector Boson, $W^\pm$, exists then it will be produced in the interaction $\nu_\mu\ (\bar{\nu}_\mu) \rightarrow \mu^\mp + W^\pm$. Conservation of energy and momentum prevent this interaction from occurring in a vacuum but the virtual muon and boson can be made real if they are scattered in the Coulomb field of a nucleus. The minimum momentum transfer to the nucleus (neglecting the mass of the muon) is $m_W^2/2E_\nu$; thus the momentum transfer, necessary to conserve momentum in the above interaction, becomes smaller for higher neutrino energies. If the momentum transfer is so large that the impact parameter approaches the nuclear radius then the scattering most probably occurs on a

single nucleon; this is termed an "incoherent" interaction. For lower momentum transfers, corresponding to peripheral collisions, the nucleus recoils as a whole; a "coherent" interaction. The critical energy for which the impact parameter is approximately equal to the nuclear radius is $E_\nu \sim 2.5\ A^{\frac{1}{3}}\ m_W^2$ GeV. Below this energy the incoherent interaction will predominate, while above it the coherent interaction becomes more important.

5.3.1 Cross-sections for $W^\pm$ Production

There have been a number of calculations of both the coherent and incoherent cross-sections for W production. Numerical methods have been used in deriving the cross-section up to 20 GeV for use in interpreting the accelerator results. The shape of the cross-section is such that when it is folded into the cosmic ray neutrino spectrum the contribution to the total interaction rate is significant up to energies beyond 1000 GeV. In this high energy region analytical expressions for the asymptotic behaviour of the total cross-section have been obtained.

Von Gehlen (1963) gives the threshold energy for incoherent interactions as $E_{th} = 0.75\ m_W\ (1 + m_W/2m_p)$ GeV; the factor 0.75 represents the lowering of the threshold due to the Fermi motion of the nucleons in the nucleus. Wu et al. (1964) have calculated the separate contributions of neutrons and protons to the incoherent cross-section from threshold to 10 GeV for m_W up to 1.5 GeV. They find that the neutron contribution, neglected in previous calculations, amounts to $\sim 30\%$ of that of the proton. They also take into account the effect of the Pauli exclusion principle. This restricts small momentum transfers to nucleons and the fractional reduction of cross-section due to it therefore increases with E_ν. Further values of the total cross-sections for E_ν up to 20 GeV and for m_W up to 2.5 GeV, obtained by these authors, are quoted by Burns et al. (1965). Crouch et al. (1965) have used

Wu's program to obtain values of the incoherent cross-section for m_W = 3.0 GeV and E_ν = 15, 38 and 100 GeV. These results taken together allow the estimation of the cross-section up to 100 GeV for m_W ranging from 1.8 to 3.0 GeV. Above 100 GeV the incoherent cross-section is only a small fraction of the total. The results are for aluminium (Z = 13, A = 27) but this is very similar to KGF rock ($\bar{Z}$ = 12.9, $\bar{A}$ = 26.3).

Values of the coherent cross-section are also given by Wu et al. (1964) up to 10 GeV and are compared with previous calculations. At these low energies the momentum transfer to the nucleus is large and the coherent cross-section is very sensitive to the little known form of the tail of the nuclear form-factor. However the contribution of the coherent interaction is only a small fraction of that of the incoherent interaction in this energy region. For high energy neutrinos an asymptotic expression for the coherent cross-section has been given by von Gehlen (1963) which is expected to be valid for $E_\nu \gtrsim 25\ m_W^2$. It can be expressed in the form of a series in $\alpha = 2\sqrt{12}\ E_\nu/m_W^2 R$ ($\underline{R}$ being the nuclear radius), the first term of which is identical to the well-known asymptotic expression of Lee et al. (1961)

$$\sigma_{coh} = \left(\frac{Z}{137}\right)^2 \frac{g^2}{6\pi m_W^2} (\ln\alpha)^3 \qquad (5.4)$$

where $\sqrt{2}\ g^2/m_W^2 = 2.26\ 10^{-19}$ cm GeV^{-1} is the vector coupling constant of muon decay. At 1000 GeV for m_W = 2 GeV (5.4) represents only 30% of the whole expression. Using a value of the coherent cross-section at 100 GeV for m_W = 3.0 GeV evaluated by Crouch et al. (1965) as a check, it is not difficult to interpolate between the 20 GeV upper limit of the numerical calculations and the 100 GeV lower limit to the validity of the asymptotic formula, and thus to obtain values for the coherent cross-sections over a

wide range of energies. The total cross-section are plotted in Fig. 5.1 for a range of values of m_W from 1.8 to 3.0 GeV, which are of present interest, together with the value for m_W = 1.2 GeV for comparison. The dashed line (A - B) intersects each curve at the energy at which the incoherent and coherent cross-sections are equal. It should be noted that these cross-sections are for the case where the anomalous magnetic moment of the boson, k, is equal to zero. This is usually implicitly assumed when experimental limits to the boson mass are quoted. Cross-sections have been calculated for $k = \pm 1$ also: for $k = +1$ the cross-section is enhanced by about 30% while for $k = -1$ it is reduced by about 20%.

Each muon-neutrino interaction in which an Intermediate Boson is produced will lead to the generation of one or two muons; we shall label the muon produced together with the boson as the 'prompt' muon. If the boson then decays in the $W \rightarrow \mu + \nu_\mu$ mode a second muon, the 'decay' muon, is also produced. Because of the relation between muon energy and the effective target thickness of rock the expected rate of detection of muons for a given value of m_W is approximately proportional to $(\bar{r}_p + b\,\bar{r}_d)$; where $\bar{r}_p$ and $\bar{r}_d$ are the mean fractions of the neutrino energy retained by the 'prompt' and 'decay' muons respectively. b is the branching ratio for muonic decay of the boson. The possible values of these parameters are discussed below.

5.3.2 The Energy of the 'Prompt' Muon

Of all the possible momentum configurations when a W is produced in the Coulomb field of the nucleus, that involving a minimum momentum transfer to the nucleus is the most likely. In this case the boson and the muon emerge in the same direction with their total energy divided between them in proportion to their mass. Thus the most probable value of r_p is $m_\mu/(m_W + m_\mu)$.

Fig. 5.1 Total Cross-section for Intermediate Boson Production

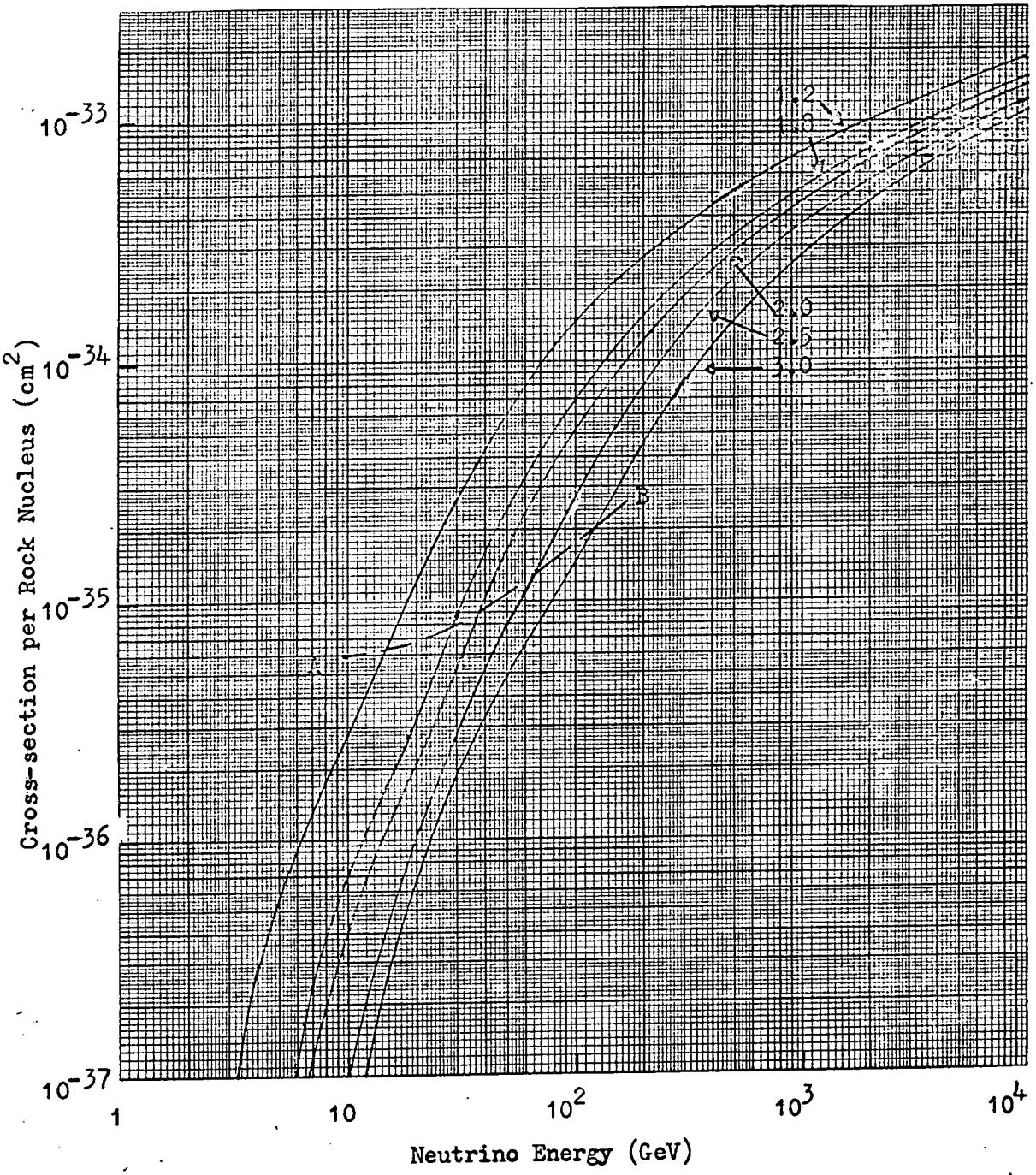

The energy spectrum of muons is therefore peaked at low energies. The sharpness of the peaking depends on the shape of the form-factor of the nucleon or nucleus near to $m_W^2/2E_\nu$: as the neutrino energy increases the spectrum becomes less sharply peaked. Veltman (1963) and Uberall (1964) have given plots of the muon spectra for coherent and incoherent interactions for a boson mass of 1 GeV and for neutrino energies up to 10 GeV. Those corresponding to the coherent interaction are very strongly peaked and the mean value, $\bar{r}_p$, can be assumed equal to the most probable value. A neutrino energy of 10 GeV for a boson mass of 1 GeV is equivalent to energies of 40 GeV and 90 GeV for m_W = 2 GeV and 3 GeV respectively, and the above result is therefore applicable at least up to these energies. In the incoherent interaction, the effect of the Pauli exclusion principle in discriminating against small momentum transfers is to broaden the high energy tail of the muon spectrum slightly. The mean value of r_p would therefore be a little higher than for the coherent interaction. It is shown in Chapter 7 that the effect of folding the cosmic ray neutrino spectrum into the total cross-section is that the median energy of neutrinos producing W's is $\sim$ 100 GeV. Therefore, up to the median energy, $\bar{r}_p \simeq m_\mu/(m_W + m_\mu)$. At very high neutrino energies the effect of the nculear form-factor is very much reduced, the muon spectrum becomes flat, and $\bar{r}_p$ will tend to 0.5. Since there is, at present, no quantitative analysis of the forms of the muon spectra at neutrino energies above those attained in accelerator experiments, the effective value of $\bar{r}_p$ that should be applied over the whole range of neutrino energies relevant to cosmic ray studies is not known. The rates of events are predicted in Chapter 7 for $\bar{r}_p$ corresponding to both the upper and lower limits. The true value will certainly be well below the upper limit and is

expected to be somewhat above the lower limit.

5.3.3 The Energy of the 'Decay' muon

Bell and Veltman (1963) and Überall (1964) have calculated the polarization of the intermediate boson and conclude that, independent of the value of $\underline{k}$, it is almost 100% circularly polarized. In this case muons from its decay are emitted predominantly backwards in the c.m.s., having an angular distribution $(1 - \cos\theta)^2$. In the laboratory system the muon therefore has a mean energy 0.25 of that of the boson. Thus $\bar{r}_d = 0.25\ (1 - \bar{r}_p)$.

5.3.4 The Muonic Branching Ratio

The rate of leptonic decay of the boson, $W \rightarrow l + \nu_l$ is $\frac{G_v m_W^3}{6\sqrt{2}\pi}$ $\simeq 6\ 10^{17} m_W^3\ \text{sec}^{-1}$, and the ratio of the decay rates $(W \rightarrow \mu + \nu_\mu)/(W \rightarrow e + \nu_e)$ is expected to be close to unity. The boson may, however, decay into two or more hadrons. The relative decay rates into two mesons have been calculated on the basis of unitary symmetry by Mani and Nearing (1964) and Namias and Wolfenstein (1965). They also give estimates of the absolute decay rates, which imply a branching ratio of non-leptonic to leptonic decay of 2 or 3 for $m_W = 2$ GeV. In a more recent work, however, Carhart and Dooher (1965), estimating the effects of strong interactions on these decay rates, conclude that boson decay into mesons is strongly suppressed and that for boson masses up to at least 3 GeV the leptonic decay modes predominate. They predict that for $m_W > 2$ GeV the decay rate into two baryons is comparable to the leptonic rate. It seems impossible, at present, to assign a value to $\underline{b}$ with any certainty from theoretical predictions. In Chapter 7 we, arbitrarily, take $b = 0.4$; the dependence on $\underline{b}$ of the rate of muons detected, for a given boson mass, is easily calculated.

5.3.5 Experimental Data on the Mass of the Boson

The Intermediate Boson has been searched for amongst the neutrino events produced in both the CERN and Brookhaven experiments. At present there is no clear evidence for the production of the W. Measured upper limits to the rate of possible boson reactions lead to lower limits to the boson mass. The lower limit from the CERN experiments (Bernardini et al. (1965)) is expressed as a function of the branching-ratio for leptonic decays (2b in our notation). In this experiment, a multiplate spark chamber containing magnetized iron was used to look for bosons decaying in the $W^+ \rightarrow \mu^+ + \nu_\mu$ mode. Of a total of about 5000 neutrino events produced in the chamber there were 33 in which two non-interacting particles with ranges > 30 cm of iron and with bending in the magnetized iron consistent with their having charges of opposite sign. This does not however exceed the background of $(\mu\pi)$ and (μp) pairs produced in inelastic interactions that would satisfy these criteria and are predicted from the bubble chamber results. Furthermore their range distributions are not consistent with their being muons from W production. A null result sets a limit of $m_W > 2.2$ GeV if the boson decays into leptons only. Non-leptonic decays of the W^+ were searched for amongst the total of 456 events observed in the HLBC where the momenta and energies of individual particles could be determined with fair accuracy. Five events were found which could be interpreted as being produced by a boson decaying into three, four or five mesons. This upper limit gives $m_W > 1.7$ GeV if the leptonic branching ratio is zero. Combining the spark chamber and HLBC results, the lower limit to m_W, expressed as a function of $\underline{b}$, is

$\underline{b}$	0.5	0.4	0.25	0.13	0
m_W (GeV)	2.2	2.2	2.1	1.9	1.7

These values are for a statistical confidence of 99%, assuming that the high energy end of the neutrino spectrum used is correct.

In the Brookhaven experiment (Burns et al. (1965)) a spark chamber was used to search for the $W^+ \rightarrow e^+ + \nu_e$ decay mode. No events were found. This result agrees with the CERN experiment but gives a less stringent lower limit to m_W.

Two experiments have been recently reported, using protons from the Argonne ZGS and the Brookhaven AGS (Lamb et al. (1965) and Burns et al. (1965a)) to look for the effects of Intermediate Bosons produced in proton-nucleus interactions. Muons from the $W \rightarrow \mu + \nu_\mu$ decay of a boson of mass > 2 GeV would typically have a much higher transverse momentum than is found in normal secondary particles from high energy interactions; thus the method used is to look for muons at large angles to the proton beam. Both experiments give only upper limits to the number of excess muons. In the first the results were interpreted, by way of a predicted production cross-section, as giving a lower limit to the boson mass of 2.5 GeV with a statistical confidence of 97%. However, in a revised prediction of the cross-section (Chilton et al. (1965)) it is stated that the previous values should be multiplied by an unknown constant factor, which may be as small as 10^{-3}. In the second experiment upper limits to the cross-section for the production of the Intermediate Boson are given as a function of assumed boson mass from 2 to 6 GeV and are $\sim 10^{-34}$ cm^2; but it is stated that present calculations of the expected cross-sections are not sufficiently certain to allow the interpretation of the data in terms of the existence of a boson with mass $m_W < 6$ GeV. Yamaguchi (1965) has pointed out that the expected rate of muons with large transverse momenta from muon pair production in nuclear interactions would be greater than that from Intermediate

Boson decay for these experiments. The best estimate of the lower limit of the boson mass therefore is still that obtained from the CERN neutrino experiment.

5.4 The Glashow Resonance Interaction.

If one considers the elastic lepton-lepton scattering interactions

$$\nu_l + e^- \rightarrow l^- + \nu_e \quad (5.5a) \quad \text{and} \quad \bar{\nu}_e + e^- \rightarrow l^- + \bar{\nu}_l \quad (5.5b)$$

then $\sigma(a) \approx 3\sigma(b) \approx \frac{G_v^2}{\pi} (\bar{E}_\nu^2) \approx 10^{-41} E_\nu \text{ cm}^2$ ($\bar{E}_\nu$ is the cms energy). If the Intermediate Boson exists and has mass m_W then this is true for cms energies $\ll m_W$ (i.e. $E_\nu \ll m_W^2/m_e$). The cross-section is down by a factor of $\sim 10^3$ on the lepton-nucleon interactions (5.1) and (5.2) because the laboratory energies required to give comparable cms energies are higher by a factor of m_p/m_e. In (5.5a) the effect of the W is to multiply the cross-section by a factor $(1 + (\bar{E}_\nu/m_W)^2)^{-1}$ which gives an asymptotic limit to σ (a) of $\sim 10^{-41}(m_W^2/m_e)$ cm^{-2}. In (5.5b), however, a real boson may be produced at a threshold laboratory energy, E_t, of $m_W^2/2m_e$ and a resonance occurs in the cross-section

$$\sigma(\theta) \approx \frac{1}{3} \frac{G_v^2}{\pi} (\bar{E}_\nu^2) \left[\frac{E_c^2}{(E_\nu - E_t)^2 + \frac{m_W}{m_e \tau_W}} \right] \quad (5.6)$$

which has a peak value, for electrons at rest, of $\sim 10^{-28}$ cm^2. This fact was first remarked upon by Glashow (1960). The velocity distribution of target atomic electrons has the effect of increasing the width of the resonance to $\sim E_t/10$ GeV; over this energy region the effective cross-section is $\sim 10^{-31}$ cm^2. In the original paper of Glashow the flux of muons produced underground by this mechanism was overestimated due to the implicit assumption that $\bar{\nu}_e = \bar{\nu}_\mu$ and $m_W \lesssim 1$GeV. Zagrebin and Zheleznykh (1964) have calculated the flux and angular distribution of muons produced by $\bar{\nu}_e$ from the decay of muons and kaons in the K_{e3} mode in the atmosphere. The absorption of neutrinos in the earth, which is important for interactions having cross-sections as high as these, was

allowed for, and a more sophisticated electron velocity distribution than that assumed by Glashow was used. In Chapter 7 their results, modified to apply to the KGF apparatus under our assumptions of the boson branching ratio, are presented. It should be noted that this interaction is the only one of those discussed so far in which a muon is produced by an electron-neutrino. It also differs from the others in that it is only initiated by the anti-neutrino. In this particular case, therefore, the rate of events is dependent upon the charge ratio of the parent mesons.

Above E_t the boson may be produced together with a γ-ray

$$\bar{\nu}_e + e^- \rightarrow W^- + \gamma . \qquad (5.7)$$

This process has been discussed by Hiroshige and Matsuda (1965). They predict that the cross-section falls with increasing energy from a maximum value at E_t to an asymptotic value $\sim 10^{-34}$ cm^2. The contribution to the muon rate would be approximately the same as from the resonance interaction.

Chapter 6

The Flux of Neutrinos at Sea Level

6.1 Introduction

Experiments in which neutrino interactions are studied differ from those with other elementary particles in that the beam of neutrinos cannot be separately monitored. In the cases of both cosmic ray and accelerator produced neutrinos, the intensity of the beam may be deduced from the measured intensities either of the parent particles or of the muons or photons which are produced from them together with the neutrinos. The type of apparatus used at present to study the high energy cosmic ray neutrinos has a threshold energy such that the interactions are detected only of the neutrinos with energies $\gtrsim$ 100 MeV. The low energy electron-neutrinos from terrestial beta decay and from nuclear reactions in the sun are thus excluded. In this case it is expected that the predominant contribution to the neutrino flux comes from the decays of mesons produced in the atmosphere. It can be shown that the flux from the decays of mesons produced in the inter-stellar material must be two orders of magnitude less than this. One cannot, however, rule out completely the possibility of an extra-terrestial flux of the same order as the atmospheric one; possible sources of high energy cosmic neutrinos are discussed in the final section of this chapter.

The neutrinos produced in the atmosphere come from the decays of pions, kaons and muons. There have been a number of calculations of

the neutrino sea level intensity. Markov and Zheleznykh (1961) derived the vertical neutrino spectrum from pion decay, which they considered to be the most important source. At energies up to 10 GeV, however, and particularly at large zenith angles, muons have a relatively high probability of decay in the atmosphere and their contribution to the neutrino intensity cannot be ignored. Zatsepin and Kuzmin (1962) calculated the neutrino intensity from both pion and muon decay and gave the variation with zenith angle from 0° to 90°. Because of the considerably greater amount of energy available to the neutrino in the decay of the kaon in the $K_{\mu 2}$ mode than in pion decay, kaons are more efficient in producing neutrinos than pions. Thus an admixture of kaons in the atmospheric meson flux, while, as has been shown, it has only a marginal effect on the muon intensities, has a considerable effect on the total neutrino intensity. Cowsik et al. (1964), taking, the ratio, $(K/\pi)_{total}$, to be 20% obtained the neutrino intensity from muons and pions and the most important decay modes of the kaons in the vertical and horizontal directions. The relative numbers of neutrinos and anti-neutrinos in the total flux were also given. The results of the present calculations, the details of which are given in the following section, have been reported by Osborne et al. (1965). In these, all decay modes of the kaons are taken into account and the variation of intensity with zenith angle is calculated. From the previous analysis, the most likely value of $(K/\pi)_{total}$ over the relevant energy range is taken to be 20%, but the effects in both the horizontal and vertical directions of the uncertainties in the ratio are also shown. Cowsik

et al. (1965) have given results of further calculations of the neutrino intensity using a similar model to that of their first paper but with slightly different basic data. These spectra, which are somewhat different from the previous ones, are compared with the present results in section 6.3.

6.2 Neutrinos Produced in the Atmosphere

In calculating the intensity of neutrinos at sea level it is necessary to differentiate between muon-neutrinos and electron-neutrinos. At the present level of sophistication of the apparatus used to examine neutrino interactions, the signs of the charges of the products of the interaction are not determined and, in general, it is not possible to differentiate between neutrinos and anti-neutrinos. The intensity that we calculate is therefore the sum of particles and anti-particles.

6.2.1 Neutrinos from Pion and Kaon Decay

The procedure used in calculating the neutrino intensity at sea level from kaon and pion decay is similar to that for the muon intensity but it is considerably simplified because no decay probability or energy loss have to be considered. The neutrino spectra are based on the OPW vertical spectrum in that the values used for the kaon and pion production spectra are those derived from it in Chapter 2. Following the same arguments as for the muon spectrum, the depth rate of production of muon-neutrinos from $\pi \Rightarrow \mu + \nu_\mu$ decay at depth x in the vertical direction (corresponding to (2.15)) is

$$n_\nu(E_\nu, x) = \frac{2.341}{120} A E_\nu^{-\gamma} \exp\left(\frac{-x}{120}\right) \int_{2.341}^{\infty} s^{-(\gamma+1)} \left(1 + \frac{s E_\nu}{B_\pi}\right)^{-1} ds \qquad (6.1)$$

Because the neutrinos do not decay and lose no energy this expression also represents the contribution to the intensity at sea level from production at a height $\underline{x}$, $M_\nu(E_\nu,x)$. The total intensity is then obtained by integrating over the entire atmosphere. In (6.1) B_π is the only term inside the integral that is dependent upon $\underline{x}$ (and this only for $x \geq 253.3$ g cm^{-2}). Taking a constant value $B_\pi = 118.1$ GeV introduces negligible error and $M_\nu(E_\nu,x)$ can then be integrated analytically, the sea level neutrino spectrum from pions becoming

$$N_\nu^\pi(E_\nu) = 2.341\, A E_\nu^{-\gamma} \int_{2.341}^{\infty} s^{-(\gamma+1)} \left(1 + \frac{s E_\nu}{B_\pi}\right)^{-1} ds \qquad (6.2)$$

All of the kaon decay modes listed in Appendix C except $K^o_{\pi 2}$, and $K^o_{\pi 3}$, contribute to the neutrino flux either directly or via the decay of charged pions. The contribution from $K_{\mu 2}$ and the leptonic three-body decays were calculated by a procedure entirely analogous to that given above for pions. The flux from two-stage decays was obtained via the production spectrum of secondary pions already calculated in deriving the muon flux. The meson production spectrum (2.25) together with the relaxation factor of Fig. 2.11 was used to obtain the neutrino intensities for the K/π ratio, $\underline{R}$, equal to 0.2. This value of $\underline{R}$ was used in the calculations of the intensities at intermediate zenith angles but vertical and horizontal intensities were calculated for R=0 and 0.4 also, in order to examine the sensitivity to the K/π ratio. In Fig. 6.1 the contributions for R = 0.2 of pions and the various decay modes of kaons to the vertical neutrino intensity at sea level are shown. They are given as fractions of the total intensity of muon-neutrinos

Fig. 6.1 Relative contributions of pions and the various decay modes of kaons to the neutrino spectrum at sea level for R = 20% at $\theta = 0^{\circ}$

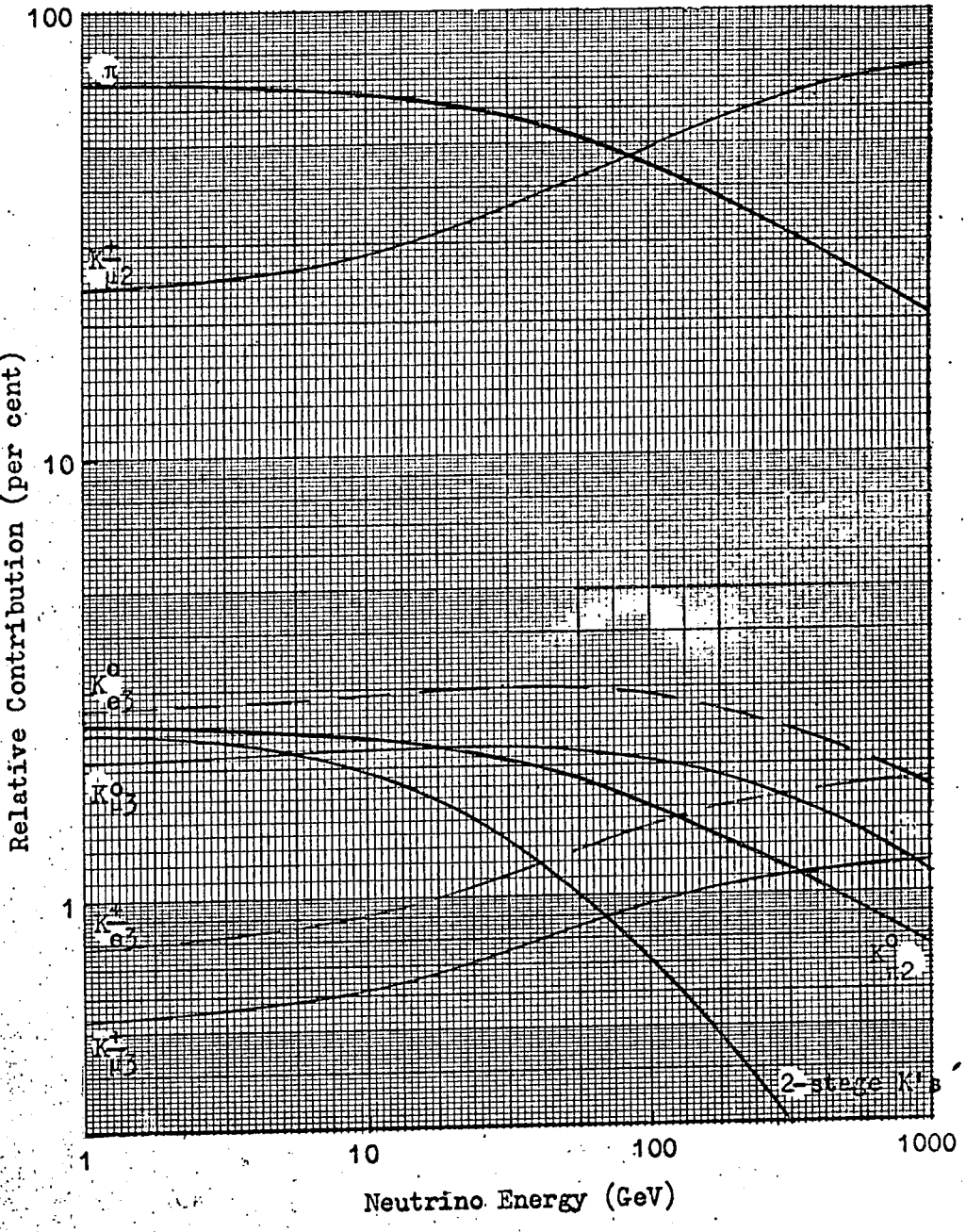

from pions and kaons; the $K^{\pm o}_{e3}$ decay modes give rise to electron-neutrinos.

In the inclined directions these expressions are modified as before. For example the depth rate of production of neutrinos from $K_{\mu 2}$ decay at a depth $l(x,\theta)$ is given by

$$n_\nu^{K_{\mu 2}}(E_\nu, l(x,\theta)) = \frac{0.58}{120} C_K \exp\left(-\frac{l}{120}\right) E_\nu^{-\gamma} 1.048 \int_{1.048}^{\infty} s^{-(\gamma+1)} \left(1 + \frac{E_\nu s}{B_K} \frac{x}{l}\right)^{-1} ds \quad (6.3)$$

Again, the total intensity at sea level is obtained by integrating over l. For $\theta \lesssim 70^\circ$, $l(x,\theta) = x \sec\theta$ and the sea level intensity is given by

$$N_\nu^{K_{\mu 2}}(E_\nu, \theta) = 0.58 C_K E_\nu^{-\gamma} 1.048 \int_{1.048}^{\infty} s^{-(\gamma+1)} \left(1 + \frac{E_\nu s}{B_K \sec\theta}\right)^{-1} ds \quad (6.4)$$

At larger zenith angles $l(x,\theta)$ is obtained by interpolation from the data of Table 2.3 and the integration over l is performed numerically. The relative contributions of the various decay modes at $\theta = 90^\circ$ are given in Fig. 6.2. In Fig. 6.3 the angular distribution of muons from kaons and pions are given, where the intensities for each sea level energy are normalised to those at 90°. The maximum at 90° is due to the greater probability of meson decay in the less dense atmosphere at large zenith angles. In the limiting case of $E_\nu >> B_K$ the ratio of the intensity at zenith angle θ to that in the vertical direction is equal to the effective value of $l(x,\theta)/x$; at 90° for example this is approximately 9.5.

6.2.2 Neutrinos from Muon Decay

In order to derive the flux of neutrinos from muon decay in the atmosphere the intensity of muons throughout the atmosphere must first be calculated. The intensity at vertical depth t of energy E_t at zenith angle θ_t^* will be denoted by $p_t(E_t,\theta_t^*)$; $\theta_t^*(t,\theta)$ is the local zenith

Fig. 6.2 Relative contributions of pions and the various decay modes of kaons to the neutrino spectrum at sea level for R = 20% for $\theta = 90^{\circ}$

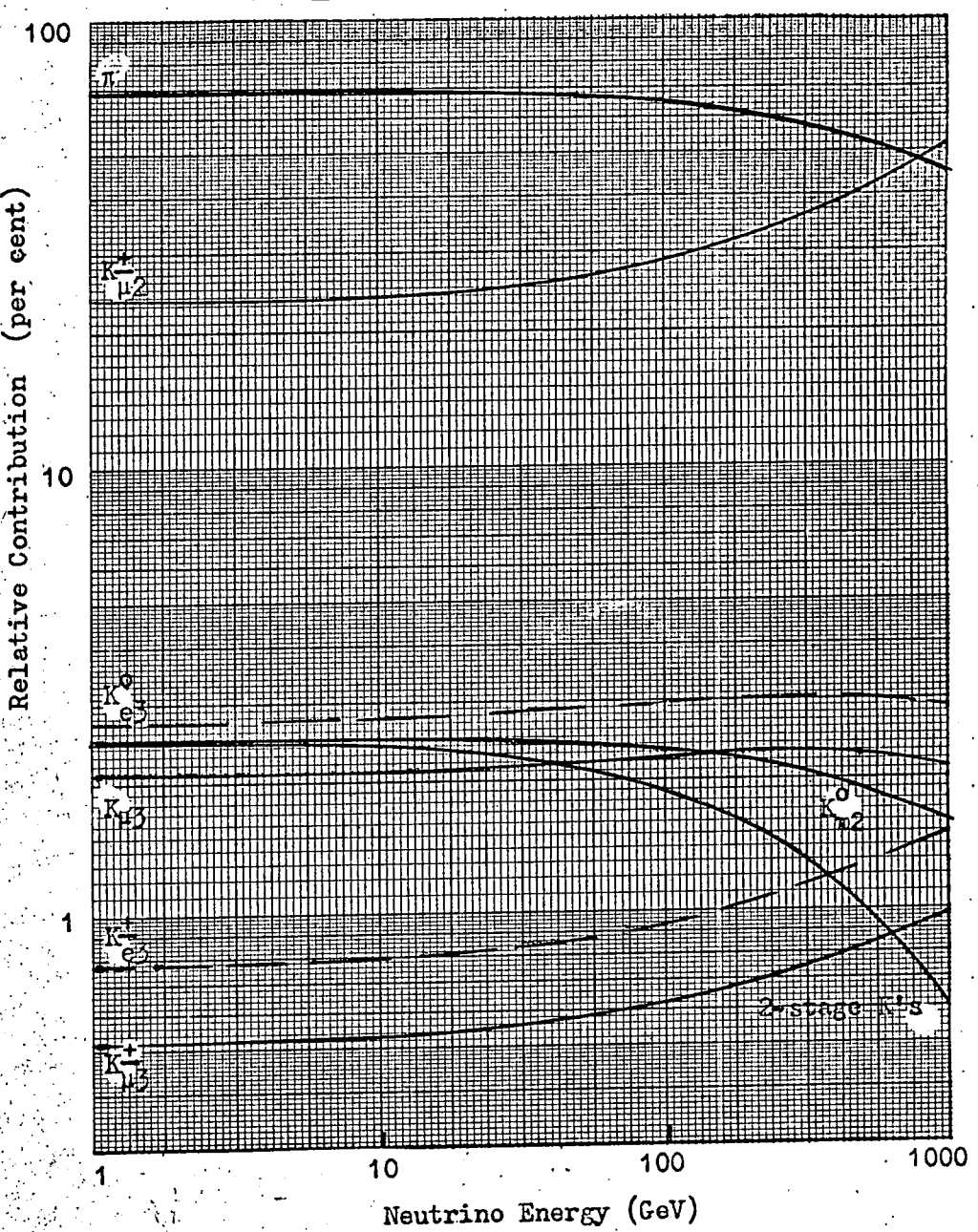

Fig. 6.3 Angular distribution at sea level of muon-neutrinos from kaon and pion decay ($K/\pi = 20\%$) with respect to the horizontal direction

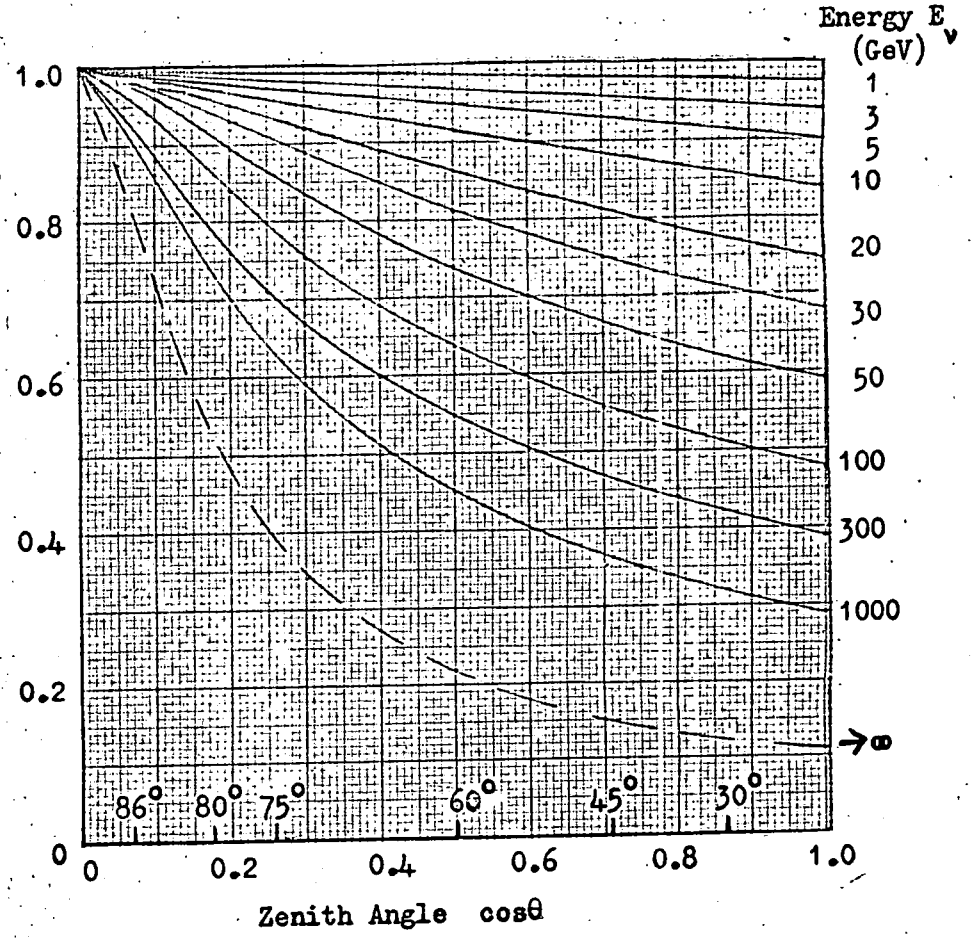

angle at $\underline{t}$ corresponding to θ at sea level. The values of this expression have already been obtained for $t = 1030$ g cm^{-2} since this is simply the muon intensity at sea level. The general expression for this intensity may be obtained from (3.5) as

$$\phi_t(E_t,\theta_t^*) = \int_0^{l(t,\theta_t^*)} n_\mu(E_\mu(x,E_t,\theta_t^*),l(x,\theta_t^*)) \cdot SP_t(x,E_t,\theta_t^*)\left[\frac{dE}{dl}(E_\mu,x)\Big/\frac{dE}{dl}(E_t,t)\right]dl \quad (6.5)$$

$E_\mu(x,E_t,\theta_t^*)$ is the energy at $\underline{x}$ of a muon having energy E_t and zenith angle θ_t^* at $\underline{t}$ and $SP_t(x,E_t,\theta_t^*)$ is the survival probability of such a muon from $\underline{x}$ to $\underline{t}$. Values of E_μ and SP_t corresponding to standard energies, E_t, for different values of $\underline{t}$ were calculated and were interpolated upon in the numerical integration of (6.5). Most of these were obtained in turn by interpolation from the values already calculated for the sea level intensity; those for the lowest energies that can be derived in this way are for energies at $\underline{t}$ corresponding to 1 GeV at sea level. For lower energies down to $E_t = 1$ GeV extra calculations of survival probability and energy loss were performed by the method outlined in section 2.3.3. For $n_\mu(E_\mu,1)$ expression (3.4) is used. Thus the neutrino flux from muon decay is calculated for the case in which the muons come from pions only. Near to the vertical direction an admixture of kaons would make no difference to the results since the vertical muon spectrum is normalised to the measured one. At large zenith angles it has been shown that a non-zero K/π ratio results in a reduction of the sea level muon intensity by up to 10 - 15%. A similar reduction in the neutrino intensity would be expected; however, the reduction in the muon intensity becomes really significant only for $E_\mu \gtrsim 500$ GeV and at these energies the relative contribution of muon

decay to the total flux is ~ 10%.

The intensity $p_t(E_t,\theta_t^*)$ was calculated for E_t from 1 to 1000 GeV for ten values of $\underline{t}$ between 0 and 1030 g cm^{-2} and for zenith angles $\theta = 0^\circ, 45^\circ, 75^\circ, 86^\circ, 90^\circ$. In Figs. 6.4, 6.5 and 6.6 $p_t(E_t,\theta_t^*)$ is plotted against $\underline{t}$ for $\theta = 0^\circ$, 75° and 90° respectively. The shapes of the curves are determined by the competing processes of enhancement of the muon intensity due to pion decay and reduction due to muon decay and energy loss. At 1000 GeV the probability of muon decay is small at all zenith angles and the intensity first increases with $\underline{t}$ due to muon production and then remains practically constant with depth. For lower energies as muon decay becomes increasingly important a distinct maximum appears in the intensity profile; this becomes more pronounced as the zenith angle increases.

Since the neutrinos do not lose energy it is of no consequence at what height in the atmosphere the muon decay occurs. Thus it is meaningful to calculate the muon decay spectrum, $D(E_\mu,\theta)$, which is the intensity of muons of energy E_μ, having a trajectory which would intersect the earth's surface at a zenith angle θ, which decay at all heights in the atmosphere. This is derived from the muon intensity versus $\underline{t}$ results:

$$D(E_\mu,\theta) = \frac{m_\mu c^2}{c\tau_\mu E_\mu} \int_0^{l(\theta,t)} p_\pi\left(E_\mu, \theta_\pi^*(t,\theta)\right) \frac{dl}{\rho(t)} \qquad (6.6)$$

The relation between $\underline{l}$ and $\underline{t}$ was obtained by interpolation from the data of Table 2.3.

Zatsepin and Kuzmin (1962) give the following expressions for the c.m.s. spectra of ν_μ and ν_e produced by muon decay

Fig. 6.4 The variation of muon intensity with depth in the atmosphere ($\theta = 0^{o}$)

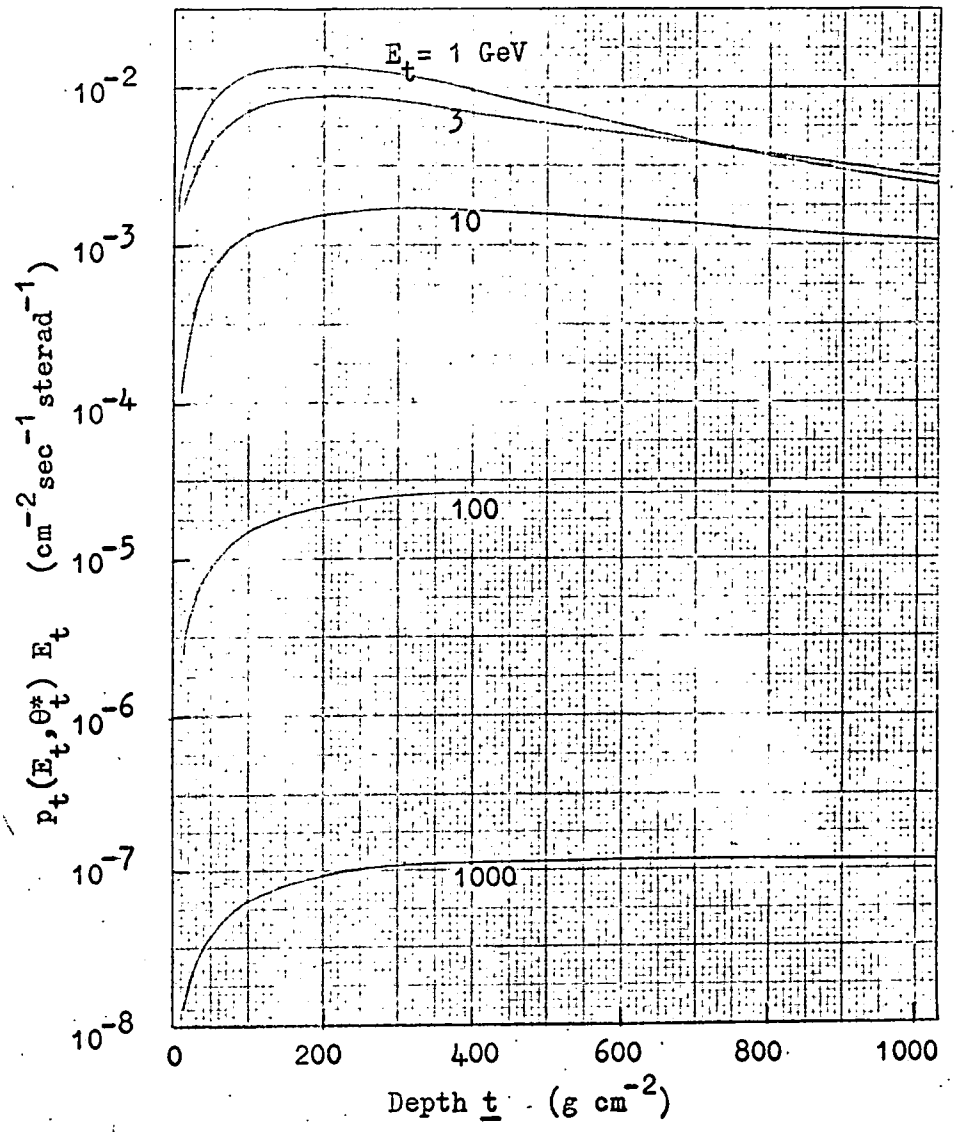

Fig. 6.5 Variation of muon intensity with depth in the atmosphere ($\theta = 75^{\circ}$)

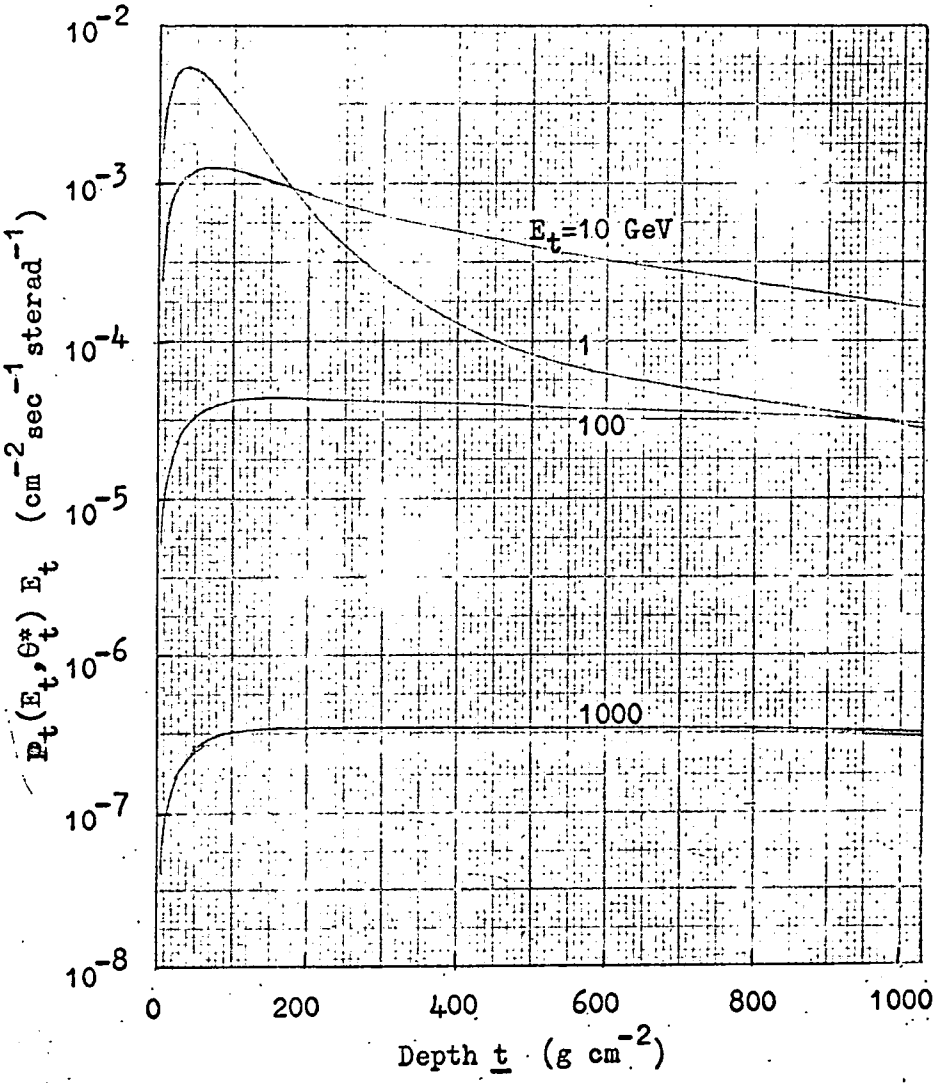

Fig. 6.6 Variation of muon intensity with depth in the atmosphere ($\theta = 90^{\circ}$)

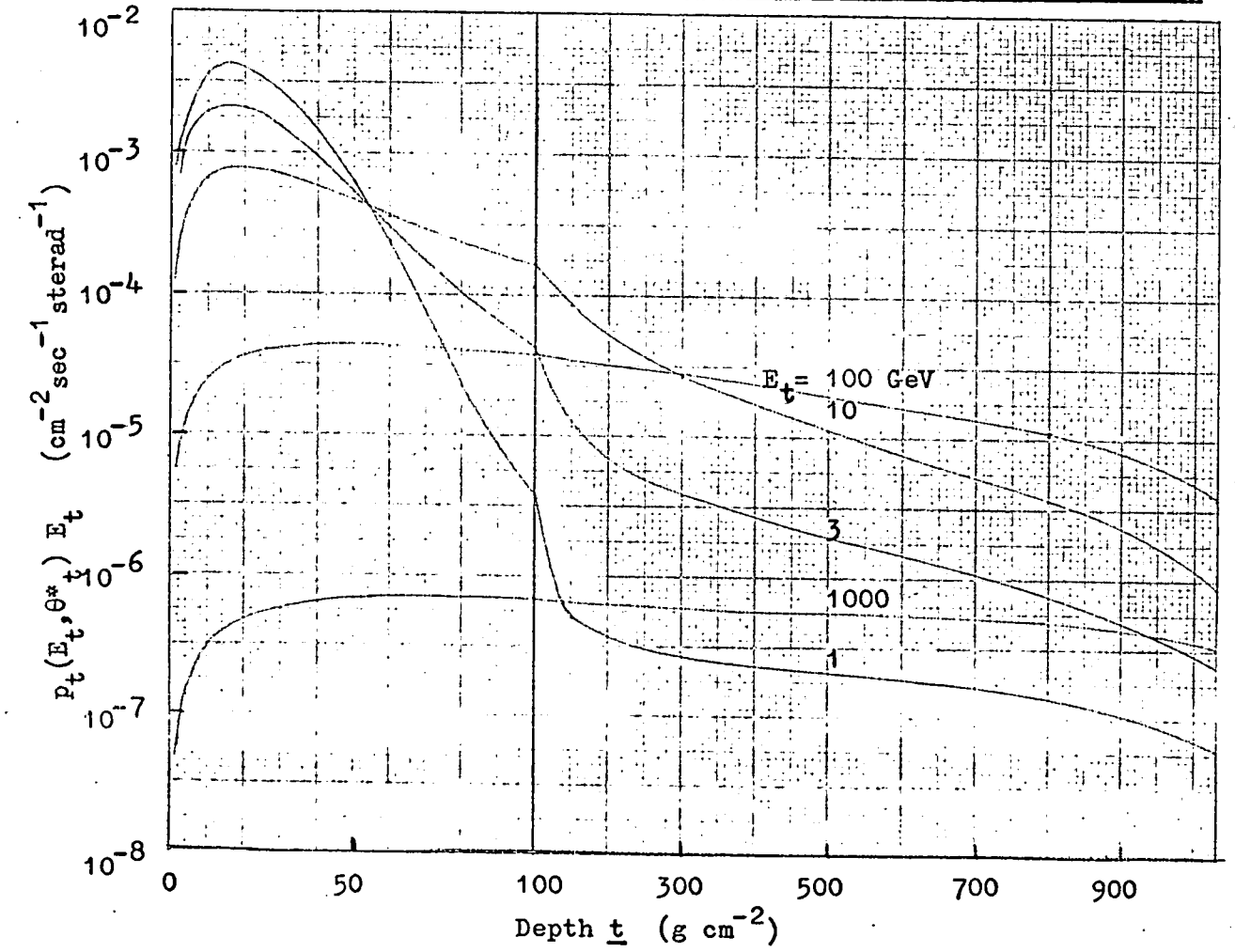

$$P^{*}_{\nu_\mu}(x)dx = 2x^2(3-2x)dx \qquad (6.7)$$

and

$$P^{*}_{\nu_e}(x)dx = 12x^2(1-x)dx \qquad (6.8)$$

where $x = E_\nu / E_{max}$, E_{max} being the maximum neutrino energy equal to $m_\mu c^2/2$. Transforming to the laboratory system, for $\beta \to 1$ these become respectively

$$P_{\nu_\mu}(y)dy = \left[\frac{5}{3} - 3y^2 + \frac{4}{3}y^3\right] dy \qquad (6.9)$$

and

$$P_{\nu_e}(y)dy = \left[2 - 6y^2 + 4y^3\right] dy \qquad (6.10)$$

where $y = E_\nu / E_\mu$. Thus the sea level spectra of ν_μ and ν_e from muon decay are

$$N^{\mu}_{\nu_\mu}(E_\nu, \theta) = \int_{E_\nu}^{\infty} D(E_\mu, \theta)\left[\frac{5}{3E_\mu} - \frac{3E_\nu^2}{E_\mu^3} + \frac{4}{3}\frac{E_\nu^3}{E_\mu^4}\right] dE_\mu \qquad (6.11)$$

and

$$N^{\mu}_{\nu_e}(E_\nu, \theta) = \int_{E_\nu}^{\infty} D(E_\mu, \theta)\left[\frac{2}{E_\mu} - \frac{6E_\nu^2}{E_\mu^3} + \frac{4E_\nu^3}{E_\mu^4}\right] dE_\mu \qquad (6.12)$$

The angular distribution of neutrinos from muon decay, normalised to the intensities at 90°, are given in Fig. 6.7. The anomalous behaviour of the distribution at 1 GeV is due to the changing slope of the pion production spectrum at low energies.

It should be noted that the values of $p_t(E_t, \theta^{*}_t)$ were obtained neglecting the effects of scattering of the muons. The value of the intensity at sea level calculated in this way for $E_t = 1$ GeV and $\theta = 90^\circ$ is increased by a factor of ~ 10 when scattering is allowed for. However, an examination of the intensity profile for $E_t = 1$ GeV in Fig. 6.6 shows that it is strongly peaked at $t = 15$ g cm^{-2}. The result of this is that

Fig. 6.7 Angular distribution of muon-neutrinos at sea level from muon decay with respect to the horizontal direction

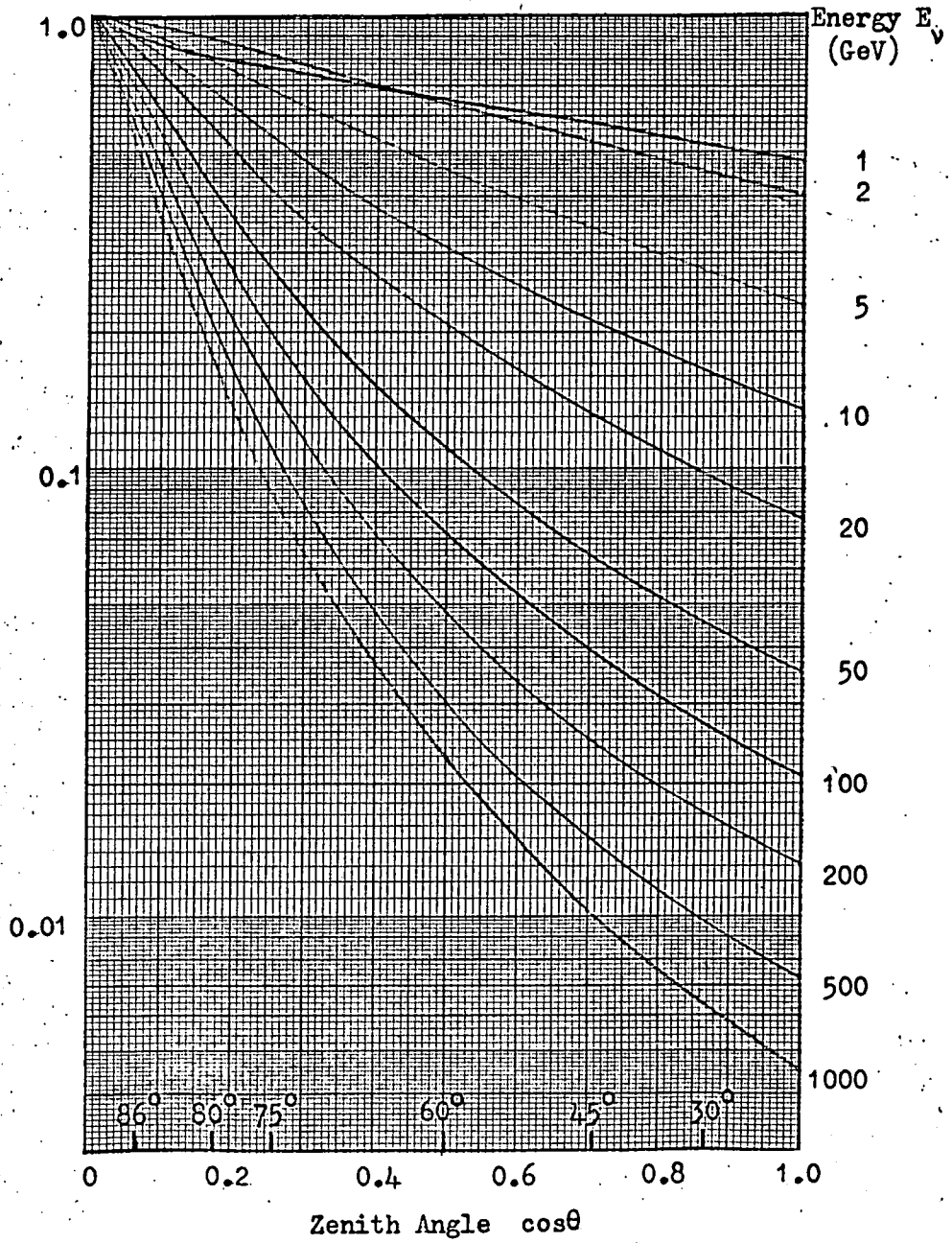

by far the greatest contribution to the muon decay spectrum at this energy comes from $t < 100$ g cm^{-2} where the effects of scattering are not important. By neglecting scattering the neutrino intensity at 1 GeV for extreme zenith angles is underestimated by a few percent.

The calculated intensities at sea level of ν_μ and ν_e from muon, pion and kaon decay for $R = 0.2$ are given in Tables 6.1 and 6.2 for the vertical and horizontal directions. The spectra are plotted in Figs. 6.8 and 6.9 and the vertical muon spectrum is also shown for comparison. In the vertical direction the relative contribution from muon decay decreases rapidly with increasing energy and at high energies, where the fractional energy loss of muons is small, the slope of these spectra is greater than that of the muon spectrum by unity because the decay probability falls as E_μ^{-1}. The ratio of the intensities of ν_μ and ν_e are almost constant, the latter being smaller because of the lower mean energy of the ν_e in the c.m.s. of muon decay. At high energies the vertical ν_μ spectrum from pion decay is approximately parallel to the muon spectrum because the majority of muons also come from pion decay. At low energies the muon spectrum is reduced below that of the neutrinos by ionisation loss and decay. In the horizontal direction the contribution of muon decay to the total neutrino intensity remains important to much higher energies because of the increased path length in the atmosphere. Fig. 6.10 gives the angular distribution of the total intensity of muon-neutrinos.

The total intensities have also been calculated in the vertical and horizontal directions for $R = 0$ and 0.4. In Fig. 6.11 they are

Fig. 6.8 Muon-neutrino and electron-neutrino intensities in the vertical direction

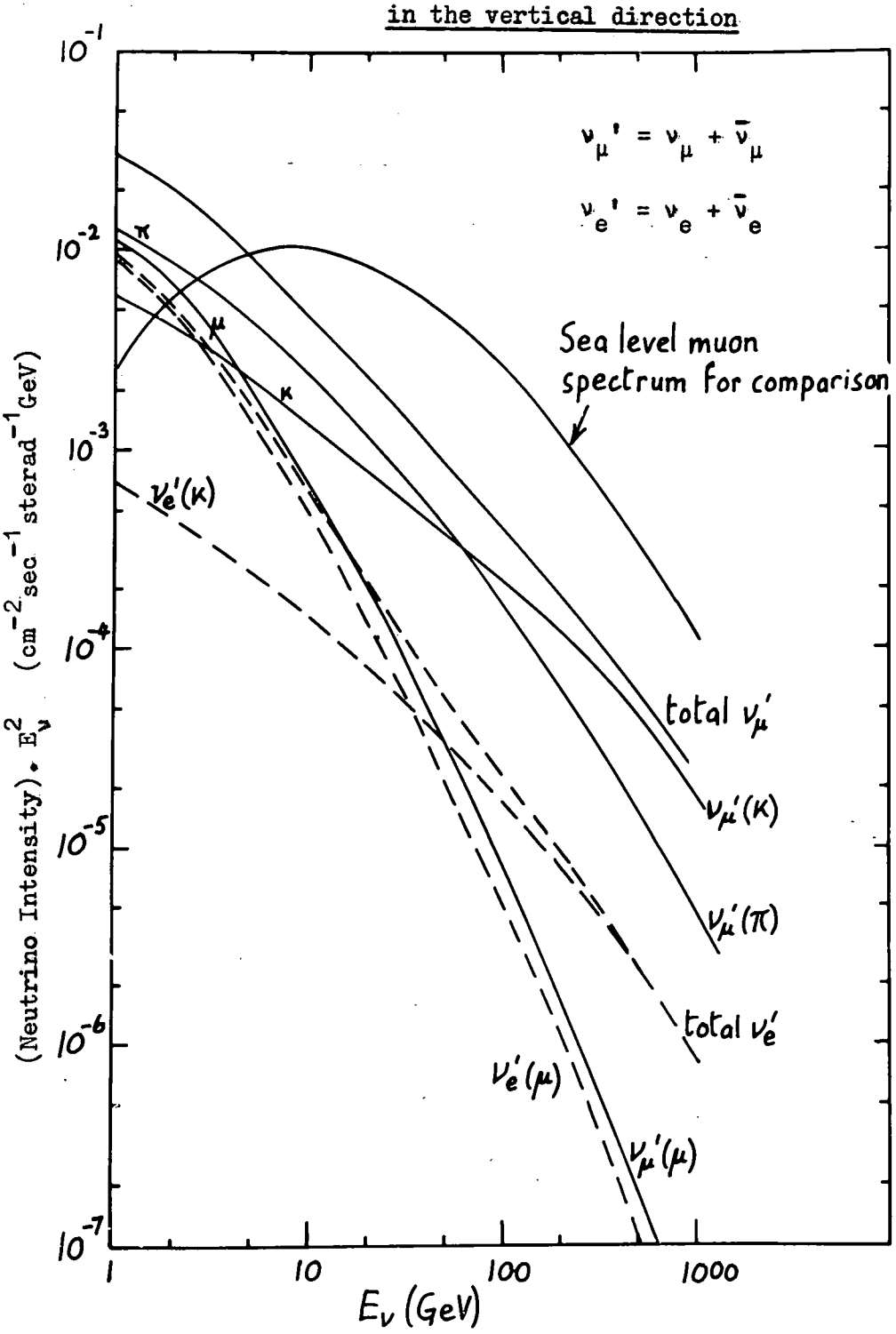

Table 6.1

Calculated Sea Level Neutrino Spectra in the Vertical Direction

Energy (GeV)	Intensity (cm^{-2} sec^{-1} $sterad^{-1}$ GeV^{-1})						
	Muon-neutrino				Electron-neutrino		
	Muon	Pion	Kaon	Total	Muon	Kaon	Total
1	1.10^{-2}	1.29^{-2}	5.94^{-3}	2.98^{-2}	8.75^{-3}	7.00^{-4}	9.45^{-3}
2	1.66^{-3}	2.23^{-3}	1.05^{-3}	4.94^{-3}	1.22^{-3}	1.17^{-4}	1.34^{-3}
3	4.53^{-4}	7.06^{-4}	3.39^{-4}	1.50^{-3}	3.24^{-4}	3.77^{-5}	3.62^{-4}
5	7.87^{-5}	1.75^{-4}	8.76^{-5}	3.41^{-4}	5.57^{-5}	9.44^{-6}	6.51^{-5}
7	2.42^{-5}	6.85^{-5}	3.55^{-5}	1.28^{-4}	1.70^{-5}	3.83^{-6}	2.09^{-5}
10	6.78^{-6}	2.46^{-5}	1.34^{-5}	4.48^{-5}	4.70^{-6}	1.44^{-6}	6.13^{-6}
20	5.09^{-7}	3.06^{-6}	1.94^{-6}	5.51^{-6}	3.45^{-7}	2.01^{-7}	5.45^{-7}
30	1.05^{-7}	8.58^{-7}	6.19^{-7}	1.58^{-6}	7.02^{-8}	6.12^{-8}	1.31^{-7}
50	1.36^{-8}	1.68^{-7}	1.48^{-7}	3.30^{-7}	9.03^{-9}	1.35^{-8}	2.25^{-8}
70	3.47^{-9}	5.63^{-8}	5.78^{-8}	1.17^{-7}	2.30^{-9}	4.96^{-9}	7.25^{-9}
100	8.07^{-10}	1.75^{-8}	2.15^{-8}	3.98^{-8}	5.30^{-10}	1.70^{-9}	2.23^{-9}
200	4.33^{-11}	1.72^{-9}	3.11^{-9}	4.87^{-9}	2.78^{-11}	2.07^{-10}	2.34^{-10}
300	7.28^{-12}	4.09^{-10}	9.19^{-10}	1.34^{-9}	4.60^{-12}	5.44^{-11}	5.90^{-11}
500	7.13^{-13}	6.12^{-11}	1.77^{-10}	2.39^{-10}	4.44^{-13}	9.04^{-12}	9.48^{-12}
700	1.49^{-13}	1.74^{-11}	5.82^{-11}	7.57^{-11}	9.11^{-14}	2.82^{-12}	2.91^{-12}
1000	2.63^{-14}	4.81^{-12}	1.84^{-11}	2.32^{-11}	1.61^{-14}	8.32^{-13}	8.48^{-13}

(the superscript denotes the power of ten)

Fig. 6.9 Muon-neutrino and electron-neutrino intensities in the horizontal direction

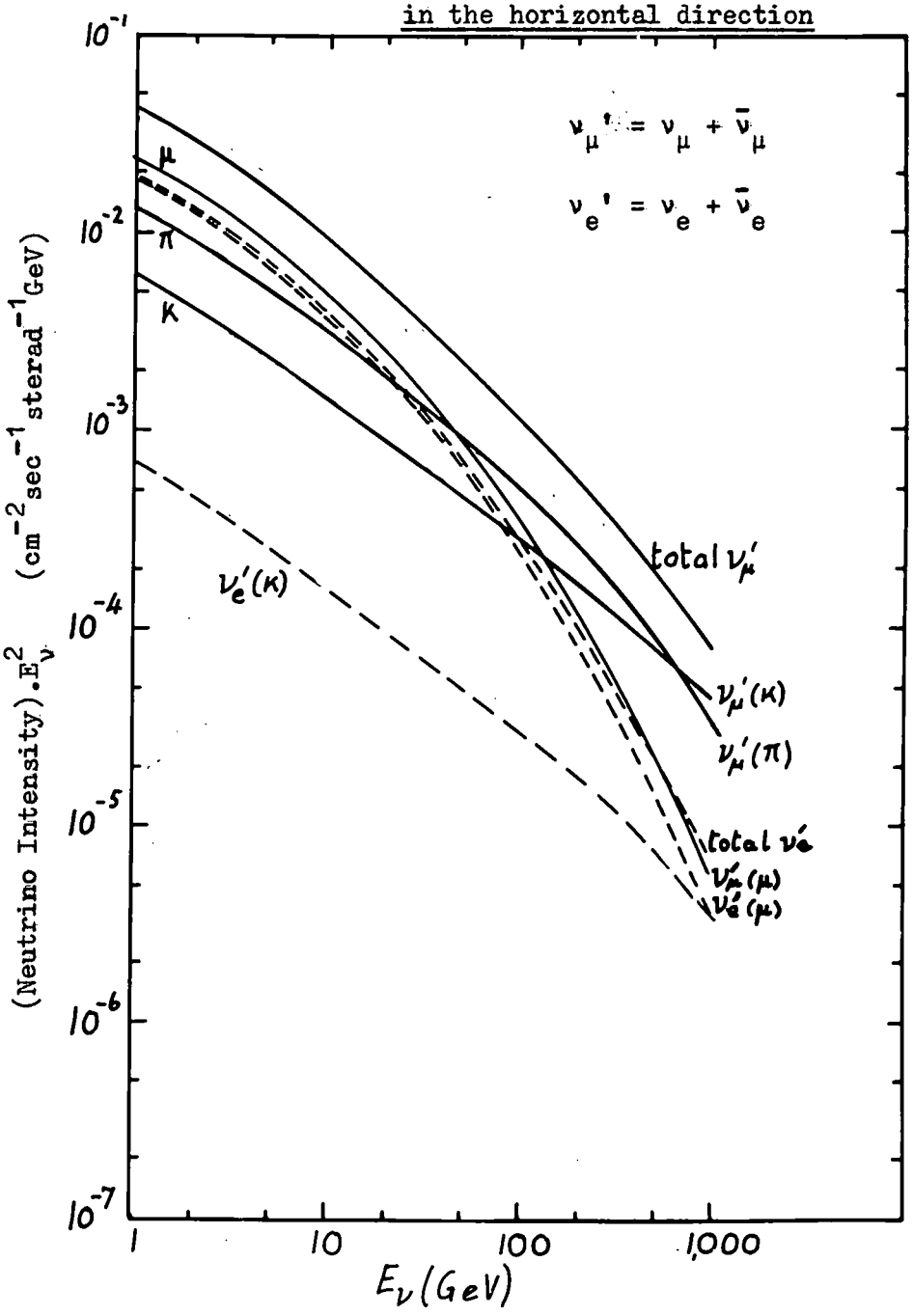

Table 6.2

Calculated Sea Level Neutrino Spectra at 90^{o} to the Zenith

Energy (GeV)	Intensity (cm^{-2} sec^{-1} $sterad^{-1}$ GeV^{-1})						
	Muon-neutrino				Electron-neutrino		
	Muon	Pion	Kaon	Total	Muon	Kaon	Total
1	2.34^{-2}	1.33^{-2}	6.02^{-3}	4.27^{-2}	1.86^{-2}	7.00^{-4}	1.93^{-2}
2	4.09^{-3}	2.35^{-3}	1.07^{-3}	7.51^{-3}	3.22^{-3}	1.20^{-4}	3.34^{-3}
3	1.39^{-3}	7.65^{-4}	3.47^{-4}	2.50^{-3}	1.08^{-3}	3.90^{-5}	1.12^{-3}
5	3.44^{-4}	2.00^{-4}	9.11^{-5}	6.35^{-4}	2.66^{-4}	9.97^{-6}	2.76^{-4}
7	1.35^{-4}	8.15^{-5}	3.74^{-5}	2.54^{-4}	1.04^{-4}	4.13^{-6}	1.08^{-6}
10	4.96^{-5}	3.10^{-5}	1.43^{-5}	9.49^{-5}	3.78^{-5}	1.59^{-6}	3.94^{-5}
20	6.57^{-6}	4.56^{-6}	2.15^{-6}	1.33^{-5}	4.91^{-6}	2.40^{-7}	5.15^{-6}
30	1.92^{-6}	1.47^{-6}	7.08^{-7}	4.09^{-6}	1.42^{-6}	7.98^{-8}	1.50^{-6}
50	3.70^{-7}	3.58^{-7}	1.79^{-7}	9.07^{-7}	2.69^{-7}	1.94^{-8}	3.03^{-7}
70	1.22^{-7}	1.41^{-7}	7.36^{-8}	3.36^{-7}	8.72^{-8}	7.86^{-9}	9.41^{-8}
100	3.63^{-8}	5.28^{-8}	2.93^{-8}	1.18^{-7}	2.62^{-8}	3.04^{-9}	2.92^{-8}
200	3.29^{-9}	7.12^{-9}	4.59^{-9}	1.50^{-8}	2.27^{-9}	4.68^{-10}	2.74^{-9}
300	7.18^{-10}	1.96^{-9}	1.43^{-9}	4.10^{-9}	4.86^{-10}	1.42^{-10}	5.28^{-10}
500	9.70^{-11}	3.53^{-10}	3.17^{-10}	7.67^{-10}	6.45^{-11}	2.89^{-11}	9.34^{-11}
700	2.49^{-11}	1.17^{-10}	1.23^{-10}	2.65^{-10}	1.64^{-11}	1.04^{-11}	2.68^{-11}
1000	5.77^{-12}	3.53^{-11}	4.47^{-11}	8.58^{-11}	3.61^{-12}	3.51^{-12}	7.32^{-12}

(the superscript denotes the power of ten)

Fig. 6.10 Variation of total muon-neutrino intensity with zenith angle

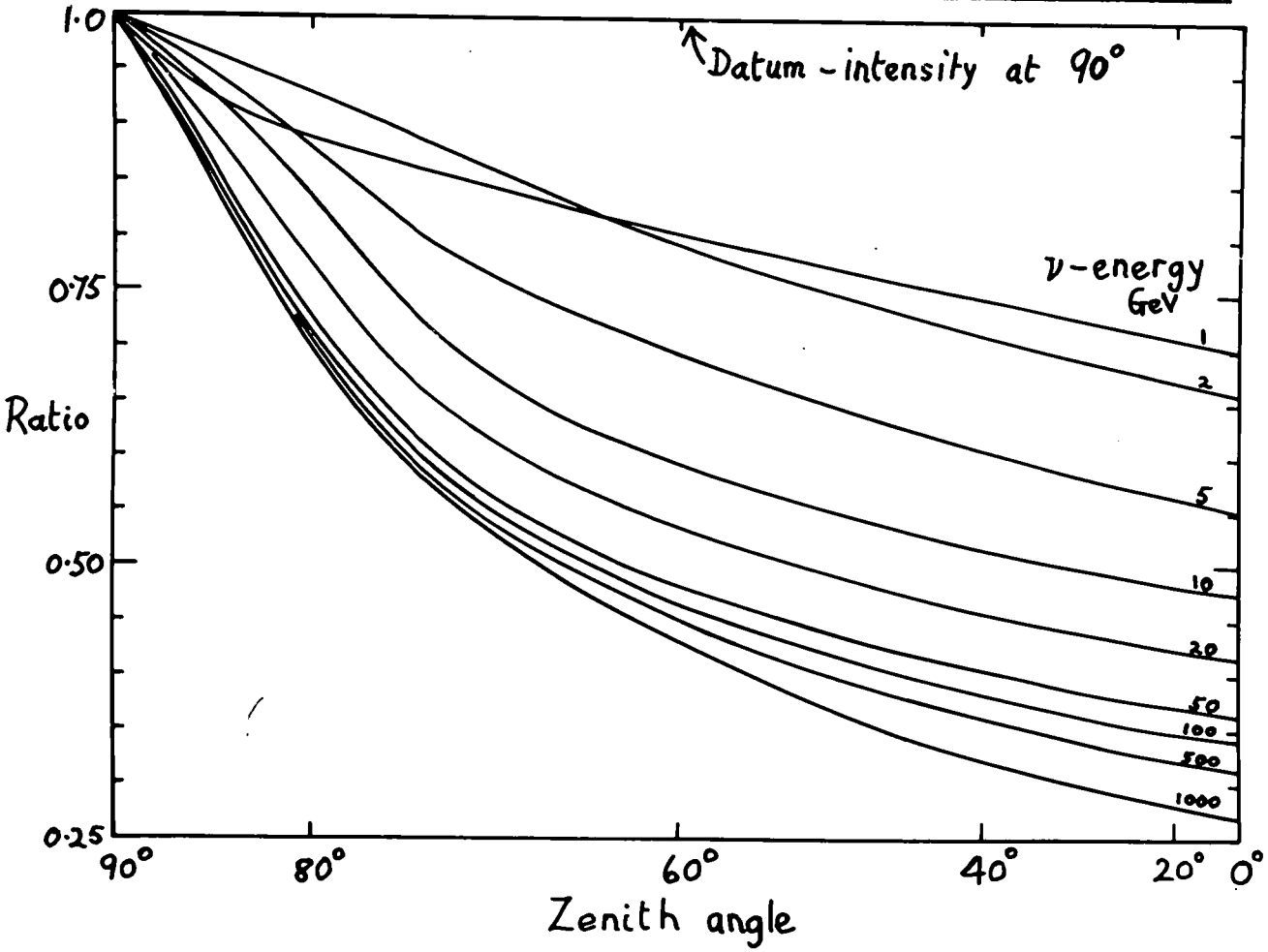

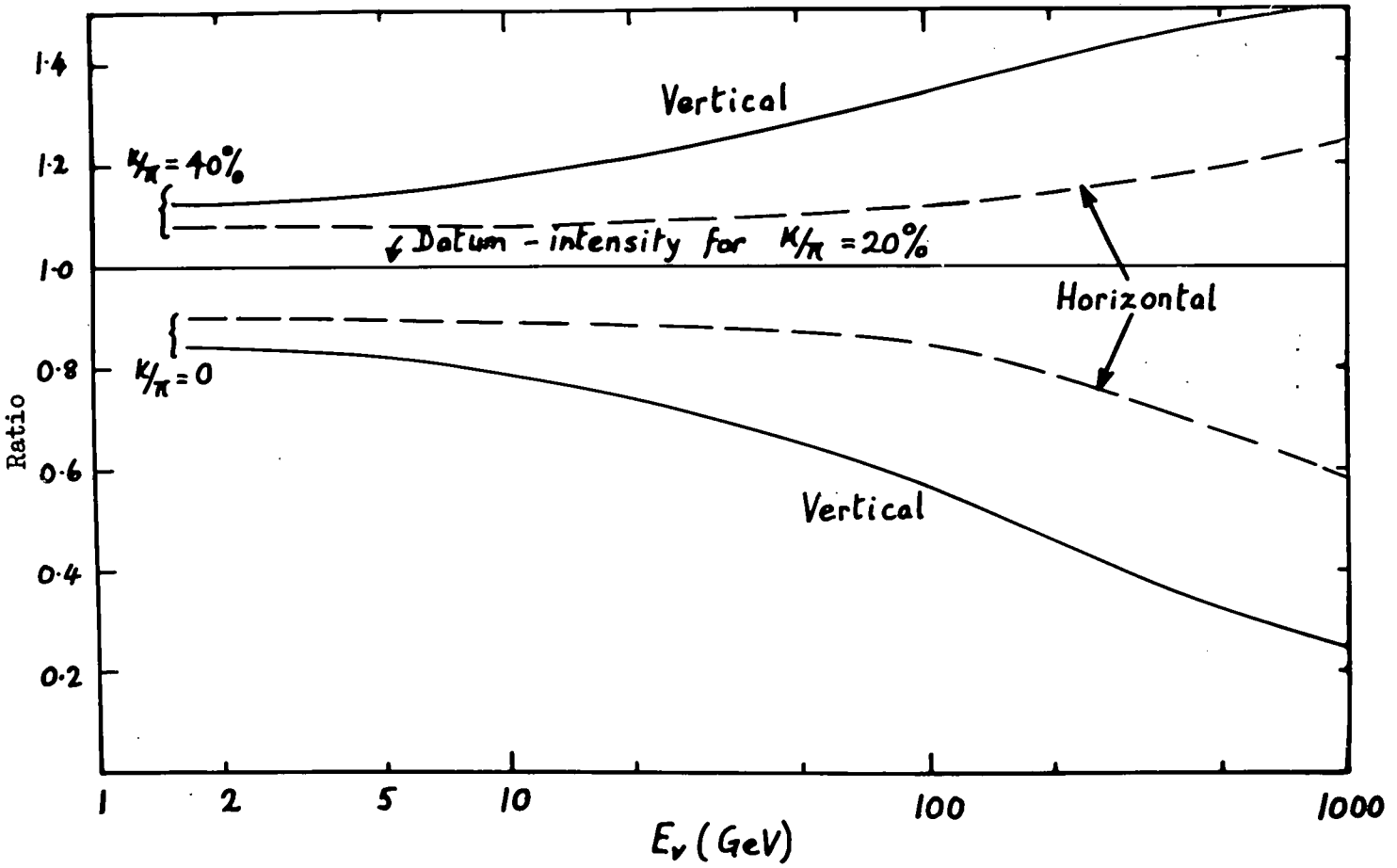

Fig. 6.11 Dependence of the muon-neutrino intensity on the K/π ratio

compared with those for R = 0.2. The considerably smaller contribution of the kaon decay to the total intensity at 90^{o} means that the horizontal intensity is much less sensitive to the value of R than the vertical one.

The division of the total fluxes of neutrinos, given above, into numbers of particles and anti-particles depends on the charge ratios of the parents. If one may assume that these ratios are independent of energy then this division can very easily be calculated; from pions $\nu_\mu/\bar{\nu}_\mu = \pi^+/\pi^-$, from muons $\bar{\nu}_\mu/\nu_\mu = \nu_e/\bar{\nu}_e = \mu^+/\mu^-$ and from charged kaons $\nu_\mu/\bar{\nu}_\mu = \nu_e/\bar{\nu}_e = K^+/K^-$ while neutral kaons produce equal numbers of neutrinos and anti-neutrinos. Cowsik et al. (1965) take μ^+/μ^- to be 1.25 as the best constant value fit to the muon charge ratio versus energy. This value is used for the pion charge ratio also; while, from measurements of kaons stopping in emulsion stacks by Lal et al. (1953), a production ratio of K^+/K^- is deduced which is assumed to apply to the whole of the relevant energy range, and has a value of 20.

6.3 Comparison with Other Results

Of the spectra given by Zatsepin and Kuzmin (1962), who do not differentiate between ν_μ and ν_e and assume that pions alone are produced in high energy collisions, only the contribution from muon decay can be compared with present work. There is agreement to within 5% in the vertical direction for energies from 10 to 1000 GeV. At lower energies the difference, which increases so that their value is 16% greater at 1 GeV, is mainly due to the adoption of a slightly different spectrum for low energy muons. In the horizontal direction their

intensity is, at 1 GeV 25% less than, at 25 GeV equal to, and at 100 GeV 20% greater than the present values. It seems that some of this discrepancy is due to the approximations they have made in the muon energy loss and survival probability.

In the published report of the present calculations (Osborne et al. (1965)) the results were compared with those of Cowsik et al. (1964). The total intensities given by the latter were found to be about 30% less in both the horizontal and vertical directions and when individual contributions were compared even greater differences were apparent. For neutrinos of kaon origin their values were only 50 to 60% of the present ones; this was partly due to their assumption that $N(K^{o}) = 1.4N(K^{+})$ and their neglecting the contribution from two-stage kaon decays but the major part of the discrepancy could not be explained.

In Fig. 6.12 the present results are compared with the total muon-neutrino spectra of Cowsik et al. (1965) in the horizontal and vertical directions. It is seen that the differences have now decreased to between 10 and 20%. Also there are no longer such large discrepancies between the individual contributions to the neutrino intensity. When their values for the kaon contribution are increased (by up to 15%) to allow for neutrinos from two-stage decays all of their intensities are less than the corresponding values of the present work by an approximately constant factor of 10 to 15%. In calculating the neutrino intensities Cowsik et al. use the treatment of Yash Pal and Peters (1964) for meson production at high energies via isobar formation. In this the calculation of the muon and neutrino intensities from the production

Fig. 6.12 Comparison of the intensities of muon-neutrinos at sea level predicted by Cowsik et al.(1965) with the values of the present work

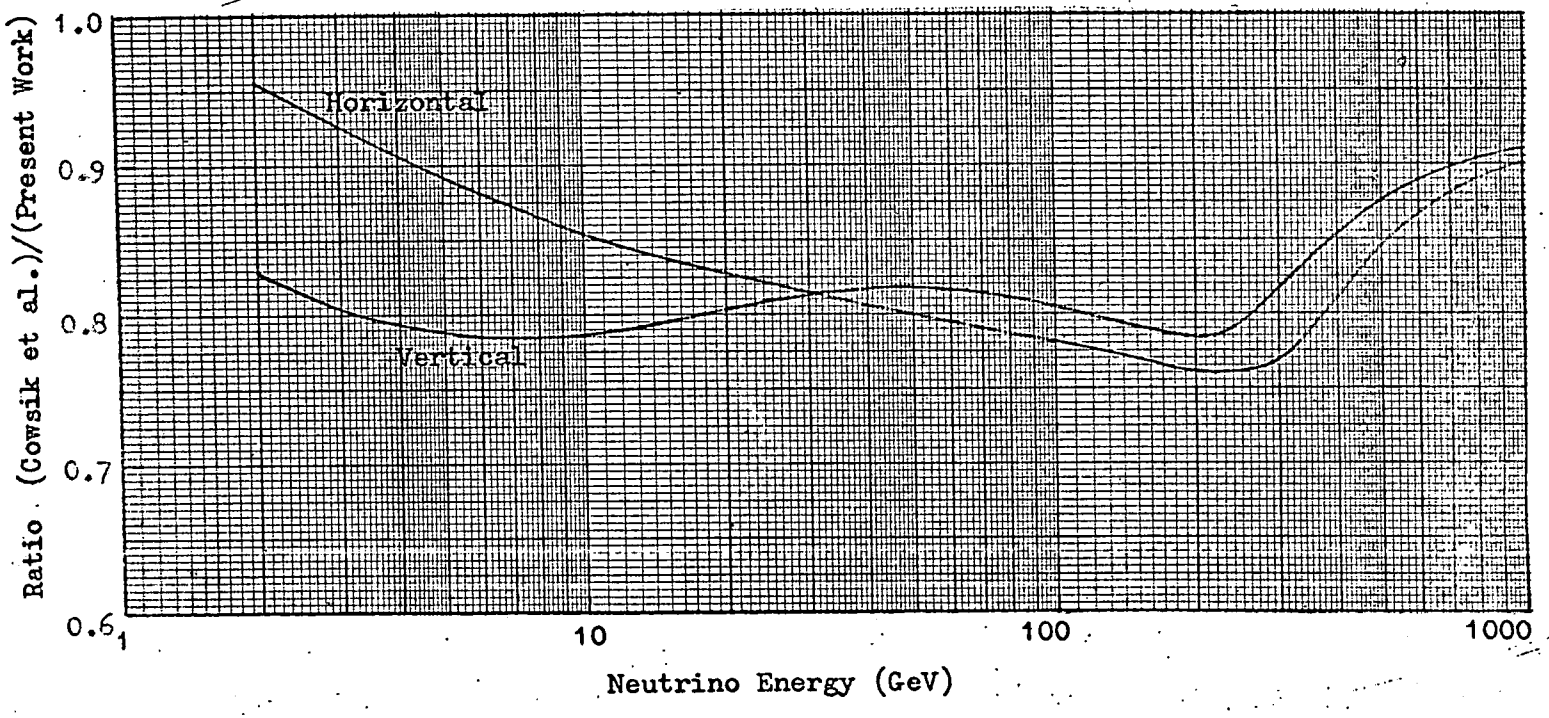

spectra of kaons and pions is essentially the same as used here. The pion and kaon production spectra are obtained, however, by taking the slope equal to that of the measured primary spectrum (a constant value, $\gamma = 2.67$) and then normalising the predicted muon intensity in the vertical direction to a measured value. The authors have normalised to the (uncorrected) intensity of Hayman and Wolfendale (1962) at 30 GeV. In Chapter 2 it was pointed out that to allow for selection bias the measured intensities must be increased by a factor that amounts to 10% at 30 GeV. Taking account of the two-stage decays of kaons and then increasing all of the neutrino intensities by 10% will bring the Cowsik et al. values to within 5% of the present results.

6.4 Extra-terrestial Neutrinos

In the previous sections it has been shown that the intensity of the 'beam' of cosmic ray neutrinos produced in the atmosphere can be calculated with sufficient accuracy that it should be possible to draw meaningful conclusions from experiments in which the products of their interactions are examined. If this is to be done then the interactions produced by neutrinos of extra-terrestial origin must be identified as such or it must be possible to assume that their contribution to the total number is negligible.

The extra-terrestial neutrinos may be divided into two classes; those produced as secondary particles in interactions between the nuclear component of the primary flux and inter-stellar or inter-galactic material and those that may be considered to be primaries themselves and come from discrete sources. The neutrinos generated by

the first mechanism are expected to be approximately isotropic in arrival direction; strong radio sources are possible candidates as generators of the second type. In present theories of the production of high energy neutrinos (e.g. Burbidge (1962)) they will be associated with a corresponding flux of high energy γ-rays. High energy neutrinos, both primaries and secondaries, are expected to be generated by the decay of pions produced in nuclear collisions. Neutrinos will come from the $\pi \rightarrow \mu \rightarrow e$ decay of charged pions while γ-rays will be produced by the neutral pions. The calculation of the relative numbers of neutrinos and γ-rays is simplified when the density of matter in the source is so low that the absorption and energy loss of the pions and muons does not occur. Assuming the production spectrum of pions to be of the form $N E^{-\alpha}$, and using the same decay spectra as before, the ratio of electron-neutrinos to γ-rays of the same energy may be shown to be

$$\frac{F(\nu_e+\bar{\nu}_e)}{F(\gamma)} = 2{\cdot}341\left[\frac{2}{\alpha}-\frac{6}{\alpha+2}+\frac{4}{\alpha+3}\right]\left[1-1{\cdot}74^{\alpha}\right] \qquad (6.13)$$

and for muon-neutrinos

$$\frac{F(\nu_\mu+\bar{\nu}_\mu)}{F(\gamma)} = 2{\cdot}341^{(1-\alpha)} + 2{\cdot}341\left[\frac{5}{3\alpha}-\frac{3}{\alpha+2}+\frac{4}{3(\alpha+3)}\right]\left[1-1{\cdot}74^{\alpha}\right] \qquad (6.14)$$

A K/π ratio of 20% will not affect (6.13) but will increase (6.14) by about 20%.

The flux of γ-rays from π^0 decay in inter-stellar space has been calculated by several authors. Hayakawa et al. (1964), using a distribution of atomic hydrogen in the Galactic disc from radio astronomical 21cm measurements together with the known cosmic ray

intensity, predict that the total intensity of γ-rays averaged over all directions is $3\ 10^{-5}$ cm^{-2}sec^{-1}sterad^{-1} and that the number with energy greater than 1 GeV is $3\ 10^{-6}$ cm^{-2}sec^{-1}sterad^{-1}. From the spectrum of γ-rays, Hayakawa et al. (1965) derive a corresponding spectrum of neutrinos. Equation (6.14) gives the ratio of muon-neutrinos to γ-rays when $\alpha = 2.65$ to be 0.64, and therefore the intensity of muon-neutrinos with energy greater than 1 GeV is $2\ 10^{-6}$ cm^{-2}sec^{-1}sterad^{-1}. This is about four orders of magnitude less than the integral intensities of atmospheric neutrinos in the horizontal and vertical directions ($2.76\ 10^{-2}$ and $1.86\ 10^{-2}$ cm^{-2}sec^{-1}sterad^{-1} respectively). The integral spectrum of Galactic neutrinos is less steep than the atmospheric one but at 10^{4} GeV the difference is still more than two orders of magnitude. The intensity of γ-rays produced in inter-galactic space is much more uncertain since it depends on the inter-galactic primary nuclear flux and density of matter, both of which are difficult to ascertain. Hayakawa et al. (1964) take the inter-galactic hydrogen density to be 10^{-5} atom cm^{-3}. The flattening of the primary spectrum, measured at the Earth, above the Galactic cut off energy ($\sim 10^{15}$eV) is taken to indicate that the inter-galactic primary spectrum is less steep than the inter-stellar one and therefore, at lower energies, the inter-galactic intensity is very much smaller than the inter-stellar intensity. The result is that, below 10^{5} GeV, the inter-galactic γ-ray flux is negligible although it dominates at higher energies. Gould and Burbidge (1965), however, assume that the inter-galactic primary intensity is the same as that at the Earth and arrive at an inter-

galactic γ-ray intensity 30 times greater than the Galactic one over the whole energy spectrum. It is also possible that there may be appreciable amounts of molecular hydrogen in association with the observed inter-stellar atomic hydrogen which could give enhanced γ-ray and neutrino intensities.

A number of experiments have been performed in which upper limits on the primary γ-ray flux incident on the Earth have been obtained. The Explorer XI Earth satellite (Kraushaar (1965)) gave an upper limit about an order of magnitude greater than the calculated Galactic intensity for energies greater than 100 MeV, and the balloon flight nuclear emulsion data of Kidd (1963) and Duthie et al. (1962) gave upper limits three orders of magnitude greater than the calculated values at 80 GeV and 470 GeV respectively. When these are converted to equivalent neutrino intensities the resultant upper limit at 1 GeV is 200 times smaller than the atmospheric muon-neutrino intensity; the difference decreases with increasing energy, and above 100 GeV the upper limit of extra-terrestial neutrinos is approximately equal to the atmospheric intensity in the vertical direction. The non-resonant neutrino interactions discussed in Chapter 5 have cross-sections which vary with energy in such a way that, when the steeply falling spectrum is taken into account, the contribution of neutrinos of energy greater than 100 GeV to the total rate of interactions is very small. Thus it seems that, unless there is some, as yet unspecified; mechanism whereby high energy neutrinos can be produced without an associated flux of γ-rays, the contribution of the isotropic extra-terrestial

neutrino flux to the total sea level flux may be neglected.

Bahcall and Frautschi (1964) have remarked on the possibility of detecting $\bar{\nu}_e$ from discrete radio sources via the Glashow resonance interaction in which the Intermediate Boson is produced. If the value of the magnetic field in the source is assumed then the spectrum of high energy electrons in the source can be calculated from the observed optical and radio synchrotron radiation and the corresponding spectrum of high energy γ-rays and neutrinos can be obtained. Assuming the mass of the boson to be about 1 GeV and calculating the spectrum of neutrinos from the Crab Nebula from the observed optical synchrotron emission, they predicted a rate of detection of muons of 100 $m^{-2}yr^{-1}$ for an apparatus of the KGF type. Bahcall (1964), however, in a later paper, points out that with a lower limit of $\sim$ 2 GeV on the Intermediate Boson mass the resonant energy will be greater than 5000 GeV while there is expected to be a cut off in the neutrino spectrum from the Crab at about 2000 GeV so that the predicted rate from this source must be drastically reduced. The fluxes of $\bar{\nu}_e$ predicted in this way from quasars and other strong radio sources are of about the same order of magnitude at 5000 GeV as the atmospheric neutrino fluxes. Gould and Burbidge (1965) do not consider that a steady state production of very high energy neutrinos by these sources is likely but supernova explosions occuring as a chain reaction within a quasar could give rise to comparable fluxes of neutrinos.

Measurements of the high energy γ-ray fluxes from discrete radio sources have been made by Chudakov et al. (1964) and Long et al. (1965).

Cherenkov telescopes, which give high angular resolution, were used to look for enhancement of the flux of Extensive Air Showers of energies greater than 5000 GeV in the directions of possible sources. The latter authors have examined the Crab Nebula, five quasars (3C48, 3C147, 3C196, 3C273, and 3C286) and three other radio sources. Their results may be summarised as giving apparent fluxes of γ-rays with energy greater than 5000 GeV as $\leq 8\ 10^{-11}\ cm^{-2}sec^{-1}$ with upper limits to the fluxes of $\sim 3\ 10^{-10}\ cm^{-2}sec^{-1}$. If the differential spectrum of the γ-rays is assumed to have an exponent of $\sim$2.5 then the ratio of $\bar{\nu}_e$ to γ-rays from (6.13) is 0.15 and the upper limit to the intensity of $\bar{\nu}_e$ with energy greater than 5000 GeV from the quasars, averaged over all directions, is $\sim 10^{-11}\ cm^{-2}sec^{-1}sterad^{-1}$. This is approximately the same as that of $\bar{\nu}_e$ produced in the atmosphere. The spectrum of the latter neutrinos is steeper than that of the former so that if the Intermediate Boson exists and has a mass greater than 2 GeV and if the neutrino intensity is close to the upper limit, interactions produced by extra-terrestial neutrinos will tend to predominate over those produced by atmospheric neutrinos. It is shown in Chapter 7, however, that with $m_W > 2$ GeV the rate of detection of muons produced by the Glashow resonance interaction for atmospheric neutrinos is considerably smaller than the observed rate. It should be noted that the quasars are among the most distant objects observed in the universe (3C147 appears to be at a distance of $5.3\ 10^9$ light years) and that attenuation of the high energy γ-ray flux by interaction with optical photons in inter-galactic space may be serious over path lengths of this magni-

tude. The upper limits to the neutrino flux obtained from the γ-ray flux from these sources could, therefore, be too low.

In conclusion it may be stated that on all present hypotheses the rate of detection of events produced by extra-terrestial neutrinos should be very small compared to that from atmospheric neutrinos. If, however, the former rate does turn out to be an appreciable fraction of the total then the most probable source will be the Glashow resonance of high energy $\bar{\nu}_e$ coming from discrete sources. Bahcall (1964) has pointed out that the muons from this interaction would be highly collimated so that plotting the arrival directions of all muons produced by neutrinos should enable any from these sources to be identified.

Chapter 7

The Kolar Gold Field Neutrino Experiment

The background to this experiment has been discussed in Chapter 1. Here the initial stages of operation are described and the first results are presented. Only those details of the apparatus relevant to the interpretation of the results are given: further information concerning the day to day running of the equipment has been given by Pattison (1965). Using values of the neutrino intensity derived in the previous chapter, the expected rates and angular distributions of muons incident on the apparatus are calculated and are compared with the preliminary results. Finally the first results of the Case-wits experiment are discussed.

7.1 The Neutrino Telescopes

The experimental site is a tunnel approximately 3.5 m wide and 4 m high running in an East-West direction at a depth of 7600 ft below ground level. The mean density of the local rock being 3.02 g cm^{-3}, this corresponds to 7000 hg cm^{-2}, or, converting to the equivalent depth in 'standard' rock ($Z^2/A = 5.5$), 7500 hg cm^{-2}. There are two identical telescopes (Tel. 1 and Tel.2) aligned in a North-South direction and thus with their vertical detecting faces parallel to the walls of the tunnel. Fig. 7.1 is an elevation corresponding to the East end of Tel. 1 or the West end of Tel. 2. Each detecting face is approximately 3 m high by 2 m wide and consists of 6 one metre squares of plastic scintillator each enclosed in an aluminium cone and viewed by two photomultipliers. There are small gaps between the scintillators so that the overall dimensions of the detecting faces are 2.07 x 3.125 m^2. The gaps have been taken into account in calculating the aperture. The two vertical walls of scintillator are 84.5 cm apart. Between them are nine boxes of neon flash

Fig 7.1 K.G.F. NEUTRINO TELESCOPE

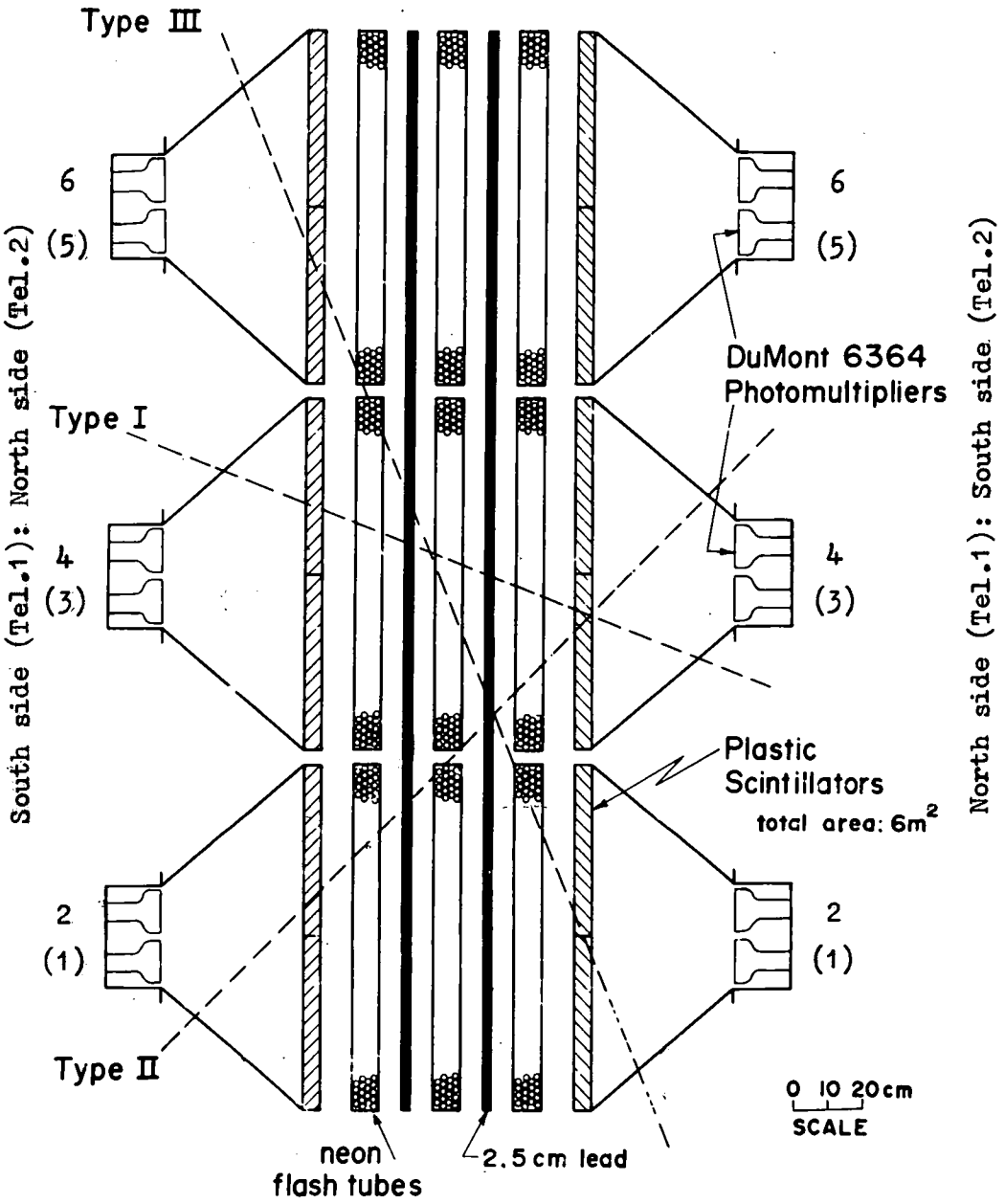

tubes in three columns separated by two walls of lead absorber each 2.5 cm thick. This 10 radiation lengths of lead serves to differentiate between high energy electrons and muons. Because of the absorber the threshold energy for muons is 100 MeV. Except for their being 2 m long the flash tubes are identical to those used in the Durham horizontal spectrograph. Each box contains 210 tubes in four columns. When a four-fold coincidence occurs between any two pairs of photomultipliers, one on each side of a telescope, the pulses are displayed on oscilloscopes and a high voltage pulse is applied to the flash tubes. The tubes which flash are recorded, together with the time of the event, by two cameras mounted on the corresponding face of the other telescope at a distance of 6 m. From the oscilloscope traces the scintillators giving the coincidence can be identified and it is possible to differentiate between a pulse due to a single particle and that produced by a number of particles. The numbering of the scintillators is shown in Fig.7.1. Those with even numbers are at the front, those with odd numbers at the back of the telescopes. The flash tubes serve three purposes: they discriminate against 'events' due to spurious four-fold coincidences; they allow the projected zenith angle of the muon tracks to be measured to within an accuracy of about 1^{o}, and they facilitate the interpretation of complex events where more than one particle is incident on the telescope or an interaction occurs inside the telescope. In the first stages of the experiment, when the observed number of events is small, it is necessary to divide the total zenith angular range covered by each telescope into a small number of cells, each covering a wide range in order that a meaningful comparison can be made between the observed and predicted angular distributions of neutrino-induced and atmospheric muons. A convenient classification is provided by the relative positions of the scintillators that

are traversed on opposite sides of the telescope. The events are then denoted as type I (opposite), type II (adjacent) and type III (top and bottom) as shown in Fig.7.1.

7.2 The Predicted Numbers of Events

7.2.1 The Aperture of the Telescopes

The aperture of each telescope is defined by the dimensions and separation of the scintillators. Expressions for the differential aperture with respect to both spatial zenith angle, θ, and projected zenith angle, β, are given in Appendix D. With the notation used there, the present telescopes have dimensions, X = 2.07 m, Y = 3.125 m and Z = 0.845 m. Thus the total aperture of each telescope, taking into account the reduction due to the small gaps between the scintillators, is 19.5 m^2 sterad. The azimuthal angles of particles incident on the telescopes are only poorly defined; for a coincidence between two even or odd numbered scintillators $47^\circ \geqslant \phi \geqslant -47^\circ$, while for an odd-even coincidence $66^\circ \geqslant \phi \geqslant -66^\circ$ ($\phi = 0^\circ$ is the normal to the detecting surface). The differential aperture with respect to projected zenith angle for the upper hemisphere is shown in Fig.7.2, together with the partial apertures for types I, II and III events.

7.2.2 The Flux of Neutrino-initiated Muons Underground

For each of the interactions discussed in Chapter 5 the flux of muons underground produced by cosmic ray neutrinos can be calculated. Using the present apparatus the intensity measured in a particular direction is that summed over all muon energies above the threshold of 100 MeV. The general expression for the intensity at a zenith angle θ is

$$I_\nu(\theta) = \frac{N_A}{A} \int_{E_{min}}^{\infty} N_\nu(E_\nu, \theta)\, R_{eff}(E_\nu)\, \sigma(E_\nu)\, dE_\nu \qquad (7.1)$$

Fig. 7.2 Differential aperture of a KGF neutrino telescope with respect to projected zenith angle

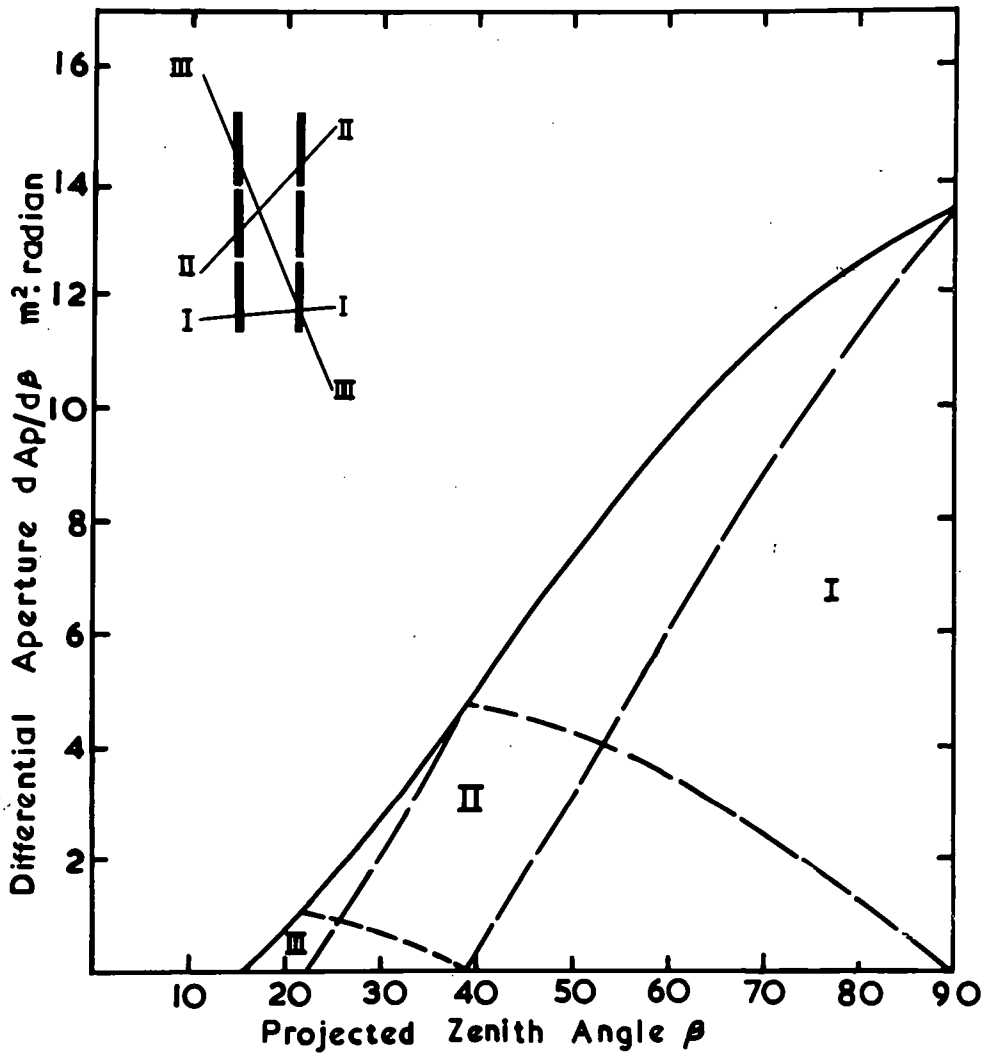

$N_\nu(E_\nu,\theta)$ is the intensity of neutrinos, of energy E_ν, at ground level, as calculated in the previous chapter. For all interactions except the Glashow resonance, the attenuation of the neutrino flux in the Earth is negligible in all directions. $\sigma(E_\nu)$ is the total cross-section per nucleus for the interaction under consideration. $R_{eff}(E_\nu)$ is the effective range in rock of muons produced by neutrinos of energy E_ν and represents the thickness of rock acting as a target for the interaction. In general we have the relation $R_{eff}(E_\nu) = R_\mu(\bar{r}E_\nu) - R_\mu(100\ \text{MeV})$, $R_\mu(E_\mu)$ being the range in rock of muons of energy E_μ as given in Fig 2,1 and $\bar{r}$ being the mean fraction of the neutrino energy retained by the muon. E_{min} is either the threshold energy of the interaction or 100 MeV, whichever is the lower. There are no simple analytical expressions for the three variables in (7.1) and the integration over energy is performed numerically. It can be seen that the median energy of neutrinos contributing to the total intensity of muons from a given interaction depends on the way in which the cross-section varies with energy; the faster the rise in cross-section the higher the median energy. In obtaining (7.1) it has been assumed that the muon enters the telescope travelling in the same direction as the interacting neutrino. In the elastic and inelastic interactions and in the production of a 'prompt' muon in association with the intermediate boson the muon is emitted in the forward direction in the c.m.s. and the laboratory angle between it and the neutrino is less than q/E, where q is the 4-momentum transfer. The Coulomb scattering of the muon in rock depends on the energy of the particle on reaching the telescope: for an energy at the telescope of 1GeV the r.m.s. projected angle of scatter is $\lesssim 3.5^\circ$. The result is that, with the possible exception of elastic interactions, the effect on the zenith angular

distribution of deviations of the muon from the neutrino direction is negligible. In the Glashow resonance interaction the neutrino direction would be particularly well defined; the angle between the neutrino and the muon would be $< 2m_e/m_W$ and the muon produced would have a very high energy and thus experience negligible scattering.

The Elastic Interaction

Because the elastic interaction has a constant cross-section above 1 GeV and the neutrino spectrum falls approximately as E^{-3}, the median energy for this interaction is only $\sim$2.5 GeV. In order to predict the contribution to the total intensity from interactions of neutrinos with energies less than 1 GeV it is necessary to extrapolate the calculated intensities below 1 GeV. The contribution of these neutrinos is $\sim$20% of the total and the uncertainty in the total intensity due to uncertainties in the extrapolation is $\sim$10%. An equally important factor is the effect of geomagnetic cut off of the primary cosmic rays of the low energy neutrino spectrum. It is assumed in calculating the total rates of events that the neutrino flux is isotropic with respect to azimuthal direction. The neutrino intensities given in Chapter 6 are derived from the vertical muon spectrum measured at Durham (53°N) where the effects of geomagnetic cut off are minimal. At KGF (13°N) the cut off becomes important in some directions, particularly in the lower hemisphere, for neutrino energies below 4 GeV. At 1 GeV the true flux is, in some directions, less by a factor of two than the assumed isotropic flux (S. Miyake, p.c.). Because of these considerations the predicted rates of elastic events quoted below must be taken to be uncertain by $\sim$30%. This applies only to this particular interaction where the median energy is close to the threshold energy of the apparatus. It is shown below that the contribution of these events to the total rate is, in any case, small.

The Inelastic Interaction

Of the very large choice of forms of the variation of the inelastic cross-section with energy, which would be compatible with the experimental results below 10 GeV, we quote the rates of events expected for four particular cases.

Inelastic (1): $\sigma = 0.45\ 10^{-38} E$ cm^2 nucleon^{-1}, with a cut off at 10 GeV. This is the minimum cross-section that would agree with machine results.

Inelastic (2): $\sigma = 0.45\ 10^{-38} E$ cm^2 nucleon^{-1}, with a cut off $\gg$10 GeV. The cross-section cannot, of course, rise linearly with energy indefinitely but if the cut off energy were $\gtrsim$ 500 GeV the predicted rate of events would not be sensitive to its actual value.

Inelastic (3): $\sigma = 0.19\ 10^{-38} E^2$ cm^2 nucleon^{-1}, with a cut off at 10 GeV.

Inelastic (4): $\sigma = 0.19\ 10^{-38} E^2$ cm^2 nucleon^{-1}, with a cut off at 40 GeV.

This quadratic rate of increase of the cross-section cannot be ruled out by the machine results.

In an inelastic interaction at least one hadron is produced in addition to the muon. If the interaction occurs in the surrounding rock sufficiently close to the telescope then a double event may be recorded in which two particles are seen to be incident on the apparatus simultaneously. Because of the strong interactions of the hadrons the effective target thickness of rock for a double event of this kind is restricted to about 120 g cm^{-2}. An estimate of the rate of double events has been made for each of the cross-sections listed above. The constant effective target thickness means that the rate is only a small fraction of that of single muons for which the target thickness is approximately proportional to the neutrino energy. An interesting point is that this results in the median energy of neutrinos causing double events being low and the rates being independent of the behaviour of the cross-section at high energies.

Production of the Intermediate Boson

The dependence of the intensity of muons, which are produced in association with the Intermediate Boson or in its decay, on the energy sharing between the 'prompt' muon and the boson and on the branching ratio, b, for $W \rightarrow \mu + \nu_\mu$ decay have been discussed in Chapter 5. The intensities are given here for b = 0.4 and the two limiting values of the energy division (i) $\bar{r}_p = m_\mu/(m_\mu + m_W)$ and (ii) $\bar{r}_p = 0.5$. The sum of the intensities of 'prompt' and 'decay' muons has been used in calculating the rate of events. The median distance from the telescopes at which detected interactions occur is from 20 to 40 metres of rock and muons from decay of the boson, being emitted predominantly in backward directions in the boson rest system, will generally travel in the laboratory system at small but finite angles to the prompt muons. Thus in only a fraction of the interactions in which two muons are produced will the two muons traverse the telescopes together. As a rough estimate, about 10% of the events due to intermediate boson production would be expected to contain two muons, for the assumed value of the muonic branching ratio. Predictions of the rates of events for three values of the boson mass above the experimental lower limit have been made (m_W = 1.8, 2.5 and 3.0 GeV).

The Glashow Resonance Interaction

There are big uncertainties in the rate of events due to the Glashow resonance interaction because of uncertainties in the flux of $\bar{\nu}_e$ at energies above 1000 GeV. The rates quoted below are obtained assuming that the K/π ratio, R, is 0.2, K^+/K^- = 1 and that the muonic branching ratio, b, is 0.4. At these high energies the majority of electron-neutrinos would be produced by K^-_{e3} and K^0_{e3} decay rather than from muon decay and therefore, for this interaction, the rate of events is approximately proportional to R. If R were

in fact zero at these energies the rates would be too high by two orders of magnitude. If there were a large positive excess of charged kaons then the neutrino fluxes assumed should be halved. Finally, the intensity of muons from this interaction is proportional to $\underline{b}$ which could have a considerably smaller value than 0.4. It is therefore apparent that the quoted rates are in the nature of upper limits. The ratio of events, initiated by neutrinos produced in the atmosphere, from the resonance production of the boson to the number from boson production on atomic nuclei is less than unity and decreases with increasing boson mass. The importance of the resonance interaction lies in the fact that it would provide a channel whereby high energy extra-terrestial neutrinos could be detected.

The intensities of muons were calculated from equation (7.1) for each of the non-resonant interactions listed above. The variation of muon intensity with zenith angle for three cases, elastic, inelastic (2) and Intermediate Boson production (m_W = 2.5 GeV) are shown in Fig. 7.3. The angular distributions are symmetrical about the horizontal plane. By folding the muon intensities into the differential aperture of the telescopes (equation D.4) the angular distributions and total rates of events detected by the telescopes were predicted. The results are given in Table 7.1, where the approximate median energies of the neutrinos causing the interactions are also indicated. Two values of the rates are given for Intermediate Boson production, corresponding to the limiting cases of energy sharing discussed in section 5.3.2. The angular distributions for some of the interactions are given in Fig. 7.4 where each curve is normalized to unit area. It is seen that the angular distribution is not very sensitive to the type of interaction but it is more strongly peaked in the horizontal direction for those where the median energy is higher.

Fig. 7.3 Intensities of neutrino-induced muons

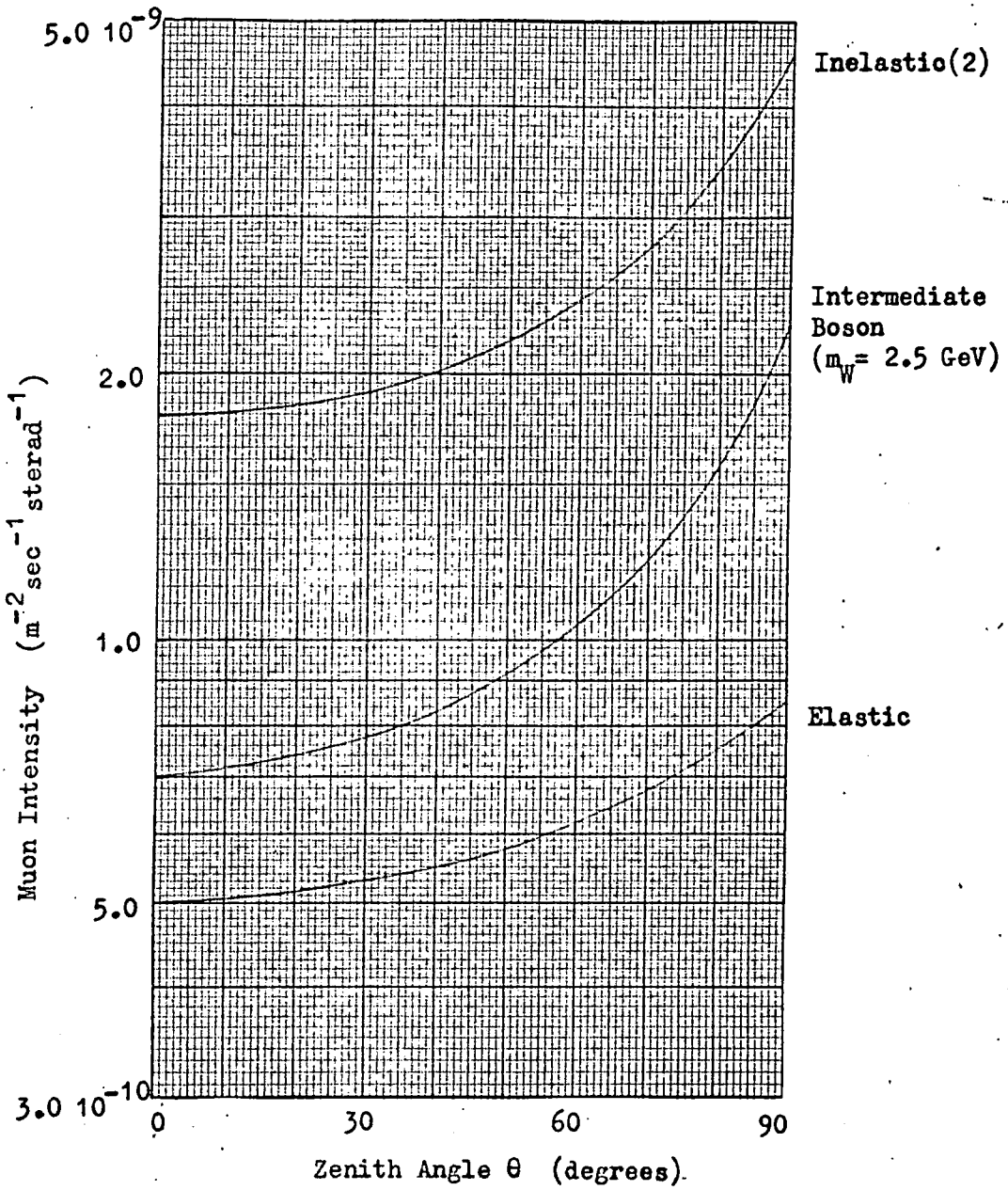

Table 7.1

Predicted Rates of Events for KGF Neutrino Telescopes

Interaction	Rate of Events (per telescope-day)	Median Neutrino Energy (GeV) (Approximate values)
(a) Elastic	$1.1\ 10^{-3}$	2.5
(b) Inelastic (1)	$2.9\ 10^{-3}$ $(2.5\ 10^{-4})$*	10
(c) Inelastic (2)	$4.9\ 10^{-3}$ $(2.5\ 10^{-4})$	25
(d) Inelastic (3)	$8.9\ 10^{-3}$ $(3.0\ 10^{-4})$	15
(e) Inelastic (4)	$3.3\ 10^{-2}$ $(3.5\ 10^{-4})$	45
(f) Intermediate Boson m_W = 1.8 GeV	(i) $4.8\ 10^{-3}$ (ii) $1.7\ 10^{-2}$	100
(g) Intermediate Boson m_W = 2.5 GeV	(i) $2.2\ 10^{-3}$ (ii) $8.0\ 10^{-3}$	200
(h) Intermediate Boson m_W = 3.0 GeV	(i) $1.5\ 10^{-3}$ (ii) $5.2\ 10^{-3}$	300
(i) Glashow Resonance m_W = 1.8 GeV	$1.5\ 10^{-3}$	3000
(j) Glashow Resonance m_W = 2.5 GeV	$3.1\ 10^{-4}$	6000
Lower Limit (a + b)	$4.0\ 10^{-3}$	

*Values in brackets are the approximate rates of double events

Fig. 7.4 Comparison of angular distributions of neutrino-induced muons on the KGF telescopes

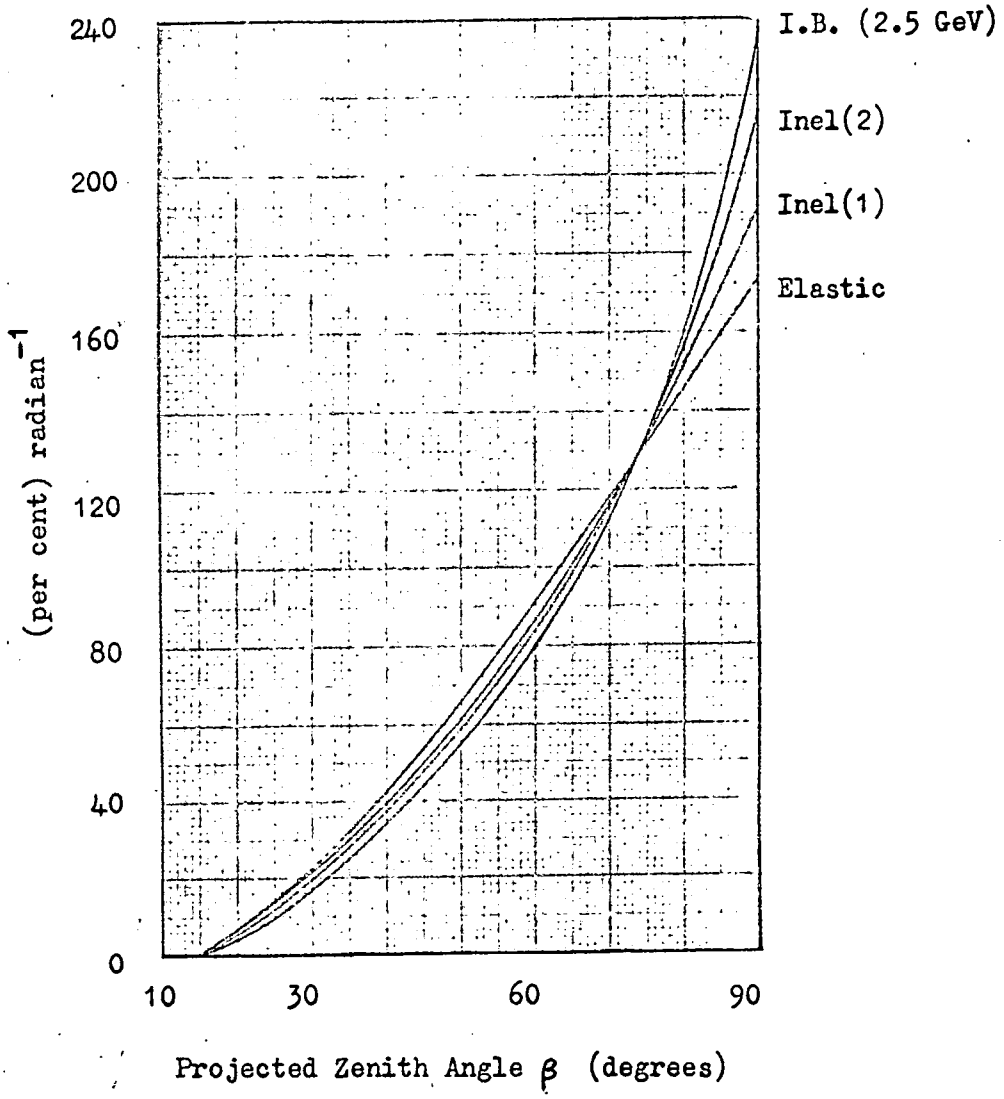

7.2.3 The Flux of Atmospheric Muons

Although the neutrino telescopes are orientated in the horizontal direction, muons are accepted which have zenith angles as low as 15°. The flux of atmospheric muons is greatly attenuated by the 7500 hg cm^{-2} of rock above the apparatus but still may be appreciable at the lower zenith angles when compared to the flux of neutrino-induced muons. Prior to the two neutrino experiments, a series of measurements of the intensity of muons, using vertically orientated detectors, had been made down to 6900 hg cm^{-2} of standard rock by Miyake et al. (1964) and a further exposure at 9200 hg cm^{-2} had yielded zero counts, resulting in an upper limit to the flux. Combining these with previous results at shallower depths the depth-intensity curve can be extrapolated to give an estimate of the vertical intensity and angular distribution of atmospheric muons at the present site. The angular distribution is simply related to the variation of vertical intensity with depth. If the vertical intensity at depth $\underline{D}$ can be represented by a power law, $I_v(D) = A.D^{-(n+1)}$, then the angular distribution is of the form $I(\theta) = I_v \cos^n\theta$. The reduction by unity of the exponent takes account of the angular distribution at sea level of muons (with sea level energy $\sim 1.5\ 10^4$ GeV) that penetrate to these depths which is proportional to sec θ. At shallower depths, where the muon range is proportional to energy, the power law expression fits the data well, but at great depths $(n + 1)$, the slope of the depth-intensity curve on a logarithmic plot, is increasing slowly with depth.

The extrapolated curve and its slope at 7500 hg cm^{-2} gives the following expression for the intensity of atmospheric muons.

$$I_A(\theta) = 8.5\ 10^{-7} \cos^{9.5}\theta\ m^{-2}\ sec^{-1}\ sterad^{-1} \qquad (7.2)$$

The uncertainty in the vertical intensity is about ± 30%. In Fig. 7.5 the differential rate of atmospheric muons with respect to projected zenith angle that is expected to be recorded by each of the KGF telescopes is given. For comparison the rate of neutrino-induced muons from the 'inelastic (2)' interaction is also shown. In this case the rate plotted is the combined value for upward and downward moving muons since the direction cannot usually be determined. The figure should be regarded as giving the form of the angular distributions only; their relative amplitudes must be determined from observation. It can be seen, however, that, unless the neutrino-induced muon flux is very much greater than that predicted for the 'inelastic (2)' case, the overwhelming majority of muons below $\beta = 30^{\circ}$ will be of atmospheric origin. Similarly any muons observed beyond $\beta = 60^{\circ}$ can be attributed to neutrino interactions with very high probability. The relative proportions of muons between 30° and 60° must be estimated from the observed angular distribution.

The continued operation of the neutrino experiments themselves will lead to more accurate values of the intensity of atmospheric muons. The Case-Wits experiment, being at a greater depth, will improve our knowledge of the angular distribution at 7500 hg cm^{-2}. The effect of the initial results from this experiment on the assumed angular distribution is discussed below.

7.3 Preliminary Results from the KGF Neutrino Experiment

The first phase of the experiment was from 1st April, 1965 to 3rd November, 1965. In this time there was a total of 298.8 telescope-days (5.03 10^{8} m^{2} sec sterad for isotropic radiation) of operation, during which 16 events were recorded. (Prior to 1st April the partly assembled apparatus was in operation for 36 telescope-days during which no definite events were seen). The 16 events are listed in Table 7.2; the events marked O.G (out of geometry)

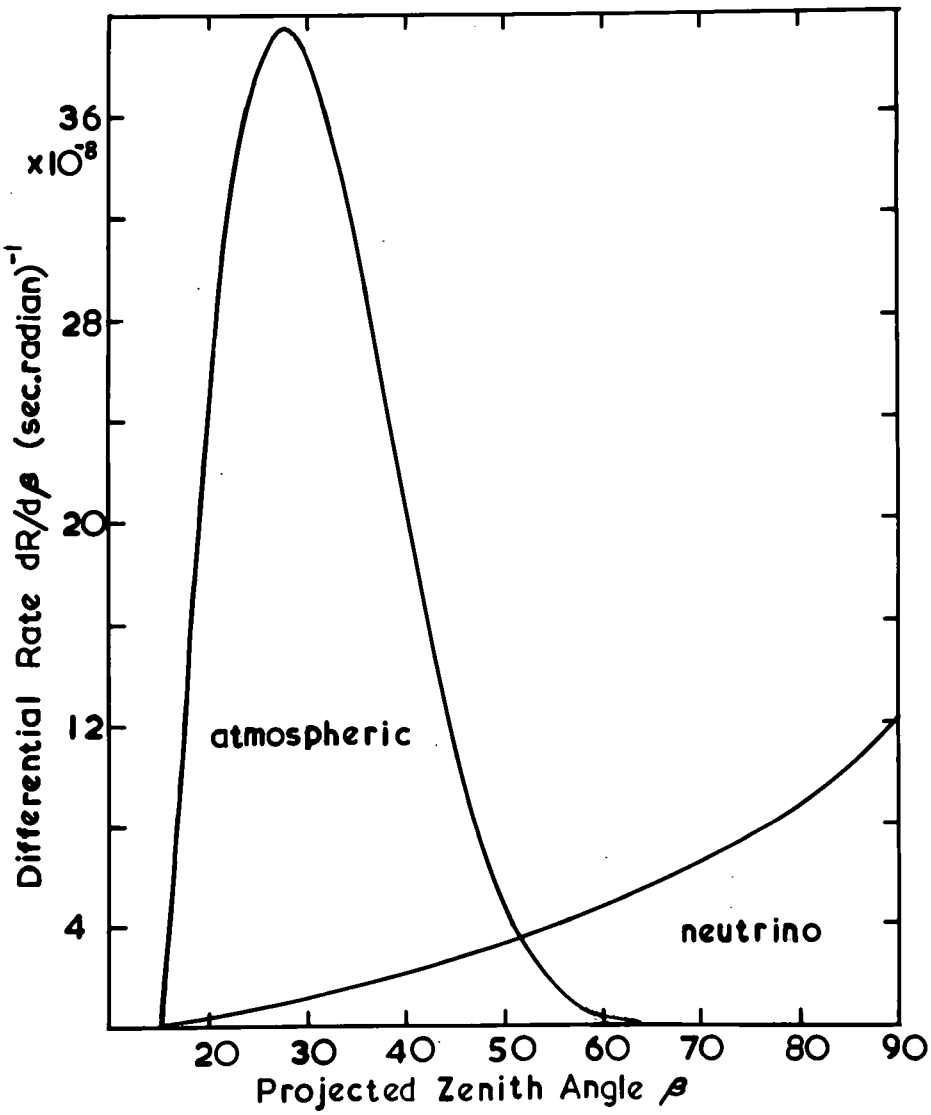

Fig. 7.5 Comparison of the forms of the angular distributions of atmospheric and neutrino-induced muons

Table 7.2

Events Recorded by the KGF Neutrino Telescopes (1/4/65 to 3/11/65)

Event No.	Date	Time IST*	Time MST+	Telescope	Scintillators	Type	Projected Zenith Angle (degrees)
1	5/4/65	20.04	08.38	1	N4 S4	I	> 39
2	27/4/65	18.26	08.30	1	N1 S1	I	48
3	25/5/65	20.03	11.58	2	N6 S6	I	75 ± 10
4	3/7/65	12.30	06.57	2	N1 S1	I	96.2 ± 0.8 99.2 ± 0.3
5	13/7/65	16.14	11.21	2	N4 S356	II	45
6	18/7/65	02.50	22.14	1	N36 S12	O.G	8.5
7	24/7/65	11.47	07.37	2	N6 S3	II	37.5
8	27/7/65	03.22	23.23	1	N6 S3	II	29.5
9	29/7/65	19.07	15.18	2	N1 S3	II	32.5
10	1/8/65	21.00	17.23	1	-	O.G	25
11	2/8/65	03.38	00.02	1	N6 S4	II	47
12	11/8/65	17.37	14.38	1	N4 S5	O.G	33
13	12/8/65	11.38	11.21		Large shower in telescope 2		
14	9/9/65	02.22	01.12	2	N5 S13	III	21
15	10/9/65	08.20	07.15	1	N6 S3	II	26.5
16	13/10/65	12.14	13.23	1	N3 S1	II	40

* Indian Standard Time + Mean Sidereal Time

are those where the muon did not pass through both scintillators, the necessary coincidence being provided by an accompanying particle or a knock-on produced inside the apparatus. Particular features of the events are listed below.

Event 1 Telescope 1 contained no flash tubes at this time. The scintillator information shows that this is a Type I event and therefore has zenith angle $\geq 39^{\circ}$.

Event 2 A single track. Only the two outer columns of flash tube boxes were installed at this time.

Event 3 A single track. Only the centre flash tube boxes were present.

Event 4 This is of particular interest since it contains two almost parallel particles incident on the telescope in the horizontal direction. Fig. 7.6 shows the two tracks in the lower third of Tel. 2. The interpretation of the event has been discussed at length in the paper by Achar et al. (1965b), where the following conclusions were drawn. The projected zenith angle between the tracks is $(3\pm1)^{\circ}$ and they appear to diverge from a point which may be at the surface of the southern rock wall or at a depth of up to 1 m, in the plane of the diagram, inside it (to the extent of 1 standard deviation). The particle producing track 'a' penetrates 10 radiation lengths of lead without scattering or producing a cascade, and is therefore not an electron and is presumably either a muon or a pion. Considering track 'b', if the two particles were produced in the southern rock wall the absence of a track in the southern flash tube tray would be due to the azimuthal angle being such that the particle, passing through the back of the telescope, missed this tray. The lead walls protrude 7 cm beyond the back of the flash tubes and it is probable that the particle passed through both lead walls. The pair of particles could, on the other hand, have been produced in the north rock wall and then have been scattered into the observed directions. In this case the particle producing track 'b' may either

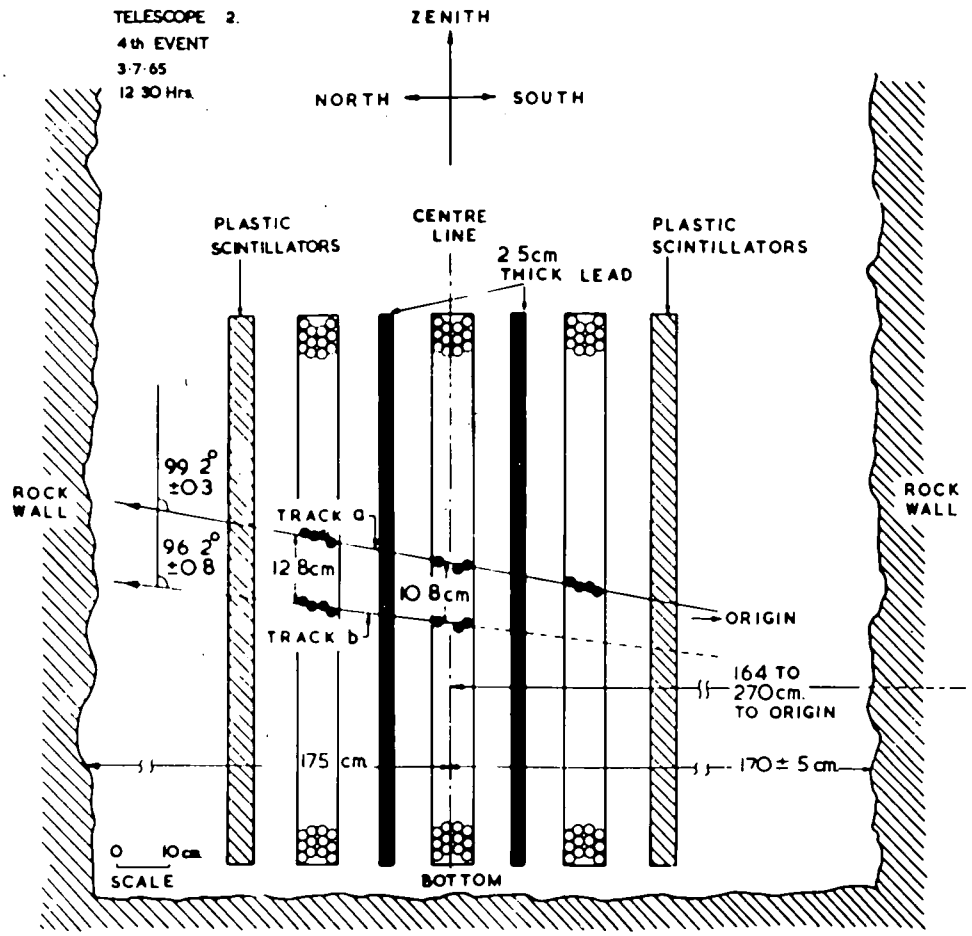

Fig. 7.6 Diagram of the lower section of Tel.2 showing the 4th event

have missed the southern flash tubes or have stopped in the second lead wall. In either case track 'b' was almost certainly caused by a muon or a pion. The simplest interpretation is that these two tracks are a muon and a pion produced in an inelastic neutrino interaction close to the surface of the rock. It is apparent from the figures given in Table 7.1, however, that if the Intermediate Boson exists with mass $\lesssim 3$ GeV there is an equal probability that the event represents the 'prompt' and 'decay' muons resulting from its production. A similar event with two, more widely separated but near parallel, penetrating tracks could be definitely attributed to a pair of muons and would be rather strong evidence for the existence of the boson.

Event 5 A single track.

Event 6 A near vertical track intersecting the S1 scintillator. The track of one of the knock-on electrons causing the coincidence with the north scintillators is visible.

Event 7 A penetrating track with a knock-on in the north flash tube tray indicating a downward moving particle.

Event 8 A penetrating track with three knock-ons in the centre tray indicating a downward moving particle.

Event 9 A penetrating track producing a shower in the north lead wall indicating a downward moving particle.

Event 10 A single track which misses the south scintillators. The coincidence was presumably caused by a knock-on from the rock.

Event 11 A single track with a small shower generated in the south lead wall indicating that the particle is travelling downwards.

Event 12 A single track which misses the south scintillators. The coincidence is caused by an associated shower from the rock wall.

Event 13 A very large shower incident on the south side of Tel. 2. All six scintillators on this side showed saturated pulses; five on the north side also gave pulses. Almost all the tubes in the south trays flashed. Pulses were also recorded from Tel. 1 although only a few tubes flashed. The shower was estimated to have an energy of several hundred GeV. No penetrating tracks were clearly defined to give the direction of the initiating particle.

Event 14 A penetrating track with a shower produced in the north lead wall indicating a downward moving particle.

Events 15 and 16 Single tracks.

7.4 Discussion of the Preliminary Results

With the small number of events so far detected it is not possible to draw any definite conclusions with regard to the character of the neutrino interactions. It is of interest, however, to compare the presently observed rates of events with those predicted in Table 7.1.

Of the 16 events, numbers 6, 10 and 12 must be ignored because they do not conform with the selection criteria and event 13 cannot be interpreted in terms of its initiating particle. The remaining 12 events contain two (2 and 4) with zenith angles greater than 60° and these can be definitely attributed to neutrino interactions. The probable division of the remaining ten into atmospheric and neutrino-induced muons can be made by comparing their angular distribution with those given in Fig. 7.5. The result is that a combination of roughly equal amplitudes of the two distributions fits the observed distribution best. An equivalent method is to compare the observed division of events into types I, II and II with the expected distributions for the two types of muons. This is shown in Table 7.3.

A total of six neutrino-initiated events gives a rate of $(2.0^{+1.2}_{-0.8})10^{-2}$ per

Table 7.3

Comparison of Observed and Predicted Angular Distributions

	Scintillator Configuration I	II	III
(i) Neutrino-induced Muons	72.6%	25.9%	1.5%
(ii) Atmospheric Muons	5.5%	61.3%	33.2%
Equal Amplitudes of (i) and (ii)	39.1%	43.6%	17.3%
Equivalent Distribution of 12 events	4.7	5.2	2.1
Observed Distribution of 12 events	4	7	1

Tel-day. This is seen to be 5 times greater than the lower limit derived from the most conservative extrapolation of the machine results, i.e. assuming that the Intermediate Boson, if it exists, has mass $\gg 3$ GeV and that the inelastic cross-section does not increase beyond 10 GeV. A continued increase in cross-section above 10 GeV is thus indicated. From the observed rates alone it is not possible to differentiate between the effect of the production of a boson with mass not much greater than the present lower limit from machine results and a rapidly increasing inelastic cross-section. For example, comparing the predictions for the 'inelastic (3)' and 'inelastic (4)' cases, the present total of six events could be explained by a quadratic increase of inelastic cross-section up to a cut off energy of~30 GeV.

It is interesting to note that, of the five events with zenith angles $\leqslant 37.5^{\circ}$, which are expected to be mostly atmospheric muons, four are either accompanied by an electromagnetic component or produce knock-ons or showers within the telescope, while of the six at larger zenith angles, which are expected to be predominantly neutrino-induced, only one shows an interaction within the telescope. This behaviour is to be expected because of the considerably higher mean energy of atmospheric muons incident on the telescopes.

The Celestial coordinates of the arrival directions of the muons have been computed and are shown in Appendix E.

7.5 Results of the Case-Wits Experiment

The experiment being performed in a collaboration between the Case Institute, Ohio and the University of Witwatersrand is basically similar to the KGF experiment. The preliminary results from it have been reported by Reines et al. (1965) and Crouch et al. (1965). The apparatus is

situated in a tunnel running in a North-South direction at a depth of 10,492 ft below ground level. The local rock having a density of 2.75 g cm^{-3} and $Z^2/A = 5.0$, this is equivalent to 8500 hg cm^{-2} of standard rock. The detector has two parallel walls of liquid scintillator of overall dimensions 37m long by 1.9m high. The walls are 1.8m apart and consist of 36 rectangular tanks 12.5 cm thick, each viewed from its two ends by four photo-multipliers. The gaps between the tanks account for 21% of the overall wall area.

The minimum requirement for the recording of an event was a coincidence between any four photo-multipliers in the same wall. Up to 2nd October 1965 a time of operation equivalent to 147 days for the complete assembly had been attained. The total of 85 events recorded are divided into four classes as follows: (i) 7 eight-fold coincidences involving one tank in each wall, (ii) 59 four-fold coincidences from a single tank in one wall, (iii) 15 multiple tank events in one wall only, (iv) 4 multiple tank events in both walls. Events of type (i) are interpreted as being due to a single particle passing through both walls of the telescope. The minimum zenith angle for these is 43° and, since the intensity of atmospheric muons at this depth and at angles greater than 43° is negligible, they can be attributed to neutrino-initiated muons. The aperture of the apparatus for type (i) events is 150 m^2 sterad. Type (ii) and (iii) events are caused by atmospheric and neutrino-initiated muons that intersect only one wall of the telescope. In the absence of visual detectors the interpretation of the type (iv) events is difficult; it is possible that they are due to two or more particles incident in the near horizontal direction and therefore attributable to neutrino interactions. On the other hand, they could be caused by near vertical atmospheric muons together with showers from the rock. The possible complexities have been

illustrated by the events recorded by the KGF telescopes. From the 7 type (i) events the intensity of neutrino-initiated muons, for an isotropic distribution is $(3.7^{+2.0}_{-1.4})10^{-9}$ m^{-2} sec^{-1} sterad^{-1}: if the four ambiguous events are included then this becomes $(5.8^{+2.3}_{-1.8})$ 10^{-9} m^{-2} sec^{-1} sterad^{-1}. This should be compared with the corresponding value of $(1.2^{+0.8}_{-0.5})10^{-8}$m^{-2}sec^{-1} sterad^{-1} for the six events from the KGF experiment. The Case-Wits result gives a lower rate, but there is no real discrepancy because of the statistical uncertainty.

It is possible to obtain an estimate of the flux of atmospheric muons at 8500 hg cm^{-2} from the above results. Using the observed rate of events at angles greater than 43°, the expected admixture of neutrino-induced muons among the type (ii) and (iii) events may be calculated and subtracted out. It is concluded that the vertical intensity of atmospheric muons is (3.4 ± 1.0) 10^{-7} m^{-2} sec^{-1} sterad^{-1}. When this result is combined with the measurements of Miyake et al. (1964) and values of the intensities at intermediate depths obtained from a direct measurement of the angular distribution of muons at 4100 hg cm^{-2} by Achar et al. (1965c), the increasing slope of a logarithmic plot of the depth-intensity curve is confirmed. Thus a $\cos^n\theta$ angular distribution somewhat overestimates the intensity of muons at large zenith angles at the KGF site. It is found that an exponential decrease of intensity with depth fits the combined data best below 4000hg cm^{-2}. In this case the angular distribution at 7500 hg cm^{-2}, neglecting the slight broadening due to muon scattering, is of the form

$$I(\theta) = I_v \exp(-8.9(\sec\theta - 1)) \sec\theta \qquad (7.3)$$

In Fig. 7.7 the resultant angular distribution in the KGF telescopes is shown compared with that obtained using (7.2). The area under both curves

Fig. 7.7 Comparison of angular distributions of atmospheric muons on the KGF telescopes

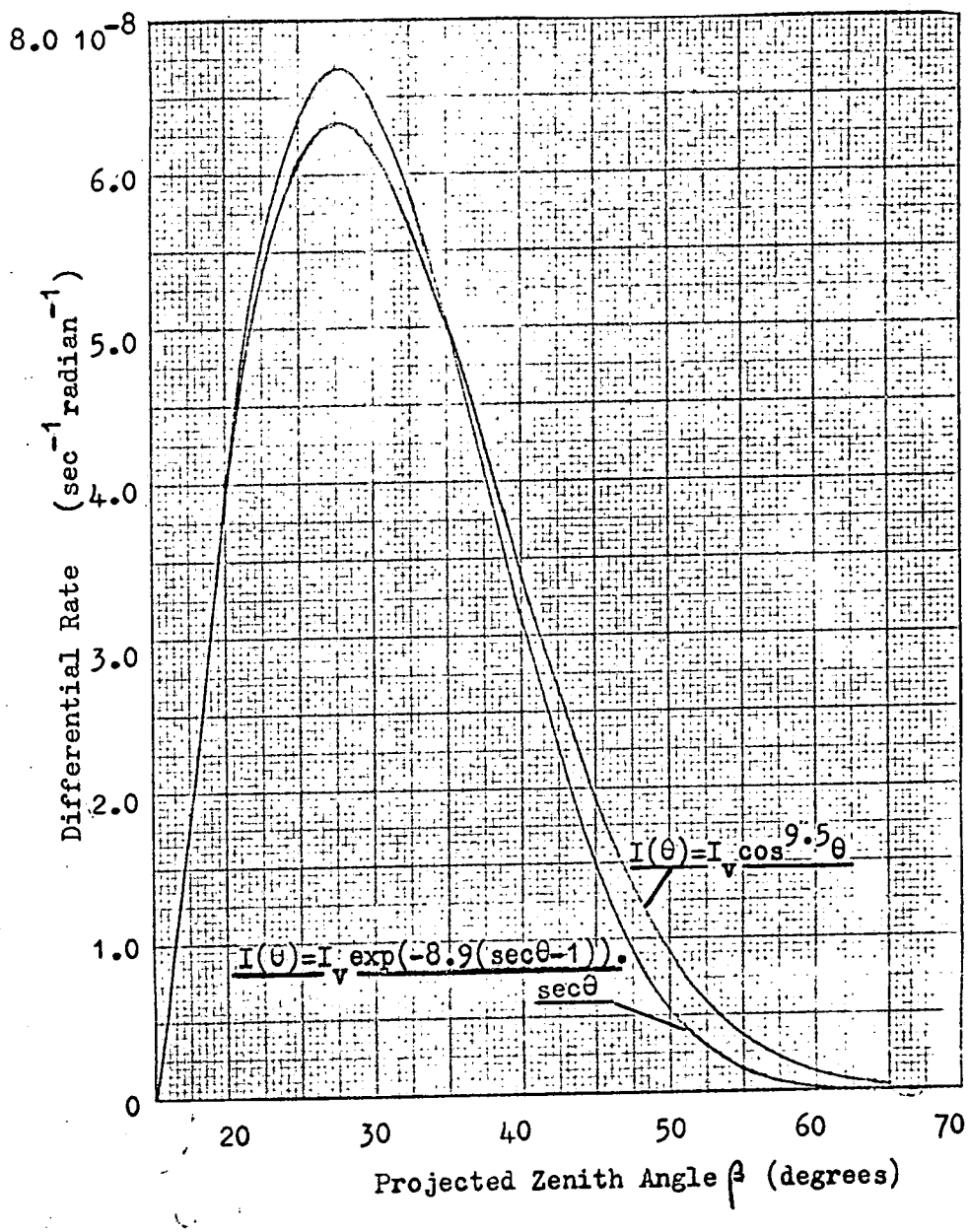

is made to agree with the observed rate of atmospheric muons, the vertical intensity derived from the six events for the angular distribution (7.3) being $(1.1^{+0.6}_{-0.5})\ 10^{-6}\ m^{-2}\ sec^{-1}\ sterad^{-1}$. It is seen that the effective cut off for atmospheric muons is reduced by about 5^{o}. None of the 16 observed events lies in the region from 50^{o} to 60^{o}, however, so that this does not affect the present interpretation.

Chapter 8

Conclusions

8.1 The Production of Kaons in High Energy Nuclear Interactions

By the combination of three methods involving measurements on cosmic ray muons an estimate was made, in Chapter 4, of R, the ratio of the production spectra of charged and neutral kaons and pions, over a range of meson energies from 3 to 5000 GeV. If the energy spectra of kaons and pions produced in individual interactions were of the same form R would be identical to the ratio of the numbers of kaons and pions produced in these interactions, R_i. If, on the other hand, the mean energy of the kaons were greater than that of the pions then, because of the rapidly falling primary spectrum, R_i would be less than R and vice versa. To compare these results with direct measurements of R_i let us initially assume equal energy spectra for kaons and pions. The set of empirical rules of Cocconi et al. (1961), the C.K.P. model, give the multiplicity of secondary particles of all charges in both the forward and backward directions in the c.m.s. from the interaction of a primary of energy E_o as $n_s = 2.7\ E_o^{0.25}$. The energy going into pions in the forward cone is approximately $E_o/3$ and the mean energy of these pions is thus $T = 2\ E_o/3\ n_s = 0.25\ E_o^{0.75}$. If, as an approximation, one assumes equipartition of energy amongst these pions then the mean energy of primary particles giving pions of energy E is

$$\bar{E}_o = 6.35\ E^{1.33} \qquad (8.1)$$

A primary of a given energy produces secondaries with a spectrum of energies, however, and because of the falling spectrum of primaries

those that retain a larger than average energy contribute most to the flux of pions of a given energy. Equation (8.1) therefore overestimates $\bar{E}_o$. The C.K.P. model gives the energy spectrum of pions as

$$N(E_\pi)\, dE_\pi = \frac{n_s}{2T} \exp(-\frac{E_\pi}{T})\, dE_\pi \qquad (8.2)$$

When this is folded into the spectrum of primary particles it is found that the mean primary energy giving pions of energy $\underline{E}$ may be expressed as

$$\bar{E}_o = 5.8\, E^{1.27} \qquad (8.3)$$

Using this expression the results of Fig. 4.13 are plotted as a function of primary energy in Fig. 8.1.

Perkins (1961) has made a summary of direct measurements of non-pion production in nuclear collisions from the study of individual interactions in multiplate cloud chambers and nuclear emulsions. By counting the number of neutral pions, identified by their decay, and assuming charge symmetry in the production of pions, the proportion of non-pions amonst all charged particles is found. The ratio of the number of secondary interactions produced by neutral particles to the total number of charged secondaries can also be measured and it is found that there are approximately equal numbers of charged and neutral non-pions. The results are plotted in Fig. 8.1. In the cloud chamber measurements (points I and II) the energy of the secondaries is such that some of the K_1^o mesons would be missed because of their rapid decay into pions; this does not apply to the emulsion results. The values are plotted as equivalent to R_i, but since the non-pions may be made up of other particles beside kaons the results must be regarded as giving an upper limit to R_i.

Fig. 8.1 A comparison of direct and indirect observations of kaon production in high energy nuclear interactions

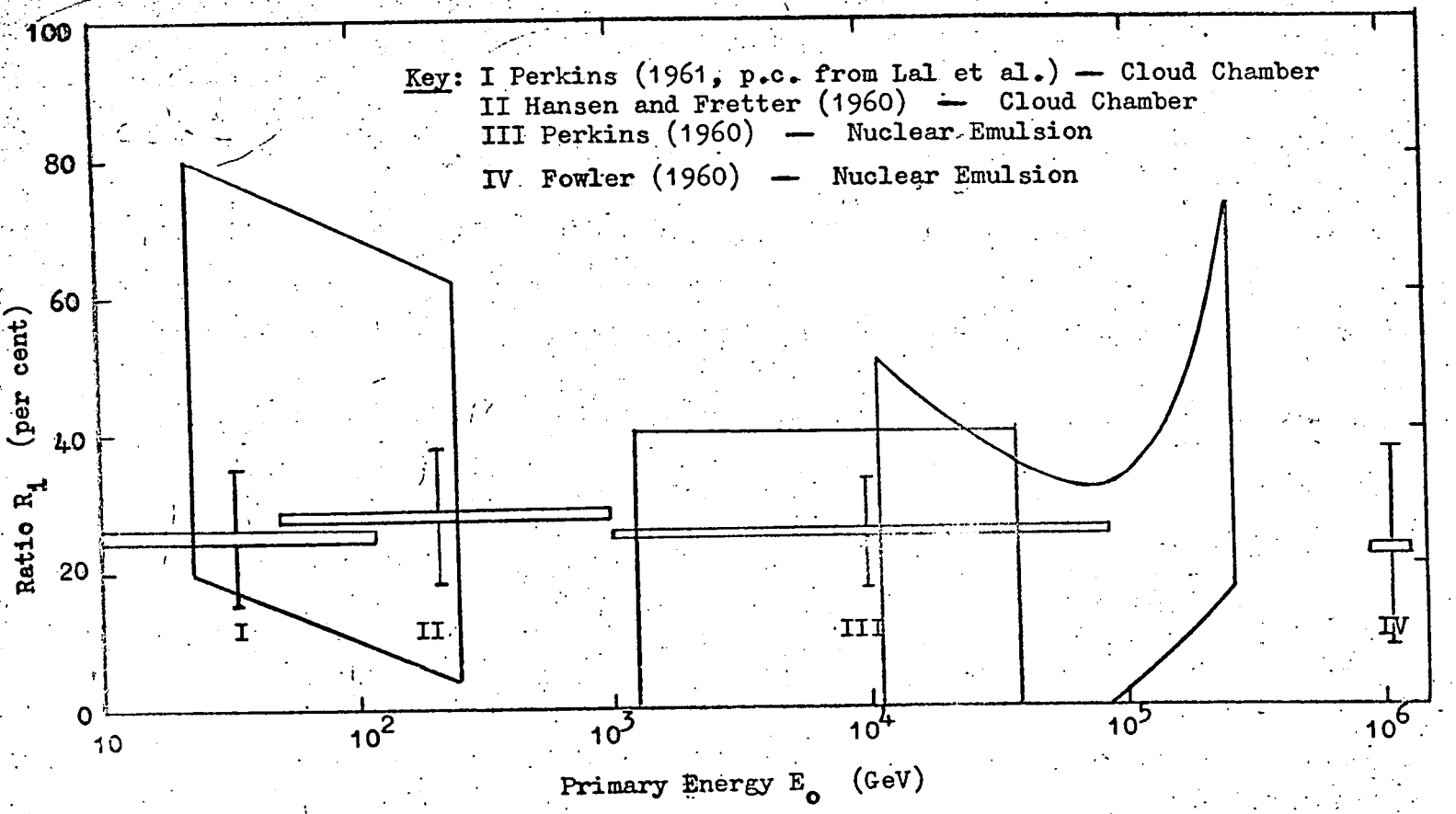

The large errors on the indirect measurements together with the appreciable errors of the directly measured values make it difficult to draw any very definite conclusions. If the majority of the non-pions produced in individual nuclear interactions are kaons then the agreement between the two types of measurement shows that there is no indication of the effective mean energies of kaons and pions from individual interactions being different. In the range of primary energies from 10^3 to 10^5 GeV the mean kaon energy could not be more than 50% greater than the mean pion energy but this limit is higher in the region where the indirect data comes from polarization measurements. If, on the other hand, as suggested by Peters, the majority of the non-pions were nucleon-antinucleon pairs the indication is that the kaons that are produced would have to have high mean energies to account for the observed value of R. This is particularly evident in the range of primary energies up to a few hundred GeV.

Particles produced in high energy interactions that move in the extreme backward direction in the c.m.s. have sufficiently low laboratory energies that their mass may be deduced from measurements of grain density and scattering in nuclear emulsions. Most models of nucleon-nucleon collisions imply forward-backward symmetry in the c.m.s. both in particle composition and angular distribution; if this is so measurements on the backward cone particles having low laboratory energy may be applied to the high laboratory energy forward cone. Kim (1964) has examined 22 jets produced by protons, neutrons and alpha particles with energies between 200 and $1.5\ 10^4$ GeV. From the identified secondary particles at

c.m.s. angles less than 175° the ratio of numbers of charged kaons to pions is 0.20 ± 0.07 and the ratio of their c.m.s. momenta is 1.4. This result does not contradict our data on the ratio of the production spectra R. For c.m.s. angles greater than 175°, however, of the observed mesons, 9 are identified as kaons and 7 as pions, the ratio of their c.m.s. momenta being 1.7. Although these particles constitute only a small fraction of the total number of secondaries their mean c.m.s. momenta are approximately an order of magnitude greater than those of the others. If forward-backward symmetry is assumed these particles would dominate the flux of mesons of a given energy at production, resulting in a value of R greater than 300%. This disagrees strongly with the observed limiting value. The simplest explanation of this discrepany would be that the identification of the particles by grain density and scattering measurements is at fault. It is possible that the assumption of symmetry in the c.m.s. is not correct for the particular interactions in which these particles were produced.

Recent measurements of the vertical intensity of muons underground by Achar et al. (1965c) have a bearing on the vertical muon sea level spectrum and thus on the value of R. There is good general agreement with the results of Miyake et al. (1964) which were used in deriving the OPW muon spectrum. The biggest difference is at 1871 hg cm^{-2} of standard rock where the former is 12% greater than the latter. Using these results, Pattison (1965) has derived new values for the muon sea level spectrum. The maximum difference from the OPW spectrum is at 1000 GeV where the former is greater by a corresponding 12%. It can

be seen from Table 2.1 that this lies within the estimated error on the OPW spectrum. If the revised spectrum is used together with the electromagnetic cascade data to estimate R, the result is that the value of R at 1500 GeV meson energy is increased to 30% and the dip in R at this energy (Fig. 4.10) largely disappears.

The ratio, R, of kaon and pion production spectra is also relevant to the observed charge ratio of muons at sea level. MacKeown (1965) has given the results of measurements using the Durham horizontal spectrograph and a comprehensive review of previous experiments. The ratio of the numbers of μ^+ to μ^- plotted against muon energy at production shows an approximately constant value of 1.20 to 1.25 above 3 GeV. Above 100 GeV the statistics are poor and an increase or decrease in the ratio cannot be ruled out. It has been shown by MacKeown and also by Cohen et al. (1965) that the production of pions by a pionisation process, taking into account statistical fluctuations in multiplicity, cannot alone account for the observed positive excess of muons. This suggests that the generation of pions via isobar production makes an important contribution to the pion production spectrum. If, however, the effective ratio of kaons to antikaons produced in high energy interactions remains at the value of 4 observed at machine energies then a kaonisation process could give results in agreement with the observed positive excess. MacKeown has shown that a value of R of 0.5 would be needed, in this case, to give results in agreement with experiment. This is somewhat higher than the most probable value that we have derived but it cannot definitely be ruled out on the basis of the present results. It has also been shown

that, if the major part of the observed positive excess is due to kaon production, either via kaonisation or isobar production, then the muon charge ratio should vary with zenith angle. The reason for this is the different relative contributions to the muon intensity from kaons in the vertical and near horizontal directions (see Figs. 2.12 and 3.3). The ratio of the values of the muon charge ratios in the horizontal and vertical directions is a function of R and the effective value of K^+/K^-. Its variation with muon energy is analogous to that of the muon intensities shown in Figs. 3.4 and 3.5, there being a maximum difference between the charge ratios in the two directions at 1000 GeV. If the charge ratio is due to pion production only, its variation with zenith angle is negligible. Thus a dependence of charge ratio on zenith angle would indicate an appreciable contribution from kaon production. The Mark II version of the Durham horizontal spectrograph will enable the charge ratio to be measured up to 1000 GeV but an accurate determination of the ratio up to this energy in the vertical direction is still lacking.

8.2 The Preliminary Results of the Neutrino Experiment

The value of R, as well as giving information on the production of kaons in high energy nuclear interactions, is needed in making calculations of muon-neutrino production in the atmosphere. It has been shown that the uncertainty in the muon-neutrino intensity in the horizontal direction due to the range of possible values of R is not greater than 15% up to a neutrino energy of 100 GeV. It has therefore been possible to make calculations of the expected rate of neutrino-induced interactions detected by the KGF neutrino telescopes under various assumptions con-

cerning the behaviour of the neutrino interaction cross-sections above machine energies.

At present the experiment is in its preliminary stages and one should not attempt to draw definite conclusions. There is a strong indication, however, that with the observed number of events, 6 in 298.8 telescope days, a conservative extrapolation of the machine data with no further appreciable increase in the inelastic cross-section above 10 GeV does not give a sufficiently high rate of events. The Case-Wits experiment, although giving a rate of neutrino events between one half and one third of that observed in the KGF experiment supports this argument. Taking into account the small number of events so far observed and some ambiguity in the interpretation of those recorded in the former experiment, there is no real discrepancy between the two sets of results.

If the present rate of events detected by the KGF telescopes is maintained then an increase in the inelastic cross-section depending on the square of the energy up to 30 GeV could be an explanation of this. Considerably enhanced statistics are needed before conclusions of this kind can be drawn, however.

Predictions of the rates of neutrino-induced muons from the production of the hypothetical Intermediate Boson in the Coulomb field of the nucleus have been given and it is shown that, even when the mass of the boson is assumed, there are considerable uncertainties in the rates. It is apparent that, with the absolute lower limit to m_W of 1.8 GeV from machine experiments and the presently unknown behaviour of the inelastic cross-section above 10 GeV, it will not be possible to gain information about the existence of the boson or its mass from measurements

of the rates alone of single neutrino-induced muons. Event 4, containing two penetrating tracks in the telescopes, has, however, demonstrated the possibility of inferring the existence of the boson from the observation of double track events where both tracks could be unambiguously identified as muons. Czyz et al. (1964) have shown that the cross-section for direct production of muons pairs in neutrino-nucleon interactions without the mediation of a real intermediate boson is approximately 1% of the elastic cross-section and we have demonstrated that elastic interactions can account for only a small fraction of the observed rate of events. The conditions for distinguishing between double events due to pairs of muons and those due to a muon and hadron are that the tracks should show no evidence of interactions inside the telescopes and that they should appear to diverge from a point at a distance inside the rock wall of several mean free paths for strong interactions. To facillitate the identification of such events, should they occur, three more telescopes are at present under construction. They are basically similar to telescopes 1 and 2 but have scintillator walls of dimensions 2 m by 2 m separated by 133 cm. The total thickness of absorber between the walls is increased to 220 g cm^{-2} of iron and in addition to the three layers of flash tubes giving the projected zenith angles of the tracks there are two layers of vertical tubes to give the azimuth.

It has been shown that the intensity of extra-terrestial neutrinos is only likely to be comparable with the intensity of those produced in the atmosphere at energies above 1000 GeV. If the intermediate boson exists then the $\bar{\nu}_e$ among these might possibly produce, via the Glashow resonance interaction, an intensity of muons that is a significant

fraction of the intensity from atmospheric neutrinos. According to present hypotheses, neutrinos of these energies are expected to be produced by only a few discrete sources. It is important therefore to examine the arrival directions of neutrino-induced muons for any anisotropies. In Appendix E the celestial coordinates of all possible neutrino-induced events at KGF are plotted. There is no evidence for any anisotropy in these events or in those from the Case-Wits experiment, whose arrival directions have also been calculated. With the very small number of events, however, this is hardly surprising. The new telescopes will enable both the Right Ascension and the Declination of the observed events to be determined with good accuracy.

In conclusion it may be stated that interactions have been observed that can definitely be attributed to cosmic ray neutrinos and that, already, interesting events have been recorded by the KGF telescopes (e.g. the double track of event 4 and the large shower event 13) that warrant further investigation by apparatus of increased size and sophistication.

Acknowledgments

The author wishes to thank Professor G.D. Rochester, F.R.S., for his continuous interest in this work and for the provision of the facilities for it.

He is grateful to his supervisor, Professor A.W. Wolfendale, for his invaluable help and advice at all stages of the work.

Members of the Cosmic Ray Group are thanked for helpful discussions. In this context the author is particularly indebted to Dr. P.K. MacKeown and Mr. S.S. Said with regard to the experimental results from the Durham horizontal spectrograph and to Dr. J.B.M. Pattison and Mr. D. R. Creed with regard to the neutrino experiment.

The staff of the University Computing Unit and its supervisor, Mrs. E. Templeton, are thanked for their assistance.

The author thanks Mr. R. White, Mr. B. Rowan and Miss C. Guyll for help with the preparation of figures and diagrams both for the present work and for previous publications during the past three years.

He is indebted to Miss A. Parnaby and Miss P. Stewart for their typing of this thesis.

Finally the Science Research Council are thanked for the provision of a Research Studentship during the period of this work.

References

Abraham, F., Kidd, J., Koshiba, M., Levi Setti,R., Tsao, C.H., and Wolter, W., (1963), Nuovo Cim., 28, 221 and 29, 315.

Achar, C.V., Menon, M.G.K.,Narasimham, V.S., Ramana Murthy, P.V., Sreekantan, B.V., Hinotani, K., Miyake, S., Creed, D.R., Osborne, J.L., Pattison, J.B.M., and Wolfendale, A.W., (1965a), Phys. Lett., 18, 196
(1965b), Phys. Lett., 19, 78
(1965d), Proc. Int. Conf. on Cosmic Rays, London, Mu-Nu 33 and 34.

Achar, C.V., Narasimham, V.S., Ramana Murthy, P.V., Creed, D.R., Pattison, J.B.M., and Wolfendale, A.W., (1965c), Proc.Phys. Soc., 86, 1305.

Akashi, M., et al. (Cooperative Japanese Emulsion Chamber Group), (1965) Proc. Int. Conf. on Cosmic Rays, London, H.E. 23.

Alikhanyan, A.I., (1959), Proc. Int. Conf. on Cosmic Rays, Moscow, Vol.1, 317.

Allen, J.E., and Apostalakis, A.J., (1961), Proc. Roy. Soc., A265, 117.

Asatiani, T.L., Krishchyan, V.M., and Sharkatunyan, R.O., (1964), Sov. Phys. JETP, 19, 1299.

Ashton, F., Kamiya, Y., MacKeown, P.K., Osborne, J.L., Pattison, J.B.M., Ramana Murthy, P.V., and Wolfendale, A.W., (1966), Proc.Phys. Soc., 87, 79.

Ashton, F., and Wolfendale, A.W., (1963), Proc. Phys. Soc. 81, 593.

Bahcall, J.N., (1964), 'Observational Neutrino Astronomy', 2nd Texas Symposium on Relativistic Astrophysics.

Bahcall, J.N., and Frautschi, S.C., (1964), Phys. Rev., 135, B788
(1964a), Phys. Rev., 136,B1547.

Baker, W.F., Cool, R.L., Jenkins, E.W., Kycia, T., Lindenbaum, S.J., Love, W.A., Luers, D., Niederer, J.A., Ozaki, S., Read, A.L., Russel, J.J., and Yuan, L.C., (1961), P.R.L., 7, 101.

Baradzei, L.T., Rubtsov, V.I., Smorodin, Yu., Solov'ev, M.V., Tolkachev, B.V., (1964), Trud. Fiz. Inst. Lebedev, Akad. Nauk, U.S.S.R., 26, 224.

Barkas, W.H., and Rosenfeld, A.H., (1965) UCRL-8030.

Barmin, V.V., Kanavets, V.P., and Morosov, B.V., (1960), Sov. Phys. JETP, 12, 683.

Barrett, P.H., Bollinger, L.M., Cocconi, G., Eisenberg, Y., and Greisen, K., (1952), Rev. Mod. Phys., 24, 133.

Becker, W., Goldberg, M., Harth, E., Leitner, J., and Lichtman, S., (1964), Nuovo Cim., 31, 1.

Bell, J.S., and Veltman, M., (1963), Phys. Lett., 5, 151.

Berezinskii, V., and Dolgoshein, B., (1962), Sov. Phys. JETP, 15, 749.

Berman, S.M., and Veltman, M., (1965), Nuovo Cim., 38, 992.

Bernardini, G., et al., (CERN Spark Chamber and HLBC Groups), (1965), Nuovo cim., 38, 608.

Bienlein, J.K., et al., (CERN Spark Chamber Group), (1964), Phys. Lett., 13,80.

Block, M.M., et al. (CERN HLBC Group), (1964), Phys. Lett., 12, 281.

Borreani, G., Gidal, G., Rinaudo, G., Werbrouch, A.E., Caforio, A., Ganelli, C.M., Natali, S., and Villani, M., (1965), Phys. Rev., 140, B1686.

Bowler, M.G., Fowler, P.H., and Perkins, D.H., (1962), Nuovo Cim. 26, 1182.

Bradt, H.V., and Clark, G.N., Phys. Rev., 132, 1306, (1963)

Brene, N., Egardt, L., and Qvist, B., (1961), Nuc. Phys., 22, 553.

Brooke, G., Meyer, M.A., and Wolfendale, A.W., (1964), Proc. Phys. Soc., 83, 871.

Burbidge, G.R., (1962), Ann. Rev. Nuc. Sci., 12, 507.

Burns, R., Goulianos, K., Hyman, E., Lederman, L., Lee, W., Mistry, N., Rettberg, J., Schwartz, M., Sunderland, J., and Danby, G., (1965), Phys. Rev. Lett., 15, 42.

Burns, R., Danby, G., Hyman, E., Lederman, L., Lee, W., Rettberg, J., and Sunderland, J., (1965a), Phys. Rev. Lett., 15, 830.

Cabibbo, N., and Chilton, F., (1965), Phys. Rev., 137, B1628.

Carhart, R., and Dooher, J., (1965) Brookhaven preprint BNL 9445.

Chilton, F., Saperstein, A.M., and Shrauner, E., (1965), Argonne preprint.

Chudakov, A.E., Dadykin, V.L., Zatsepin, V.I., Nesterova, N.M., (1964), Proc. Int. Conf. on Cosmic Rays, Jaipur, Vol.4, 199.

Cocconi, G., Koester, L.J., and Perkins, D.H., (1961), Lawrence Radiation Lab. High Energy Physics Study Seminars No. 28 pt. 2 (UCID)-1444).

Cohen, L., Fowler, G.N., and Poulopoulos, P., (1965), Nuc. Phys., 74, 619.

Cousins, J.E., and Nash, W.F., (1962), Phil. Mag. Supp., 11, 349.

Cowsik, R., Yash Pal, Rengarajan, T.N., and Tandon, S.N., (1964), Proc. Int. Conf. on Cosmic Rays, Jaipur, 6, 211.

Cowsik, R., Yash Pal, and Tandon, S. N., (1965) Preprint TIFR, Bombay, (Submitted to Proc. Indian Acad. Sci.)

Crouch, M.F., Gurr, H.S., Jenkins, T.L., Kropp, W.R., Reines, F., Smith, G.R., Meyer, B., and Sellschop, J.P.F., (1965), Int. Conf. on Weak Interactions, Argonne.

Csejthey-Barth, M., (1964), Nuovo Cim., 32, 545.

Cutts, D., Elioff, E., and Steining, R., (1965), Phys. Rev., 138, B968.

Danby, G., Gaillard, J.M., Goulianos, K., Lederman, L.M., Mistry, N., Schwartz, M., and Steinberger, (1962), Phys. Rev. Lett., 9, 36.

Davis, R., (1964), Phys. Rev. Lett., 12, 303.

Dekkers, D., Geibel, J.A., Mermod, R., Weber, G., Willits, T.R., Winter, K., Jordan, B., Vivargent, M., King, N.M., and Wilson, E.J.N., (1965), Phys. Rev., 137, B962.

Dolgoshein, B., Luchkov, B., and Ushakov, V., (1962), Sov. Phys. JETP., 15, 654.

Duthie, J., Fowler, P.H., Kaddoura, A., Perkins, D.H., and Pinkau, K., (1962), Nuovo Cim., 24, 122.

Erlykin, A.D., (1965), Proc. Int. Conf. on Cosmic Rays, London, Mu-Nu 29.

Fowler, G.N., and Wolfendale, A.W., (1958), Prog. in Elementary Particle and Cosmic Ray Physics, Vol IV, Chapter 3, (Ed. J.G. Wilson and S.A. Wouthuysen: North-Holland).

Fowler, P., (1960), Proc. 1960 Rochester Conf. on High Energy Physics, 829.

Fujimoto, Y., (1964), Proc. Int. Conf. on Cosmic Rays, Jaipur, 5, 326.

Fujimoto, Y., Hasegewa, S., Kazuno, M., Nishimura, J., Niu, K., and Ogita, N., (1959), Proc. Int. Conf. on Cosmic Rays, Moscow,Vol 1, 41.

Furuichi, S., (1958), Nuovo Cim, 7, 269.

Gardener, M., Jones, D.G., Taylor, F.E., and Wolfendale, A.W., Proc. Phys. Soc., 80, 697 (1962).

von Gehlen, G., Nuovo Cim., 30, 859 (1963).

Glashow, S.L., (1960), Phys. Rev., 118, 316.

Goody, R.M., 'The Physics of the Stratosphere', (Cambridge U.P. 1954)

Gould, R.J., and Burbidge, G.R., (1965), Ann. d'Astrophysique, 28, 171.

Hansen,L, and Fretter, W., (1960), Phys. Rev., 118, 812.

Hayakawa, S., Okuda, H., Tanaka, Y., and Yamamoto, Y., (1964), Prog. Theor. Phys. Supp., 30, 153.

Hayakawa, S., Nishimura, J., Yamamoto, Y., to be published in Prog. Theor. Phys. Supp. 32 (1965)

Hayman, P.J., Palmer, N.S., and Wolfendale, A.W., Proc. Roy. Soc., A275, 391, (1963).

Hayman, P.J., and Wolfendale, A.W., (1962), Proc. Phys. Soc., 80, 710.

Higashi, S., Kitamura, T., Mishima, Y., Mitani, S., Miyamoto, S., Oshio, T., Shibata, H., Watanabe, K., and Watase, Y., (1962), J. Phys. Soc. Japan, (Supp. AIII), 17, 362.

Higashi, S., Kitamura, T., Oda, M., Tanaka, Y., and Watase, Y., (1964), Nuovo Cim., 32, 1.

Higashi, S., Kitamura, T., Miyamoto, S., Mishima, Y., Takahashi, T., and Watase, Y., (1965), preprint Osaka City University.

Hiroshige, N., and Matsuda, N., (1965), Prog. Theor. Phys., 33, 764.

Judge, R.J.R., and Nash, W.F., (1965), Nuovo Cim, 35, 1025.

Kalmus, G.E., Kernan, A, Pu, R.T., Powell, W.M., and Dawd, R., (1964), Phys. Rev. Lett., 13, 99.

Kidd, J.M., (1963), Nuovo Cim., 27, 57.

Kim, C.O., (1964), Phys. Rev., 136, B515.

Kocharyan, N, Kirakosyan, Z.A., Sharoyan, E.G., and Pikalow, A.P., (1960), Sov. Phys. JETP, 11, 12.

Krasilnikov, D.D., (1964), Proc. Int. Conf. on Cosmic Rays, Jaipur, Vol 6, 124.

Kraushaar, W.L., (1965), Ann. d'Astrophysique, 28, 202.

Lal, D., Yash Pal, and Peters, B., (1953), Proc. Indian Acad. Sci., 38, 398.

Lamb, R.C., Lundy, R.A., Novey, T.B., Yovanovitch, D.D., Good, M.L., Hartung, R., Peters, M.W., and Subramanian, A., (1965), Phys. Rev. Lett., 15, 800.

Lee, T.D., (1961), CERN report 61-30.

Lee, T.D., Markstein, P., and Yang, C.N., Phys. Rev. Lett., 7, 429, (1961).

Lee, T.D., and Yang, C.N., (1960), Phys. Rev., 119, 1410.

Lloyd, J.L., and Wolfendale, A.W., Proc. Phys. Soc. A., 68, 1045, (1955).

Long. C.D., McBreen, B., Porter, N.A., and Weekes, T.C., (1965), Proc. Int. Conf. on Cosmic Rays, London, Spec. 3.

MacKeown, P.K., (1965), Ph.D. Thesis, University of Durham.

Maeda, K., (1960), Journ. of Atmos. and Terr. Phys., 19, 184 (1964), Journ.of Geophysical Research, 69, 1725.

Malhotra, P.K., Shukla, P.G., Stephens, S.A., Vijayalakshmi, B., Boult, J., Bowler, M.G., Fowler, P.H., Hackforth, H.L., Keereetaveep, J., Mayes, V.M., and Tovey, S.N., (1965), Nuovo Cim., 40A, 385.

Mani, H.S., and Nearing, J.S., (1964), Phys. Rev., 135, B1009.

Markov, M.A., and Zheleznykh, I.M., (1961), Nucl. Phys., 27, 385.

Menon, M.G.K., (1963), Proc. Int. Conf. on Cosmic Rays, Jaipur, Vol 6, 152.

Menon, M.G.K., and Ramana Murthy, P.V., (1965), Prog. in Cosmic Ray and Elementary Particle Physics, Vol 9, (ed. J.G. Wilson and S.A. Wothuysen: North-Holland)

Menon, M.G.K., Ramana Murthy, P.V., Sreekantan, B.V., and Miyake, S., (1963), Nuovo Cim., 30, 1208.

Miyake, S., Narasimham, V.S., and Ramana Murthy, P.V., (1964), Nuovo Cim., 32, 1505.

Namias, V., and Wolfenstein, L., (1965), Nuovo Cim., 36, 542.

Nishimura, J., (1965), Proc. Int. Conf. on Cosmic Rays, London.

Olbert, S., Phys. Rev., 96, 400, (1964).

Osborne, J.L., (1964), Nuovo Cim., 32, 816.

Osborne, J.L., Said, S.S., and Wolfendale, A.W., (1965), Proc. Phys. Soc., 86, 911.

Osborne, J.L., and Wolfendale, A.W., (1963), Proc. Int. Conf. on Cosmic Rays, Jaipur, Vol. 6, 36.

Osborne, J.L., and Wolfendale, A.W., (1964), Proc. Phys, Soc., 84, 901.

Osborne, J.L., Wolfendale, A.W., and Palmer, N.S.,(1964), Proc. Phys. Soc., 84, 911.

Yash Pal, and Peters, B., Mat. Fys. Medd. Dan. Vid. Selsk., Vol 33 no. 15, (1964)

Pattison, J.B.M., (1965), Ph. D. Thesis, University of Durham.

Paty, M., (1965), CERN report 65-12.

Perkins, D.H., (1960), Prog. in Cosmic Ray and Elementary Particle Physics, Vol 5 , Chapter 3.

Perkins, D.H., (1961), Proc. Int. Conf. on the Theoretical Aspects of Very High Energy Phenomena, CERN report 61-22, p 99.

Peters, B., Proc. Int. Conf. on Cosmic Rays, London, (1965), Rapporteur paper.

Ramana Murthy, P.V., (1962), Ph.D. Thesis, Bombay.

Rogers, I.W., Ph. D. Thesis, University of Durham (1965).

Reines, F., Crouch, M.F., Jenkins, T.L., Kropp, W.R., Gurr, H.S., Smith, G.R., Sellschop, J.P.F., and Meyer, B., (1965), Phys. Rev. Lett., 15, 429.

Reines, F., Jenkins, T.L., Crouch, M.F., and Sellschop, J.P.F., (1963), Proc. Int. Conf. on Cosmic Rays, Jaipur, Vol 6, 182.

Rossi, B., (1948), Rev. Mod. Phys., 20, 537.

Rossi, B., (1952), 'High Energy Particles', (New York: Prentice-Hall).

Sands, M., (1950), Phys. Rev., 77, 180.

Smith, J.A., and Duller, N.M., (1959), Journ. of Geophysical Research, 64, 2297.

Sen Gupta, S.N., and Sinha, M.S., (1962), Proc. Phys. Soc., 79, 1183.

Shafer, J.B., et al., (1963), Phys. Rev., 130, 2077.

Tanikawa, Y., and Watanabe, S., (1959), Phys. Rev., 113,1344.

Uberall, H., (1964), Phys. Rev., 133, B444.

Veltman, M., (1963), CERN report 63-37, p 21.

Wu, A.C.T., Chen-Ping Yang, Fuchel, K., and Heller, S., (1964), Phys. Rev. Lett., 12, 57.

Yamaguchi, Y., (1961), CERN report 61-2.

Yamaguchi, Y., (1965), CERN preprint Th 634.

Zagrebin, V.A., and Zheleznykh, I.M., (1964), preprint, Lebedev Institute Moscow.

Zatsepin, G.T., and Kuz'min, V.A., (1961), Sov. Phys. JETP, 12, 1171.
(1962), Sov. Phys. JETP, 14, 1294.

Zatsepin, G.T., and Mikhalchi, E.D., J. Phys. Soc. Japan, Supp. AIII, 356, (1961); Proc. Int. Conf. on Cosmic Rays, London, Mu-Nu 28, (1965).

Appendix A

Rate of Energy loss of High Energy Muons

A.1 Introduction

Calculations of the propagation of cosmic ray muons in the atmosphere require knowledge of the rate of energy loss in air, ($Z = 7.2$, $A = 14.2$, variable density). The rate of energy loss in 'standard' rock, ($Z = 11$, $A = 22$, density $\rho = 2.65$ g cm^{-3}), is used in deriving the muon sea level spectrum from the depth-intensity measurements. The processes by which muons lose energy have been discussed in detail by Cousins and Nash (1962) and Hayman et al. (1963). Only the final expressions are given here together with the numerical values for air and rock.

A.2 Collision

Energy losses by ionisation and excitation, caused by inelastic collisions of the muon with atomic electrons, are given by

$$-\left(\frac{dE}{dx}\right)_{col} = K\left\{\ln\left[\frac{2m_e c^2 E_m}{I^2(Z)(\varepsilon-1)}\right] - \left(\frac{1-\varepsilon\beta^2}{\varepsilon-1}\right) - 2\beta^2 + \frac{1}{4}\left(\frac{E_m}{E+m_\mu c^2}\right)^2\right\} \quad \text{MeV g}^{-1}\text{cm}^{-2} \quad \text{(A1)}$$

for $\beta \geq \frac{1}{\varepsilon^{\frac{1}{2}}}$ and

$$-\left(\frac{dE}{dx}\right)_{col} = K\left\{\ln\left[\frac{2m_e c^2 E_m}{(1-\beta^2)I^2(Z)\varepsilon}\right] - 2\beta^2 + \frac{1}{4}\left(\frac{E_m}{E+m_\mu c^2}\right)^2\right\} \quad \text{MeV g}^{-1}\text{cm}^{-2} \quad \text{(A2)}$$

for $\beta \leq \frac{1}{\varepsilon^{\frac{1}{2}}}$. K is a constant, $\frac{2\pi N_A r_0^2 m_e c^2}{\beta^2} \cdot \frac{Z}{A}$, (for both air and rock, where $Z/A = 0.5$, $K = 7.66\ 10^{-2}$ MeV g^{-1}cm^{-2}). $I(Z)$ is the ionization potential of the atom, which is taken to be $1.35\ 10^{-5}$ Z MeV. $E_m = E^2(E + m_\mu^2 c^2/2m_e)^{-1}$ is the maximum transferable energy of a muon to an electron. $\varepsilon = 1 + \frac{Ze^2 k^2 N_A}{\pi A m_e I^2(Z)} \cdot \rho$ is the dielectric constant of

the medium. The other symbols have their conventional meanings.

For rock $\beta^2 = \frac{1}{\varepsilon}$ when E = 0.5 GeV and for energies higher than this (A.1) becomes $-\left(\frac{dE}{dx}\right)_{col} = 1.505 + 0.0766\left\{\ln E_m + \frac{1}{4}\left(\frac{E_m}{E+105.7}\right)^2\right\}$ MeV $g^{-1}cm^2$ (A.3)

For $E \gtrsim 10$ GeV this reduces to

$$-\left(\frac{dE}{dx}\right)_{col} = 1.524 + 0.0766 \ln E_m \quad \text{MeV } g^{-1}cm^2 \qquad (A.4)$$

For air (A.1) and (A.2) become

$$-\left(\frac{dE}{dx}\right)_{col} = 0.5499 + 0.0766\left\{\ln E_m + 2\ln E + \frac{1}{4}\left(\frac{E_m}{E+105.7}\right)^2\right\} \quad \text{MeV } g^{-1}cm^2 \qquad (A.5)$$

for $E < 105.7\ (\frac{22.74}{\rho} + 1)^{\frac{1}{2}} \simeq \frac{503.8}{\rho^{\frac{1}{2}}}$ MeV, and

$$-\left(\frac{dE}{dx}\right)_{col} = 1.580 + 0.0766\left\{\ln E_m + \frac{1}{4}\left(\frac{E_m}{E+105.7}\right)^2 - \frac{2.538\,10^{-5}}{E^2\rho}\right\} \quad \text{MeV } g^{-1}cm^2 \qquad (A.6)$$

for $E > \frac{503.8}{\rho^{\frac{1}{2}}}$ MeV.

A.3 Pair Production

The creation of an electron pair in the Coulomb field of the nucleus by a muon gives the following contribution to the energy loss.

$$-\left(\frac{dE}{dx}\right)_{pp} = \frac{N_A m_e (\alpha r_0)^2}{\pi}\frac{Z^2}{A} E\left[19.3 \ln\left(\frac{E}{m_\mu c^2}\right) - 53.7\right] \quad \text{MeV } g^{-1}cm^2 \qquad (A.7)$$

When E > 25 GeV a screening factor

$$f = \left[\ln(183Z^{\frac{1}{3}}) + 9/16\right]\left[\ln\left(E/m_\mu c^2\right) - 7/8 + 9/16 \ln Z\right]^{-1} \qquad (A.8)$$

must be applied hence

$$-\left(\frac{dE}{dx}\right)_{pp} = 3.778\ 10^{-3} Z \cdot E \cdot [5.772 - \tfrac{1}{3}\ln Z]\left[\ln E - 7.443\right]\left[\ln E - 5.145\right]^{-1} \text{ MeV } g^{-1}cm^2 \qquad (A.9)$$

This expression may be approximated up to 10^4 GeV by

$$-\left(\frac{dE}{dx}\right)_{pp} = 1.6\ 10^{-6} E \quad \text{MeV } g^{-1}cm^2, \text{ for rock} \qquad (A.10)$$

and

$$-\left(\frac{dE}{dx}\right)_{pp} = 1.0\ 10^{-6} E \quad \text{MeV } g^{-1}cm^2, \text{ for air.} \qquad (A.11)$$

These approximations introduce an error of less than 1% into the total rate of energy loss.

A.4 Bremsstrahlung

The average rate of radiation of energy from the acceleration of the muon in the Coulomb field of the nucleus is given by the following expressions. For $E \lesssim 4000$ GeV the effects of atomic screening are ignored and

$$-\left(\frac{dE}{dx}\right)_B = C\,E\left[\ln\left(\frac{12\,E\,Z^{\frac{1}{2}}}{5\,m_\mu c^2}\right) - \frac{1}{3}\right] \quad \text{MeV g}^{-1}\text{ cm}^2 \qquad \text{(A.12)}$$

For $E > 4000$ GeV

$$-\left(\frac{dE}{dx}\right)_B = C.E\left[\ln\left(\frac{m_\mu}{m_e}\,183\,Z^{-\frac{1}{3}}\right) + \frac{1}{8}\right] \quad \text{MeV g}^{-1}\text{cm}^2 \qquad \text{(A.13)}$$

where the constant $C = 4\alpha N_A r_0^2 \left(\frac{m_e}{m_p}\right)^2 \frac{Z}{A}$ MeV g^{-1}cm^2. Again (A.12) and (A.13) may be approximated by linear relationships

$-\left(\frac{dE}{dx}\right)_B = 1.7\ 10^{-6}\ E$ MeV g^{-1}cm^2 for rock, and

$-\left(\frac{dE}{dx}\right)_B = 1.0\ 10^{-6}\ E$ MeV g^{-1}cm^2 for air, with an error of less than 1% in the total rate of energy loss.

A.5 Nuclear Interaction

The contribution to the muon energy loss due to nuclear interaction becomes increasingly important at high energies. The interaction is assumed to occur between the virtual photon cloud surrounding the muon, and the nucleus. There is, however, some uncertainty in the calculation of the spectrum of virtual photons and in the photo-nuclear cross-section, $\sigma_{\gamma-N}$, at high energies. Hayman et al. (1963), using the Williams-Weiszacker equation for the virtual photon spectrum, express the energy loss as

$$-\left(\frac{dE}{dx}\right)_N = \frac{2\alpha\,\sigma_{\gamma-N}\,N_A\,E}{\pi} \quad \text{MeV g}^{-1}\text{cm}^2 \qquad \text{(A.14)}$$

and, with a value $\sigma_{\gamma-N} = 2.6\ 10^{-28}$ cm^2 nucleon^{-1}, from Higashi et al. (1962), obtain the expression

$$-\left(\frac{dE}{dx}\right)_N = 7 \cdot 10^{-7} E \quad \text{MeV g}^{-1}\text{cm}^2 \qquad \text{(A.15)}$$

This is the value used here. It must be noted, however, that nuclear interactions give the least certain contribution to the total energy loss. The effect of this uncertainty on the range-energy relation in rock and the derivation of the muon sea level spectrum at energies above 1 TeV is discussed in Chapter 2. On the other hand, the fractional energy loss of muons of energies above 1 TeV in traversing the whole of the atmosphere is small so that the effect of the uncertainty in the contribution of nuclear interactions to the total rate of energy loss in air is not important.

A.6 Total Rate of Energy Loss

Summing the four contributions and expressing E and E_m in GeV, we have the following expressions. For rock

$$-\left(\frac{dE}{dx}\right)_{tot} = 2.05\ 10^{-3} + 7.66\ 10^{-5}\left[\ln E_m\right] + 4.0\ 10^{-6} E \quad \text{GeV g}^{-1}\text{cm}^2 \qquad \text{(A.16)}$$

and for air

$$-\left(\frac{dE}{dx}\right)_{tot} = 2.137\ 10^{-3} + 7.66\ 10^{-5}\left[\ln E_m + 2\ln E + \frac{1}{4}\left(\frac{E_m}{E+0.106}\right)^2\right] + 2.73\ 10^{-6} E \quad \text{GeV g}^{-1}\text{cm}^2 \qquad \text{(A.17)}$$

for $E \leq \frac{0.504}{\rho^{\frac{1}{2}}}$ GeV and

$$-\left(\frac{dE}{dx}\right)_{tot} = 2.109\ 10^{-3} + 7.66\ 10^{-5}\left\{\ln E_m + \frac{1}{4}\left(\frac{E_m}{E+0.106}\right)^2 - \ln\rho - \frac{0.2538}{E^2\rho}\right\} + 2.73\ 10^{-6} E \quad \text{GeV g}^{-1}\text{cm}^2 \qquad \text{(A.18)}$$

for $E \geq \frac{0.504}{\rho^{\frac{1}{2}}}$ GeV.

APPENDIX B

PROPERTIES OF THE ATMOSPHERE

Relations between pressure, x, density, ρ, and altitude, h, are derived below. (Subscript T refers to values at the tropopause; subscript o to those at sea level).

$$dx = \rho \, dh \ g \ cm^{-2} \tag{B1}$$

$$\rho = \frac{x \, g}{R \, T(h)} \ g \ cm^{-3} \tag{B2}$$

where $R = 2.888 \ 10^6$ erg $^oK^{-1}$ g^{-1} and T(h) is the absolute temperature at altitude h.

Combining (B1) and (B2) and integrating

$$\frac{x}{x_o} = \exp\left(-\frac{g}{R} \int_o^h \frac{dh}{T(h)} \right) \tag{B3}$$

For $h \leqslant h_T$, $T(h) = T_o - \Gamma h$, where Γ is the lapse rate in $^oK \ km^{-1}$, and (B3) becomes, for $x \geqslant x_T$

$$x = x_o \left(1 - \frac{\Gamma}{T_o} h\right)^{g/\Gamma R} \tag{B4}$$

For the stratosphere $h \geqslant h_T$, $T(h) = T_T$ and (B3) becomes for $x \leqslant x_T$

$$x = x_T \exp\left[-\frac{g}{R \, T_T} (h - h_T) \right] \tag{B5}$$

Goody (1954) gives the following values at the latitude of Durham (55°N).

Mean annual height of tropopause	$h_T = 10.3$ km
Mean annual temperature at sea level	$T_o = 282^oK$
Mean annual temperature of tropopause	$T_T = 219^oK$
Pressure at sea level	$x_o = 1030$ g cm^{-2}
thus the lapse rate	$\Gamma = 6.078$ ^oK km^{-1}

Then (B4) and (B5) become

$$x = 1030 \ (1 - 0.02156 \ h)^{5.587} \ g \ cm^{-2} \quad \text{when } h \leqslant 10.3 \text{ km} \tag{B6}$$

$x = 253.3 \exp(-0.1549 (h - 10.3))$ g cm^{-2} when $h \geqslant 10.3$ km (B7)

Conversely

$h(x) = 46.380 - 13.398\, x^{0.179}$ km when $x \geqslant 253.3$ g cm^{-2} (B8)

$h(x) = 46.040 - 64.576 \ln(x)$ km when $x \leqslant 253.3$ g cm^{-2} (B9)

and from (B2)

$\rho(x) = 4.170\, 10^{-6}\, x^{0.821}$ g cm^{-3} when $x \geqslant 253.3$ g cm^{-2} (B10)

$\rho(x) = 1.548\, 10^{-6}\, x$ g cm^{-3} when $x \leqslant 253.3$ g cm^{-2} (B11)

Appendix C

Kaon Decay Modes and Energy Spectra of Decay Particles

C.1 Decay Modes

The following decay modes and branching ratios have been used in calculating the spectra of muons, neutrinos and photons produced by kaon decays.

Decay Mode	Branching Ratio (%)
1) Charged Kaons	
($\tau_{K^\pm} = 1.22\ 10^{-8}$ sec)	
$K^\pm_{\mu 2} \rightarrow \mu^\pm + \nu_\mu(\bar{\nu}_\mu)$	58
$K^\pm_{\pi 2} \rightarrow \pi^\pm + \pi^0$	26
$K^\pm_{\pi 3} \rightarrow \pi^\pm + \pi^+ + \pi^-$	6
$K^\pm_{\pi 3}{}' \rightarrow \pi^\pm + \pi^0 + \pi^0$	2
$K^\pm_{\mu 3} \rightarrow \mu^\pm + \pi^0 + \nu_\mu(\bar{\nu}_\mu)$	4
$K^\pm_{e 3} \rightarrow e^\pm + \pi^0 + \nu_e(\bar{\nu}_e)$	5
2) Neutral Kaons	
i) K^0_1 ($\tau_{K^0_1} = 0.9\ 10^{-10}$ sec)	
$K^0_{\pi 2} \rightarrow \pi^+ + \pi^-$	34.5
$K^0_{\pi 2}{}' \rightarrow \pi^0 + \pi^0$	15.5
ii) K^0_2 ($\tau_{K^0_2} = 6\ 10^{-8}$ sec)	
$K^0_{\mu 3} \rightarrow \mu^\pm + \pi^\mp + \nu_\mu(\bar{\nu}_\mu)$	16
$K^0_{e 3} \rightarrow e^\pm + \pi^\mp + \nu_e(\bar{\nu}_e)$	17
$K^0_{\pi 3} \rightarrow \pi^+ + \pi^- + \pi^0$	6.5
$K^0_{\pi 3}{}' \rightarrow \pi^0 + \pi^0 + \pi^0$	10.5

Notes

1) Branching ratios are given to the nearest 0.5%; only those with branching ratios greater than 1% are included.

2) The branching ratio of the $K^o_{\pi 3}$' mode of K^o_2 in which only neutral particles are produced is difficult to measure. Experimental values varying from 8% to 19% have been quoted. The present estimate from experiment is $13.6 \pm 1.0\%$ (Barkas and Rosenfeld (1965)). The value of 10.5% is obtained from the measured decay rates of the charged kaon under the assumption that $\Delta T = \frac{1}{2}$ is valid.

3) Barkas and Rosenfeld give a branching ratio of 63.2% for $K_{\mu 2}$, which is based mainly on a xenon bubble chamber experiment. The value of 58% comes from a nuclear emulsion experiment of Becker et al. (1964), who point out that all results from emulsion work are systematically lower than the bubble chamber value.

C.2 Two-body Kaon Decay Modes

The $K_{\mu 2}$ decay is analogous to the $\pi \rightarrow \mu + \nu_\mu$ decay. In the laboratory system the muon has energy between $0.0458\ E_K$ and E_K and the neutrino has energy between 0 and $0.9542\ E_K$.

If the small differences in mass between charged and neutral pions and charged and neutral kaons are ignored, then in all kaon decays into two pions the pion energy in the laboratory system lies between $0.086\ E_K$ and $0.914\ E_K$.

C.3 Three-body Kaon Decay Modes

For kaon decay into pions the c.m.s. spectrum of Kalmus et al. (1964) has been used. The c.m.s. spectra of the decay products in three-body leptonic decay modes have been calculated by Furuichi (1958) and Brene et al. (1961)

on the basis of the Universal Fermi Interaction for various values of the ratio, $\xi = f_-/f_+$, of the form factors describing the effects of strong interaction. All recent measurements of the energy spectra and polarisation of the decay particles (e.g. Cutts et al. (1965)) are consistent with the real part of ξ being zero. We shall therefore use the calculated spectra for $\xi = 0$.

Let the energy spectrum of a decay particle $\underline{i}$ in the c.m.s. be $P(\overline{E_i})$ where $\overline{E_i}$ is the c.m.s. energy and $\overline{E_i}$ max is the maximum energy. In the laboratory system where the energy of the particle $\underline{i}$ is expressed as $\varepsilon = E_i/E_K$ the minimum and maximum energies of the particle are

$$\varepsilon_{min} = \frac{1}{m_K c^2}\left(\overline{E}_{i\,max} - \left((\overline{E}_{i\,max})^2 - m_i^2 c^4\right)^{\frac{1}{2}}\right) \qquad (C.1)$$

and

$$\varepsilon_{max} = \frac{1}{m_K c^2}\left(\overline{E}_{i\,max} + \left((\overline{E}_{i\,max})^2 - m_i^2 c^4\right)^{\frac{1}{2}}\right) \qquad (C.2)$$

respectively, and the energy spectrum is

$$Q(\varepsilon) = \frac{m_K c^2}{2} \int_{\frac{1}{2}\left(m_K c^2 \varepsilon + \frac{m_i^2 c^4}{\varepsilon m_K c^2}\right)}^{\overline{E}_{i\,max}} \frac{P(\overline{E}_i)\, d\overline{E}_i}{\left(\overline{E}_i^2 - m_i^2 c^4\right)^{\frac{1}{2}}} \qquad (C.3)$$

The spectra obtained from this integral are not in the form of simple analytical expressions; however, with the required accuracy they may be represented by 3rd order polynomials. As a test of the accuracy of the polynomials giving least squares fits to each of the numerically evaluated spectra, the mean energies of the polynomial expression and the true spectrum were compared; in no case was there a discrepancy of more than 3% between the mean energies.

The polynomial expressions are as follows.

1) $K_{\mu 3} \rightarrow \pi + \mu + \nu_\mu$

(a) Pion

$$Q(\varepsilon) = -0.7822 + 16.74\varepsilon - 31.42\varepsilon^2 + 15.50\varepsilon^3 \qquad (C.4)$$

$$.0830 \leq \varepsilon \leq .9548$$

(b) Muon

$$Q(\varepsilon) = -0.3903 + 19.70\varepsilon - 45.29\varepsilon^2 + 26.69\varepsilon^3 \qquad (C.5)$$

$$.0496 \leqslant \varepsilon \leqslant .9165$$

(c) Muon-neutrino

$$Q(\varepsilon) = 2.522 + 0.01823\varepsilon - 11.86\varepsilon^2 + 9.745\varepsilon^3 \qquad (C.6)$$

$$0 \leqslant \varepsilon \leqslant 0.7340$$

2) $K_{e3} \rightarrow \pi + e + \nu_e$

(a) Pion

$$Q(\varepsilon) = -0.4293 + 12.42\varepsilon - 21.63\varepsilon^2 + 9.777\varepsilon^3 \qquad (C.7)$$

$$.0793 \leqslant \varepsilon \leqslant 1.0$$

(b) Electron-neutrino

$$Q(\varepsilon) = 2.241 + 0.2246\varepsilon - 9.191\varepsilon^2 + 6.862\varepsilon^3 \qquad (C.8)$$

$$0 \leqslant \varepsilon \leqslant 0.862$$

3) $K_{\pi 3} \rightarrow \pi + \pi + \pi$

$$Q(\varepsilon) = -8.306 + 93.91\varepsilon - 233.0\varepsilon^2 + 166.8\varepsilon^3 \qquad (C.9)$$

$$0.1234 \leqslant \varepsilon \leqslant 0.6430$$

All of the spectra given above are normalised to unit area. Certain of these spectra may be combined before being used to calculate the muon and neutrino intensities. The pion spectrum from $K_{\mu 3}$ and K_{e3}, combining (C.4) and (C.7) in the ratio 16:17, is

$$Q(\varepsilon) = -0.6004 + 14.53\varepsilon - 26.38\varepsilon^2 + 12.55\varepsilon^3 \qquad (C.10)$$

$0.0811 \leqslant \varepsilon \leqslant 0.9781$ with a total branching ratio of 33%.

The pion spectrum from $K^{\pm}_{\pi 3}$ and $K^{\pm}_{\pi 3}{}'$ is, allowing for three pions from the first decay and one from the second in the ratio 6:2,

$$Q(\varepsilon) = -20.77 + 234.8\varepsilon - 582.5\varepsilon^2 + 417.0\varepsilon^3 \qquad (C.11)$$

$0.1234 \leqslant \varepsilon \leqslant 0.6430$ for a total branching ratio of 8%.

To obtain the spectrum for $K^{o}_{\pi\,3}$ decay in which two charged pions are produced the coefficients of (C.9) must be doubled.

Appendix D

The Differential Aperture of Horizontally Orientated Telescopes

General expressions for the differential aperture of simple rectangular telescopes of the type in current use in the two cosmic ray neutrino experiments are given below. Consider a telescope with two parallel vertical detecting areas of height Y and width X separated by a distance Z. If, in a direction that makes an angle ξ with the normal to the detecting surfaces, the area of the front surface projected on to the back surface is $A(\theta,\phi)$, where θ and ϕ are the spherical coordinates of zenith and azimuth respectively corresponding to ξ, then the aperture is given by

$$d\Omega = A(\theta,\phi)\cos\xi \sin\theta\, d\theta\, d\phi \qquad (D.1)$$

With $\cos\xi = \cos\phi \sin\theta$ and substituting for $A(\theta,\phi)$ the differential aperture with respect to spatial zenith angle becomes

$$\frac{d\Omega}{d\theta} = 4\int_0^{\phi_{max}} (X - Z\tan\theta)\left(Y - \frac{Z}{(\cos\phi\tan\theta)}\right)\cos\phi \sin^2\theta\, d\phi \qquad (D.2)$$

The value of ϕ_{max} depends on θ. For $\tan\theta \geqslant (X^2 + Z^2)^{\frac{1}{2}}/Y$, ϕ is limited by the vertical edge of the detecting surface and $\tan\phi_{max} = X/Z$. For smaller values of θ, ϕ is limited by the horizontal edge of the detecting surface and $\sec\phi_{max} = Y\tan\theta/Z$. Substituting for ϕ_{max} in (D.2) we have

$$\frac{d\Omega}{d\theta} = 4\left[\sin^2\theta\left\{Y\left[(X^2+Z^2)^{\frac{1}{2}} - Z\right]\right\} - \sin\theta\cos\theta\left\{XZ\tan^{-1}\frac{X}{Z} - Z^2\ln\left(\frac{(X^2+Z^2)^{\frac{1}{2}}}{Z}\right)\right\}\right] \qquad (D.3a)$$

for $\frac{\pi}{2} \geqslant \theta \geqslant \tan^{-1}((X^2 + Z^2)^{\frac{1}{2}}/Y)$ and

$$\frac{d\Omega}{d\theta} = 4\sin\theta\left[XY\left(\sin^2\theta - \frac{Z^2}{Y^2}\cos^2\theta\right)^{\frac{1}{2}} - YZ\sin\theta + \cos\theta\left\{Z^2 - XZ\cos^{-1}\left(\frac{Z}{Y}\cot\theta\right) + Z^2\ln\left(\frac{Y}{Z}\tan\theta\right)\right\}\right] \qquad (D.3b)$$

for $\tan^{-1}((X^2 + Z^2)^{\frac{1}{2}}/Y) \geqslant \theta \geqslant \tan^{-1}(Z/Y)$.

Over the range $\pi > \theta > \frac{\pi}{2}$ the relation $\frac{d\Omega}{d\theta}(\theta) = \frac{d\Omega}{d\theta}(\pi - \theta)$ may be used. When calculating the total aperture, (D.3a) may be integrated analytically over the relevant range of θ but (D.3b) must be evaluated numerically.

If the differential aperture with respect to projected zenith angle β in the YZ plane is required then $\tan\beta = \cos\phi \tan\theta$ and (D.2) becomes

$$\frac{d\Omega}{d\beta} = 4\int_0^{\tan^{-1}\frac{X}{Z}} (x - z\tan\phi)(Y - z\cot\beta)\frac{\cos^2\phi \sin^2\beta}{(\cos^2\beta\cos^2\phi + \sin^2\beta)^2}\, d\phi \qquad (D.4)$$

for $\frac{\pi}{2} \geqslant \beta \geqslant \tan^{-1}(Z/Y)$. This must be evaluated numerically.

Appendix E

Celestial Coordinates of Muons in the KGF Neutrino Experiment

In Chapter 6 it was shown that the rate of events detected by the KGF telescopes due to the interactions of extra-terrestial neutrinos is expected to be considerably smaller than that due to neutrinos produced in the atmosphere. If this is not the case, the most probable source of the latter events would be the Glashow resonance interaction of very high energy $\bar{\nu}_e$. These high energy neutrinos are likely to come from only a limited number of discrete sources. It is therefore important to plot the arrival directions of all possible neutrino-induced muons in Celestial coordinates and to look for any anisotropies.

The telescopes are aligned in a North-South direction and are at a latitude of 12.9°N. If the arrival direction of the muon with repect to the telescope has a zenith angle θ and an azimuth angle ϕ, then the Celestial coordinates are given by

$$\cos\theta' = \cos\theta \cos\theta_o + \sin\theta \sin\theta_o \cos\phi \qquad (E.1)$$

and $$\cos(\phi_o - \phi') = (\cos\theta \sin\theta_o - \cos\phi \sin\theta \cos\theta_o)/(1 - \cos^2\theta')^{\frac{1}{2}} \qquad (E.2)$$

where ϕ' is the Right Ascension and the Declination is $(90^{\circ} - \theta')$N for $\theta' < 90^{\circ}$ and $(\theta' - 90^{\circ})$S for $\theta' > 90^{\circ}$. θ_o and ϕ_o define the position of the telescope: $\theta_o = 77.1^{\circ}$ and ϕ_o is the Sidereal Time in degrees.

The Celestial coordinates of the 11 events with known projected zenith angle that fell within the geometry of the telescopes are shown in Figs. E.1 and E.2, which represent the North and South Celestial hemispheres repectively. With the present telescopes only the limits of azimuth are known and this results in uncertainty mainly in the

Fig. E.1 The North Celestial Hemisphere

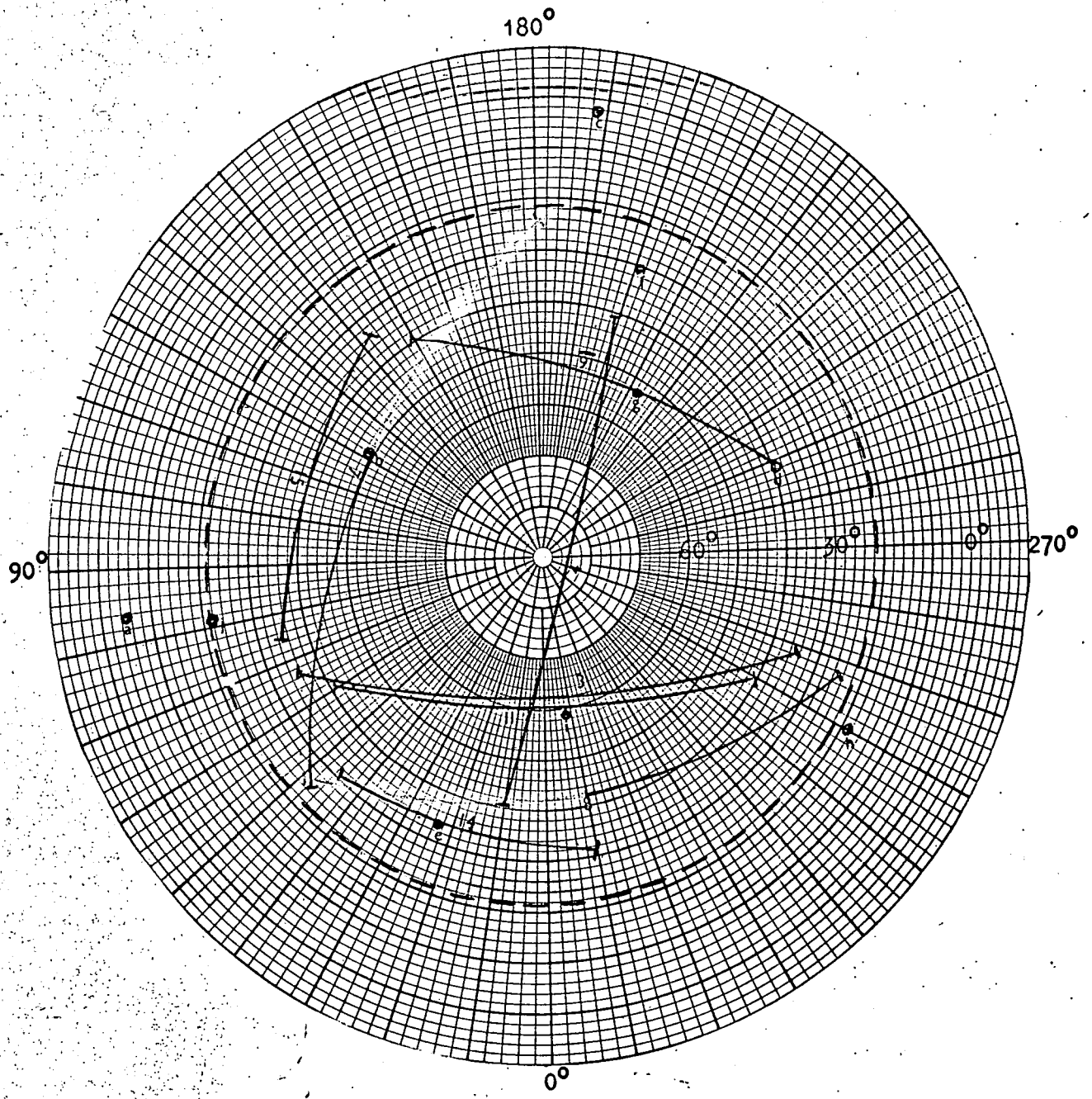

Key Quasars: a 3C147, b 3C196, c 3C273, d 3C345, e 3C48, f 3C286
Colliding galaxies: g 3C295, h Cyg. A
Supernova remains: i Cass. A, j Crab Nebula (M1)

Fig. E.2 The South Celestial Hemisphere

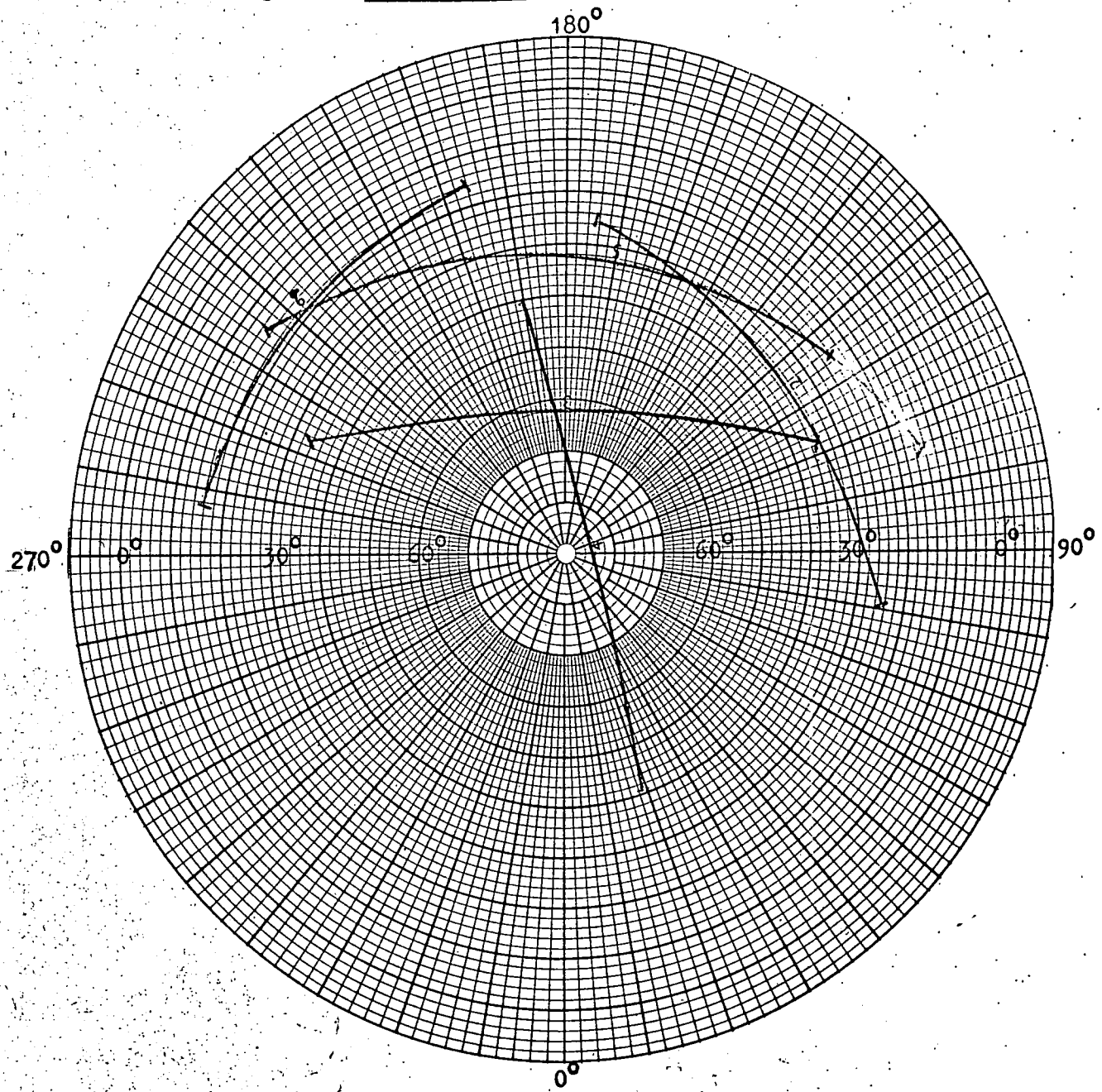

coordinate of Right Ascension. In general it is not possible to tell whether a particle traverses the telescope in an upward or downward direction. For muons induced by non-resonant neutrino interactions either is equally probable. Neutrinos taking part in the Glashow resonance interaction would, however, have an absorption length of a few hundred kilometres of rock. Thus the number of muons incident on the telescopes from this interaction at zenith angles greater than about 120° would be quite negligible. Only events 3 and 4 satisfy this criterion for upward going particles and they are plotted twice, once in each hemisphere. With this restriction on θ, it is apparent that not all of the North Celestial hemisphere is covered by the telescopes. For particles with azimuth angle $\phi = 0^{\circ}$ the minimum declination is 27.9°N, while for particles with the largest possible azimuth angle this is reduced to 21.6°N. This limiting value is shown in Fig. E.1. The whole of the southern hemisphere is covered.

The positions of some possible sources of high energy neutrinos are shown. It should be noted that the Crab Nebula (M1) does not lie within the field of view of the present telescopes.